From Continuous Modelling to Discrete Constrained Optimal Control of Distributed Parameter Systems

by

Guilherme Ozorio Cassol

A thesis submitted in partial fulfillment of the requirements for the degree of

Doctor of Philosophy

in

Process Control

Department of Chemical and Materials Engineering

University of Alberta

Abstract

Distributed parameter systems (DPS) are systems that have their evolution through time and in space. These systems are present in every type of industrial process, from chemical to electrical applications. Thus, proper modeling and control of DPS are indispensable for the optimization and control of such processes. Due to their spatiotemporal dynamics, these systems are generally represented by partial integro-differential equations (PIDEs), which brings issues with the control and monitoring of such applications. This thesis studies the modeling and control of such systems, specifically the ones modelled by first and second-order hyperbolic PDEs, not relying on the spatial approximation generally applied to deal with the PIDEs. First, an alternative model for transport-reaction processes is analyzed, taking into account the possible inertia present in the transport. Second, the regulator design of a heat exchanger system in the continuous-time setting is developed, ensuring disturbance rejection and proper output tracking. Then, the leap from the continuous to the discrete-time is taken by studying the regulator design for the sediment-filled water canal dynamics. Lastly, the optimal constrained controller is developed in the last chapters to take into account constraints applied to the system. First, an autothermal reactor operating in an unstable condition is considered. The simulations show the controller performance and proper convergence to the desired steady-state. In the subsequent chapter, the constrained control problem is solved for the alternative model of transport-reaction processes. The difference in the system response of the commonly used model and the

proposed model is noticeable. The discrete representation used for the systems in the discrete-time setting does not consider the early spatial approximation generally used when dealing with DPS.

Preface

This thesis resulted in five papers:

Chapter 2 of this work has been published as Guilherme Ozorio Cassol, Stevan Dubljevic, "Hyperbolicity of reaction-transport processes", AIChE Journal (2021). I was responsible for the theory development, numerical simulations, analysis of the results, and manuscript composition. Stevan Dubljevic was the supervisory author involved with concept formation and manuscript composition.

Chapter 3 was published as Guilherme Ozorio Cassol, Dong Ni, Stevan Dubljevic, "Heat exchanger system boundary regulation", AIChE Journal (2019). I was responsible for the theory development, numerical simulations, analysis of the results, and manuscript composition. Dong Ni and Stevan Dubljevic were the supervisory authors involved with concept formation and manuscript composition.

Chapter 4 has been published as Guilherme Ozorio Cassol, Stevan Dubljevic, "Discrete output regulator design for the linearized Saint-Venant-Exner model" , Processes (2020). I was responsible for the theory development, numerical simulations, analysis of the results, and manuscript composition. Stevan Dubljevic was the supervisory author involved with concept formation and manuscript composition.

Chapter 5 of this work is published as Guilherme Ozorio Cassol, Stevan Dubljevic, "Dynamical Analysis and Model Predictive Control of an Auto-Thermal Reactor" , Industrial and Engineering Chemistry Research (2019). I was responsible for the theory development, numerical simulations, analysis of the results, and manuscript composition. Stevan Dubljevic was the supervisory author involved with concept formation and manuscript composition.

Chapter 6 has been submitted for publication as Guilherme Ozorio Cassol, Stevan Dubljevic, "Model Predictive Control of a Second-order Hyperbolic transport-reaction process", AIChE Journal. I was responsible for the theory development, numerical simulations, analysis of the results, and manuscript composition. Stevan Dubljevic was the supervisory author involved with concept formation and manuscript composition.

Acknowledgements

First, I would like to express my profound gratitude to my supervisor, Prof. Stevan Dubljevic. His assistance and involvement made this journey tolerable and exhilarating. Although we started working together by the end of my studies, I also want to thank Prof. Youssef Belhamadia for his patience.

I thank my family for their emotional support throughout these years.

I am also grateful to my colleagues in the distributed parameter systems group and the visiting students I had the pleasure to work with: Junyao Xie, Lu Zhang, Jukka-Pekka Humaloja, Seyedhamidreza Khatibi, Azzam Hazim, Xiaodong Xu, Jie Qi, Yanjiu Zhou, and Behrad Moadeli.

Last but not least, I thank CAPES for the financial support, and I am grateful for this opportunity.

Contents

List of Tables

List of Figures

Chapter 1

Introduction

When "Stirred pots and empty tubes" [1] was written by Aris and Varma, the mathematical models for ideal reactors and the diffusion-reaction in porous catalysts were being studied. The researchers were trying to determine the criteria for the uniqueness, multiplicity, and stability for such systems' steady-states. About 40 years later, these mathematical models are still used, as stirred tanks and tubular reactors are extensively used in chemical and biochemical transformations.

The dynamics of tubular reactors are represented as mathematical models having both temporal and spatial characteristics, and these processes are named distributed parameter systems (DPS). Examples of applications include heavy oil recovery in the petroleum industry, tubular and plug-flow reactor systems used for chemical production and refinement and heat exchangers used in various industries. In the same line, in manufacturing industries, phase transitions and thermal treatment, represented by DPS models, are critical factors in the fabrication and processing of materials, such as crystal growth methods for semiconductor production.

The mathematical models of this kind of system are given by partial differential equations (PDEs), and they belong to the class of infinite-dimensional systems. Due to the existence of the spatial variable in the mathematical model, the state estimation and control of distributed parameter systems are challenging and interesting. Hence, there is a rich and active research interest in this field that draws upon the well-established classical tools of mathemati-

cal analysis and employs the recent advancements in computer technology for process simulation and numerical studies of complex problems.

A PDE includes partial derivatives of a function regarding two or more independent variables. The distributed nature of the state is the distinguishing feature of process variables modelled by PDEs in contrast to those represented by ordinary differential equations (ODEs), for which the process variables are represented by functions of only a single independent variable. Consider $x(\zeta, t)$, a dependent variable, function of other independent variables: ζ, an independent spatial variable belonging to a domain $\Omega \in \Re$; t, the independent time variable, considered as $t \in \Re^+$. The function $x(\zeta, t)$ represents the system's state at the time t along with the space domain and is the process variable of interest.

Linear (or linearized) PDEs can describe many transport-reaction processes in chemical and materials engineering. The system properties strongly depend on the type of PDE that models the system. These types of equations have their classification defined based on the following form:

$$\alpha \frac{\partial^2 x}{\partial t^2}(\zeta, t) + \beta \frac{\partial^2 x}{\partial t \partial \zeta}(\zeta, t) + \gamma \frac{\partial^2 x}{\partial \zeta^2}(\zeta, t) = F\left(x, \frac{\partial x}{\partial t}, \frac{\partial x}{\partial \zeta}, t, z, u\right) \tag{1.1}$$

If $\beta^2 - 4\alpha\gamma > 0$, the PDE is hyperbolic; if $\beta^2 - 4\alpha\gamma = 0$, it is a parabolic PDE; finally, if $\beta^2 - 4\alpha\gamma < 0$, the system is represented by an elliptic PDE. An axial dispersion chemical reactor is described by parabolic PDE, while a plug flow reactor is modelled by a hyperbolic PDE.

A general representation of a linear PDE with input is given as below:

$$\frac{\partial x}{\partial t}(\zeta, t) = A(\zeta, t)x(\zeta, t) + B(\zeta, t)u(t) \tag{1.2}$$

where $A(\zeta, t)(\cdot)$ is the spatial operator, and, for most common chemical processes, it can be written as:

$$A(\zeta, t)(\cdot) = \frac{\partial}{\partial \zeta}\left(D(\zeta, t)\frac{\partial(\cdot)}{\partial \zeta}\right) + v(\zeta, t)\frac{\partial(\cdot)}{\partial \zeta} + k(\zeta, t)(\cdot) \tag{1.3}$$

This generic type of PDE given in (1.2)-(1.3) includes two important transport mechanisms: the diffusion (represented by the diffusion coefficient $D(\zeta, t)$) and convection (represented by the velocity $v(\zeta, t)$). This type of equation

also accounts for a generation/consumption term, represented by $k(\zeta, t)$. The $B(\zeta, t)$ term in (1.2) represents the input operator and depends on the type of actuation imposed on the system.

In both PDEs and ODEs, the system is not properly posed without specifying the initial conditions. For PDEs, not only the initial conditions ($x(\zeta, t = 0) = x_o(\zeta)$) are necessary, but also the boundary conditions. These conditions are generally of three types:

- **Dirichlet** (also called **first-type**) boundary condition: specify the function at the boundary:

$$ax(\zeta = \zeta_o, t) = c \tag{1.4}$$

- **Neumann** (or **second-type**) boundary condition: specify the value of the spatial derivative at the boundary:

$$b\frac{\partial x}{\partial \zeta}(\zeta = \zeta_o, t) = c \tag{1.5}$$

- **Robin** (or **third-type**) boundary condition: specify a linear combination of the function and its spatial derivative at the boundary:

$$ax(\zeta = \zeta_o, t) + b\frac{\partial x}{\partial \zeta}(\zeta = \zeta_o, t) = c \tag{1.6}$$

The type of actuation applied to the system also significantly influences how to properly design the controller. Generally, three different types of input can be considered on the controller design for a DPS, as illustrated in Figure 1.1. The first type of actuation, shown on the top of the figure, considers that the input is distributed throughout the domain and that it is possible to control the actuation at any point (i.e., $u(\zeta, t)$). Thus, both the inputs and states belong to infinite-dimensional spaces. Unfortunately, although the assumption of an infinite-dimensional space is mathematically correct, the possibility of implementation is near impossible. As illustrated at the top of Figure 1.1, if we consider a reactor, this assumption would only be realizable if an infinite number of heat elements were acting on the reactor, making it possible to manipulate the input at any point.

The illustration at the center of Figure 1.1 represents the second type of input, one that belongs to a finite-dimensional space and acts on the states in an in-domain distributed manner. A reactor surrounded by a jacket with a high flow (or heat capacity) heating/cooling fluid inside is an example of this input type. In this case, the fluid temperature inside the jacket will not change throughout the domain. Thus, the temperature of the heating/cooling fluid that enters the jacket remains the same. The inlet temperature to the jacket is this system input and affects the states due to the temperature difference between the two fluids.

The last type of input is similar to the second case and represented at the bottom of Figure 1.1. Instead of considering that the jacket's temperature is constant, now it is assumed that both the jacket and reactor's temperatures will change throughout the domain and are states of the system. The input only changes the jacket inlet temperature, which corresponds to the boundary condition of the jacket's states. These instances, where the actuation is applied at the boundary, are called boundary control problems. The input acts only at the domain boundary and is not spatially distributed. Notice that all the types of boundary conditions shown above can be considered in boundary control problems (i.e., $c = u(t)$ in the Dirichlet, Neumann or Robin boundary conditions).

Due to these characteristics, the DPS regulator design is more complex than in the finite-dimensional systems (also called Lumped Parameter System - LPS and generally represented by ODEs). The presence of spatial variables presents limitations to the controller design accomplished in the LPS setting. For instance, in some cases, the inputs and outputs can be given as boundary conditions, which adds to design complexity. In general, there are two approaches taken for controller design and state estimation of DPS, as illustrated in Figure 1.2:

1. **Early lumping**: the DPS is first discretized into an approximate LPS, leading to a system of ODEs. The LPS control theory is then applied for the controller design and state estimation. As the resulting system

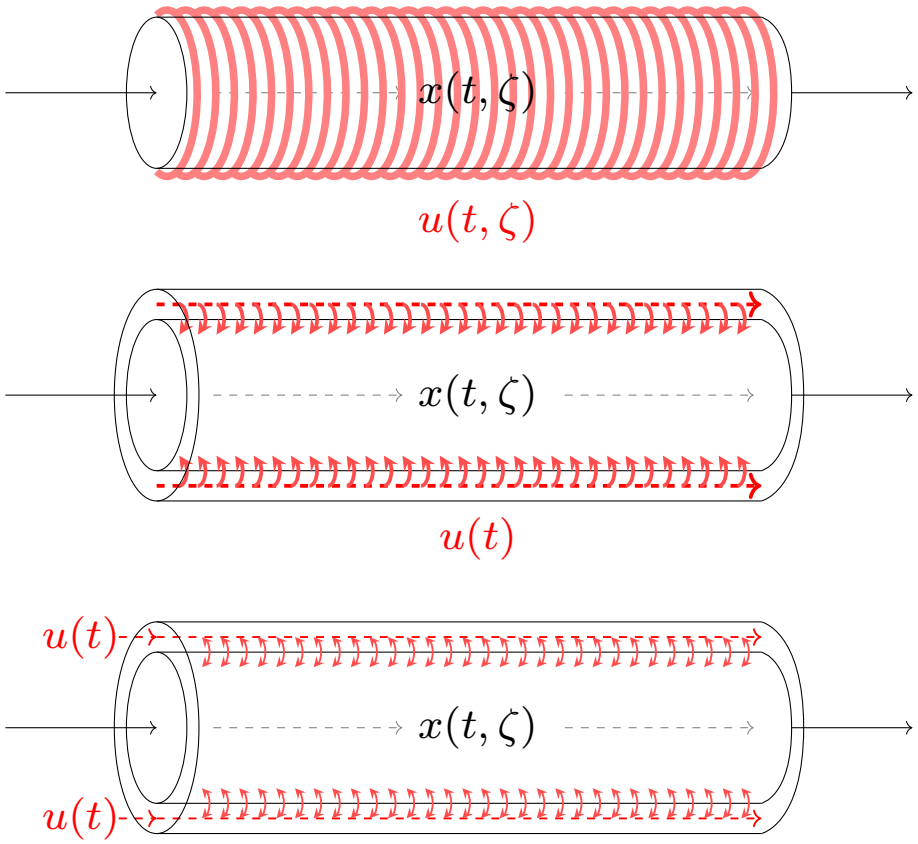

Figure 1.1: Types of DPS Inputs: (Top) Infinite-dimensional in-domain input; (Center) Finite-dimensional in-domain input; (Bottom) Finite-dimensional boundary input;

of ODEs depends on the discretization method and the number of the discretization points, the conditions for controllability, stabilizability and observability can also vary, which is a drawback of this methodology.

2. **Late lumping**: the control theory is applied directly to the DPS, and discretization is used at the final stage for implementation. This methodology considers the theory and analysis of PDEs to define the system properties (controllability, stabilizability, and observability).

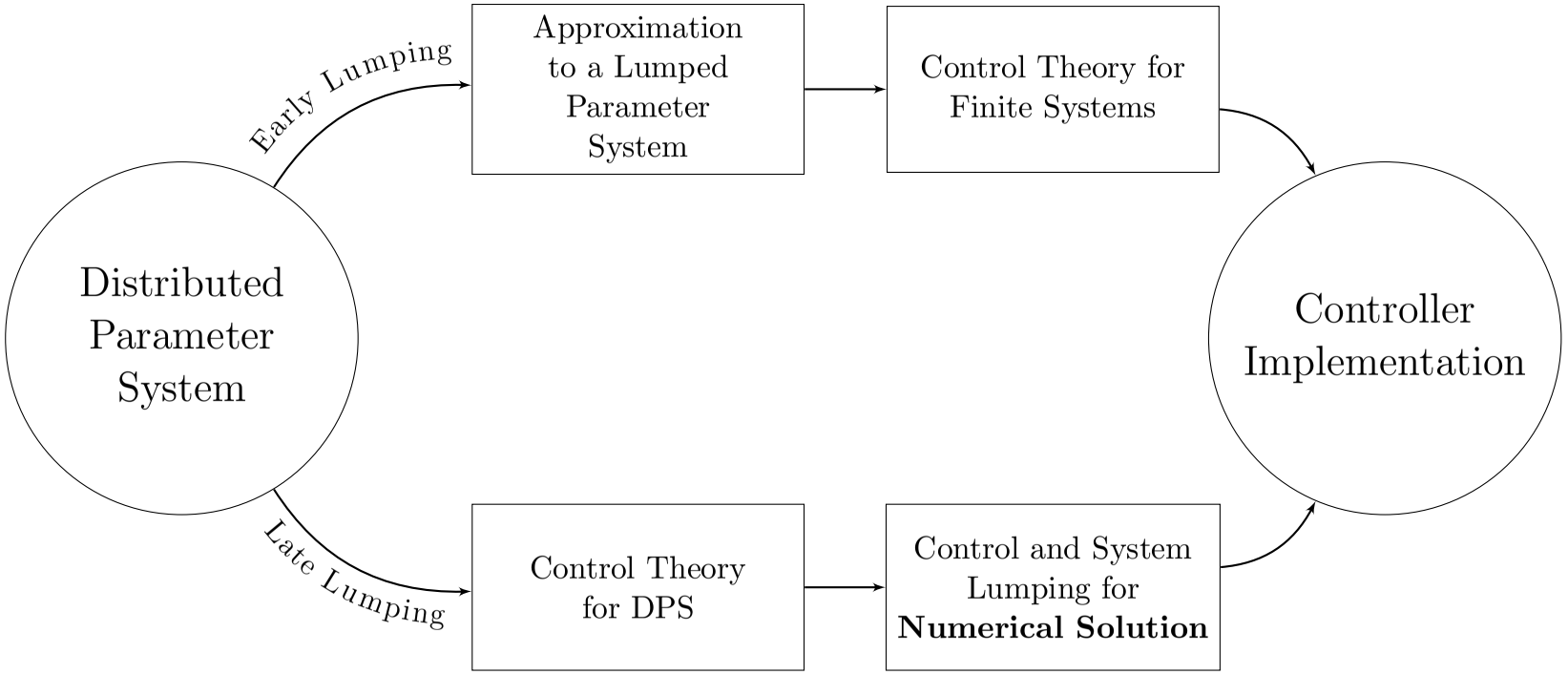

Figure 1.2: Early and late lumping controller design

The difference between these methodologies can be seen in the following example. Considering the following PDE, represented in Figure 1.3:

$$\begin{cases} \dfrac{\partial x(\zeta,t)}{\partial t} = A(\zeta,t)x(\zeta,t) = -v\dfrac{\partial x(\zeta,t)}{\partial \zeta} \\ x(\zeta=0,t) = u(t) \\ y(t) = x(\zeta=1,t) \end{cases} \tag{1.7}$$

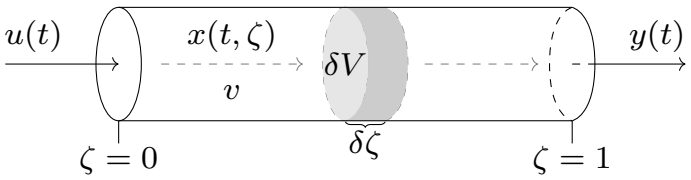

Figure 1.3: Hyperbolic system (Eq. 1.7) representation

The finite differences method can be used to get a system of ODE that approximately represents the partial differential equation. Once the finite-dimensional representation is obtained, standard finite system control definitions such as controllability, stabilizability, observability and transfer function representation can be explored. Considering the early and late lumping methodologies, the results shown in Table 1.1 are obtained for the transfer function representation, where N represents the number of intervals in the discretization (i.e., number of total points minus one) and v is the system velocity.

$A(\zeta,t) = -v\dfrac{\partial}{\partial\zeta}$, $\begin{cases} x(\zeta=0,t) = u(t) \\ y(t) = x(\zeta=1,t) \end{cases}$	Methodology	Transfer Function
	Early Lumping	$G(s) = \frac{1}{\left(1+\frac{s}{vN}\right)^N}$
	Late Lumping	$G(s) = \mathrm{e}^{-\frac{s}{v}}$

Table 1.1: Tranfer functions obtained using early and late lumping

The transfer function obtained by applying finite differences in the partial differential equation shows that the system is supposed to have poles at $s = -vN$ with multiplicity N. The analytical transfer function does not display any poles; in fact, as expected, it only represents a time delay. It is possible

to show that as $N \to \infty$ the transfer function obtained with the discretized system converges to the analytical solution, i.e.:

$$\lim_{N\to\infty} G(s) = \lim_{N\to\infty} \frac{1}{\left(1+\frac{s}{vN}\right)^N} = \mathrm{e}^{-\frac{s}{v}} \tag{1.8}$$

Therefore, if a large number of discretization points are used, the system of ODEs obtained by the early lumping methodology approximately well represents the system. This is one of the drawbacks of the early lumping methods, as a higher number of discretization points increases the computational cost to represent the distributed parameter system properly.

This thesis proposal aims to study the modeling and controller design for DPS without the use of early lumping in the context of chemical systems, considering the design in both continuous and discrete-time settings. Specifically, systems that can be modelled by hyperbolic PDEs are studied.

1.1 Literature Review

One of the main goals of any control strategy is to make the system dynamics behave in a specified, desired manner. Therefore, the classical problem of a servo-design regulator is defined as the design of the closed-loop control system, which tracks a prescribed signal, rejects possible disturbances applied to the system, and guarantees the closed-loop stability with some degree of robustness [2]. The distributed parameter system class includes a diversity of important processes in science, and engineering [3]–[5]. In the literature, this type of system is addressed with two approaches: finite-dimensional approximation of the distributed system followed by finite-dimensional design and functioning assessment (the early lumping methodology); and a direct infinite-dimensional design for the distributed parameter systems followed by finite-dimensional (numerical solution) implementation [6]–[8].

By following the well-known regulator designs from the finite-dimensional systems theory, one possible way to design the regulator for the distributed parameter systems is to use the early lumping approach. Hence, standard regulator design methods applicable to ODE systems can be realized, and

several contributions deal with the regulator problem for finite-dimensional linear systems [9], [10]. However, the early lumping approach also results in a possible mismatch between the dynamical properties of the original distributed parameter and the lumped parameter models, which inevitably affects the designed regulator performances [11].

A more rigorous way to address regulator design in the realm of distributed parameter processes is to exploit the infinite-dimensional characteristic of the system, as past contributions in the literature have done: the PI-controller for distributed parameter systems with constant disturbance was developed [12]; the use of the geometric theory for the regulation problem for infinite-dimensional linear systems driven by finite-dimensional exosystems was also studied [13] and the regulator design was proposed for a class of first-order hyperbolic PDE systems with space-varying coefficients [14]and for a system of hyperbolic transport equations [6]. The output and error feedback regulators design for a linear scalar nonspectral hyperbolic system with boundary and in-domain actuation was developed [15].

Furthermore, the type of information available for the regulator also determines its features. For example, given that the full-state information is available, which rarely happens in practice for a DPS, one can design a full-state feedback regulator. The spatial and temporal properties of the distributed parameter systems, coupled with the spatially distributed or boundary actuation and measurement, make it impractical to measure the system states at all points [16], [17]. The practical design realizations need to account for scenarios when only output and/or error measurements are available. Thus, using the states reconstructed by observers, filters, and estimators is interesting [6].

With the early lumping methodology, the observation problem is addressed with the tools available in the more developed field of finite-dimensional systems [18], [19]. The infinite-dimensional designs have been conceived by using different strategies, such as the geometric control method equipped with manifold theory [4], back-stepping integral transformations [8], variable structure estimation schemes [20], nonlinear evolution equations [21], open-loop observers [22], and absolute stability [7]. The infinite-dimensional observer

design problem was also addressed with an adjustable-weight Lyapunov function [23], and the related convergence inequalities were handled with a linear matrix inequality approach recalled from optimal boundary control design [24]. The optimal constrained state estimation problem has also been addressed by the use of a sequential, algorithmic optimal constrained state estimator, capable of dealing with boundary actuation and point measurement [25].

A state-of-the-art controller realization is ultimately digital, therefore, discrete. This motivates the search for a control design that considers the closed-loop system's discrete-time nature. Modern control techniques (such as the model predictive control) generally use a discrete version of the overall system. Therefore, the traditional numerical time discretization schemes are frequently considered to transform models and/or controllers for implementation. But, the accuracy of the discrete system representation may be impacted as the sampling period is increased, which adversely may affect the overall model and closed-loop stability [26].

From the linear systems theory, it is known that simple explicit and implicit Euler time discretization may impact the systems' stability by mapping stable continuous to possible unstable discrete counterpart system and vice versa [27]. This issue becomes even more prominent in the case of controller design and/or realizations for DPS. Hence, it is essential to explore time discretization schemes that provide an accurate and reliable transformation of continuous linear infinite-dimensional systems to the linear discrete-time infinite-dimensional one. The application of Crank-Nicolson midpoint integration rule [28], a type of discretization in the systems science also known as Cayley-Tustin time discretization, has been shown to preserve the intrinsic energy and dynamical characteristics of the linear distributed parameter system [29], with no spatial discretization or/and spatial model reduction needs to be applied.

In reality, actuators and sensors have their limits due to physical properties, or the desired output is required to be within a specific range. This adds constraints to the control problem. Among modern control designs, if optimal control is considered and constraints are imposed in the systems' settings, advanced control strategies - such as model predictive control (MPC) - can

be used to achieve the optimal system response without constraints violation. MPC incorporates constraints explicitly, is easily formulated as a constrained optimization problem, and can be solved with standard software. It also can anticipate future events and take control actions accordingly. This predictive ability is something classic controllers like PID controllers do not have.

In essence, a linear MPC refers to a class of control algorithms that compute the controlled variables profiles by utilizing a linear process model to optimize an open-loop quadratic objective function subject to constraints over a future time-horizon [30], [31]. Only the first control action of the computed profile is applied, and this process is repeated at each time interval [32], [33]. In the case of linear models, the model predictive control utilizes a linear state space or transfer function representations obtained by modeling or empirical response of the controlled plant [30]. The outstanding feature of linear model predictive control is that constrained and multivariable processes can be addressed with emphasis on a robust algorithm realization that can be implemented online.

The MPC for DPS has to consider the distributed nature, the naturally present constraints, and limitations on available measurements into its optimal performance. In particular, there are similarities among constrained optimal controller design formulations for finite and infinite-dimensional systems. The differences in the controller synthesis are associated with how the stable and unstable infinite-dimensional systems are treated. Along the line of similarities, the well-known formulation of the quadratic form optimization functional on the infinite horizon is used for both infinite, and finite-dimensional systems [34]. Various development of MPC for distributed parameter systems have been explored considering distributed actuation [35], boundary actuation [36], and output and full-state feedback control [37].

1.2 Thesis Outline

This thesis proposal aims to study the modeling and control of DPS without using early lumping techniques, considering the design in both continuous and discrete-time settings. Hyperbolic models are the focus of this thesis, which is

divided as follows:

In Chapter 2, common chemical engineering transport-reaction systems are modeled by considering the inertia in the transport phenomena. This results in second-order hyperbolic PDEs, which account for a finite speed of propagation. The findings provide the derivation of the hyperbolic transport-reaction partial differential equations and a direct comparison with their corresponding dissipative parabolic PDEs. The stability analysis of the dynamical systems is considered and complemented by numerical simulations for typical processes, such as the heat diffusion in a slab, transport-reaction inside a chemical reactor, and a phase change problem. The results show the effects of the modeling and/or limits of the approximation used in deriving and considering the hyperbolic PDE for transport-reaction systems.

In Chapter 3, the boundary feedback regulator design for heat exchangers with delayed feedback is developed. Counter-flow/parallel-flow heat exchanger systems described by a pair of coupled transport hyperbolic partial differential equations (PDEs) with delayed boundary feedback loop are considered. By applying a boundary transformation, the coupled transport hyperbolic PDEs and boundary delay are changed into a corresponding linear infinite-dimensional system used in the regulator design. The design initially addresses a full state feedback controller realization augmented by the observer design to simultaneously output exponential stabilization and tracking and disturbance rejection of polynomial and/or harmonic type of reference signals. The simulations studies demonstrate the proposed design for counter-flow and parallel-flow heat exchangers, two standard configurations present in industrial practice.

In Chapter 4, the regulator design in the discrete-time setting for the unstable linearized Saint-Venant-Exner model is addressed. The proposed regulator ensures the closed-loop stability and proper tracking of polynomial and periodic reference signals using output feedback in a sample-data setting. The system discrete representation is achieved by applying the structure-preserving Cayley-Tustin time discretization, and the direct relation with the regulator in the continuous-time setting is shown. The regulator design is developed using the backstepping methodology to provide the closed-loop stability and

the observer design. At the same time, the Sylvester equations are solved to achieve proper tracking. Finally, the numerical simulation results show the regulator's performance.

In Chapter 5, the design of a model predictive controller for the auto-thermal reactor with an internal counter-current heat exchanger (ARICHE) is considered. This system is modelled by a system of quasilinear hyperbolic PDEs and can exhibit a multiplicity of steady states, which is explored by considering a parametric analysis of the model. Generally, the unstable steady-state, which provides optimal conversion and selectivity, is regarded as the steady-state of interest. The linearization is utilized to obtain a linear system of coupled transport-reaction hyperbolic PDEs. The structure-preserving Caley-Tustin discretization is employed without any spatial approximation and/or order reduction. The discrete model is utilized in the model predictive controller (MPC) design, and it successfully addresses the control scenarios which account for the optimality, stability, and constraints satisfaction.

In Chapter 6, the model predictive controller design is developed for the type of PDEs studied in Chapter 2. The dynamics of a tubular chemical reactor with boundary actuation is assumed to be modelled by a second-order hyperbolic equation. The discrete Luenberger observer design for state reconstruction is addressed and integrated with the MPC design. The observer gain is obtained by solving the operator Ricatti equation in the discrete-time setting using the bi-orthonormal basis defined for the system operator. At the same time, the MPC accounts for constrained and optimal control. In addition, the results for considering both parabolic and hyperbolic equations are presented and discussed.

Finally, Chapter 7 outlines the results of this thesis and discusses the present and future research plans.

Chapter 2

Hyperbolicity of reaction-transport processes

2.1 Introduction

The heat transport thorough a solid is one of the simplest transport-reaction processes one can come across in chemical/process engineering. The conductive transport of heat across the macroscopic scale is generally described by a parabolic partial differential equation (PDE) obtained by defining the heat flux given by the Fourier's law. In Fourier's law, an initial temperature gradient in a conductive medium causes an immediate heat flux, thus, any initial disturbance in the material body is propagated instantly [38]. However, it has been experimentally shown that, in some cases, the parabolic heat conduction equation may not accurately describe the process. Materials with non-homogeneous structures, for instance, present thermal waves that travel with a finite speed of propagation [39]. A similar behavior is seen when extremely fast thermal disturbances are induced by a laser [40] or a flash lamp [41].

To deal with the undesirable feature characteristic of the parabolic PDE, Cattaneo [42] proposed a modified Fourier's law that took into account the thermal inertia and, when applied to the energy balance, the resulting PDE is a hyperbolic equation. This type of equation is physically relevant and has the desired finite speed of propagation [42], [43]. Furthermore, the hyperbolicity mathematically ensures the well-posedness of the local Cauchy problems [44]. The hyperbolicity of the transport phenomena has been analyzed in different

contributions. In particular in King et al. [45], the numerical and analytical solutions of the hyperbolic heat equation were analyzed in an infinite space. Similarly, in Novikov [46], the temperature propagation in an infinite one-dimensional plate with a stationary heat sensor was solved considering a hyperbolic heat-conduction equation. In Mitra et al. [47], the experimental evidence of the heat propagation in processed meat demonstrated that the hyperbolic model is an accurate representation of heat conduction on a macroscopic level. More recently, a modified equilibrium model of a heat-conducting, heterogeneous mixture was proposed using the modified flux, and a set hyperbolic equations was obtained [48]. The study of Nosko [39] proposed different non-Fourier models to simulate temperatures in materials subjected to extremely fast thermal disturbances, specifically for the microscopic sliding contact. In addition, in Abbasi et al. [49], the optimal control in a biological tissue modeled by a thermal wave equation, i.e., a hyperbolic heat equation, was proposed.

The modeling feature associated with this delayed flux in the chemical engineering process, for instance in tubular reactors [50], [51]), is interesting as generally the models of reaction-diffusion nature are represented by parabolic PDEs originated by assuming that the flux in the mass balance is given by Fick's law. As Cattaneo's and Fick's (or Fourier's) laws are equivalent in the steady-state condition, for some applications, the differences are generally seen in small timescales. But, for systems characterized by long relaxation times, such as polymeric fluids, heat and electric conductor at high temperatures, the difference is noticeable. For mass transfer, where relaxation time might be several orders of magnitude larger than in heat propagation, the same behavior might hold [52]. This potential has been noticed in the literature, and was considered to potentially represent anomalous mass transport phenomena [53], [54].

Furthermore, the Cattaneo-type of flux has been shown to arise from statistical mechanics as well. For example: in Nonnenmacher [55] the nonlinear constitutive laws were derived from the nonlinear Boltzmann equation, which was then linearized and, in turn, lead to Cattaneo's modified flux. In Godoy [56],

the quantum random walk was used to study diffusion in one dimensional crystalline nanostructures. A hyperbolic equation was derived to represent the dynamic in the mesoscopic diffusion regime. The differences between these classes of PDEs are also important when designing a controller since the deviation in the system's dynamics might affect the controller's performance and the closed-loop stability, as a model-based controller for transport problems generally considers the parabolic model [36], [57].

In this contribution, the effects of the transport delay in a moving boundary problem, specifically, a Stefan problem, are also analyzed. This type of system is a specific class of boundary value problem for partial differential equations that generally focus on the heat distribution in a body with a phase transition. A common example of a Stefan problem is the diffusion of heat in ice melting: the interface between the solid and liquid phase will change its position as the ice melts [58]. The solution of this type of system needs to take into account the determination of the moving boundary position as it changes with time and cannot be determined a priori. Although this type of problem is generally associated with melting and solidification problems, there are contributions that address the fluid flow in porous media or even shock waves in gas dynamics using Stefan-like problems [58].

This chapter analyzes the distinct characteristics of the second-order hyperbolic and parabolic PDEs obtained for different mass or heat transport processes. First, the heat transfer in a finite body with different boundary conditions is considered. The derivation and stability analysis of the parabolic and hyperbolic equations are shown. In this case, an open-form analytical solution can be obtained and the comparison between the results is made. Then, the same characteristics are studied for an axial dispersion reactor considering open and closed boundary conditions, which is a typical chemical engineering example. Finally, a moving boundary problem is explored considering the two types of PDEs and the numerical results of the simulations are discussed.

2.2 The heat equation

Considering a fluid at rest with constant density and neglecting non-linear terms in gradients and time-derivatives, the energy balance for the system, considering only the transport in one dimension, leads to the following equation:

$$C\partial_t T + \partial_\zeta q = 0 \tag{2.1}$$

where C is material heat capacity per unit of volume. The heat flux (q) can be defined by the Fourier's law if only diffusion is considered:

$$q = -k\partial_\zeta T \tag{2.2}$$

where k is the material thermal conductivity, assumed to be constant in the space. The energy balance can be rewritten as:

$$\partial_t T + \partial_\zeta q = 0 \implies \partial_t T = \alpha \partial_{\zeta\zeta} T \tag{2.3}$$

with $\alpha = \frac{k}{\rho c} = \frac{k}{C}$, ρ is the material density and c is the material heat capacity per unit of mass. For an initial value problem ($T(\zeta, t = 0) = T_0(\zeta)$) in a one dimensional infinite spatial domain, the solution of this PDE is given as:

$$T(\zeta, t) = \frac{1}{(4\pi\alpha t)^{3/2}} \int_{-\infty}^{\infty} T(z, 0) \exp\left(-\frac{(z-\zeta)^2}{4\alpha t}\right) dz \tag{2.4}$$

As long as the initial condition is different from 0, this solution predicts an instant heat propagation, which is called the Heat Conduction Paradox. Cattaneo [42] wrote a paper at which the question of the paradox of heat conduction was addressed. The author modified Fourier's law, based on the elementary kinetic theory of gases. It was argued that there is a time-lag between the start of the particles at their point of departure and the time of passage through the middle layer. Therefore, if the temperature changes in time then, the heat flux at a certain time should depend on the temperature gradient of an earlier time. This assumption leads to the following definition of a modified heat flux:

$$q = -k(1 - \tau\partial_t)\partial_\zeta T \tag{2.5}$$

where τ is called the characteristic time. If $\tau \to 0$, the following approximation can be used:

$$(1 - \tau\partial_t)^{-1} \approx (1 + \tau\partial_t) \tag{2.6}$$

and the energy balance can be rewritten as a second order hyperbolic PDE:

$$\tau\partial_{tt}T + \partial_t T = \alpha\partial_{\zeta\zeta}T \tag{2.7}$$

with the understanding that, if $\tau = 0$, the original parabolic PDE from Eq. 2.3 is obtained.

2.2.1 Boundary Conditions

Considering the heat conduction equations shown in Eq. 2.3 and Eq. 2.7, three different sets of boundary conditions are assumed and will be used in the following sections:

$$1. \begin{cases} T(0,t) = 0 \\ T(1,t) = 0 \end{cases} \tag{2.8}$$

$$2. \begin{cases} \partial_\zeta T(0,t) = 0 \\ T(1,t) = 0 \end{cases} \tag{2.9}$$

$$3. \begin{cases} \partial_\zeta T(0,t) = 0 \\ \partial_\zeta T(1,t) = 0 \end{cases} \tag{2.10}$$

The first set of boundary conditions (Eq. 2.8) represents two Dirichlet boundary conditions and assumes the direct control of the temperature on the boundaries, which physically represent the case when large heat sinks/sources with constant temperature placed at the boundaries. Eq. 2.10 represents two Neumann boundary conditions, which assumes the possibility that the flux can be controlled. Eq. 2.9 has mixed boundary conditions as the types of boundary conditions at the two boundaries are different.

2.2.2 Eigenvalue Analysis

In this section, a comparison among the eigenvalue distribution of the parabolic and second order hyperbolic is made to understand how the system dynamics

are different in these two modeling settings. As the results for the parabolic have been extensively studied and reported, the outcome for this type of equation is shown in Table 2.1.

The eigenvalue problem is defined as $A\phi = \lambda\phi$, where A is the operator considered, ϕ is the eigenfunction and λ is the eigenvalue.

Table 2.1: Properties of the parabolic heat equation (Eq. 2.3)

Boundary Condition	B.C. 1 (Eq. 2.8)	B.C. 2 (Eq. 2.9)	B.C. 3 (Eq. 2.10)
Eigenvalues	$\lambda_k = -\alpha\pi^2 k^2, \text{ for } k > 0$	$\lambda_k = -\alpha\pi^2 \left(\frac{2k+1}{2}\right)^2, \text{ for } k \geq 0$	$\lambda_k = -\alpha\pi^2 k^2, \text{ for } k \geq 0$
A **Eigenfunctions**	$\phi_k(\zeta) = a_k \sin(\pi k\zeta)$	$\phi_k(\zeta) = a_k \cos\left(\frac{2k+1}{2}\pi\zeta\right)$	$\phi_k(\zeta) = a_k \cos(\pi k\zeta), \phi_0(\zeta) = a_0$
Adjoint Op. (A^*)	$A^* = \alpha\partial_{\zeta\zeta}$		
Adjoint B.C.	$\begin{cases} y(0) = 0 \\ y(1) = 0 \end{cases}$	$\begin{cases} \partial_\zeta y(0) = 0 \\ y(1) = 0 \end{cases}$	$\begin{cases} \partial_\zeta y(0) = 0 \\ \partial_\zeta y(1) = 0 \end{cases}$
Adj. Eigenfunctions	$\psi_k(\zeta) = \phi_k(\zeta)$	$\psi_k(\zeta) = \phi_k(\zeta)$	$\psi_k(\zeta) = \phi_k(\zeta)$
a_k	$a_k = \sqrt{2}$	$a_k = \sqrt{2}$	$a_0 = 1$ and $a_k = \sqrt{2}$ for$k \geq 1$
PDE Solution	$T(\zeta, t) = \sum_k^\infty \mathrm{e}^{\lambda_k t} A_k Z_k(\zeta)$		
Z_k	$Z_k = \phi_k(\zeta)$	$Z_k = \phi_k(\zeta)$	$Z_k = \phi_k(\zeta)$
A_k	$A_k = \langle T(\zeta, 0), \psi_k(\zeta) >$		
Semigroup	$\mathcal{T}(t)(\cdot) = \int_0^1 \sum_k^\infty \mathrm{e}^{\lambda_k t} Z_k(\zeta)\psi_k(\eta)(\cdot)d\eta$		

For the second order hyperbolic, the partial differential equation shown in Eq. 2.7 can be written as:

$$\frac{\partial}{\partial t}\begin{bmatrix} T \\ \dfrac{\partial T}{\partial t} \end{bmatrix} = \begin{bmatrix} 0 & 1 \\ \dfrac{\alpha}{\tau}\dfrac{\partial^2}{\partial \zeta^2} & \dfrac{-1}{\tau} \end{bmatrix}\begin{bmatrix} T \\ \dfrac{\partial T}{\partial t} \end{bmatrix} \tag{2.11}$$

such that the operator A is defined as:

$$A = \begin{bmatrix} 0 & 1 \\ \dfrac{\alpha}{\tau}\dfrac{\partial^2}{\zeta^2} & \dfrac{-1}{\tau} \end{bmatrix} \tag{2.12}$$

thus, as the eigenvalue problem is defined as $A\phi = \lambda\phi$, the following system of equations is solved as:

$$\begin{cases} \phi_2 = \lambda\phi_1 \\ \dfrac{\alpha}{\tau}\dfrac{\partial^2\phi_1}{\partial\zeta^2} - \dfrac{\phi_2}{\tau} = \lambda\phi_2 \end{cases} \tag{2.13}$$

which leads to the following second order ODE:

$$\frac{d^2\phi_1}{d\zeta^2} = \frac{\lambda}{\alpha}(\lambda\tau + 1)\phi_1 \tag{2.14}$$

This second order equation has a general solution given as:

$$\begin{bmatrix} \phi \\ d_\zeta\phi \end{bmatrix} = \mathrm{e}^{\bar{A}(\zeta-\zeta_0)}\begin{bmatrix} \phi(\zeta_0) \\ d_\zeta\phi(\zeta_0) \end{bmatrix} \implies \bar{A} = \begin{bmatrix} 0 & 1 \\ \frac{\lambda}{\alpha}(\lambda\tau+1) & 0 \end{bmatrix} \tag{2.15}$$

where $\phi = \phi_1$ and $\lambda' = \frac{\lambda}{\alpha}(\lambda\tau + 1)$ and $\zeta_0 = 0$. Applying the assumed boundary conditions gives the following distribution of eigenvalues and eigenfunctions:

1. $\phi_{1,k}(\zeta) = a_k \sin(\pi k\zeta), \phi_{2,k}(\zeta) = a_k\lambda_k \sin(\pi k\zeta)$ and $\lambda_k = \frac{-1}{2\tau} \pm \sqrt{\frac{1}{4\tau^2} - \frac{\alpha\pi^2k^2}{\tau}}$, for $k > 0$

2. $\phi_{1,k}(\zeta) = a_k \cos\left(\frac{2k+1}{2}\pi\zeta\right), \phi_{2,k}(\zeta) = a_k\lambda_k \cos\left(\frac{2k+1}{2}\pi\zeta\right)$ and $\lambda_k = \frac{-1}{2\tau} \pm \sqrt{\frac{1}{4\tau^2} - \frac{\alpha\pi^2}{\tau}\left(\frac{2k+1}{2}\right)^2}$, for $k \geq 0$

3. $\phi_{1,k}(\zeta) = a_k \cos(\pi k\zeta), \phi_{1,0}(\zeta) = a_0, \phi_{2,k}(\zeta) = a_k\lambda_k \sin(\pi k\zeta), \phi_{2,0} = a_0\lambda_k$ and $\lambda_k = \frac{-1}{2\tau} \pm \sqrt{\frac{1}{4\tau^2} - \frac{\alpha\pi^2k^2}{\tau}}$, for $k \geq 0$

Remark 2.1 *: The solution of the eigenvalues problem of the hyperbolic PDEs results in a different set of eigenvalues when compared to the parabolic equation (shown in Table 2.1). For the parabolic case, it can be seen that the dynamics of the heat transport problem contains only negative real eigenvalues that are distributed apart of each other in a quadratic sense, reflecting the exponential attenuated dynamical response of the system (the response does not have oscillatory behavior). The second order hyperbolic PDE does not have an infinite set of real eigenvalues as shown above (for the parabolic equation, $\lambda_k \to -\infty$ as $k \to \infty$), in fact, for all solutions, the whole set of eigenvalues are constrained in a region where $\frac{-1}{\tau} \leq Re(\lambda_n) \leq 0$, as it is shown in Figure 2.1, for $\alpha = 0.25$ and $\tau = 0.01$. Furthermore, the complex eigenvalues of the hyperbolic equation will have the same real part $(-1/2\tau)$. This infinity number of eigenvalues with the same real part is manifested in the hyperbolic PDE modeling as the finite speed of propagation. For the same value of α, the hyperbolic (λ_H) and parabolic eigenvalues (λ_P) are, for the heat diffusion in a resting body, related by:*

$$\lambda_H(\lambda_H\tau + 1) = \lambda_P \tag{2.16}$$

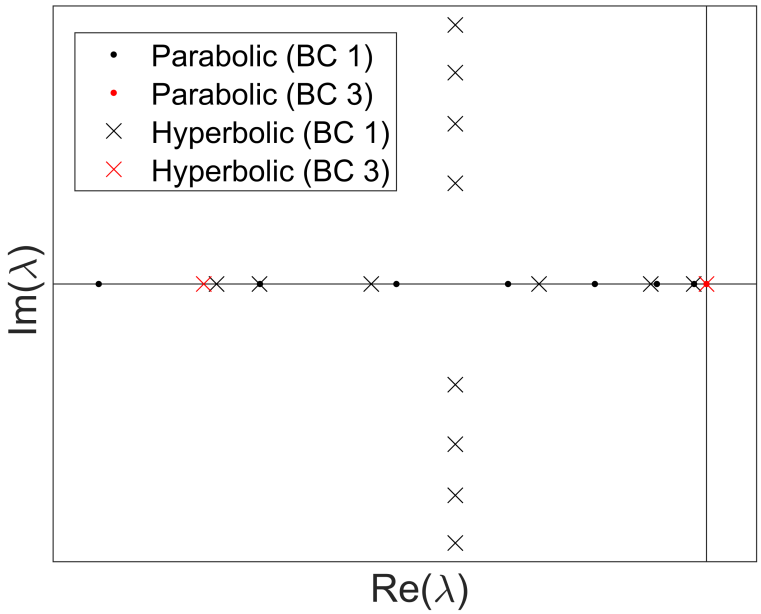

Figure 2.1: Parabolic (circle) and hyperbolic (cross) PDEs' eigenvalues distribution for BC 1 (Eq.2.8) and BC 3 (Eq.2.10). The red values are added for the third set of boundary condition.

Limit of the approximation

As the assumption that $\tau \to 0$ was used to transform the modeling setting from hyperbolic to parabolic PDE, one can also expect an upper limit for τ, at which the hyperbolic equation will not be physically meaningful. By examining the solutions for the eigenvalue problem, there is a value for $\tau > \tau_{max}$ at which all eigenvalues of the hyperbolic equation will be complex eigenvalues with a common real part but different imaginary parts:

1. $\frac{1}{4\tau_{max}^2} - \frac{\alpha\pi^2}{\tau_{max}} < 0 \implies \tau_{max} = \frac{1}{4\pi^2\alpha}$
2. $\frac{1}{4\tau_{max}^2} - \frac{\alpha\pi^2}{\tau_{max}} \left(\frac{1}{2}\right)^2 < 0 \implies \tau_{max} = \frac{1}{\pi^2\alpha}$
3. $\frac{1}{4\tau_{max}^2} - \frac{\alpha\pi^2}{\tau_{max}} < 0 \implies \tau_{max} = \frac{1}{4\pi^2\alpha}$

Thus, for cases 1 and 2, the system will present only complex eigenvalues if $\tau > \tau_{max}$. Case 3 will always have 2 real eigenvalues $\lambda_{0,1} = 0, \lambda_{0,2} = 1/\tau$, but all others will be complex if $\tau > \tau_{max}$. Thus, for $\tau > \tau_{max}$, the eigenvalues distributions predict a response of the system with attenuating oscillations, which might not have physical meaning. However, the finite speed, associated with the multiplicity of eigenvalues with the same real part, is still present.

2.2.3 Adjoint operators and the orthonormal basis

In the next section, the open-form analytical solutions of the parabolic and hyperbolic equations are developed. The motivation for this analysis stems from the need to provide an analytic solution for the unforced system dynamics evolution. To obtain these analytic solutions, we first derive the adjoint of the operators, which is used to define an orthonormal base and is then employed in the analytical solution. To find the adjoint operator, the general definition of inner product is used:

$$\langle Ax, y\rangle_Y = \langle x, A^*y\rangle_X \tag{2.17}$$

where $x \in X$, $y \in Y$, $A : X \to Y$, $A^* : Y \to X$, and $\langle\cdot,\cdot\rangle_Y$, $\langle\cdot,\cdot\rangle_X$ are the inner products.

Next, the eigenvalue problem of the adjoint operator is considered, as its eigenfunctions will build the orthonormal base used in the solution. As it can be noticed from Table 2.1, for all boundary conditions and the adjoint operator defined for the parabolic PDE, $A = A^*$ and $D(A) = D(A^*)$. Thus, the operator is self-adjoint, which implies a spatial symmetry of the dynamics. As the parabolic operator is self-adjoint the solution of the eigenvalue problem for A^* will give the same result as A, thus $\psi(\zeta) = \phi(\zeta)$, where $\psi(\zeta)$ is the eigenfunction of the adjoint operator. The orthonormal basis can be constructed with $\phi(\zeta)$ and $\psi(\zeta)$, such that:

$$\langle \phi_i(\zeta), \psi_j(\zeta) \rangle = \delta_{ij} = \begin{cases} 0, \text{ if } i \neq j \\ 1, \text{ if } i = j \end{cases} \tag{2.18}$$

and with the solutions of the eigenvalue problem for the different boundary conditions, it is possible to define a_k such that the above condition is true. For the hyperbolic PDE, the operator defined in 2.12, the following is obtained:

$$\begin{aligned} \left\langle A \begin{bmatrix} x_1 \\ x_2 \end{bmatrix}, \begin{bmatrix} y_1 \\ y_2 \end{bmatrix} \right\rangle_Y = \int_0^1 \begin{bmatrix} x_2 \\ \frac{\alpha}{\tau}\partial_{\zeta\zeta} x_1 - \frac{x_2}{\tau} \end{bmatrix}^T \begin{bmatrix} y_1 \\ y_2 \end{bmatrix} d\zeta = \\ \int_0^1 \begin{bmatrix} x_1 \\ x_2 \end{bmatrix}^T A^* \begin{bmatrix} y_1 \\ y_2 \end{bmatrix} d\zeta = \langle x, A^* y \rangle_X \end{aligned} \tag{2.19}$$

which gives the following adjoint operator ($A^* = A^T$ in Eq. 2.12):

$$A^* = \begin{bmatrix} 0 & \frac{\alpha}{\tau}\partial_{\zeta\zeta} \\ 1 & \dfrac{-1}{\tau} \end{bmatrix} \tag{2.20}$$

with the following boundary conditions:

1. $\begin{cases} y_2(0) = 0 \\ y_2(1) = 0 \end{cases}$
2. $\begin{cases} \partial_\zeta y_2(0) = 0 \\ y_2(1) = 0 \end{cases}$
3. $\begin{cases} \partial_\zeta y_2(0) = 0 \\ \partial_\zeta y_2(1) = 0 \end{cases}$

As $A^* \neq A$, the operator of the hyperbolic PDE is not self-adjoint, thus, the eigenvalue problem needs to be solved to find the eigenfunctions of the adjoint

operator. The eigenvalue problem $A^*\psi = \lambda\psi$ has the same characteristic equation as A, thus, the same eigenvalues. Its eigenfunctions, however, are given by:

$$\begin{cases} \lambda\psi_1 = \partial_{\zeta\zeta}\psi_2 \\ \lambda\psi_2 = \psi_1 - \frac{\psi_2}{\tau} \end{cases} \implies \begin{cases} \psi_1 = \frac{1+\lambda\tau}{\tau}\psi_2 \\ \psi_2 = a\mathrm{e}^{\sqrt{\lambda'}\zeta} + b\mathrm{e}^{-\sqrt{\lambda'}\zeta} \end{cases} \tag{2.21}$$

where: $\lambda' = \frac{\lambda(1+\lambda\tau)}{\tau}$ and a and b are found using the boundary conditions defined above, which leads to the following solution:

1. $\psi_{1,k}(\zeta) = a_k^* \frac{1+\lambda_k\tau}{\tau}\sin(\pi k\zeta), \psi_{2,k}(\zeta) = a_k^*\sin(\pi k\zeta)$, with $a_k^* = a_k = \sqrt{\frac{2\tau}{1+2\tau\lambda_k}}$, for $k > 0$
2. $\psi_{1,k}(\zeta) = a_k^* \frac{1+\lambda_k\tau}{\tau}\cos\left(\frac{2k+1}{2}\pi\zeta\right), \psi_{2,k}(\zeta) = a_k\cos\left(\frac{2k+1}{2}\pi\zeta\right)$, with $a_k^* = a_k = \sqrt{\frac{2\tau}{1+2\tau\lambda_k}}$, for $k \geq 0$
3. $\psi_{1,k}(\zeta) = a_k^* \frac{1+\lambda_k\tau}{\tau}\cos(\pi k\zeta), \psi_{1,0}(\zeta) = \frac{1+\lambda_k\tau}{\tau}a_0^*, \psi_{2,k}(\zeta) = a_k^*\cos(\pi k\zeta)$, $\psi_{2,0} = a_0^*$, with $a_k^* = a_k = \sqrt{\frac{2\tau}{1+2\tau\lambda_k}}$ for $k \geq 0$

where the condition $a_k^* = a_k$ was assumed such that $\langle\phi_i(\zeta), \psi_j(\zeta)\rangle = \delta_{ij}$ and ϕ_i, ψ_j form a biorthonormal basis of the hyperbolic PDE.

2.2.4 Analytic Solutions

The analytic solutions of the PDEs are obtained in this section using the method of separation of variables. In this method, the solution $T(\zeta, t)$ is assumed to be a product of a spatial function $Z(\zeta)$ and a temporal function $\Theta(t)$, i.e., $T(\zeta) = Z(\zeta)\Theta(t)$. As before, the solution of the parabolic PDE will not be shown in detail and is presented in Table 2.1. For the hyperbolic PDE, substituting $T(\zeta, t)$ in Eq. 2.7 and dividing both sides by $Z(\zeta)\Theta(t)$ leads to:

$$\tau\frac{d^2\Theta(t)}{dt^2}\frac{1}{\Theta(t)} - \frac{d\Theta(t)}{dt}\frac{1}{\Theta(t)} = \alpha\frac{d^2Z(\zeta)}{d\zeta^2}\frac{1}{Z(\zeta)} = c \tag{2.22}$$

where c is a constant that does not depend on time or space. This gives following ODEs:

$$\begin{cases} \frac{d^2Z(\zeta)}{d\zeta^2} = \frac{c}{\alpha}Z(\zeta) \\ \tau\frac{d^2\Theta(t)}{dt^2} + \frac{d\Theta(t)}{dt} = c\Theta(t) \end{cases} \tag{2.23}$$

The general solution of the ODE for $Z(\zeta)$ is $Z(\zeta) = a\mathrm{e}^{\sqrt{\frac{c}{\alpha}}\zeta} + b\mathrm{e}^{-\sqrt{\frac{c}{\alpha}}\zeta}$, where the coefficients are calculated using the boundary conditions:

1. $Z_k(\zeta) = a_k \sin(\pi k \zeta)$ with: $c_k = -\alpha \pi^2 k^2$, for $k > 0$

2. $Z_k(\zeta) = a_k \cos\left[\pi \left(k + \frac{1}{2}\right) \zeta\right]$ with: $c_k = -\alpha \pi^2 \left(\frac{2k+1}{2}\right)^2$, for $k \geq 0$

3. $Z_k(\zeta) = a_k \sin(\pi k \zeta)$ with: $c_k = -\alpha \pi^2 k^2$, for $k \geq 0$

Notice that c_k is not the same as the system eigenvalues, as the ODE for the time-dependent part is a second order equation and it can be written as a system of first-order ODEs:

$$\frac{d}{dt}\begin{bmatrix} \Theta_k(t) \\ \frac{d\Theta_k(t)}{dt} \end{bmatrix} = \begin{bmatrix} 0 & 1 \\ \frac{c_k}{\tau} & \frac{-1}{\tau} \end{bmatrix} \begin{bmatrix} \Theta_k(t) \\ \frac{d\Theta_k(t)}{dt} \end{bmatrix} \tag{2.24}$$

The solution is given by:

$$\begin{bmatrix} \Theta_k(t) \\ \frac{d\Theta_k(t)}{dt} \end{bmatrix} =$$

$$\underbrace{\begin{bmatrix} \frac{e^{\lambda_k^- t} - e^{\lambda_k^+ t} + \left(e^{\lambda_k^+ t} + e^{\lambda_k^- t}\right)\sqrt{4c_k\tau+1}}{2\sqrt{4c_k\tau+1}} & \frac{e^{\lambda_k^+ t} - e^{\lambda_k^- t} + \left(e^{\lambda_k^- t} - e^{\lambda_k^+ t}\right)(4c_k\tau+1)}{4c_k\sqrt{4c_k\tau+1}} \\ \frac{c_k\left(e^{\lambda_k^- t} - e^{\lambda_k^+ t}\right)}{\sqrt{4c_k\tau+1}} & \frac{e^{\lambda_k^+ t} - e^{\lambda_k^- t} + \left(e^{\lambda_k^- t} + e^{\lambda_k^+ t}\right)\sqrt{4c_k\tau+1}}{2\sqrt{4c_k\tau+1}} \end{bmatrix}}_{\Lambda_k(t)} \begin{bmatrix} \Theta_k(0) \\ \frac{d\Theta_k(0)}{dt} \end{bmatrix} \tag{2.25}$$

where λ_k^+ and λ_k^- are the two possible solutions of λ_k (λ_k is the solution of a second order polynomial - the same shown in section 2.2.2). Using the principle of superposition, the general solution of the hyperbolic PDE can be written as:

$$\begin{bmatrix} T(\zeta,t) \\ \frac{dT(\zeta,t)}{dt} \end{bmatrix} = \sum_k^{\infty} \Lambda_k(t) \begin{bmatrix} A_k \\ B_k \end{bmatrix} Z_k \tag{2.26}$$

where $\Lambda_k(t)$ can be simplified to:

$$\Lambda_k(t) = \begin{bmatrix} \Lambda_k^{1,1}(t) & \Lambda_k^{1,2}(t) \\ \Lambda_k^{2,1}(t) & \Lambda_k^{2,2}(t) \end{bmatrix} \tag{2.27}$$

with:

$$\begin{aligned}
\Lambda_k^{1,1}(t) &= e^{-\frac{t}{2\tau}}\left[\cosh\left(\frac{t}{\tau}\sqrt{c_k\tau + \frac{1}{4}}\right) + \frac{\sinh\left(\frac{t}{\tau}\sqrt{c_k\tau+\frac{1}{4}}\right)}{2\sqrt{c_k\tau+\frac{1}{4}}}\right] \\
\Lambda_k^{1,2}(t) &= \frac{2\tau e^{-\frac{t}{2\tau}}\sinh\left(\frac{t}{2\tau}\sqrt{c_k\tau+\frac{1}{4}}\right)}{\sqrt{4c_k\tau+1}} \\
\Lambda_k^{2,1}(t) &= \frac{2c_k e^{-\frac{t}{2\tau}}\sinh\left(\frac{t}{2\tau}\sqrt{c_k\tau+\frac{1}{4}}\right)}{\sqrt{4c_k\tau+1}} \\
\Lambda_k^{2,2}(t) &= e^{-\frac{t}{2\tau}}\left[\cosh\left(\frac{t}{\tau}\sqrt{c_k\tau + \frac{1}{4}}\right) - \frac{\sinh\left(\frac{t}{\tau}\sqrt{c_k\tau+\frac{1}{4}}\right)}{2\sqrt{c_k\tau+\frac{1}{4}}}\right]
\end{aligned} \tag{2.28}$$

To find the coefficients A_k and B_k, the initial conditions and the orthogonality of Z_k are used. For each Z_k we can find a Z_k^* such that $\langle Z_k, Z_k^* \rangle = \delta_{ij}$:

1. $Z_k^*(\zeta) = a_k^* \sin(\pi k \zeta)$ with: $a_k = a_k^* = \sqrt{2}$, for $k > 0$
2. $Z_k^*(\zeta) = a_k^* \cos\left[\pi \left(k + \frac{1}{2}\right) \zeta\right]$ with: $a_k = a_k^* = \sqrt{2}$, for $k \geq 0$
3. $Z_k^*(\zeta) = a_k^* \cos(\pi k \zeta)$ with: $a_k = a_k^* = \sqrt{2}$, for $k > 0$ and $a_0 = a_0^* = 1$

Thus, if the inner product with respect to $Z_k^*(\zeta)$ is taken in both sides of the solution at $t = 0$ (thus $\Lambda(0) = I$), the following is obtained:

$$\begin{array}{l} \langle T(\zeta,0), Z_m^*(\zeta)\rangle = \sum_k^\infty A_k \langle Z_k(\zeta), Z_m^*(\zeta)\rangle \implies A_k = \langle T(\zeta,0), Z_k^*(\zeta)\rangle \\ \langle \frac{dT(\zeta,0)}{dt}, Z_m^*(\zeta)\rangle = \sum_k^\infty B_k \langle Z_k(\zeta), Z_m^*(\zeta)\rangle \implies B_k = \langle \frac{dT(\zeta,0)}{dt}, Z_k^*(\zeta)\rangle \end{array} \tag{2.29}$$

where the fact that $\left\langle Z_i(\zeta), Z_j^*(\zeta) \right\rangle = \delta_{ij}$ was used to simplify the summation. Thus, given the initial condition, the solution of the hyperbolic PDE can be written as:

$$\begin{array}{l} T(\zeta,t) = \sum_k^\infty \left[\begin{array}{cc} \Lambda_k^{1,1}(t) & \Lambda_k^{1,2}(t) \end{array} \right] \left[\begin{array}{c} \langle T(\zeta,0), Z_k^*(\zeta)\rangle \\ \langle \frac{dT(\zeta,0)}{dt}, Z_k^*(\zeta)\rangle \end{array} \right] Z_k = \\ \int_0^1 \sum_k^\infty \left[\begin{array}{cc} Z_k(\zeta)\Lambda_k^{1,1}(t) Z_k^*(\eta) & Z_k(\zeta)\Lambda_k^{1,2}(t) Z_k^*(\eta) \end{array} \right] \left[\begin{array}{c} T(\zeta,0) \\ dT(\zeta,0) \end{array} \right] \end{array} \tag{2.30}$$

2.2.5 Simulation Results for the Heat Transport

In this section, the simulation results for the heat transport are discussed. First, as it is not possible to realize an infinite number of eigenvalues in the solution of the PDEs, the high fidelity approximation is considered and the approximation error of the initial conditions is analyzed. One thousand eigenvalues (and eigenfunctions) were used in the simulation, and the integrals were calculated using the trapezoidal rule with one thousand discretization points in space. The norm of the error in the approximation of the initial condition is defined as:

$$||e(0)|| = ||x(0) - x_A(0)|| = \sqrt{\int_0^L \left[x(\zeta,0) - x_A(\zeta,0)\right]^2 d\zeta} \tag{2.31}$$

where $x(0)$ are the chosen initial conditions (just $T(\zeta, 0)$ for the parabolic; $T(\zeta, 0)$ and $\partial_t T(\zeta, 0)$ for the hyperbolic) and $x_A(0)$ is the approximation (given by the truncation at $t = 0$ of the sum for the parabolic PDE shown in Table 2.1 and Eq. 2.30 for the hyperbolic). Table 2.2 shows the values of the initial errors and the initial conditions chosen. As the initial velocity is considered to be zero for the hyperbolic PDE, the approximation error depends only on the initial condition for T, which was set as the same function for the parabolic and hyperbolic PDEs.

Table 2.2: Initial conditions and initial errors in the approximation

PDE Type	**Initial condition**	**Initial Error**
Parabolic (B.C. 1)	$T(0) = -\zeta^2 + \zeta$	1.6912e-14
Parabolic (B.C. 2)	$T(0) = -\zeta^2 + 1$	4.4495e-14
Parabolic (B.C. 3)	$T(0) = -2\zeta^3 + 3\zeta^2$	6.3790e-14
Hyperbolic (B.C. 1)	$T(0) = -\zeta^2 + \zeta$	1.6912e-14
	$\partial_t T(0) = 0$	
Hyperbolic (B.C. 2)	$T(0) = -\zeta^2 + 1$	4.4495e-14
	$\partial_t T(0) = 0$	
Hyperbolic (B.C. 3)	$T(0) = -2\zeta^3 + 3\zeta^2$	6.3790e-14
	$\partial_t T(0) = 0$	

The simulation results are presented for arbitrary values of $\alpha = 1$ and $\tau = 0.01$. The spatial profiles of $T(\zeta, t)$ and $\partial_t T(\zeta, t)$ for the parabolic PDE are shown in Figure 2.2. Due to the initial conditions, it is easy to see that $\partial_t T(\zeta, 0)$ is going to be different than zero for all cases and it is at its maximum at the beginning. As shown in the previous sections, all the boundary conditions used result in stable systems.

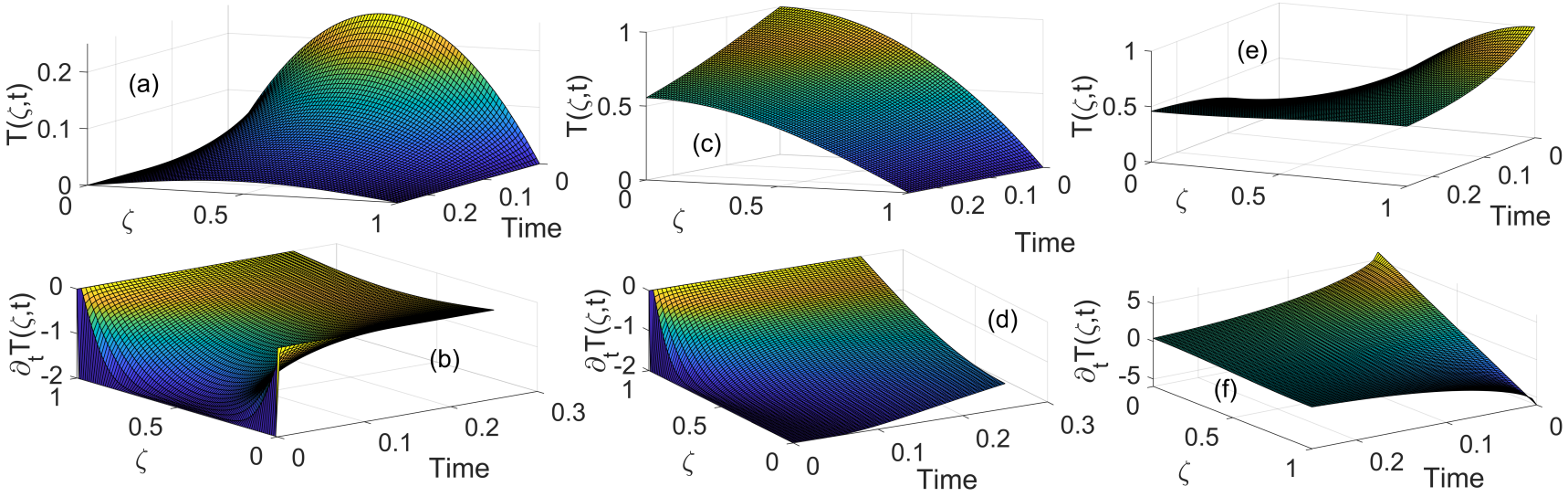

Figure 2.2: Simulation results for the Parabolic PDE, with initial conditions given in Table 2.2: (a) and (b) $T(\zeta, t)$ and $\partial_t T(\zeta, t)$ for B.C. 1; (c) and (d) $T(\zeta, t)$ and $\partial_t T(\zeta, t)$ for B.C. 2; (e) and (f) $T(\zeta, t)$ and $\partial_t T(\zeta, t)$ for B.C. 3.

The same results are shown for the hyperbolic PDE in Figure 2.3. It is possible to see that the velocities profiles, i.e., the rates of temperature change, are completely different from the results presented in the parabolic PDE case. The system takes some time to reach the maximum velocity, not instantaneously as was the case for the parabolic. The velocities profiles are initially different, as the parabolic presents a smooth profile, while the hyperbolic presents sudden changes. As expected, the PDEs converge to the same steady-state profile, although the apparent difference is seen in the initial dynamic response. This difference also shown in Cassol et al. [59], which showed the distinct slope in the profiles of the hyperbolic and parabolic PDEs.

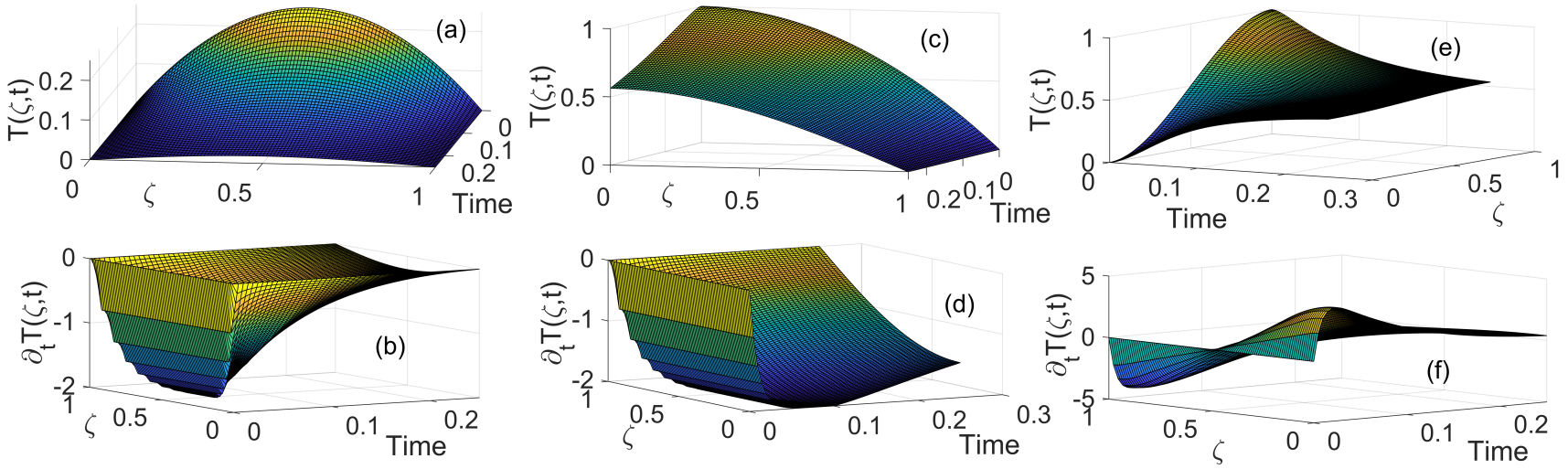

Figure 2.3: Simulation results for the Hyperbolic PDE, with initial conditions given in Table 2.2: (a) and (b) $T(\zeta, t)$ and $\partial_t T(\zeta, t)$ for B.C. 1; (c) and (d) $T(\zeta, t)$ and $\partial_t T(\zeta, t)$ for B.C. 2; (e) and (f) $T(\zeta, t)$ and $\partial_t T(\zeta, t)$ for B.C. 3.

Next, a comparison for different initial conditions for the $\partial_t T(\zeta, t)$, as one might argue that the previous results show a distinguished difference between the hyperbolic and parabolic because the initial condition was $\partial_t T(\zeta, 0) = 0$. The system responses, only considering the second set of boundary conditions, for different initial conditions of $\partial_t T(\zeta, 0)$, but with the same $T(\zeta, 0)$, are displayed in Figure 2.4. The initial conditions used and the initial error are shown in Table 2.3.

Table 2.3: Initial conditions and initial errors in the approximation

PDE Type	**Initial conditions**	**Initial Error**
Hyperbolic (B.C. 2)	1: $T(0) = -\zeta^2 + 1$ & $\partial_t T(0) = 0$	4.4495e-14
	2: $T(0) = -\zeta^2 + 1$ & $\partial_t T(0) = \cos(\frac{\pi}{2}\zeta)$	6.0266e-14
	3: $T(0) = -\zeta^2 + 1$ & $\partial_t T(0) = 2(\zeta^2 - 1)$	9.9493e-14

The responses show that, as $\partial_t T(\zeta, t)$ are initially different, the profiles of $T(\zeta, t > 0)$ are distinct at the same time, as expected. For $t > 0$, the difference between the values of $\partial_t T(\zeta, t)$ starts to decrease and the rate of change converge to the same spatial profile. Thus, the rate of change of the hyperbolic PDE will be the same after some time, independent of the initial condition used for $\partial_t T(\zeta, 0)$.

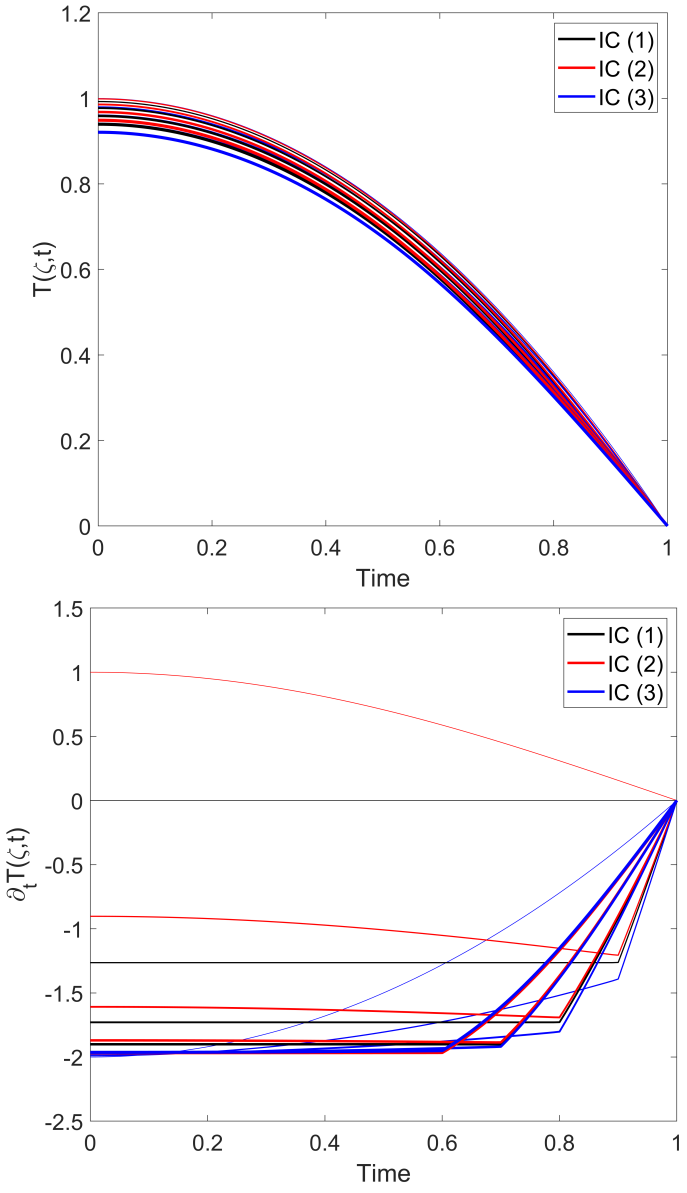

Figure 2.4: Comparison of the simulation for the Hyperbolic PDE with B.C. 2 and three different initial velocities (time increases with the line width).

One last comparison is made considering the hyperbolic PDE with different values of τ, as shown in Figure 2.5. Three different values are considered ($\tau = \{0.01, 0.1, 1\}$) and the same initial condition ($\partial_t T(0) = 0$) is used. The responses are distinct from each other, and, as expected, the higher the value of τ, the slower is the system's response. But, a higher value of τ may also lead to a physically unfeasible response, as discussed in Section 2.2.2 and shown in Figure 2.5 (c) and (d). In this figure, the responses are shown at $\zeta = 0.5$ and the different values of τ are considered. The maximum value for which the approximation should hold is $\tau_{max} \approx 0.0253$. For $\tau = 0.01$ the response exponentially converges to the steady-state without showing oscillations; $\tau = 0.1$ produces a response with oscillations and these oscillations become greater for $\tau = 1$. This type of behavior is not expected in a finite slab.

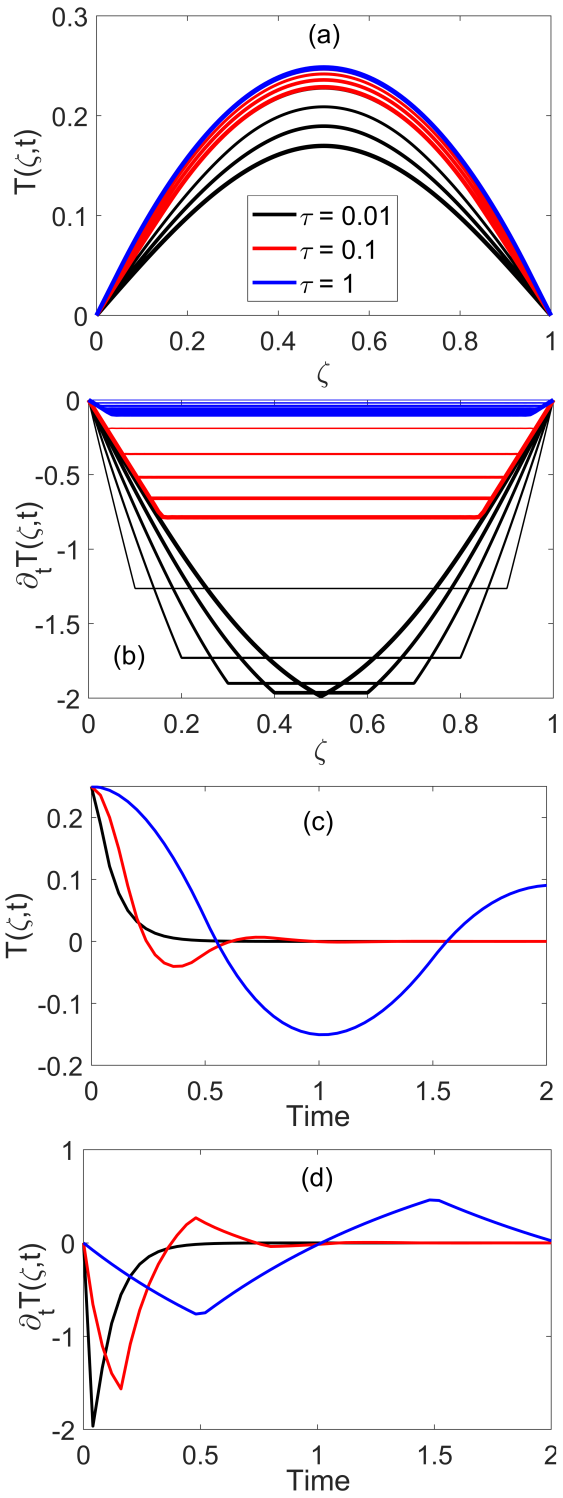

Figure 2.5: Comparison of the simulation results for the Hyperbolic PDE with B.C. 1 and three different values of τ: (a) Spatial profile for $T(\zeta, t)$ at different times; (b) Spatial profile for$\partial_t T(\zeta, t)$ at different times. Time increases with the line width. (c) Response of $T(\zeta = 0.5, t)$; (d) Response of $\partial_t T(\zeta = 0.5, t)$.

2.3 The Axial Tubular Reactor

Considering a fluid, with a constant density and diffusivity (D), moving inside a tube with velocity (v). The tube has a constant cross-sectional area and a first-order reaction happens inside of it. The fluid's velocity is not high enough to neglect the diffusive effects. If the radial and angular diffusion can be neglected, the mass balance for the system leads to the following equation:

$$\frac{\partial C}{\partial t} = -\partial_\zeta F + r = -\partial_\zeta F - kC \tag{2.32}$$

where F is the mass flux and r is the reaction term (in this case a first-order reaction with constant specific reaction rate). The mass flux can be given by the sum of the diffusive term (Fick's law) and advective term. If only the axial effects are considered, the flux is defined as:

$$F = -D\partial_\zeta C + vC \tag{2.33}$$

This leads to the following parabolic PDE:

$$\frac{\partial C}{\partial t} = D\partial_{\zeta\zeta} C - v\partial_\zeta C - kC \tag{2.34}$$

Fick's law does not consider any inertia, thus, similarly to the heat diffusion, it is possible to assume that a delay is present in the mass flux as well:

$$F = -D(1 - \tau\partial_t)\partial_\zeta C + vC \tag{2.35}$$

This leads to the following PDE:

$$\frac{\partial C}{\partial t} = D(1 - \tau\partial_t)\partial_{\zeta\zeta} C - v\partial_\zeta C - kC \tag{2.36}$$

If $\tau \to 0$, then $(1 - \tau\partial_t)^{-1} \approx (1 + \tau\partial_t)$, the equation becomes:

$$\tau\partial_{tt} C + \partial_t C = D\partial_{\zeta\zeta} C - v\partial_\zeta C - v\tau\partial_{\zeta t} C - kC - k\tau\partial_t C \tag{2.37}$$

Lastly, one could also argue that the delay is present in both diffusive and advective terms, leading to:

$$F = (1 - \tau\partial_t)(-D\partial_\zeta C + vC) \tag{2.38}$$

Substituting in the mass balance gives:

$$\frac{\partial C}{\partial t} = (1 - \tau\partial_t)\left[D\partial_{\zeta\zeta}C - v\partial_\zeta C\right] - kC \tag{2.39}$$

Using the approximation for $\tau \to 0$ gives the following second order hyperbolic PDE:

$$\tau\partial_{tt}C + \partial_t C = \alpha\partial_{\zeta\zeta}C - v\partial_\zeta C - kC - k\tau\partial_t C \tag{2.40}$$

Thus, the two different second-order PDEs take into account different physical assumptions. If it is considered that the delay on the particles only occur in their response to a concentration gradient, then the delayed diffusion PDE shown in Eq. 2.37 would be more appropriate. If the time-lag that happens until the particles start moving, as proposed by Cattaneo [42], also happens in the advective transport, then, the total flux is considered to have a delay and Eq. 2.40 represents this assumption better.

2.3.1 Boundary Conditions

Two types of boundary conditions are considered: closed vessels and open vessels [51], [60], as represented in Figure 2.6. An open condition means that dispersion occurs, while a closed condition does not take dispersion into account. Thus, for closed-closed vessels, represented on the top of Figure 2.6, there is no dispersion in concentration either upstream (right before the inlet of the reactor, at $\zeta = 0^-$) or downstream (right after the outlet, at $\zeta = L^+$). In an open-open vessel, represented on the bottom of Figure 2.6, the dispersion occurs both upstream and downstream. Thus, these are different possible sets of boundary conditions that can be achieved by assuring the continuity of the flux in the inlet and outlet:

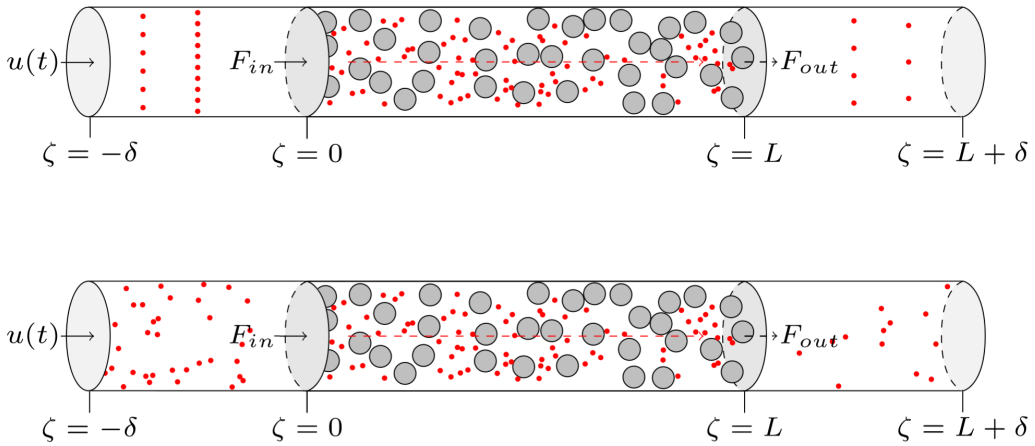

Figure 2.6: Tubular reactor representation: (top) Closed-Closed boundary condition; (bottom) Open-Open boundary conditions.

1. Closed-closed: No dispersion in the flux upstream and downstream, thus $F(0^-) = vC(0^-)$ and $F(L^+) = vC(L^+)$. Considering that the reaction just occurs inside the reactor, $C(L^+) = C(L^-)$, this leads to the following boundary conditions:

$$vC(0^-) = vC(0^+) - D\partial_\zeta C(0^+) \text{ and } \partial_\zeta C(L^-) = 0 \tag{2.41}$$

2. Open-Open: dispersion happens upstream and downstream, thus $F(0^-) = vC(0^-) - D\partial_\zeta C(0^-)$ and $F(L^+) = vC(L^+) - D\partial_\zeta C(L^+)$. For this case, the continuity of concentration is also considered, such that $C(0^-) = C(0^+)$ and $C(L^+) = C(L^-)$, leading to the following boundary conditions:

$$\partial_\zeta C(0^-) = \partial_\zeta C(0^+) \text{ and } \partial_\zeta C(L^-) = \partial_\zeta C(L^+) \tag{2.42}$$

If a delay is considered only in the diffusive term, the boundary conditions are going to change for the hyperbolic PDE:

1. Closed-closed:

$$vC(0^-) = vC(0^+) - D(1 - \tau\partial_t)\partial_\zeta C(0^+) \text{ and } \partial_\zeta C(L^-) = 0 \tag{2.43}$$

If $\tau \to 0$, the boundary condition becomes:

$$(1+\tau\partial_t)vC(0^-) = (1+\tau\partial_t)vC(0^+) - D\partial_\zeta C(0^+) \text{ and } \partial_\zeta C(L^-) = 0 \tag{2.44}$$

2. Open-Open: $F(0^-) = vC(0^-) - D(1-\tau\partial_t)\partial_\zeta C(0^-)$ and $F(L^+) = vC(L^+) - D(1-\tau\partial_t)\partial_\zeta C(L^+)$. Assuming continuity of concentration, the following boundary conditions are obtained:

$$\partial_\zeta C(0^-) = \partial_\zeta C(0^+) \text{ and } \partial_\zeta C(L^-) = \partial_\zeta C(L^+) \tag{2.45}$$

Therefore, by considering delay in the total flux, the boundary conditions become:

1. Closed-closed:

$$vC(0^-) = \left[vC(0^+) - D\partial_\zeta C(0^+)\right] \text{ and } \partial_\zeta C(L^-) = 0 \tag{2.46}$$

2. Open-Open: $F(0^-) = (1-\tau\partial_t)\left[vC(0^-) - D\partial_\zeta C(0^-)\right]$ and $F(L^+) = (1-\tau\partial_t)\left[vC(L^+) - D\partial_\zeta C(L^+)\right]$. With the continuity of concentration:

$$\partial_\zeta C(0^-) = \partial_\zeta C(0^+) \text{ and } \partial_\zeta C(L^-) = \partial_\zeta C(L^+) \tag{2.47}$$

2.3.2 Eigenvalue Problem

In this section, the difference in the PDEs' dynamics is examined by exploring the differences in their eigenvalues distributions, taking into account the closed and open boundary conditions defined in the previous section.

Closed-closed Boundary Conditions

1. Parabolic PDE: For the parabolic PDE, the operator A can be defined as:

$$Ax = D\partial_{\zeta\zeta}x - v\partial_\zeta x - kx = \lambda x \tag{2.48}$$

with the boundary conditions defined in Section 2.3.1. As defined previously, the eigenvalue problem is given as the solution of $A\phi = \lambda\phi$. Substituting the operator and solving for ϕ gives the following ODE:

$$\frac{d}{d\zeta}\begin{bmatrix}\phi \\ d_\zeta\phi\end{bmatrix} = \begin{bmatrix}0 & 1 \\ \frac{\lambda+k}{D} & \frac{v}{D}\end{bmatrix}\begin{bmatrix}\phi \\ d_\zeta\phi\end{bmatrix} \tag{2.49}$$

And its general solution is given by:

$$\begin{bmatrix} \phi \\ d_\zeta \phi \end{bmatrix} = \begin{bmatrix} f_{11}(\zeta,\lambda) & f_{12}(\zeta,\lambda) \\ f_{21}(\zeta,\lambda) & f_{22}(\zeta,\lambda) \end{bmatrix} \begin{bmatrix} \phi(\zeta_0) \\ d_\zeta \phi(\zeta_0) \end{bmatrix} \tag{2.50}$$

with:

$$\begin{aligned} f_{11}(\zeta,\lambda) &= \mathrm{e}^{\frac{b}{2}(\zeta-\zeta_0)} \left[\cosh\left((\zeta-\zeta_0)\sqrt{\tfrac{b^2}{4}+a} \right) - \frac{b}{2} \frac{\sinh\left((\zeta-\zeta_0)\sqrt{\frac{b^2}{4}+a} \right)}{\sqrt{\frac{b^2}{4}+a}} \right] \\ f_{12}(\zeta,\lambda) &= \frac{\mathrm{e}^{\frac{b}{2}(\zeta-\zeta_0)} \sinh\left((\zeta-\zeta_0)\sqrt{\frac{b^2}{4}+a} \right)}{\sqrt{\frac{b^2}{4}+a}} \\ f_{21}(\zeta,\lambda) &= a \frac{\mathrm{e}^{\frac{b}{2}(\zeta-\zeta_0)} \sinh\left((\zeta-\zeta_0)\sqrt{\frac{b^2}{4}+a} \right)}{\sqrt{\frac{b^2}{4}+a}} \\ f_{22}(\zeta,\lambda) &= \mathrm{e}^{\frac{b}{2}(\zeta-\zeta_0)} \left[\cosh\left((\zeta-\zeta_0)\sqrt{\tfrac{b^2}{4}+a} \right) + \frac{b}{2} \frac{\sinh\left((\zeta-\zeta_0)\sqrt{\frac{b^2}{4}+a} \right)}{\sqrt{\frac{b^2}{4}+a}} \right] \end{aligned} \tag{2.51}$$

And, in this case, $a = \frac{\lambda+k}{D}$, $b = \frac{v}{D}$ and $\zeta_0 = 0$. Using the closed-closed boundary conditions defined in Section 2.3.1 with zero inlet flux (i.e., $C(0^-) = 0$), the boundary conditions are $0 = v\phi(0) - D\partial_\zeta\phi(0)$ and $\partial_\zeta\phi(L) = 0$, resulting in the following equations:

$$\begin{cases} \partial_\zeta \phi(0) = \frac{v}{D}\phi(0) \\ f_{21}(L,\lambda)\phi(0) + f_{22}(L,\lambda)\partial_\zeta\phi(0) = 0 \\ \implies \phi(0)\left[f_{21}(L,\lambda) + \frac{v}{D} f_{22}(L,\lambda) \right] = 0 \end{cases} \tag{2.52}$$

If $\phi(0) = 0$, the eigenfunction will be the trivial solution, which is not desired. Thus, $f_{21}(L,\lambda) + \frac{v}{D} f_{22}(L,\lambda) = 0$ must hold. Replacing by the functions given in Eq. 2.51, the following equation is obtained:

$$\tanh\left(\frac{L}{D}\sqrt{\frac{v^2}{4} + D(k+\lambda)} \right) = \frac{-v\sqrt{\frac{v^2}{4} + D(k+\lambda)}}{\frac{v^2}{2} + D(k+\lambda)} \tag{2.53}$$

Differently from the eigenvalue problem considered in Section 2.2.2 for the heat equation, this is a transcendental equation and its analytical solution is not available. Thus, a numerical method is used to find λ_k.

2. Hyperbolic PDE - Delayed diffusion: For the hyperbolic PDE there are two different scenarios for the flux. First, the operator that considers the delay in the diffusive term is analyzed:

$$\begin{gathered}\frac{\partial}{\partial t}\begin{bmatrix} C(t) \\ \partial_t C(t) \end{bmatrix} = A \begin{bmatrix} C(t) \\ \partial_t C(t) \end{bmatrix} = \\ \begin{bmatrix} 0 & 1 \\ \frac{D\partial_{\zeta\zeta} - v\partial_\zeta - k}{\tau} & -v\partial_\zeta - k - \frac{1}{\tau} \end{bmatrix} \begin{bmatrix} C(t) \\ \partial_t C(t) \end{bmatrix}\end{gathered} \tag{2.54}$$

which is equivalent to write the PDE shown in Eq. 2.37 and its boundary conditions were shown in Section 2.3.1. Thus, the system of equations obtained is given by:

$$\begin{cases} \phi_2 = \lambda\phi_1 \\ \frac{D}{\tau}\partial_{\zeta\zeta}\phi_1 - \frac{v}{\tau}\partial_\zeta\phi_1 - \frac{k}{\tau}\phi_1 - \frac{1}{\tau}\phi_2 - v\partial_\zeta\phi_2 - k\phi_2 = \lambda\phi_2 \end{cases} \tag{2.55}$$

which can be written in the following form:

$$\frac{d}{d\zeta}\begin{bmatrix} \phi_1 \\ d_\zeta\phi_1 \end{bmatrix} = \begin{bmatrix} 0 & 1 \\ \frac{(k+\lambda)(1+\lambda\tau)}{D} & \frac{v(1+\lambda\tau)}{D} \end{bmatrix} \begin{bmatrix} \phi_1 \\ d_\zeta\phi_1 \end{bmatrix} \tag{2.56}$$

The solution of this system has the same structure as Eq. 2.50 with $a = \frac{(k+\lambda)(1+\lambda\tau)}{D}$, $b = \frac{v(1+\lambda\tau)}{D}$ and $\zeta_0 = 0$. Applying closed-closed boundary conditions and the relation $\phi_2 = \lambda\phi_1$, the following conditions need to be satisfied:

$$\begin{gathered}\begin{cases} \partial_\zeta\phi_1(0) = v\frac{1+\tau\lambda}{D}\phi_1(0) \\ f_{21}(L,\lambda)\phi_1(0) + f_{22}(L,\lambda)\partial_\zeta\phi_1(0) = 0 \end{cases} \\ \implies \phi_1(0)\left[f_{21}(L,\lambda) + v\tfrac{1+\tau\lambda}{D}f_{22}(L,\lambda)\right] = 0\end{gathered} \tag{2.57}$$

Thus, $f_{21}(L,\lambda) + v\frac{1+\tau\lambda}{D}f_{22}(L,\lambda) = 0$ is the characteristic equation for this case. Substituting the functions given in Eq. 2.51, the following equation is obtained:

$$\begin{gathered}\tanh\left(\tfrac{L}{D}\sqrt{\tfrac{v^2(1+\lambda\tau)^2}{4} + D(k+\lambda)(1+\lambda\tau)}\right) = \\ \frac{-v(1+\lambda\tau)\sqrt{\frac{v^2(1+\lambda\tau)^2}{4} + D(k+\lambda)(1+\lambda\tau)}}{\frac{v^2(1+\lambda\tau)^2}{2} + D(k+\lambda)(1+\lambda\tau)}\end{gathered} \tag{2.58}$$

which is solved with a numerical method. It can be seen that in the limit $\tau \to 0$ the above expression becomes the expression Eq.2.53 which is related to parabolic spectral characteristics.

3. Hyperbolic PDE - Delayed total flux: For the delay in the total flux, the operator is defined as:

$$\frac{\partial}{\partial t}\begin{bmatrix} C(t) \\ \partial_t C(t) \end{bmatrix} = A\begin{bmatrix} C(t) \\ \partial_t C(t) \end{bmatrix} = \begin{bmatrix} 0 & 1 \\ \frac{D\partial_{\zeta\zeta} - v\partial_\zeta - k}{\tau} & -k - \frac{1}{\tau} \end{bmatrix}\begin{bmatrix} C(t) \\ \partial_t C(t) \end{bmatrix} \tag{2.59}$$

which is equivalent to writing the PDE shown in Eq. 2.40, with boundary conditions presented in Section 2.3.1. The following system is obtained from the eigenvalue problem:

$$\begin{cases} \phi_2 = \lambda\phi_1 \\ \frac{D}{\tau}\partial_{\zeta\zeta}\phi_1 - \frac{v}{\tau}\partial_\zeta\phi_1 - \frac{k}{\tau}\phi_1 - \frac{1}{\tau}\phi_2 - k\phi_2 = \lambda\phi_2 \end{cases} \tag{2.60}$$

resulting in:

$$\frac{d}{d\zeta}\begin{bmatrix} \phi_1 \\ d_\zeta\phi_1 \end{bmatrix} = \begin{bmatrix} 0 & 1 \\ \frac{(k+\lambda)(1+\lambda\tau)}{D} & \frac{v}{D} \end{bmatrix}\begin{bmatrix} \phi_1 \\ d_\zeta\phi_1 \end{bmatrix} \tag{2.61}$$

The solution has the same structure as Eq. 2.50 with $a = \frac{(k+\lambda)(1+\lambda\tau)}{D}$, $b = \frac{v}{D}$ and $\zeta_0 = 0$. Applying the boundary conditions results in the condition below:

$$\begin{cases} \partial_\zeta\phi(0) = \frac{v}{D}\phi(0) \\ f_{21}(L,\lambda)\phi(0) + f_{22}(L,\lambda)\partial_\zeta\phi(0) = 0 \end{cases} \Longrightarrow \tag{2.62}$$
$$\phi(0)\left[f_{21}(L,\lambda) + \frac{v}{D}f_{22}(L,\lambda)\right] = 0$$

Setting aside the trivial solution, the characteristic equation for this operator is given by $f_{21}(L,\lambda) + \frac{v}{D}f_{22}(L,\lambda) = 0$, which leads to:

$$\tanh\left(\frac{L}{D}\sqrt{\frac{v^2}{4} + D(k+\lambda)(1+\lambda\tau)}\right) = \frac{-v\sqrt{\frac{v^2}{4} + D(k+\lambda)(1+\lambda\tau)}}{\frac{v^2}{2} + D(k+\lambda)(1+\lambda\tau)} \tag{2.63}$$

Remark 2.2 *Although this is a transcendental equation, a direct relation with the Eq. 2.53, obtained for the parabolic PDE, can be derived:*

$$\lambda_P = (k+\lambda_H)(1+\lambda_H\tau) \implies \lambda_H = \frac{-(1+k\tau) \pm \sqrt{(1+k\tau)^2 + 4\tau\lambda_P}}{2\tau} \tag{2.64}$$

where λ_P is the eigenvalue of the parabolic PDE and λ_H is the solution for the delay in the total flux.

The eigenvalues distributions for a set of parameters are shown in Figure 2.7, for $0.1 \leq v \leq 15$. The same behavior seen in the heat transport by conduction is observed in the case of reactor dynamics. The eigenvalues for the parabolic PDE are all placed apart in the quadratic manner at the real axis, while just a finite number of the eigenvalues of the hyperbolic PDE follow the same trend. These eigenvalues are placed at the real axis within a finite interval. As the velocity increases, it is expected that the eigenvalues are going to shift to the left side, as a plug-flow reactor (obtained when $\frac{v}{D} \to \infty$) would be inherently stable. Furthermore, an increase in the velocity also helps to discern the difference between the delayed diffusion and the delayed total flux. Although they both have a similar response to the increase in the velocity, the effects are different. For the total delayed flux (Figure 2.7 (c)), all the eigenvalues shifted from the real axis to the complex plane. For the delayed diffusive flux (Figure 2.7 (b)), the shift for the left side of the complex plane is more evident and the distance between the real eigenvalues decreases as v increases.

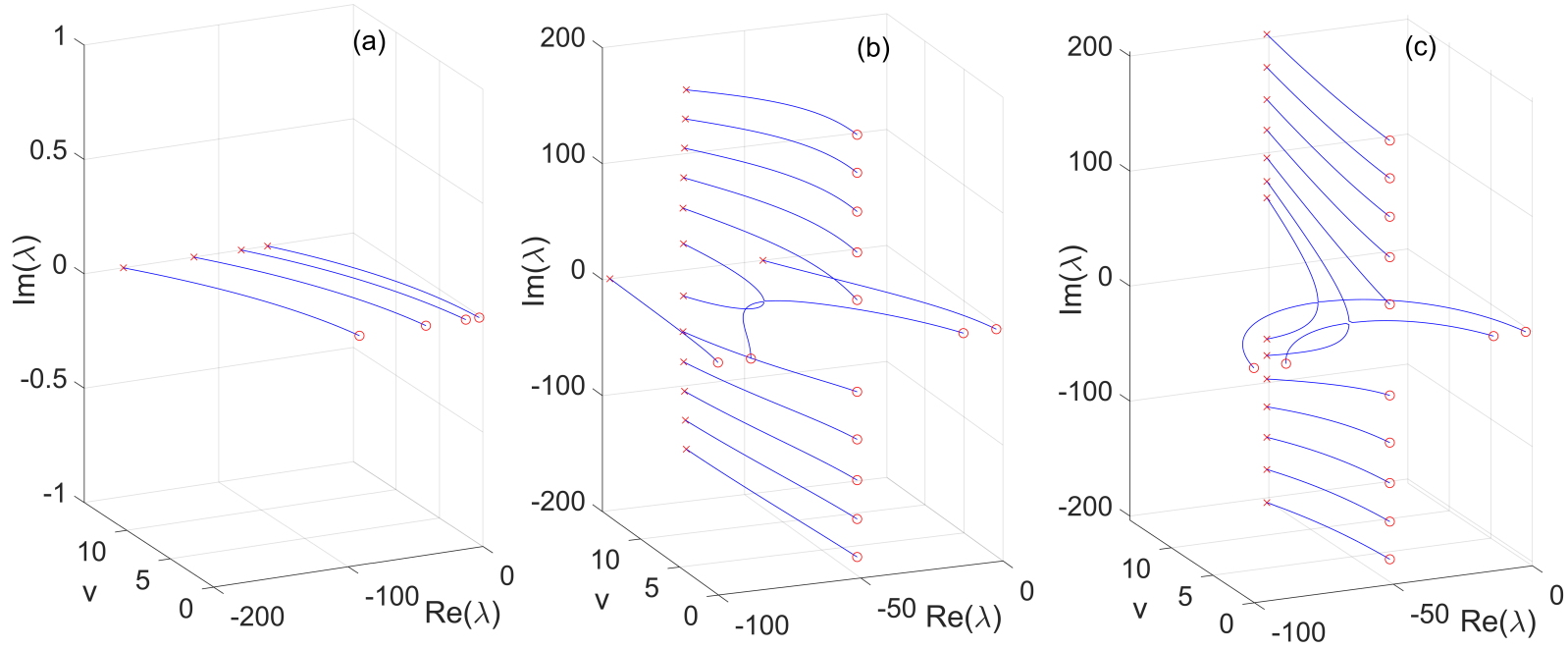

Figure 2.7: Tubular reactor eigenvalue distribution for Closed-Closed B.C. with $D = 1$, $k = 2$ and $\tau = 0.01$ for $0.1 \leq v \leq 15$: (a) Parabolic; (b) Hyperbolic (Delayed Diffusion); (c) Hyperbolic (Delayed Flux). $\circ$ represents the beginning of the line ($v = 0.1$) and $\times$ the end value ($v = 15$).

2.3.3 Simulation Results for the Closed-Closed Boundary Conditions

Lastly, the simulation results for the closed-closed boundary conditions are shown in Figure 2.8. For this simulation the initial conditions used were $T(\zeta, 0) = -3\zeta^2 + 6\zeta + 1$, with $v = 6$, $D = 1$, $k = 2$, $\tau = 0.01$ and $\partial_t T(\zeta, 0) = 0$ for the hyperbolic. Once more, the difference in the rate of change ($\partial_t T(\zeta, t)$) is clearly noticeable, as the rate for the parabolic PDE starts at its maximum at some points. The hyperbolic cases take some time to reach the same rate as the parabolic and the responses never get to the same magnitude when compared to the parabolic values. This behavior causes a delay in $T(\zeta, t)$ for the hyperbolic PDE, as expected.

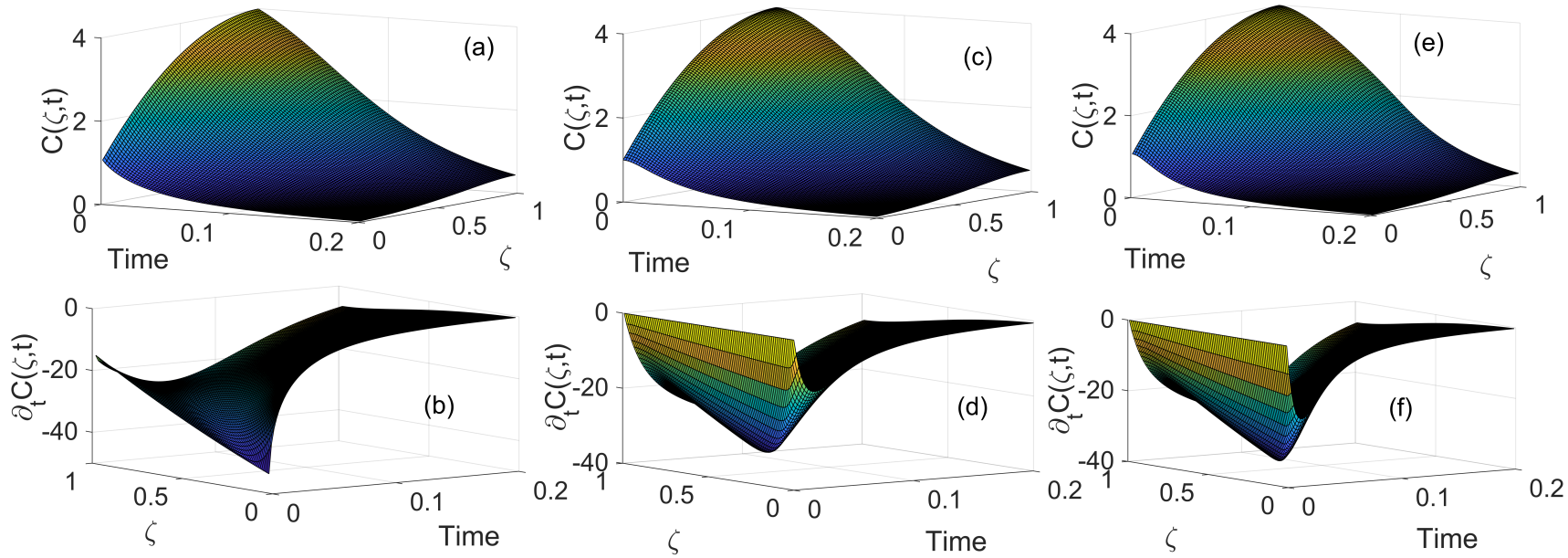

Figure 2.8: Tubular reactor simulation results with Closed-Closed B.C. considering $v = 6$, $D = 1$, $k = 2$ and $\tau = 0.01$ for the hyperbolic PDE: (a) and (b) $C(\zeta, t)$ and $\partial_t C(\zeta, t)$ for Parabolic; (c) and (d) $C(\zeta, t)$ and $\partial_t C(\zeta, t)$ for Hyperbolic (delayed Diffusion); (e) and (f) $C(\zeta, t)$ and $\partial_t C(\zeta, t)$ for Hyperbolic (delayed total Flux).

Open-open Boundary Conditions:

Unlike the closed-closed boundary conditions, the open-open boundary conditions assume that the upstream and downstream flux will have a diffusive term as well, thus, the movement driven by the gradient of concentration is added to the front wave that is characteristic of the advective term. The boundary conditions for the rector generally assume continuity of the total flux and concentration in the beginning of the reactor (i.e., $F(0^-) = F(0^+)$ and $C(0^-) = C(0^+)$) and at the end of the reactor (i.e., $F(L^-) = F(L^+)$ and $C(L^-) = C(L^+)$). The total flux, as considered previously, is different for each type of PDE and the complete operator (represented by $\mathcal{A}$), that consider both the transport zones and the reaction zone, can be defined as:

$$\mathcal{A} = \begin{bmatrix} A_T & 0 & 0 \\ 0 & A & 0 \\ 0 & 0 & A_T \end{bmatrix} \tag{2.65}$$

where A_T is used to represent the transport happening upstream and downstream, such that $A_T = -\partial_\zeta F$. A is the operator for the reactions zone (i.e., $A = -\partial_\zeta F - r$) and can be one of the operators defined in Equation 2.48, 2.54 or 2.59.

1. Parabolic PDE: the flux for the parabolic is defined as $F = vC - D\partial_\zeta C$, thus $A_T C = D\partial_{\zeta\zeta} C - v\partial_\zeta C$ and $AC = D\partial_{\zeta\zeta} C - v\partial_\zeta C - kC$. A transport zone with length δ is considered before and after the reaction zone (one could consider two transport zones with different lengths, but, for the sake of simplicity, the same length is considered in this contribution). The eigenvalue problem is given by $\mathcal{A}\Phi = \lambda\Phi$ and besides the four boundary conditions already shown in Section 2.3.1, two more boundary conditions are necessary. It is assumed that there is no incoming flux at $\zeta = -\delta$, thus $F(-\delta) = vC(-\delta) - D\partial_\zeta C(-\delta) = 0$; and that at the end ($\zeta = L + \delta$) the concentration does not change further ($\partial_\zeta C(L + \delta) = 0$). Finally, the eigenfunctions will be the solution of the following differential equations:

$$\begin{cases} Dd_{\zeta\zeta}\phi_1 - vd_\zeta\phi_1 = \lambda\phi_1 \\ Dd_{\zeta\zeta}\phi_2 - vd_\zeta\phi_2 - k\phi_2 = \lambda\phi_2 \\ Dd_{\zeta\zeta}\phi_3 - vd_\zeta\phi_3 = \lambda\phi_3 \end{cases} \tag{2.66}$$

with the boundary conditions:

$$\begin{array}{ccc} v\phi_1(-\delta) - Dd_\zeta\phi_1(-\delta) = 0 & \phi_1(0) = \phi_2(0) & d_\zeta\phi_1(0) = d_\zeta\phi_2(0) \\ \phi_2(L) = \phi_3(L) & d_\zeta\phi_2(L) = d_\zeta\phi_3(L) & d_\zeta\phi_3(L+\delta) = 0 \end{array} \tag{2.67}$$

Each eigenfunction will have the same structure defined in Eq. 2.50, with $a = \frac{\lambda}{D}$, $b = \frac{v}{D}$ and $\zeta_0 = -\delta$ for ϕ_1; $a = \frac{\lambda+k}{D}$, $b = \frac{v}{D}$ and $\zeta_0 = 0$ for ϕ_2; and $a = \frac{\lambda}{D}$, $b = \frac{v}{D}$ and $\zeta_0 = L$ for ϕ_3. Applying the boundary conditions to the solution gives the following equation:

$$\begin{bmatrix} f_{21}^{(3)}(L+\delta,\lambda) & f_{22}^{(3)}(L+\delta,\lambda) \end{bmatrix} \begin{bmatrix} f_{11}^{(2)}(L,\lambda) & f_{12}^{(2)}(L,\lambda) \\ f_{21}^{(2)}(L,\lambda) & f_{22}^{(2)}(L,\lambda) \end{bmatrix} \begin{bmatrix} f_{11}^{(1)}(0,\lambda) & f_{12}^{(1)}(0,\lambda) \\ f_{21}^{(1)}(0,\lambda) & f_{22}^{(1)}(0,\lambda) \end{bmatrix} \begin{bmatrix} 1 \\ \frac{v}{D} \end{bmatrix} \phi_1(-\delta) = 0 \tag{2.68}$$

where k in the superscript of $f_{ij}^{(k)}$ indicates to which eigenfunction (ϕ_k) is the function related to and each component is given by Eq. 2.51.

2. Hyperbolic PDE - Delayed diffusion: the flux is defined as $F = vC - (1 - \tau\partial_t)D\partial_\zeta C$ and using the approximation for $\tau \to 0$, A is the same as in Eq. 2.54. Similarly, A_T will be defined with the same structure, but with $k = 0$. Considering the same transport zone with length δ before and after the reaction zone, no incoming flux at $\zeta = -\delta$ and continuity of concentration at $\zeta = L + \delta$, the eigenvalue problem gives the following system of equations:

$$\begin{cases} \phi_{2,l} = \lambda\phi_{1,l} \\ \frac{D}{\tau}d_{\zeta\zeta}\phi_{1,1} - \frac{v}{\tau}d_\zeta\phi_{1,1} - \frac{1}{\tau}\phi_{2,1} - vd_\zeta\phi_{2,1} = \lambda\phi_{1,k} \\ \frac{D}{\tau}d_{\zeta\zeta}\phi_{1,2} - \frac{v}{\tau}d_\zeta\phi_{1,2} - \frac{k}{\tau}\phi_{1,2} - \frac{1}{\tau}\phi_{2,2} - vd_\zeta\phi_{2,2} - k\phi_{2,2} = \lambda\phi_{2,2} \\ \frac{D}{\tau}d_{\zeta\zeta}\phi_{1,3} - \frac{v}{\tau}d_\zeta\phi_{1,3} - \frac{1}{\tau}\phi_{2,3} - vd_\zeta\phi_{2,3} = \lambda\phi_{2,3} \end{cases} \tag{2.69}$$

where $l = \{1, 2, 3\}$ in the subscript indicates to which eigenfunction is $\phi_{1,l}$ or $\phi_{2,l}$ assigned to. The boundary conditions for the eigenfunctions are given as:

$$\begin{cases} v(1+\tau\lambda)\phi_{1,1}(-\delta) - Dd_\zeta\phi_{1,1}(-\delta) = 0 \\ \phi_{1,1}(0) = \phi_{1,2}(0) \\ d_\zeta\phi_{1,1}(0) = d_\zeta\phi_{1,2}(0) \\ \phi_{1,2}(L) = \phi_{1,3}(L) \\ d_\zeta\phi_{1,2}(L) = d_\zeta\phi_{1,3}(L) \\ d_\zeta\phi_{1,3}(L+\delta) = 0 \end{cases} \tag{2.70}$$

The solution will have the same structure as Eq. 2.50, with $a = \frac{\lambda(1+\lambda\tau)}{D}$, $b = \frac{v(1+\lambda\tau)}{D}$ and $\zeta_0 = -\delta$ for $\phi_{1,1}$; $a = \frac{(\lambda+k)(1+\lambda\tau)}{D}$, $b = \frac{v(1+\lambda\tau)}{D}$ and $\zeta_0 = 0$ for $\phi_{1,2}$; and $a = \frac{\lambda(1+\lambda\tau)}{D}$, $b = \frac{v(1+\lambda\tau)}{D}$ and $\zeta_0 = L + \delta$ for $\phi_{1,3}$. And, by applying the boundary conditions to the solution of the ODEs, the equation obtained is very similar to Eq. 2.68:

$$\begin{bmatrix} f_{21}^{(3)}(L+\delta,\lambda) & f_{22}^{(3)}(L+\delta,\lambda) \end{bmatrix} \begin{bmatrix} f_{11}^{(2)}(L,\lambda) & f_{12}^{(2)}(L,\lambda) \\ f_{21}^{(2)}(L,\lambda) & f_{22}^{(2)}(L,\lambda) \end{bmatrix} \\ \begin{bmatrix} f_{11}^{(1)}(0,\lambda) & f_{12}^{(1)}(0,\lambda) \\ f_{21}^{(1)}(0,\lambda) & f_{22}^{(1)}(0,\lambda) \end{bmatrix} \begin{bmatrix} 1 \\ \frac{v+\lambda\tau}{D} \end{bmatrix} \phi_{1,1}(-\delta) = 0 \tag{2.71}$$

where k in the superscript of $f_{ij}^{(l)}$ indicates to which eigenfunction ($\phi_{1,l}$) is the function related to and each component is given by Eq. 2.51 for a, b and ζ_0 given above for each eigenfunction. Then, the eigenfunctions $\phi_{2,l}$ can be easily found using the relation $\phi_{2,l} = \lambda\phi_{1,l}$.

3. Hyperbolic PDE - Delayed total flux: the flux is defined as $F = (1 - \tau\partial_t)(v - D\partial_\zeta)C$, thus, A is defined as in Eq. 2.59 and A_T is the same, with $k = 0$. With the same previous assumptions regarding the transport zone and boundary conditions, the new system of equations given by the eigenvalue problem is:

$$\begin{cases} \phi_{2,l} = \lambda\phi_{1,l} \\ \frac{D}{\tau}d_{\zeta\zeta}\phi_{1,1} - \frac{v}{\tau}d_\zeta\phi_{1,1} - \frac{1}{\tau}\phi_{2,1} = \lambda\phi_{1,k} \\ \frac{D}{\tau}d_{\zeta\zeta}\phi_{1,2} - \frac{v}{\tau}d_\zeta\phi_{1,2} - \frac{k}{\tau}\phi_{1,2} - \frac{1}{\tau}\phi_{2,2} - k\phi_{2,2} = \lambda\phi_{2,2} \\ \frac{D}{\tau}d_{\zeta\zeta}\phi_{1,3} - \frac{v}{\tau}d_\zeta\phi_{1,3} - \frac{1}{\tau}\phi_{2,3} = \lambda\phi_{2,3} \end{cases} \tag{2.72}$$

where l in the subscript indicates to which eigenfunction is $\phi_{1,l}$ or $\phi_{2,l}$ related. The boundary conditions for the eigenfunctions are given as:

$$\begin{cases} v\phi_{1,1}(-\delta) - Dd_\zeta\phi_{1,1}(-\delta) = 0 \\ \phi_{1,1}(0) = \phi_{1,2}(0) \\ d_\zeta\phi_{1,1}(0) = d_\zeta\phi_{1,2}(0) \\ \phi_{1,2}(L) = \phi_{1,3}(L) \\ d_\zeta\phi_{1,2}(L) = d_\zeta\phi_{1,3}(L) \\ d_\zeta\phi_{1,3}(L+\delta) = 0 \end{cases} \tag{2.73}$$

The solution is given by Eq. 2.50, with $a = \frac{\lambda(1+\lambda\tau)}{D}$, $b = \frac{v}{D}$ and $\zeta_0 = -\delta$ for $\phi_{1,1}$; $a = \frac{(\lambda+k)(1+\lambda\tau)}{D}$, $b = \frac{v}{D}$ and $\zeta_0 = 0$ for $\phi_{1,2}$; and $a = \frac{\lambda(1+\lambda\tau)}{D}$, $b = \frac{v}{D}$

and $\zeta_0 = L + \delta$ for $\phi_{1,3}$. And, by applying the boundary conditions to the solution of the ODEs, the equation obtained has the same structure as Eq. 2.68, with each component given by Eq. 2.51 for the a, b and ζ_0 defined above for each eigenfunction.

Remark 2.3 *The Closed-Closed boundary conditions can be solved in the same way as the Open-Open boundary conditions (i.e., considering that there are also two eigenfunctions related to the transport zones). But, as the transport zones would be represented by hyperbolic equations and, as the condition in $\zeta = -\delta$ is the no incoming flux, the only solution for ϕ_1 is $\phi_1(\zeta) = 0$. Thus, the boundary conditions for ϕ_2 are the same as shown in Section 2.3.2 and, as continuity of concentration is assumed at the end of the reaction zone, $\phi_3(L) = \phi_2(L)$. As $\phi_3(L)$ is also given by the solution of a first order hyperbolic equation, it does not have any influence in the system stability. Thus, only the solution of the eigenvalue problem in the reaction zone (ϕ_2) and its boundary conditions are necessary to analyze the system's stability for closed-closed boundary conditions. But, for the open-open boundary conditions, the transport zones influence the system's stability.*

The eigenvalues' distribution for the same set of parameters used in Section 2.3.2, considering a transport zone of $\delta = 1$, is shown in Figure 2.9 for $0.1 \leq v \leq 15$. As the open-open boundary conditions consider the transport before and after the reaction zone, the effects are seen in the eigenvalue distribution, as the number of eigenvalues increased in the same interval in comparison to Figure 2.7. The overall behavior is similar to the previously obtained, with the eigenvalues of the parabolic PDE placed in the real axis, while most of the eigenvalues of the hyperbolic PDEs are in the complex plane with a finite number of the eigenvalues in the real axis. When the velocity is increased, the same behavior for the closed-closed boundary conditions is seen once again, with the whole set of eigenvalues shifting to the left for all PDEs and some of the eigenvalues of the hyperbolic PDEs shifting from the real axis to the complex plane.

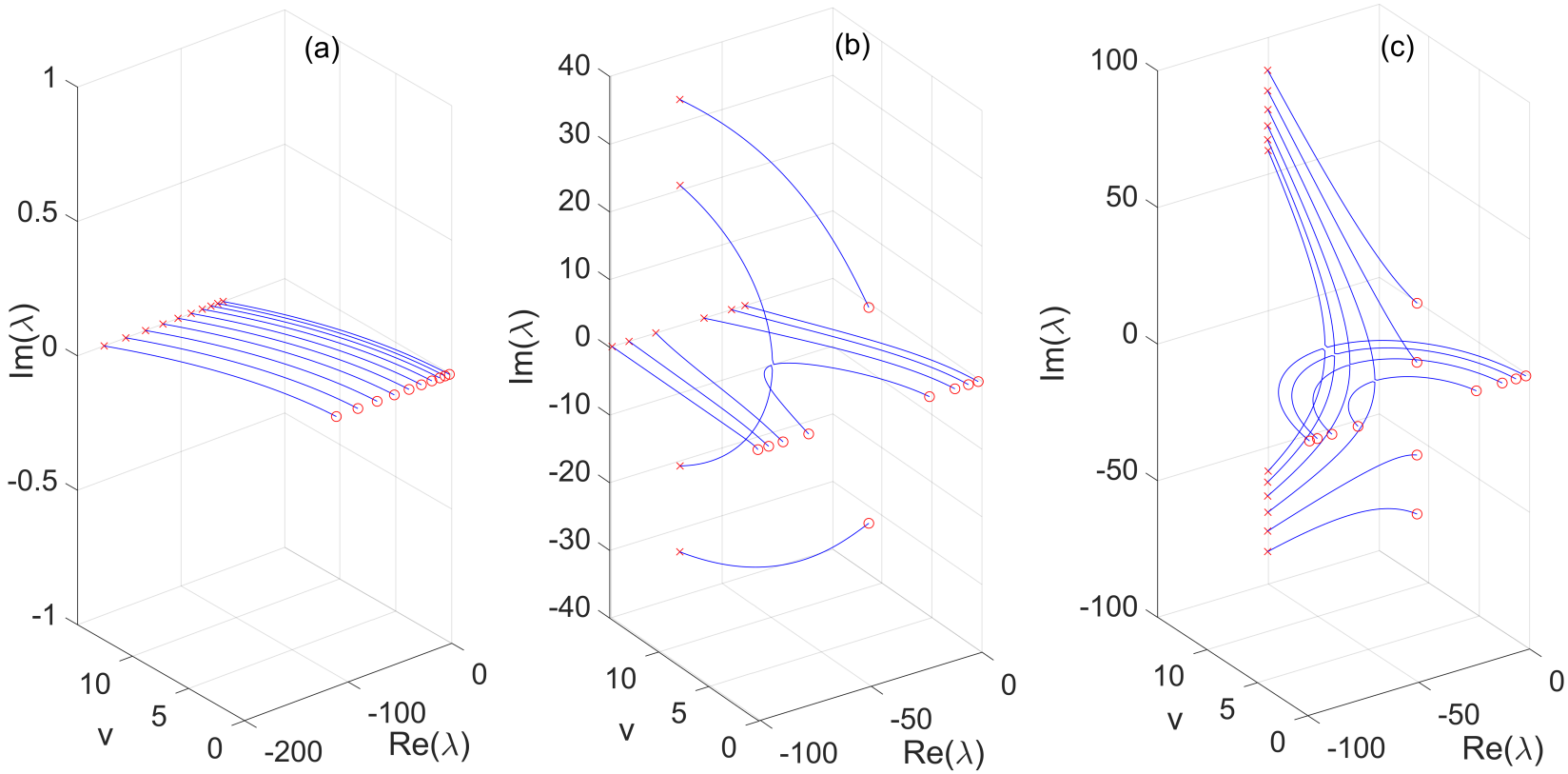

Figure 2.9: Tubular reactor eigenvalue distribution for Closed-Closed B.C. with $D = 1$, $k = 2$ and $\tau = 0.01$ for $0.1 \leq v \leq 15$: (a) Parabolic; (b) Hyperbolic (Delayed Diffusion); (c) Hyperbolic (Delayed Flux). $\circ$ represents the beginning of the line ($v = 0.1$) and $\times$ the end value ($v = 15$).

Simulation Results for the Open-Open Boundary Conditions

In this section, the simulation results for the open-open boundary conditions are discussed. Figure 2.10 shows the time-spatial profiles for $T(\zeta, t)$ and $\partial_t T(\zeta, t)$ for the parabolic and the hyperbolic PDEs, considering delayed diffusive flux and total flux. The same set of parameter used in the simulation of the closed-closed boundary conditions were considered and $\delta = 1$. The initial conditions used were $T(-\delta \leq \zeta \leq 0, 0) = 0.25(\zeta + 1)^2 + 6\zeta + 1$, $T(0 \leq \zeta \leq 1, 0) = 0.25\zeta^2 + 6.5\zeta + 7.25$ and $T(1 \leq \zeta \leq 2, 0) = -3.5(\zeta - 1)^2 + 7\zeta + 14$ and $\partial_t T(\zeta, 0) = 0$ for the hyperbolic. As discussed previously, the difference in the initial rate of change ($\partial_t T(\zeta, t)$) of the parabolic and the hyperbolic PDEs in clearly noticeable, as the hyperbolic takes into account the delay, resulting an initial difference in $T(\zeta, t)$ between the PDEs.

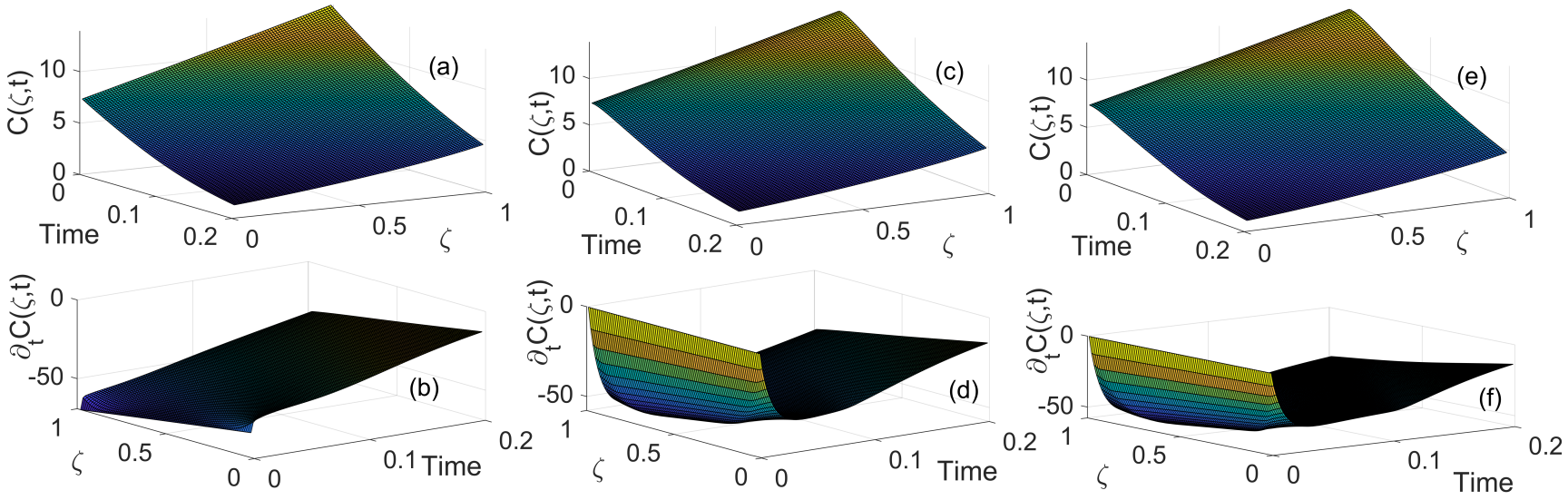

Figure 2.10: Tubular reactor simulation results with Open-Open B.C. considering $v = 6$, $D = 1$, $k = 2$ and $\tau = 0.01$ for the hyperbolic: (a) and (b) $C(\zeta, t)$ and $\partial_t C(\zeta, t)$ for Parabolic; (c) and (d) $C(\zeta, t)$ and $\partial_t C(\zeta, t)$ for Hyperbolic (delayed Diffusion); (e) and (f) $C(\zeta, t)$ and $\partial_t C(\zeta, t)$ for Hyperbolic (delayed total Flux).

2.4 Heat Equation and Stefan Problem

To analyze the difference between the results obtained by the hyperbolic and parabolic PDEs, a heat diffusion problem with phase change is also considered. One of the simplest mathematical model to describe the phase transition phenomenon is called Stefan problem [61]. If a phase change of a material occurs at a given point, latent heat is released or absorbed and the temperature of the material at that point remains constant. It is assumed that the phase change temperature is constant and that the temperature across the material is continuous. For the sake of simplicity, a one dimensional case is considered in a material with constant cross sectional area. If the phase change happens at a point $\zeta = \epsilon(t)$, then:

$$T_I(\zeta = \epsilon(t) - \delta, t) = T_{II}(\zeta = \epsilon(t) + \delta, t) = T_C \tag{2.74}$$

where δ is a small spatial variation (such that $\delta \to 0$), T_C is the phase change temperature and the subscripts I and II are used to represent two different phases. Therefore, this condition implies that the temperature close to the phase transition point is continuous and is the same in both phases. The Stefan condition is obtained by applying a energy balance between two instants t_0 and t_1 in a control volume that is going through the phase change. Assuming that the phase transition point moved from $\epsilon(t_0)$ to $\epsilon(t_1)$ and $\epsilon(t_1) > \epsilon(t_0)$, the energy involved in the phase change is given by the volume of the material that went through phase change between these two instants and the latent heat required for the transition:

$$Q = C_{lat} A[\epsilon(t_1) - \epsilon(t_0)] \tag{2.75}$$

where Q is the energy involved in the phase transition, C_{lat} is the latent heat (per unit of volume) and A is the constant cross sectional area. The amount of energy released/required in the phase transition should be equivalent to the heat provided by the heat diffusion in both sides of the interface in this time interval, that is:

$$Q = \int_{t_0}^{t_1} \int_A (q_I - q_{II}) dA dt = A \int_{t_0}^{t_1} (q_I - q_{II}) dt \tag{2.76}$$

where q_I and q_{II} represents the heat fluxes from the phases and it is assumed that the cross sectional area does not change. Then:

$$\begin{gathered} Q = C_{lat} A[\epsilon(t_1) - \epsilon(t_0)] = A \int_{t_0}^{t_1} (q_I - q_{II}) dt \implies \\ C_{lat}[\epsilon(t_1) - \epsilon(t_0)] = \int_{t_0}^{t_1} (q_I - q_{II}) dt \end{gathered} \tag{2.77}$$

Dividing the equation by $t_1 - t_0$ and setting $t_1 \to t_0$, finally gives the Stefan condition:

$$C_{lat} d_t \epsilon(t) = q_I(t, \zeta = \epsilon - \delta) - q_{II}(t, \zeta = \epsilon + \delta) \tag{2.78}$$

The system considered here is shown in Figure 2.11, which could represent the phase transition of water and ice.

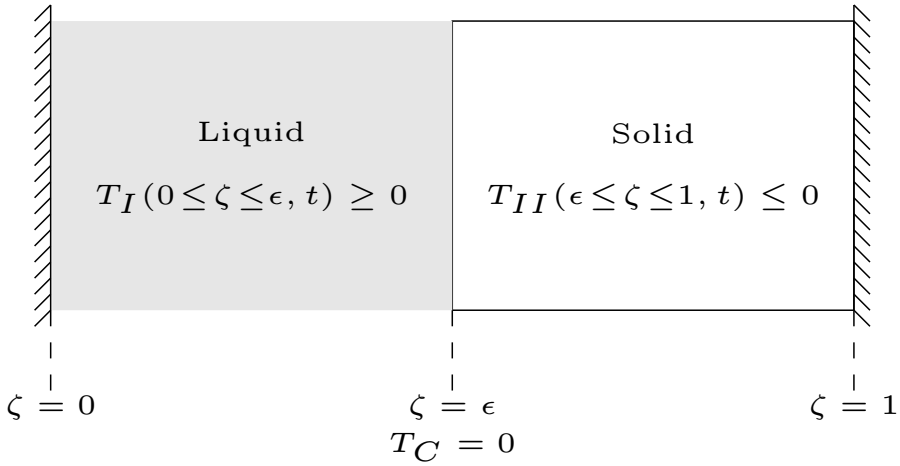

Figure 2.11: Representation of the system with phase transition.

The transition temperature is considered to be $T_C = 0$. An initial temperature of $T_I(0 < \zeta < \epsilon(0), 0) \neq 0$ and $T_{II}(\epsilon(0) < \zeta < 1) \neq 0$ is considered throughout the system. It is also assumed that there are no heat sinks or sources in-domain and that the temperatures at both ends are at the transition temperature (i.e., $T_I(0,t) = T_{II}(1,t) = T_C = 0$). This implies that, initially, there are two flows in the system, coming to the interface from each side of the system, until the temperature in the whole domain reaches the transition temperature. This is called a two-phase Stefan problem as both phases have temperature profiles to be determined.

The Stefan condition for the moving boundary, using the Fourier's law, is given as:

$$\dot{\epsilon} = -\beta_I \, \partial_\zeta T_I|_{\zeta = \epsilon(t)} + \beta_{II} \, \partial_\zeta T_{II}|_{\zeta = \epsilon(t)} \tag{2.79}$$

where $\beta_i = \frac{k_i}{C_{lat}}$, with k_i as the material thermal conductivity, and $\dot{\epsilon} = \frac{d\epsilon}{dt}$. If the modified heat flux shown in Eq. 2.5 is used, considering the same τ for the two phases, the Stefan condition obtained is:

$$\tau\ddot{\epsilon} + \dot{\epsilon} = -\beta_I \, \partial_\zeta T_I|_{\zeta=\epsilon(t)} + \beta_{II} \, \partial_\zeta T_{II}|_{\zeta=\epsilon(t)} \tag{2.80}$$

where $\ddot{\epsilon} = \frac{d^2\epsilon}{dt^2}$. Thus, the modified heat flux results in a second order ordinary differential equation for the moving boundary, while the original Fourier's law results in a first order ordinary differential equation. These equations need to be solved along with the corresponding hyperbolic and parabolic PDEs, Eq. 2.7 and Eq. 2.3, respectively. As the resulting system has a time-dependent domain, a change of coordinates is applied to the system prior to its solution:

- Liquid domain (Phase *I*): the following change of coordinates is used:

$$l = \frac{\zeta}{\epsilon(t)}, \text{ for } 0 \leq \zeta \leq \epsilon(t) \tag{2.81}$$

  where $l \in [0, 1]$ is the new coordinate, which has a fixed domain. This change of coordinates makes it necessary to redefine the partial derivatives as well. For the spatial derivatives, the following is obtained:

$$\partial_\zeta T_I(\zeta, t) = \frac{1}{\epsilon}\partial_l T_I(l, t) \tag{2.82}$$

$$\partial_{\zeta\zeta} T_I(\zeta, t) = \frac{1}{\epsilon^2}\partial_{ll} T_I(l, t) \tag{2.83}$$

  The time derivatives become:

$$\partial_t T_I(\zeta, t) = \partial_t T_I(l, t) - \frac{l}{\epsilon}\dot{\epsilon}\partial_l T_I(l, t) \tag{2.84}$$

$$\partial_{tt} T_I(\zeta, t) = \partial_{tt} T_I(l, t) - \frac{2l}{\epsilon}\dot{\epsilon}\partial_l\partial_t T_I(l, t) + \partial_l T_I(l, t)\left[\frac{2l}{\epsilon^2}(\dot{\epsilon})^2 - \frac{l}{\epsilon}\ddot{\epsilon}\right] \tag{2.85}$$

  Substituting in the parabolic PDE leads to the following non-linear PDE:

$$\partial_t T_I(l, t) = \frac{l}{\epsilon}\dot{\epsilon}\partial_l T_I(l, t) + \alpha_I \frac{1}{\epsilon^2}\partial_{ll} T_I(l, t) \tag{2.86}$$

  And for the hyperbolic PDE:

$$\begin{aligned}\partial_{tt} T_I(l, t) = {} & \frac{2l}{\epsilon}\dot{\epsilon}\partial_l\partial_t T_I(l, t) - \partial_l T_I(l, t)\left[\frac{2l}{\epsilon^2}(d_t\epsilon)^2 - \frac{l}{\epsilon}\ddot{\epsilon}\right] \\ & + \frac{1}{\tau}\left[-\partial_t T_I(l, t) + \frac{l}{\epsilon}\dot{\epsilon}\partial_l T_I(l, t) + \alpha_I \frac{1}{\epsilon^2}\partial_{ll} T_I(l, t)\right]\end{aligned} \tag{2.87}$$

- Solid domain (Phase *II*): Similarly to the liquid, the change of coordinates used in the solid phase is given by:

$$s = \frac{\zeta - \epsilon(t)}{1 - \epsilon(t)}, \text{ for } \epsilon(t) \leq \zeta \leq 1 \tag{2.88}$$

such that $g \in [0, 1]$ has a fixed-domain. The new spatial derivatives are defined as:

$$\partial_\zeta T_{II}(\zeta, t) = \frac{1}{1-\epsilon}\partial_s T_{II}(s, t) \tag{2.89}$$

$$\partial_{\zeta\zeta} T_{II}(\zeta, t) = \frac{1}{(1-\epsilon)^2}\partial_{ss} T_{II}(s, t) \tag{2.90}$$

And the time derivatives:

$$\partial_t T_{II}(\zeta, t) = \partial_t T_{II}(s, t) - \frac{1-s}{1-\epsilon}\dot{\epsilon}\partial_s T_{II}(s, t) \tag{2.91}$$

$$\begin{aligned}\partial_{tt} T_{II}(\zeta, t) = \partial_{tt} T_{II}(s, t) - \frac{2(1-s)}{1-\epsilon}\dot{\epsilon}\partial_s\partial_t T_{II}(s, t) + \\ \partial_s T_{II}(s, t)\left[\frac{2(s-1)}{(1-\epsilon)^2}(\dot{\epsilon})^2 - \frac{s-1}{1-\epsilon}\ddot{\epsilon}\right]\end{aligned} \tag{2.92}$$

Thus, for the parabolic PDE, the following equation is obtained:

$$\partial_t T_{II}(s, t) = \frac{1-s}{1-\epsilon}\dot{\epsilon}\partial_s T_{II}(s, t) + \alpha_{II}\frac{1}{(1-\epsilon)^2}\partial_{ss} T_{II}(s, t) \tag{2.93}$$

The hyperbolic PDE gives:

$$\begin{aligned}\partial_{tt} T_{II}(s, t) = \\ \frac{2(1-s)}{1-\epsilon}\dot{\epsilon}\partial_s\partial_t T_{II}(s, t) - \partial_s T_{II}(s, t)\left[\frac{2(s-1)}{(1-\epsilon)^2}(\dot{\epsilon})^2 - \frac{s-1}{1-\epsilon}\ddot{\epsilon}\right] \\ + \frac{1}{\tau}\left[-\partial_t T_{II}(s, t) + \frac{1-s}{1-\epsilon}\dot{\epsilon}\partial_s T_{II}(s, t) + \alpha_{II}\frac{1}{(1-\epsilon)^2}\partial_{ss} T_{II}(s, t)\right]\end{aligned} \tag{2.94}$$

- Moving boundary: Lastly, it is necessary to rewrite the Stefan condition in the new coordinates. For the parabolic PDE, the moving boundary dynamics were given by a first order ODE, which becomes:

$$\dot{\epsilon} = -\beta_I \left.\frac{1}{\epsilon}\partial_l T_I(l, t)\right|_{l=1} + \beta_{II} \left.\frac{1}{1-\epsilon}\partial_s T(s, t)\right|_{s=0} \tag{2.95}$$

Similarly, for the second order ODE derived from the delayed flux:

$$\tau\ddot{\epsilon} + \dot{\epsilon} = -\beta_I \left.\frac{1}{\epsilon}\partial_l T_I(l, t)\right|_{l=1} + \beta_{II} \left.\frac{1}{1-\epsilon}\partial_s T(s, t)\right|_{s=0} \tag{2.96}$$

Thus, for the non-delayed flux, Eq. 2.95 must be solved simultaneously with Eq. 2.86 for the Liquid Phase and Eq. 2.93 for the Solid Phase. Similarly, for the delayed flux, Eq. 2.96 for the moving boundary, Eq. 2.87 for the Liquid Phase and Eq. 2.94 for the Solid Phase are numerically solved together.

Simulation results of the Stefan problem

For the results shown in this section, the following system parameters were used: $\alpha_I = 0.5$, $\alpha_{II} = 1$, $\beta_I = \beta_{II} = 1$ and $\tau = 0.01$ for the hyperbolic case. The initial conditions were chosen as:

$$\begin{aligned} \epsilon(0) &= 0.5 \\ T_I(\zeta, 0) = -2\zeta\frac{(\zeta - \epsilon(0))}{\epsilon(0)^2} &\implies T_I(l, 0) = -2l(l-1) \\ T_{II}(\zeta, 0) = 4\frac{(\zeta - \epsilon(0))(\zeta - 1)}{(1 - \epsilon(0))^2} &\implies T_{II}(s, 0) = 4s(s-1) \end{aligned} \tag{2.97}$$

The spatial-time evolution of the parabolic and hyperbolic PDEs, together with the time evolution of the moving boundary, are shown in Figure 2.12. It is possible to see some differences between the time evolution of the two phases for each type of PDE considered. However, the divergence becomes more noticeable in the evolution of the moving boundary. At a first instance, the solid phase increases due to the initial temperature profile. But, due to its higher thermal diffusion, the temperature reaches the transition temperature faster. Then, in the liquid phase, with a lower thermal diffusion, it takes more time to reach the transition temperature, thus after some time, this phase starts to increase up until the steady-state is reached. As the dynamics of the moving boundary depends completely on the incoming fluxes, a difference in the behavior of the parabolic is expected and is clearly seen in Figure 2.12 (c). The overall behavior between the phases, as described above, is still present, however, as the hyperbolic PDE takes into account a delay, the transitions take some time to happen.

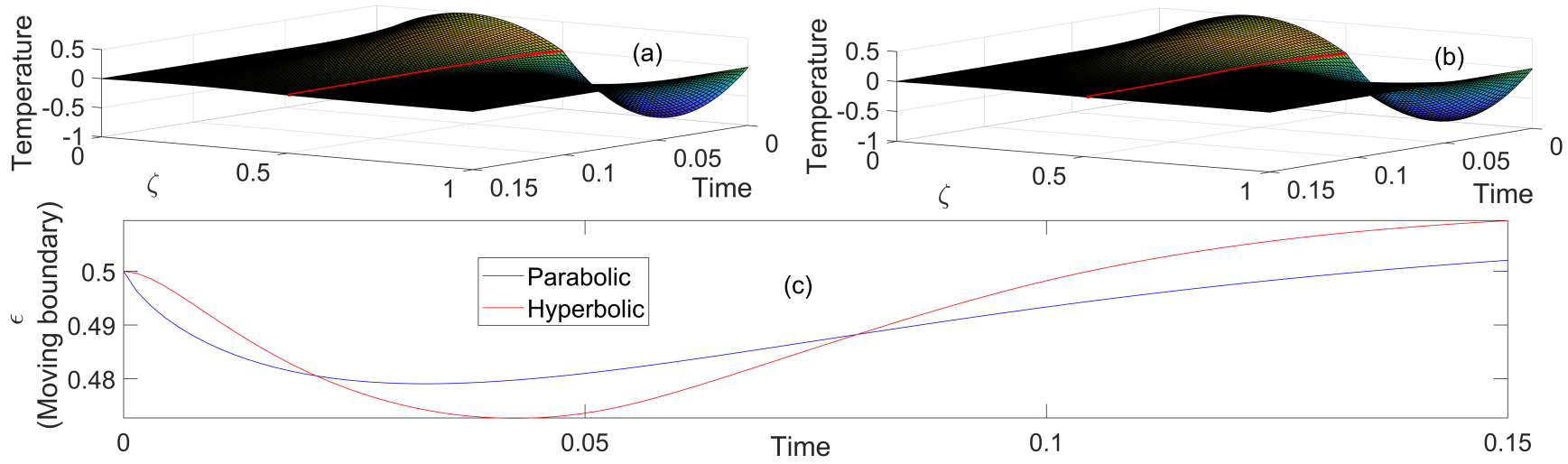

Figure 2.12: Stefan problem simulation results. considering $\alpha_I = 0.5$, $\alpha_{II} = 1$, $\beta_I = \beta_{II} = 1$ and $\tau = 0.01$ for the hyperbolic: (a) Space-time result of $T(\zeta, t)$ for the Parabolic; (b) Space-time result of $T(\zeta, t)$ for the Hyperbolic; In both cases, the red line indicates the boundary between the two phases; (c) Time evolution of the moving boundary for the Parabolic (blue line) and Hyperbolic (red line).

2.5 Conclusion

In this chapter the differences between the parabolic partial differential equations, generally derived from diffusive transport, and the hyperbolic PDEs, which arise if the delay in the transport is considered were explored. In the non-delayed diffusion, any initial disturbance in the material body is propagated instantly with maximum rate, which is characteristic of the parabolic equation. To eliminate this undesirable feature, a delayed flux is considered to take into account the initial inertia, and, with an approximation, a hyperbolic equation is derived, which avoids the phenomenon of infinite propagation.

The eigenvalues of the systems were analyzed whenever possible and the results of numerical simulations were presented to show the distinction between these two types of equations. All the reaction-transport processes considered, that is, a one-dimensional heat diffusion, an axial tubular reactor and a phase change system, presented similar differences between the hyperbolic and parabolic PDEs. Overall, the properties' rate of change presented a noticeable distinction from the hyperbolic and parabolic equation. As a consequence, a disparity is also seen in the property itself. Specifically for the system with a phase transition (modeled as a Stefan problem), the type of flux influences the boundary's dynamics. Thus, for this system the discrepancy between the hyperbolic and parabolic PDE modeling was apparent.

This difference in the dynamics can be crucial for some applications in material processing and subsequently will impinge on the controller design. If a model based controller is designed, although it can guarantee the closed-loop stability with some degree of robustness, the controller's performance would be affected by the modeling setting, which is a topic for future contributions.

2.6 Acknowledgments

The support provided by CAPES - 88881.128514/2016-01 (Brazil) for Guilherme Ozorio Cassol is gratefully acknowledged.

Chapter 3

Heat Exchanger System Boundary Regulation

3.1 Introduction

The process industry and large utility plants operations are constantly monitored and analyzed for novel ways to reduce energy consumption and increase operational profitability. Heat exchangers are ubiquitously present in the process industry and included in industrial plants, where they account for heat recovery and ultimately improvement in process energy efficiency [62]. Also, they are used to minimize the loss of heat by recovering some of energy from the process discharge streams and/or applied to recover the heat contained in a later stages process streams to preheat the earlier stages stream entering the plant.

A counter current flow and a parallel flow, two heat exchanger system configurations that are frequently found in practice are considered in this contribution. The counter current configuration has some advantages over the parallel design since the counter current configuration provides temperature uniformity between the two liquids that minimizes the thermal stresses throughout the exchanger. In addition, the outlet temperature of the cooled liquid can approach the most noteworthy temperature of the hot fluid; therefore this configuration achieves a more uniform rate of energy exchange throughout the heat exchanger, see Xu et. al. [6]. These systems, which are distributed parameter systems (DPS) are commonly modelled by partial differential equations

(PDEs), and in general are more complex to deal with compared to the lumped parameter systems, that are commonly modelled by ordinary differential equations (ODEs). Specifically, heat exchangers are modelled by applying mass, momentum and energy conservation principles endowed with constitutive relations that render a system of coupled transport hyperbolic PDE equations. Due to their frequent presence in an industrial setting, most important aspects of the dynamical stability and system theoretic properties have been thoroughly investigated. Namely, if there is no time lag in the boundary feedback loop, the exponential stability is shown for the counter-flow type by using the port-Hamiltonian approach as well as by using the spectral analysis [63], [64]. Along the same line, if the boundary delay is considered in a dynamical representation, the stability of this system is explored by transformation of the time lag dynamics to the corresponding transport equation and by applying the port-Hamiltonian approach to the transformed system to get necessary stability conditions for the system for both configurations [65].

One of the main goals of any control strategy is to be able to make the system dynamics behave in a specified, desired manner. Therefore, the classical problem of a servo-design regulator is defined as the design of the closed-loop control system which tracks a prescribed signal and rejects possible disturbance signals applied to the system with guarantees on the closed-loop stability with some degree of robustness. Furthermore, the type of information available in the regulator design also determines features of the regulator. For example, given that the full state information is available, which rarely happens in practice and/or in an DPS setting, one can design a full state feedback regulator. In effect, more appealing practical design realizations account for scenarios when only error and/or output measurements are available (in some cases, the measured output does not account for the regulated output whose behaviour is enforced), see Xu. et. al. [6]. In general, it is considered in the regulator design that the desired reference signals to be tracked and the known disturbances to be rejected are generated by an exosystem [2]. Furthermore, by following the well known regulator designs from the finite dimensional systems theory, one possible way to design the regulator for the distributed parameter

systems is to use a lumping approach, which implies that some type of model approximation or/and model reduction is applied (which converts the PDEs to sets of ODEs). Hence, standard regulator design methods applicable to ODE systems can be realized and there are several contributions that deal with the regulator problem for linear finite-dimensional systems [2], [9], [10]. However, this approach of early lumping also results in a possible mismatch between dynamical properties of the original distributed parameter and the lumped parameter models, which inevitably affect the designed regulator performances [11].

A more rigorous way to address regulator design in the realm of distributed parameter processes is to exploit the infinite-dimensional characteristic of the system and design in the DPS setting. In particular, the method of design of output and error feedback regulators for linear scalar hyperbolic PDE infinite-dimensional system is explored and addresses boundary and in-domain regulation problem for infinite-dimensional nonspectral linear system [15]. Along the same line, the PI-controller for distributed parameter systems with constant disturbance was realized by Kobayashi et. al. [12], while the geometric theory for the regulation problem for infinite-dimensional linear systems driven by finite-dimensional exosystems was developed in Byrnes et. al. [13]. Furthermore, the geometric theory for the regulator design problem was proposed for a class of first order hyperbolic PDE systems with space-varying coefficients [14], while the regulator design through internal model principle for the system of hyperbolic transport equation was addressed by solving a constrained Sylvester equation in Xu et. al. [6]. Boundary control problems are, as the name suggests, problems that have a boundary condition as a function of the manipulated variable. Many contributions have addresses this case for hyperbolic systems, for instance, in Prieur et. al. [66], a Riemann invariants approach was used to develop a robust boundary controller, in Krstic [67], the boundary control of partial differential equations using the backstepping method is developed. Along the same line of backstepping design, in Bastin [68], the boundary stabilization of systems of two balance laws by both full-state and dynamic output feedback was explored, while in Krstic and Smyshlyaev [69],

the backstepping methodology was use to stabilize first order linear hyperbolic PDE systems. The backstepping method has been generally used to achieve exponential stabilization in boundary control problems: in Di Meglio et. al [70], the boundary stabilization controller was designed for a linear system of coupled first-order hyperbolic PDEs; in Deutscher (2015) [71] backstepping methodology was used to simplify the design of output regulators for a linear parabolic PDE system; and in Deutscher (2019) [72], backstepping was used to solve the output regulation problem for coupled parabolic partial integro-differential equations. In the same spirit, in Xu et. al. [73], the output regulation problem for a linear multiple input multiple output system of hyperbolic partial integro-differential equations was considered also using the backstepping methodology.

In the early works, in the case of regulator designs for heat exchangers, an approximate modelling and control of nonlinear processes using a polynomial expansion was applied with PI and PID regulators, but the system was not considered to be distributed [74], [75]. Recently, the boundary geometric control was applied to a counter-current heat exchanger, considering a model based of two coupled hyperbolic PDEs, with the purpose of controlling the internal fluid temperature by manipulating the jacket temperature at its inlet boundary, which resulted in good regulation and tracking performances [76]. A control strategy based on the state-feedback using a Kalman filter to reconstruct the entire state of the system was used in a parallel-flow heat exchanger to control the internal fluid temperature by manipulating the inlet external fluid temperature [77]. A repetitive control strategy was implemented in a tubular heat-exchanger system to deal with intrinsic resonance dynamics when residence time is variable and achieves fast, well-damped responses in the control of the outlet fluid temperature [78]. A model based control strategy that uses the thermal energy in the fluids as a controlled variable instead of the outlet temperature was used in compact plate heat exchangers to achieve a robust control that does not rely on the specification of the overall heat transfer coefficient, as it can strongly vary with a specific manufacturer [79]. Along the line of the heat exchanger dynamics, common configurations of counter or

cocurrent two flows exchanging heat across the exchanger are inherently stable systems [6], [14], [80], whereas heat exchangers with reverse flow can lead to unstable dynamics, so that regulation of more complex and physically relevant models of reverse flow heat exchanger realizations needs to be addressed.

Motivated by the above considerations, the manuscript main contribution is the design of output regulators (servo-mechanism) for realistic and complex heat exchanger systems in both the counter and/or cocurrent flow configuration with boundary returned flow modelled by time lag dynamics which exhibits unstable dynamical behaviour. In particular, we address the modelling framework by considering the initial setting of heat transport hyperbolic PDEs endowed by the time lag dynamics representing boundary feedback flow that is adequately transformed in the boundary infinite-dimensional state space setting amenable to stability analysis and subsequent regulator design. The manuscript contribution also accounts for stability analysis of the two configurations of the heat exchanger system and is followed by regulator designs. The full state feedback regulator design is provided as an initial design which ensures stabilization of the hyperbolic PDE system and also accounts for the perfect trajectory tracking and/or disturbance rejection of any polynomial functions and/or harmonic functions tracking and disturbance signals. Further, we demonstrate that the important issue of the gain based output feedback regulator realization cannot be realized without the observer design, and therefore the output and error feedback regulator designs are developed (prior assumes that only output is available to the regulator, while former accounts for the scenario when only an error between the regulated output and reference is given). In all three regulator designs presented, the full state, the output and the error feedback design, the salient feature of solution of the Sylvester equation for the system of hyperbolic PDEs are realized and presented. Finally, we demonstrate three different designs and corroborate on the designs characteristics associated with numerical simulations and presented results.

3.2 System Description

The system of 1-D linear hyperbolic partial differential equations PDEs on domain $\{t \in \Re_+, \zeta \in [0,1]\}$, representing a counter current heat exchanger system with a delayed boundary feedback is given in the following Figure 3.1 and as system by:

$$\begin{cases} \dfrac{\partial \theta_1}{\partial t} = -\nu_1 \dfrac{\partial \theta_1}{\partial \zeta} + h_1 \left(\theta_2 - \theta_1\right) + B_d d \\ \dfrac{\partial \theta_2}{\partial t} = \quad \nu_2 \dfrac{\partial \theta_2}{\partial \zeta} - h_2 \left(\theta_2 - \theta_1\right) + B_d d \\ \theta_1 \left(t, \zeta = 0\right) = \theta_{in}(t) \\ \theta_2 \left(t, \zeta = 1\right) = -k\, \theta_1 \left(t - \tau, \zeta = 1\right) \\ \theta_1 \left(0, \zeta\right) = \theta_{1,0}(\zeta),\ \theta_2 \left(0, \zeta\right) = \theta_{2,0}(\zeta) \\ \theta_1 \left(s, \zeta = 1\right) = \phi(s),\ s \in (-\tau, 0) \end{cases} \tag{3.1a}$$

$$y(t) = \theta_2(t, \zeta = 0), y_m(t) = \theta_2(t, \zeta = z_m) \tag{3.1b}$$

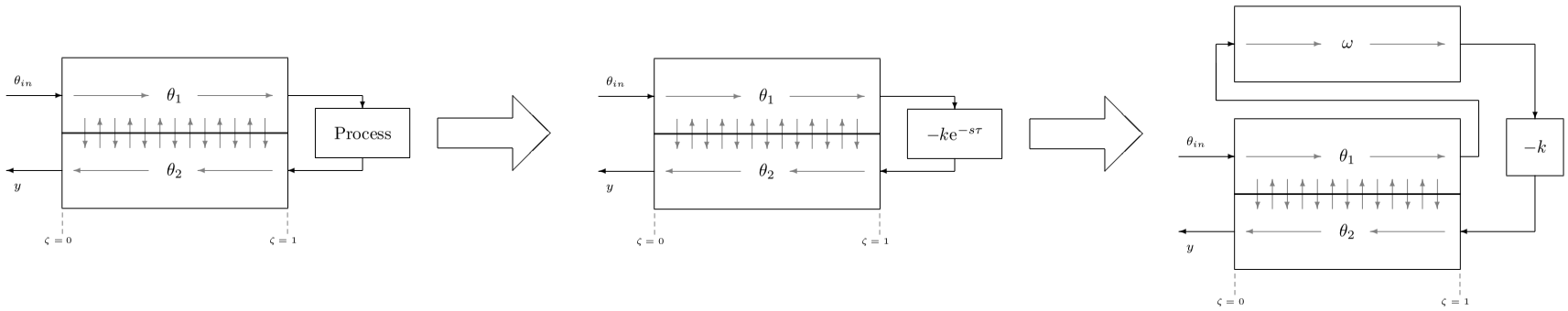

Figure 3.1: (Left): The counter current heat exchanger used in a process for heat integration; (Center): The process is represented as boundary delayed flow feedback; (Right) Schematics of modelling transformation of (3.1a)-(3.1b) to (3.2a)-(3.2b).

where the heat exchanger states $\theta_1(\cdot,t)$ and $\theta_2(\cdot,t) \in H = \mathcal{L}^2(0,1)$ represent the state variables (dimensionless fluid temperatures) while the boundary input is applied at the inlet of θ_1 and the output is at the outlet of the θ_2. The space of interest is a Hilbert space $H = \mathcal{L}^2(0,1)$ equipped with the norm $\|\cdot\| = \int_0^1 (\cdot)\, d\zeta$, and h_1 and h_2 are constant heat exchange coefficients, while ν_1 and ν_2 are positive and represent the constant transport velocities. This model can represent a process where the outlet of the first part of the heat-exchanger (tube) is passed through other stages of the process and then comes back to the heat exchanger into the second part (shell surrounding tube). Throughout the other process stages, the temperature of the stream is changed, which could be represented by the gain k. Furthermore, the time it takes for the stream to come back to the heat-exchanger can be represented by the time delay τ. In the special case of a reaction happening inside one section of the heat-exchanger, the case of an auto-thermal reactor can be considered as analyzed by Bonvin et. al. [81]–[83]. The disturbance applied, $d(t)$, is applied on the system and $B_d(\zeta)$ is the disturbance input spatial distribution function. The controlled output $y(t)$ and the measured output $y_m(t)$ do not necessarily coincide and in this work they are taken from different spatial locations along the second heat exchanger state domain, that is $y(t) = \theta_2(t, z_0)$ and $y_m(t) = \theta_2(t, z_m)$.

The boundary applied time delay dynamics associated with the boundary feedback flow is appropriately represented by a scalar transport equation, and the stability of the input and disturbance free setting of the (3.1a)-(3.1b) has been already addressed [65]. In order to address the system response in the presence of boundary input and disturbance present one needs to account for design of regulators to guarantee closed-loop stability and reference tracking.

Hence, we transform the system as follows:

$$\begin{cases} \dfrac{\partial \theta_1}{\partial t} = -\nu_1 \dfrac{\partial \theta_1}{\partial \zeta} + h_1 \left(\theta_2 - \theta_1\right) + B_d d \\ \dfrac{\partial \theta_2}{\partial t} = \quad \nu_2 \dfrac{\partial \theta_2}{\partial \zeta} - h_2 \left(\theta_2 - \theta_1\right) + B_d d \\ \dfrac{\partial \omega}{\partial t} = -\mu \dfrac{\partial \omega}{\partial \zeta} \\ \theta_1 \left(0, \zeta\right) = \theta_{1,0}(\zeta),\ \theta_2 \left(0, \zeta\right) = \theta_{2,0}(\zeta) \\ \omega \left(0, \zeta\right) = \phi((\zeta - 1)\frac{1}{\mu}) \end{cases} \tag{3.2a}$$

$$y(t) = \theta_2(t, z_0 = 0),\ y_m(t) = \theta_2(t, z_m) \tag{3.2b}$$

with $\omega \in H = \mathcal{L}^2(0,1)$ being the state variable representing a transport delay, and $\phi(s)$ is an arbitrary function that represents the initial conditions associated with the time delay (when $0\langle t\langle \tau$ with μ positive and representing the constant transport velocity (it is related with the time delay by $\mu = 1/\tau$). The boundary conditions for this configuration are:

$$\begin{cases} \theta_1 \left(t, \zeta = 0\right) = \theta_{in}(t) = u(t) \\ \theta_2 \left(t, \zeta = 1\right) = -k\, \omega \left(t, \zeta = 1\right) \\ \omega \ \left(t, \zeta = 0\right) = \theta_1 \left(t, \zeta = 1\right) \end{cases} \tag{3.3}$$

where $\theta_{in}(t)$ is the dimensionless temperature input at the boundary of the first tube of the heat exchanger and is the manipulated variable ($u(t)$) considered in this work, while k is a positive constant that represents the static feedback gain.

The parallel heat exchanger configuration is described by the following system of partial differential equations:

$$\begin{cases} \dfrac{\partial \theta_1}{\partial t} = -\nu_1 \dfrac{\partial \theta_1}{\partial \zeta} + h_1 \left(\theta_2 - \theta_1\right) + B_d d \\ \dfrac{\partial \theta_2}{\partial t} = -\nu_2 \dfrac{\partial \theta_2}{\partial \zeta} - h_2 \left(\theta_2 - \theta_1\right) + B_d d \\ \theta_1 \left(t, \zeta = 0\right) = \theta_{in}(t) \\ \theta_2 \left(t, \zeta = 0\right) = -k\, \theta_1 \left(t - \tau, \zeta = 1\right) \\ \theta_1 \left(0, \zeta\right) = \theta_{1,0}(\zeta),\ \theta_2 \left(0, \zeta\right) = \theta_{2,0}(\zeta) \\ \theta_1 \left(s, \zeta = 1\right) = \phi(s),\ s \in (-\tau, 0) \end{cases} \tag{3.4a}$$

$$y(t) = \theta_2(t, z_0 = 1),\ y_m(t) = \theta_2(t, z_m) \tag{3.4b}$$

As it can be seen, the parallel heat exchanger configuration given by (3.4a)-(3.4b) differs from the counter current configuration (3.2a)-(3.2b) by the flow

direction, the boundary condition and the second heat exchanger output. This configuration can also be represented by three linear hyperbolic equations by transforming the delay dynamics into a scalar hyperbolic PDE:

$$\begin{cases} \dfrac{\partial \theta_1}{\partial t} = -\nu_1 \dfrac{\partial \theta_1}{\partial \zeta} + h_1 \left(\theta_2 - \theta_1\right) + B_d d \\ \dfrac{\partial \theta_2}{\partial t} = -\nu_2 \dfrac{\partial \theta_2}{\partial \zeta} - h_2 \left(\theta_2 - \theta_1\right) + B_d d \\ \dfrac{\partial \omega}{\partial t} = -\mu \dfrac{\partial \omega}{\partial \zeta} \\ \theta_1 \left(0, \zeta\right) = \theta_{1,0}(\zeta),\ \theta_2 \left(0, \zeta\right) = \theta_{2,0}(\zeta) \\ \omega \left(0, \zeta\right) = \phi((\zeta - 1)\frac{1}{\mu}) \end{cases} \tag{3.5a}$$

$$y = \theta_2(t, \zeta = 1), y_m = \theta_2(t, \zeta = z_m), \tag{3.5b}$$

As in the counter current configuration, θ_1, θ_2 and ω represent the state variables, $\phi(s)$ is the arbitrary initial condition of the time delay (when $0\langle t\langle \tau$), ν_1, ν_2 and μ are the constant transport velocities, h_1 and h_2 are the constant heat exchange coefficients, $d(t)$ is the disturbance and $B_d(\zeta)$ is the disturbance input. This new set of equations has the following boundary conditions:

$$\begin{cases} \theta_1 \left(t, \zeta = 0\right) = \theta_{in}(t) = u(t) \\ \theta_2 \left(t, \zeta = 0\right) = -k\, \omega \left(t, \zeta = 1\right) \\ \omega \ \left(t, \zeta = 0\right) = \theta_1 \left(t, \zeta = 1\right) \end{cases} \tag{3.6}$$

Therefore, both configurations can be represented in the unified manner as boundary control problem on space $\{t \in \Re_+, \zeta \in [0, 1]\}$:

$$\dot{x}(t) = \mathfrak{A} x(t) + \bar{B}_d d(t) \tag{3.7a}$$

$$y(t) = C x(t) \tag{3.7b}$$

$$y_m(t) = C_m x(t) \tag{3.7c}$$

$$\mathfrak{B} x(t) = u(t) \tag{3.7d}$$

where $x(t, \cdot) \in \mathcal{H} = \mathcal{L}^2(0, 1)^3$ is the state variables, $y(t) \in \Re$ is the output variable, $y_m(t) \in \Re$ is the measured variable and $u(t) \in \Re$ is the input variable. The spatial operator $\mathfrak{A}$ is a linear operator with the following domain $\mathcal{D}(\mathfrak{A}) = \left\{h(z) \in \mathcal{L}^2(0, 1)^3 | h(z) \text{ is abs. cont., and } \dfrac{dh(z)}{dz} \in \mathcal{L}^2(0, 1)^3\right\}$, $\mathfrak{B} \in \mathfrak{L}(\mathcal{H}, \Re)$ is a linear boundary operator, $\bar{B}_d \in \mathfrak{L}(\Re, \mathcal{H})$ is a linear disturbance location operator, $C \in \mathfrak{L}(\mathcal{H}, \Re)$ is the output operator and $C_m \in \mathfrak{L}(\mathcal{H}, \Re)$ is

the measure input operator. Therefore, for the counter current configuration:

$$\mathfrak{A} = \begin{bmatrix} -\nu_1\partial_\zeta - h_1 & h_1 & 0 \\ h_2 & \nu_2\partial_\zeta - h_2 & 0 \\ 0 & 0 & -\mu\,\partial_\zeta \end{bmatrix} \tag{3.8a}$$

$$C\Psi(\zeta) = \Psi_2(\zeta = 0)\,, C_m\Psi(\zeta) = \Psi_2(\zeta = z_m)\,, \mathfrak{B}\Psi(\zeta) = \Psi_1(\zeta = 0) \tag{3.8b}$$

and for the parallel configuration one obtains:

$$\mathfrak{A} = \begin{bmatrix} -\nu_1\partial_\zeta - h_1 & h_1 & 0 \\ h_2 & -\nu_2\partial_\zeta - h_2 & 0 \\ 0 & 0 & -\mu\,\partial_\zeta \end{bmatrix} \tag{3.9a}$$

$$C\Psi(\zeta) = \Psi_2(\zeta = 1)\,, C_m\Psi(\zeta) = \Psi_2(\zeta = z_m)\,, \mathfrak{B}\Psi(\zeta) = \Psi_1(\zeta = 0) \tag{3.9b}$$

where $\partial_\zeta(\cdot)$ is the linear differential operator $\dfrac{\partial(\cdot)}{\partial\zeta}$ and $\Psi(\zeta) = [\Psi_1(\zeta)\,\Psi_2(\zeta)\,\Psi_3(\zeta)]^T$ is a vector of three spatial functions, while $B_d(\zeta)$ and $\bar{B}_d(\zeta)$ for both configurations are defined as:

$$\bar{B}_d(\zeta) = \begin{bmatrix} B_d(\zeta) \\ B_d(\zeta) \\ 0 \end{bmatrix}, \qquad B_d(\zeta) = \begin{cases} 0, \zeta\langle 0.4 \\ 1, 0.4 \leq \zeta \leq 0.6 \\ 0, 0.6\langle\zeta \end{cases} \tag{3.10a}$$

Physically the disturbance can be seen as a heat source that is constantly adding heat to the heat exchanger. In general, one can consider any location along the domain and the analysis and results can be adequately adjusted to account for any disturbance placement and/or type. Furthermore, these configurations can be represented as regular well-defined distributed parameter system [80] by:

$$\dot{x}(t) = \mathfrak{A}x(t) + \bar{B}_d d(t), x_0 \in H \tag{3.11a}$$

$$y(t) = C_\Lambda x(t) \tag{3.11b}$$

$$y_m(t) = C_{m,\Lambda} x(t) \tag{3.11c}$$

$$\mathfrak{B}x(t) = u(t) \tag{3.11d}$$

where $C_\Lambda \in \mathfrak{L}(\mathcal{H}, \Re)$ and $C_{m,\Lambda} \in \mathfrak{L}(\mathcal{H}, \Re)$ are the Λ-extension of the operators C and C_m, and are defined as $C_\Lambda x(t) = \lim_{\lambda\to+\infty} C\lambda(\lambda I - A)^{-1}x(t)$, $C_{m,\Lambda}x(t) = \lim_{\lambda\to+\infty} C_m\lambda(\lambda I - A)^{-1}x(t)$, $x(t) \in \mathcal{H}$. Throughout this work, the following exogenous system as a integral part of the regulator design is considered. The

importance of exogenous system is that it generates desired output signal tracking signal and also accounts for the generation of the family of considered disturbances. In particular, the exogenous system accounts for generation of polynomial and harmonic reference and/or disturbance signals, and is given as:

$$\begin{aligned} \dot{v}(t) &= Sv(t), \quad v(0) = v_0 && (3.12) \\ y_r(t) &= Qv(t) && (3.13) \\ d(t) &= Fv(t) && (3.14) \end{aligned}$$

where the matrix S is spectral and generates dynamics of the exosystem states, Q is a matrix that gives the desired output tracking signal $y_r(t)$ and F is the matrix that generates disturbance dynamics. In this manuscript, the tracking reference signals are given as family of steps, ramps and harmonic periodic functions. Hence, for these functions the proper exosystem is given by:

$$S = \begin{bmatrix} 0 & 1 & 0 & 0 \\ 0 & 0 & 0 & 0 \\ 0 & 0 & 0 & \alpha \\ 0 & 0 & -\alpha & 0 \end{bmatrix} \tag{3.15}$$

Q is defined accordingly with the desired tracking signals characteristics and F is associated with the disturbance step signal. Finally, the important formulation of tracking error used in the design is given as:

$$e(t) = y(t) - y_r(t) \tag{3.16}$$

which implies that output regulator design needs to ensure $e(t) \to 0$ as $t \to \infty$.

3.2.1 Spectral Properties of the System

The underlying dynamical system which is given by the operator $\mathfrak{A}$ in (3.11a) represents a system of heterodirectional coupled hyperbolic PDEs, with boundary and in domain coupling. In general, a scalar hyperbolic PDEs or homodirectional system of hyperbolic PDEs without boundary coupling is characterized with the empty spectrum and ultimate dynamical stability on the finite spatial domain, hence it is of importance to address the operator $\mathfrak{A}$ features

in the light of the intrinsic stability of the operator and/or spectral operator properties. It can be shown that $\mathfrak{A}$ is a spectral operator and the eigenvalues and eigenfunctions of $\mathfrak{A}$ can be found by solving the corresponding eigenvalue problem given as:

$$\mathfrak{A}\phi = \lambda\phi \tag{3.17}$$

where ϕ correspond to the eigenfunctions of the system and λ the corresponding eigenvalues. The operator shown in (3.17) can be written as $\mathfrak{A} = V\partial_\zeta + \hat{A}$, where V is a diagonal matrix with the system velocities and $\hat{A}$ is a matrix that contains the system constants, defined in Eq. (3.18), where the sign of ν_2 depends on the heat exchanger configuration.

$$V = \begin{bmatrix} -\nu_1 & 0 & 0 \\ 0 & \pm\nu_2 & 0 \\ 0 & 0 & -\mu \end{bmatrix} \quad \hat{A} = \begin{bmatrix} -h_1 & h_1 & 0 \\ h_2 & -h_2 & 0 \\ 0 & 0 & 0 \end{bmatrix} \tag{3.18}$$

The eigenvalue problem for the error operator is given as:

$$\mathfrak{A}\phi = (V\partial_\zeta + \hat{A})\phi = \lambda\phi, \tag{3.19}$$

for $\phi = \begin{bmatrix} \phi_1 \\ \phi_2 \\ \phi_3 \end{bmatrix}$ which belongs to domain of $\mathfrak{A}$, which can be written as $\partial_\zeta\phi = V^{-1}(\lambda I - \hat{A})\phi$ and has a general solution given as:

$$\phi(\zeta) = M(\zeta)\phi(\zeta = 0) \tag{3.20}$$

where $M(\zeta)$ is the matrix exponential of $V^{-1}(\lambda I - \hat{A})$ and is given as:

$$M(\zeta) = \mathrm{e}^{V^{-1}(\lambda I - \hat{A})\zeta} = \begin{bmatrix} M_{1,1}(\zeta) & M_{1,2}(\zeta) & 0 \\ M_{2,1}(\zeta) & M_{2,2}(\zeta) & 0 \\ 0 & 0 & M_{3,3}(\zeta) \end{bmatrix}$$

$$M_{1,1}(\zeta) = \mathrm{e}^{\frac{a}{2}\zeta}\left[\cosh\left(\tfrac{b}{2}\zeta\right) + \frac{\left(\frac{a}{2} - \frac{h_2+\lambda}{\nu_2}\right)\sinh\left(\frac{b}{2}\zeta\right)}{\frac{b}{2}}\right]$$

$$M_{1,2}(\zeta) = \tfrac{h_1}{\nu_1}\mathrm{e}^{\frac{a}{2}\zeta}\tfrac{\sinh\left(\frac{b}{2}\zeta\right)}{\frac{b}{2}}$$

$$M_{2,2}(\zeta) = \mathrm{e}^{\frac{a}{2}\zeta}\left[\cosh\left(\tfrac{b}{2}\zeta\right) + \frac{\left(\frac{a}{2} + \frac{h_1+\lambda}{\nu_1}\right)\sinh\left(\frac{b}{2}\zeta\right)}{\frac{b}{2}}\right] \tag{3.21}$$

$$M_{2,1}(\zeta) = -\tfrac{h_2}{\nu_2}\mathrm{e}^{\frac{a}{2}\zeta}\tfrac{\sinh\left(\frac{b}{2}\zeta\right)}{\frac{b}{2}}$$

$$a = -\left(\tfrac{h_1+\lambda}{\nu_1} - \tfrac{h_2+\lambda}{\nu_2}\right)$$

$$b = \sqrt{\left(\tfrac{h_1+\lambda}{\nu_1} - \tfrac{h_2+\lambda}{\nu_2}\right)^2 + \tfrac{4\lambda(\lambda+h_1+h_2)}{\nu_1\nu_2}}$$

$$M_{3,3}(\zeta) = \mathrm{e}^{-\frac{\lambda}{\mu}\zeta}$$

Using the boundary conditions:

$$\begin{cases} \phi_1(\zeta = 0) = 0 \\ \phi_2(\zeta = 1) = -k\,\phi_3(\zeta = 1) \\ \phi_3\ (\zeta = 0) = \phi_1(\zeta = 1) \end{cases} \tag{3.22}$$

The spectral set for this system $\sigma(\mathfrak{A}) = \{\lambda_1, \lambda_2, ...\}$ with $\lambda_i \in \mathbb{C}$, where $\mathbb{C}$ represents the set of complex numbers, is given by the solution of the following non-linear algebraic equation:

$$\left[\cosh\left(\frac{b}{2}\right) + \frac{\left(\frac{a}{2} + \frac{h_1+\lambda}{\nu_1}\right)\sinh\left(\frac{b}{2}\right)}{\frac{b}{2}}\right] = -k\frac{h_1}{\nu_1}\frac{\sinh\left(\frac{b}{2}\right)}{\frac{b}{2}}\mathrm{e}^{-\frac{\lambda}{\mu}} \tag{3.23}$$

with a and b given in (3.21). The eigenvalue problem can also be solved for the parallel configuration and has the same general solution as given in (3.20). With the boundary conditions:

$$\begin{cases} \phi_1(\zeta = 0) = 0 \\ \phi_2(\zeta = 0) = -k\,\phi_3(\zeta = 1) \\ \phi_3\ (\zeta = 0) = \phi_1(\zeta = 1) \end{cases} \tag{3.24}$$

And exponential matrix given as:

$$M(\zeta) = \mathrm{e}^{V^{-1}(\lambda I - \hat{A})\zeta} = \begin{bmatrix} M_{1,1}(\zeta) & M_{1,2}(\zeta) & 0 \\ M_{2,1}(\zeta) & M_{2,2}(\zeta) & 0 \\ 0 & 0 & M_{3,3}(\zeta) \end{bmatrix}$$

$$M_{1,1}(\zeta) = \mathrm{e}^{\frac{a}{2}\zeta}\left[\cosh\left(\tfrac{b}{2}\zeta\right) + \frac{\left(\frac{a}{2} + \frac{h_2+\lambda}{\nu_2}\right)\sinh\left(\frac{b}{2}\zeta\right)}{\frac{b}{2}}\right]$$

$$M_{1,2}(\zeta) = \frac{h_1}{\nu_1}\mathrm{e}^{\frac{a}{2}\zeta}\frac{\sinh\left(\frac{b}{2}\zeta\right)}{\frac{b}{2}}$$

$$M_{2,2}(\zeta) = \mathrm{e}^{\frac{a}{2}\zeta}\left[\cosh\left(\tfrac{b}{2}\zeta\right) + \frac{\left(\frac{a}{2} + \frac{h_1+\lambda}{\nu_1}\right)\sinh\left(\frac{b}{2}\zeta\right)}{\frac{b}{2}}\right] \tag{3.25}$$

$$M_{2,1}(\zeta) = \frac{h_2}{\nu_2}\mathrm{e}^{\frac{a}{2}\zeta}\frac{\sinh\left(\frac{b}{2}\zeta\right)}{\frac{b}{2}}$$

$$a = -\left(\frac{h_1+\lambda}{\nu_1} + \frac{h_2+\lambda}{\nu_2}\right)$$

$$b = \sqrt{\left(\frac{h_1+\lambda}{\nu_1} + \frac{h_2+\lambda}{\nu_2}\right)^2 - \frac{4\lambda(\lambda+h_1+h_2)}{\nu_1\nu_2}}$$

$$M_{3,3}(\zeta) = \mathrm{e}^{-\frac{\lambda}{\mu}\zeta}$$

And the spectral set for this system $\sigma(\mathfrak{A}) = \{\lambda_1, \lambda_2, ...\}$ with $\lambda_i \in \mathbb{C}$ is given by the solution of:

$$k\frac{h_1}{\nu_1}\frac{\sinh\left(\frac{b}{2}\right)}{\frac{b}{2}}\mathrm{e}^{\frac{a}{2}-\frac{\lambda}{\mu}} = -1 \tag{3.26}$$

with a and b given in (3.25). In the ensuing sections, we will consider a set of parameters so that the underlying $\mathfrak{A}$ is unstable with finite number of unstable eigenvalues.

The eigenvalue problem solution shown in (3.17) for different values of the boundary feedback gain k gives the spectral eigenvalue distribution of two heat exchanger configurations and it is shown in Figure 3.2. It is possible to see that the system becomes unstable as the value of k increases, as the eigenvalues are shifted to the right complex plane. For the conditions used, $k = 2$ results in one pair of unstable complex eigenvalues and $k = 2.5$ results in two pairs. The results for the parallel configuration are very similar to the countercurrent, as $k = 2$ results in one pair of unstable complex eigenvalues and $k = 2.5$ results in two pairs.

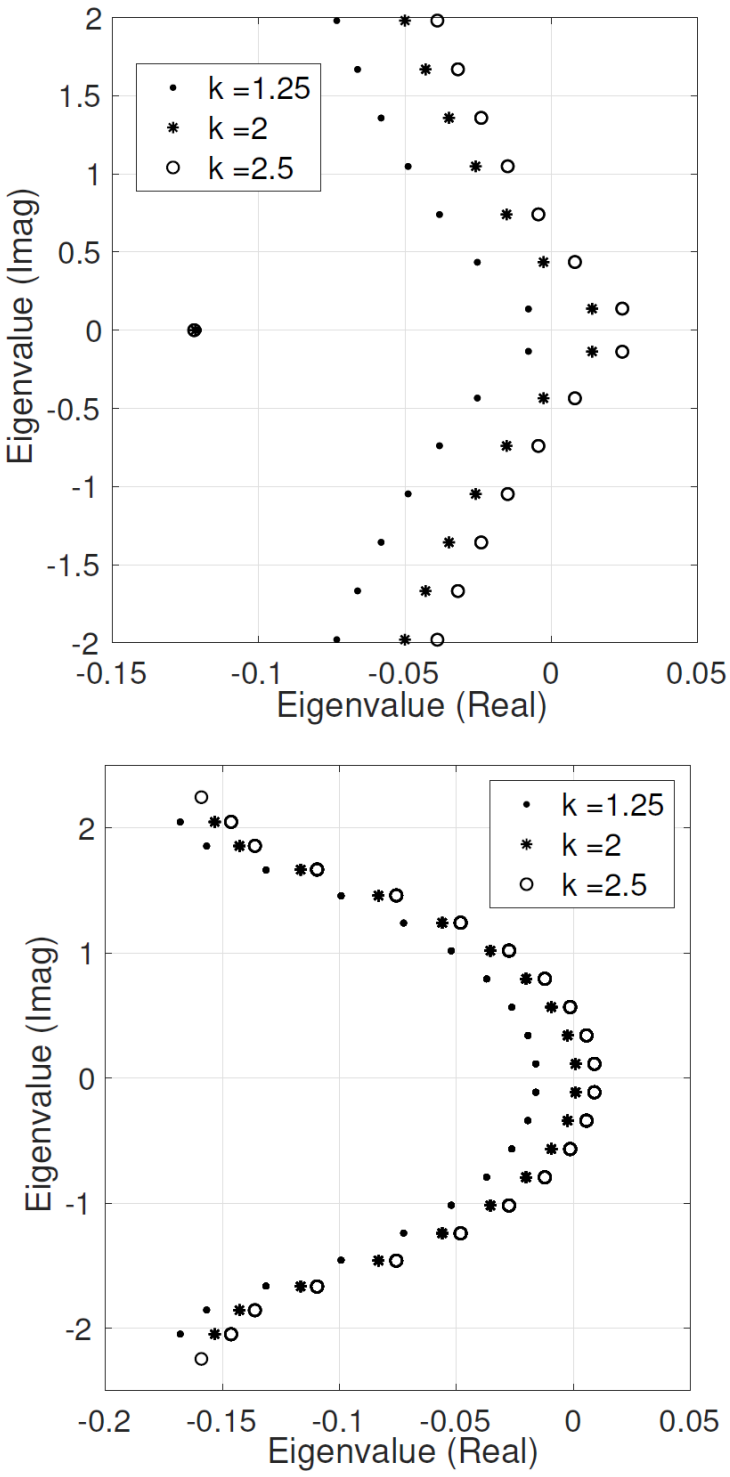

Figure 3.2: Calculated eigenvalues for different values of the boundary feedback gain k: (Top) counter current configuration; (Bottom) parallel configuration.

3.2.2 Boundary Control Transformation

Along the line of the well-posed system description and associate controller design we consider the following state transformation, which converts the unbounded boundary control input operator into a corresponding in-domain operator:

$$p(t) = x(t) + \beta u(t) \tag{3.27}$$

and the system can be rewritten as:

$$\begin{aligned} \dot{p}(t) &= \dot{x}(t) + \beta\dot{u}(t) = \mathfrak{A}x(t) + \beta\dot{u}(t) + B_d d(t) \\ &= Ap(t) + \mathfrak{A}\beta u(t) + \beta\dot{u}(t) + B_d d(t) \end{aligned} \tag{3.28a}$$

$$y(t) = C_\Lambda x(t) = C_\Lambda p(t) - C_\Lambda \beta u(t) \tag{3.28b}$$

In general, in order to decouple states one needs to find β such as $\mathfrak{A}\beta = 0$ and $\mathfrak{B}p(t) = 0$, so that the above system can be reduced and represented as:

$$\begin{cases} \dot{p}(t) = Ap(t) + \beta\dot{u}(t) + B_d d(t) \\ p(\zeta = 0, t) = 0 \end{cases} \tag{3.29a}$$

$$y(t) = C_\Lambda p(t) - C_\Lambda \beta u(t) = \underbrace{[-C_\Lambda\beta \; C_\Lambda]}_{C_\Lambda^e} \begin{bmatrix} u(t) \\ p(t) \end{bmatrix} \tag{3.29b}$$

where A has the same elements as in (3.8a) and (3.9a), but its first boundary condition is defined as $\theta_1(\zeta = 0) = 0$. The system can be represented as the following state space form:

$$\begin{bmatrix} \dot{u}(t) \\ \dot{p}(t) \end{bmatrix} = \underbrace{\begin{bmatrix} 0 & 0 \\ 0 & A \end{bmatrix}}_{A^e} \underbrace{\begin{bmatrix} u(t) \\ p(t) \end{bmatrix}}_{x^e} + \underbrace{\begin{bmatrix} 1 \\ \beta \end{bmatrix}}_{B^e} \dot{u}(t) + \underbrace{\begin{bmatrix} 0 \\ B_d \end{bmatrix}}_{B_d^e} d(t) \tag{3.30}$$

where $\dot{u}(t)$ is the new manipulated variable and the manipulated boundary input was changed to a correspondent in-domain input.

3.3 Regulator Design

In this section, the regulator design is proposed and the methodology necessary to guarantee simultaneous stabilization and proper output tracking for the system is explained. First, we consider the design of stabilizing full state feedback gain based control law. Secondly, motivated with technical limitations to measure full state of the temperature along the heat exchanger system,

we design a boundary observer which is utilized in the state reconstruction. Finally, we construct the output regulation equations in the form of the Sylvester equation which provides a solution to the feedforward gains deployed in the output regulation and tracking as well as disturbance rejection.

3.3.1 System Stabilization with Output Feedback

The simplest possible way to consider stabilization of the heat exchanger is to apply gain based output feedback $u(t) = Ky(t)$. Then, the eigenvalue problem (3.17) for a output feedback control law, shown in (3.31):

$$u(t) = Ky(t) \tag{3.31}$$

induces the following form of the boundary condition for both (3.22) and (3.24) configurations:

$$\phi_1(\zeta = 0) = u(t) = KC_\Lambda \phi \tag{3.32}$$

where C_Λ is the output operator defined in (3.11b) regarding (3.8b) and (3.9b). For the counter-current configuration ($\phi_1(\zeta = 0) = KC\phi = K\phi_2(\zeta = 0)$) the spectral set of $\sigma(\mathfrak{A})$ is the solution of:

$$\begin{aligned} -K\frac{h_2}{\nu_2}\frac{\sinh\left(\frac{b}{2}\right)}{\frac{b}{2}} - \left[\cosh\left(\frac{b}{2}\right) + \frac{\left(\frac{a}{2} + \frac{h_1+s}{\nu_1}\right)\sinh\left(\frac{b}{2}\right)}{\frac{b}{2}}\right] - k\frac{h_1}{\nu_1}\frac{\sinh\left(\frac{b}{2}\right)}{\frac{b}{2}}\mathrm{e}^{-\frac{s}{\mu}} \\ +kK\left[\cosh\left(\frac{b}{2}\right) + \frac{\left(\frac{a}{2} - \frac{h_2+s}{\nu_2}\right)\sinh\left(\frac{b}{2}\right)}{\frac{b}{2}}\right]\mathrm{e}^{-\frac{\lambda}{\mu}} = 0 \end{aligned} \tag{3.33}$$

with a and b defined at (3.21).

And for the parallel system ($\phi_1(\zeta = 0) = KC_\Lambda\phi = K\phi_2(\zeta = 1)$) spectral set

is given by:

$$
\begin{aligned}
&K\frac{h_2}{\nu_2}\frac{\sinh\left(\frac{b}{2}\right)}{\frac{b}{2}} - k\frac{h_1}{\nu_1}\frac{\sinh\left(\frac{b}{2}\right)}{\frac{b}{2}}\mathrm{e}^{-\frac{\lambda}{\mu}} \\
&- kK\mathrm{e}^{\frac{a}{2}}\left[\cosh\left(\frac{b}{2}\right) + \frac{\left(\frac{a}{2}+\frac{h_2+\lambda}{\nu_2}\right)\sinh\left(\frac{b}{2}\right)}{\frac{b}{2}}\right] \\
&\left[\cosh\left(\frac{b}{2}\right) + \frac{\left(\frac{a}{2}+\frac{h_1+\lambda}{\nu_1}\right)\sinh\left(\frac{b}{2}\right)}{\frac{b}{2}}\right]\mathrm{e}^{-\frac{\lambda}{\mu}} \\
&+ kK\frac{h_1}{\nu_1}\frac{h_2}{\nu_2}\mathrm{e}^{\frac{a}{2}-\frac{\lambda}{\mu}}\left(\frac{\sinh\left(\frac{b}{2}\right)}{\frac{b}{2}}\right)^2 = \mathrm{e}^{-\frac{a}{2}}
\end{aligned}
\tag{3.34}
$$

and a and b defined at (3.25). It will be clear, in the ensuing sections that parameter K can not ensure stability of the closed-loop system (in both configurations), since the spectral properties of the overall system remain invariant with respect to gain modulation in the output feedback structure.

The eigenvalue problem solution for (3.17) with the boundary condition shown in (3.32) gives the results shown in Figure 3.3. For both configurations the gain based output feedback control (that is $u(t) = Ky(t)$) is not able to stabilize the system, as the input is not able to shift all the unstable complex pair to the left plane. In Figure 3.3 (Top), for the counter current configuration, the output feedback is just able to shift the eigenvalues that are real and has almost no influence exerted to the complex eigenvalues (the complex eigenvalues do not change for different values of gain). As the output feedback gain is changed ($K = [-10 : 10]$), the real part of the unstable eigenvalue is barely changed, as shown in the left subplot. For the parallel configuration, the output feedback has influence on entire spectrum, but it is not possible to find a stabilizing gain that guarantees that all the spectrum will be placed to the interior of left complex plane. The right subplot in Figure 3.3 shows that as the output feedback gain changes, there is always at least one unstable eigenvalue pair in the system. Therefore, it is not possible to guarantee stability for the system using the gain based output feedback.

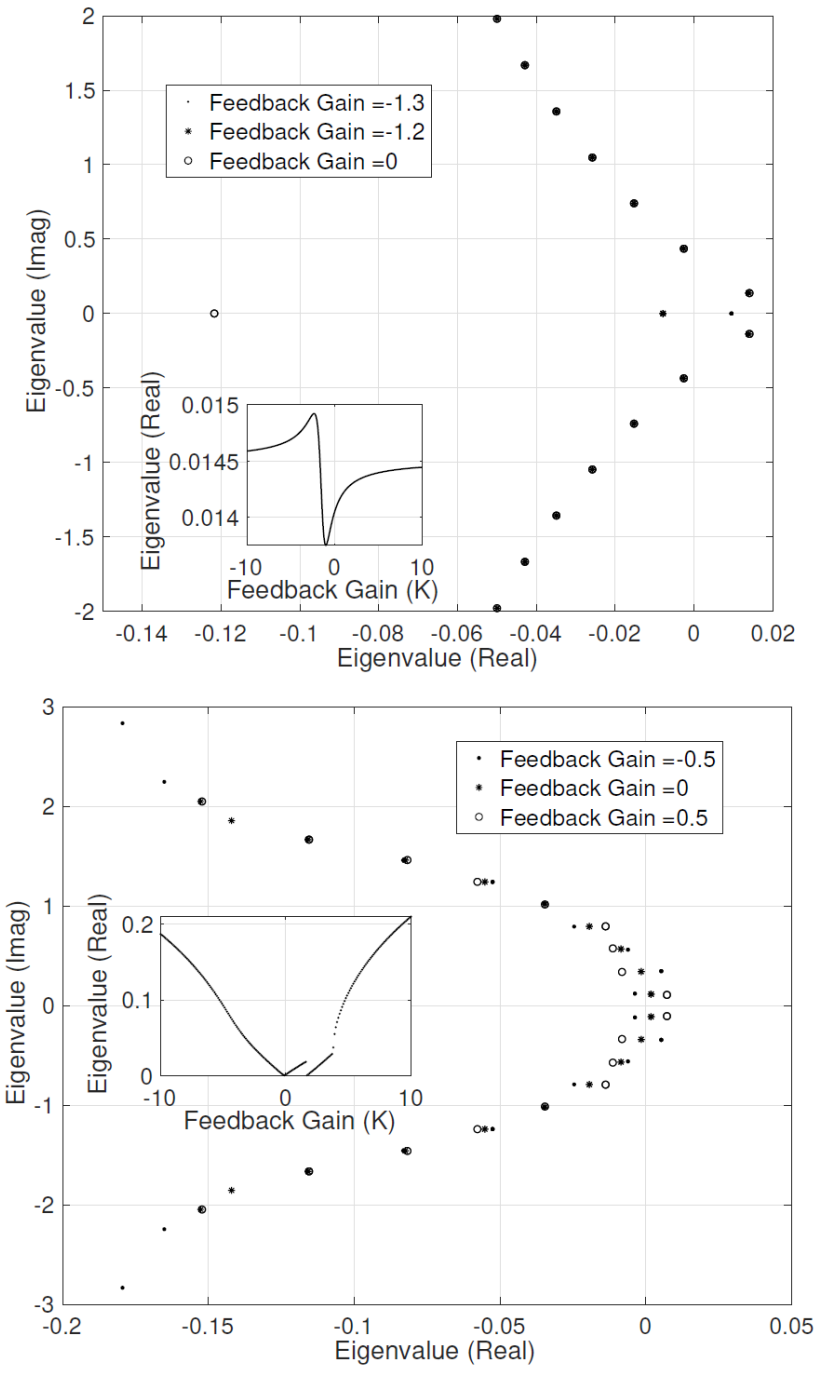

Figure 3.3: Calculated eigenvalues for different values of the feedback gain K in: (Top) counter current configuration; (Bottom) parallel configuration.

The simulation results using an output feedback with the feedback gain $K = -1.2$ in the counter current configuration are shown in Figure 3.4, and as expected, the system is unstable and the output grows exponentially.

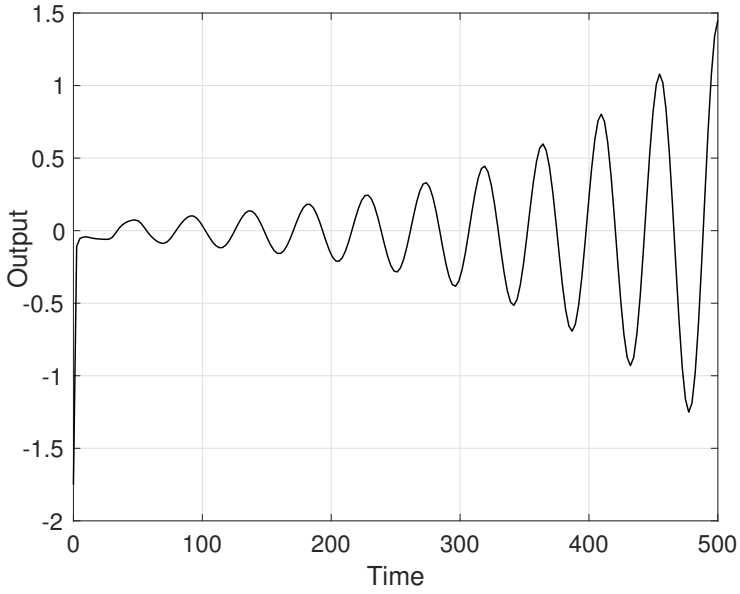

Figure 3.4: System output response with feedback gain $K = -1.2$.

3.3.2 Full-state feedback control

In this section, a full-state feedback controller design is considered as the initial step in system stabilization. The closed-loop schematic representation for this scenario is shown in Figure 3.5 and it is considered that all state variables are available for design and for implementation (which means that we assume that infinite dimensional states are available and can be directly measured).

The fundamental characteristic of dissipative spectral systems is that the system eigenspectrum can be separated in finite dimensional unstable state (X_U), and stable infinite dimensional state space complement (X_S), which are related to the corresponding eigenfunctions (ϕ_i), adjoint eigenfunctions (ψ_i) and eigenvalues (λ_i):

$$\begin{array}{rcl} X_U & = & \{\psi_1, \psi_2, ..., \psi_n\} \\ X_S & = & \{\psi_{n+1}, \psi_{n+2}, ..., \psi_\infty\} \end{array} \tag{3.35}$$

where n is the number of unstable eigenfunctions (associated with a set of unstable eigenvalues). The following theorem is used to guarantee the system closed loop stability:

Theorem 3.1 *Given a system* $\dot{x} = Ax + Bu$, $x \in X$ *and* $B \in \mathbb{L}(\mathbb{C}, X)$, *and if the following holds:*

- X_U *is finite dimensional*
- $\mathcal{T}(t)X_U \subset X_S$, $\tau(t)X_S \subset X_S$, *given* $X = X_U \oplus X_S$
- *The unstable part of the system,* X_U, *is controllable*

then the $(A + BK)$ *generates an exponentially stable semigroup* $\mathcal{T}(t)$.

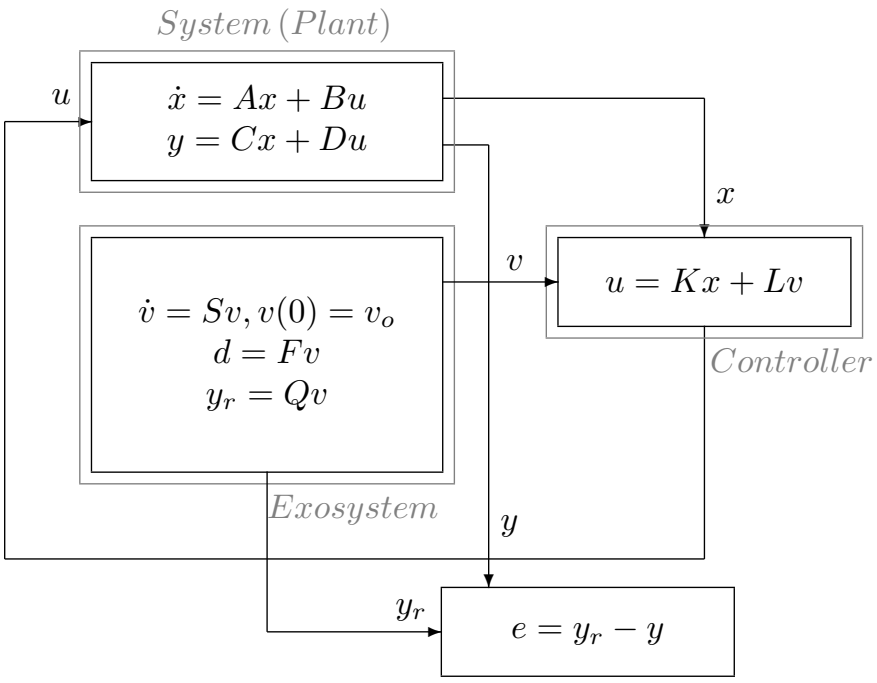

Figure 3.5: Closed system representation using a full-state feedback.

Proof: The first condition is satisfied by analyzing the eigenvalue distribution shown in Figure 3.2, as the value of k was chosen such that the system has only a pair of unstable eigenvalues. The second and third conditions can be proved by analyzing the dynamics of the unstable eigenmodes, which are the conjugated complex of each other:

$$X_U = \{\psi_1, \psi_2\} \rightarrow \lambda_1 = \bar{\lambda}_2 \rightarrow \psi_1 = \bar{\psi}_2 \tag{3.36}$$

$$\dot{X}_U(t) = A_U X_U(t) + B_U u(t) = \begin{bmatrix} \alpha + j\beta & 0 \\ 0 & \alpha - j\beta \end{bmatrix} X_U(t) + B_U u(t) \quad (3.37)$$

where $B_U = \begin{bmatrix} b_{U,1} \\ \bar{b}_{U,1} \end{bmatrix}$, with $b_{U,1} = \langle B, \psi_1 \rangle$. Thus, it is easy to see that the pair (A_U, B_U) is controllable. If (A_U, B_U) is controllable, then there is a K such that $(A_U + B_U K)$ is stable. Then, for any $x \in X_U$, $\mathcal{T}(t)x \in X_S$, where $\mathcal{T}(t)$ is the closed-loop semigroup.

The appropriate value of K for the full-state control law is derived below. Using the state transformation $W = T^{-1}X$, we get the following system:

$$\dot{W}_U(t) = \bar{A}_U W_U(t) + \bar{B}_U u(t) \quad (3.38)$$

with:

$$T = \begin{bmatrix} \frac{1}{2} & -\frac{1}{2}j \\ \frac{1}{2} & \frac{1}{2}j \end{bmatrix}, \bar{A}_U = \begin{bmatrix} \alpha & \beta \\ -\beta & \alpha \end{bmatrix}, \bar{B}_U = T^{-1} \begin{bmatrix} \langle B, \psi_1 \rangle \\ \langle B, \bar{\psi}_1 \rangle \end{bmatrix} \quad (3.39)$$

which yields the following control law:

$$u(t) = -K W_U(t) \quad (3.40)$$

that leads to the following equation:

$$\dot{W}_U(t) = \left[\bar{A}_U - \bar{B}_U K\right] W_U(t) \quad (3.41)$$

and it is possible to find values for K that makes subsystem $\left[\bar{A}_U - \bar{B}_U K\right]$ stable and therefore, the entire system is stabilized in exponential manner. The stabilizing final control law is given by:

$$u(t) = -\bar{K}(X(t)) = -K T^{-1} \langle X(t), \psi_U \rangle \quad (3.42)$$

where $\bar{K}$ is an operator that acts on the full-state of the system. Along the same line, the same procedure could be utilized to design pole placement controller if more unstable eigenvalue pairs are considered.

Figure 3.6 shows results associated with deployment of the full state feedback control law presented in Eq.(3.42), and as it can be demonstrated the exponential stabilization is achieved with some oscillations which are associated

with the transients related to initial conditions response contribution. Therefore, once the stabilization of unstable dynamics is guaranteed, it is possible to implement an output tracking design for the system.

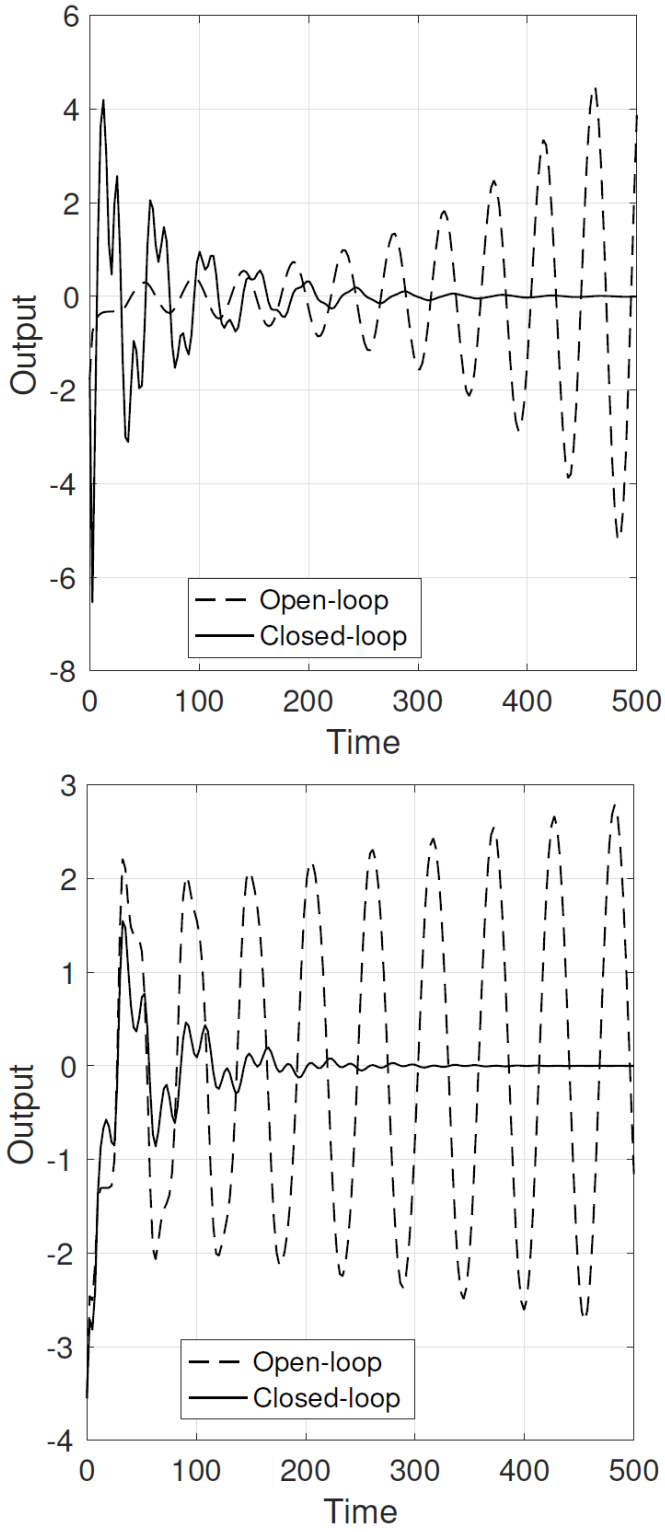

Figure 3.6: System stabilization with fullstate feedback: (Top) counter current configuration; (Bottom) parallel configuration.

3.3.3 Observer Stability

The results of the previous section imply that the full state feedback control law is utilized for the stabilization purposes. However, this is simply not feasible and possible in any realistic application and/or setting. Therefore, the way to address this problem is to use an observer to reconstruct the state variables information by considering the output measurement and having in mind that the heat exchanger outlet is only available output measurement. The reconstructed states $\hat{x}$ dynamics associated with the heat exchanger system is the copy of the system model dynamics and takes into account information given by the output in affine manner. The type of the Luenberger observer design considered here has the form given as:

$$\dot{\hat{x}}(t) = A\hat{x}(t) + Bu(t) + B_d d(t) + \gamma C(x(t) - \hat{x}(t))(t) \tag{3.43}$$

Hence, by considering the general representation of the system:

$$\begin{array}{l} \dot{x}(t) = Ax(t) + Bu(t) + B_d d(t) \\ y(t) = Cx(t) \end{array} \tag{3.44}$$

and by subtracting these equations, one can define the observer error as $\hat{e}(t) = x(t) - \hat{x}(t)$:

$$\dot{\hat{e}}(t) = (A - \gamma C_m)\hat{e}(t), \quad \hat{e}(0) \neq 0; \tag{3.45}$$

Therefore, the observer stability depends on the choice of observer gain γ. We emphasize that the observer gain is spatial operator which is given as $\gamma = [\ \ell \quad \ell \quad \ell\ ]^T$. This choice of the observer gain means that the same constant observer gain is used throughout the system (there is no spatial variation, although it could be considered). In order to guarantee the observer stability, it is necessary to choose a ℓ such that observer error (shown in (3.45)) is stable. The analysis of the observer error dynamics can be used to achieve this goal. The operator shown in (3.8a) and (3.9a) can be written as $\mathfrak{A} = V\partial_\zeta + \hat{A}$, where V is a diagonal matrix with the system velocities and $\hat{A}$ is a matrix that contains the system constants. The eigenvalue problem for the error operator is given as:

$$(\mathfrak{A} - \gamma C_m)\phi = (V\partial_\zeta + \hat{A} - \gamma C_m)\phi = \lambda\phi, \tag{3.46}$$

for $\phi = [\ \phi_1 \quad \phi_2 \quad \phi_3\ ]^T$ belonging to the domain of $\mathfrak{A}$. This equation can be written as:

$$\partial_\zeta \phi = V^{-1}(\lambda I - \hat{A})\phi + V^{-1}\gamma C_m \phi = \underbrace{V^{-1}(\lambda I - \hat{A})}_{A^*}\phi + V^{-1}\gamma\phi_2(\zeta = \zeta_m) \quad (3.47)$$

where ζ_m is the given output location. Hence, the general solution is given as:

$$\begin{aligned} \phi(\zeta) &= M(\zeta)\phi(\zeta = 0) + \phi_2(\zeta = \zeta_m)\int_0^\zeta M(\zeta - \eta)V^{-1}\gamma d\eta \\ &= M(\zeta)\phi(\zeta = 0) + \phi_2(\zeta = \zeta_m)\underbrace{A^{*-1}[M(\zeta) - I]V^{-1}\gamma}_{B^*(\zeta)} \end{aligned} \quad (3.48)$$

where $M(\zeta)$ is the matrix exponential of A^* (the same matrix defined in (3.21) and (3.25)) and $B^*(\zeta) = [B_1^*(\zeta)\, B_2^*(\zeta)\, B_3^*(\zeta)]^T$. For the counter current configuration, the boundary conditions are the same as given in (3.22) and are used to find $\phi(\zeta = 0)$:

$$\phi(\zeta=0)=\begin{bmatrix} 0 \\ -\phi_2(\zeta=\zeta_m)\dfrac{[B_2^*(\zeta=1)+kB_3^*(\zeta=1)+kM_{3,3}(\zeta=1)B_1^*(\zeta=1)]}{M_{2,2}(\zeta=1)+M_{1,2}(\zeta=1)M_{3,3}(\zeta=1)\,k} \\ -\phi_2(\zeta=\zeta_m)\dfrac{[B_2^*(\zeta=1)M_{1,2}(\zeta=1)+kB_3^*(\zeta=1)M_{1,2}(\zeta=1)-M_{2,2}(\zeta=1)B_1^*(\zeta=1)]}{M_{2,2}(\zeta=1)+M_{1,2}(\zeta=1)M_{3,3}(\zeta=1)\,k} \end{bmatrix} \tag{3.49}$$

where $M_{i,j}(\zeta)$ are the elements (functions of ζ) of the exponential matrix (given in (3.21)). By evaluating the solution at $\zeta = \zeta_m$ the following result is obtained for $\phi_2(\zeta)$:

$$\begin{aligned}\phi_2(\zeta = \zeta_m) = &-M_{2,2}(\zeta = \zeta_m)\phi_2(\zeta = \zeta_m) \\ &\frac{[B_2^*(\zeta = 1) + kB_3^*(\zeta = 1) + kM_{3,3}(\zeta = 1)B_1^*(\zeta = 1)]}{M_{2,2}(\zeta = 1) + M_{1,2}(\zeta = 1)M_{3,3}(\zeta = 1)\,k} \\ &+ \phi_2(\zeta = \zeta_m)B_2^*(\zeta = \zeta_m)\end{aligned} \tag{3.50}$$

Which leads to the following non-linear equation:

$$\begin{aligned}1 + M_{2,2}(\zeta = \zeta_m)&\frac{[B_2^*(\zeta = 1) + kB_3^*(\zeta = 1) + kM_{3,3}(\zeta = 1)B_1^*(\zeta = 1)]}{M_{2,2}(\zeta = 1) + M_{1,2}(\zeta = 1)M_{3,3}(\zeta = 1)\,k} \\ &- B_2^*(\zeta = \zeta_m) = 0\end{aligned} \tag{3.51}$$

Notice that $M(\zeta)$ is a function of λ, which also makes $B^*(\zeta)$ not only a function of ℓ (the observer gain) but also of λ. If λ is set as $\lambda = 0 + \alpha j$ (where $j = \sqrt{-1}$ and $\alpha \in \Re$), the Eq.(3.51) can be solved for ℓ. As the system is unstable, setting $\ell = 0$ will result in an unstable observer. Therefore, the value of ℓ found in (3.51) by setting $\lambda = 0 + \alpha j$ gives the value of gain ℓ for the case of observer marginal stability (the eigenvalues cross the imaginary axes at this ℓ). Figure 3.7 (Top) shows the eigenvalues behaviour for different values of ℓ. As the value of ℓ is increased, the unstable pair of eigenvalues are shifted to the left side of the complex plan, however as ℓ increases one pair of stable eigenvalues are shifted to the right side which makes system unstable again. Therefore, there is a stability region for the values of gain ℓ for this observer gain design and the values of ℓ for these stability regions can be calculated by considering Eq.(3.51).

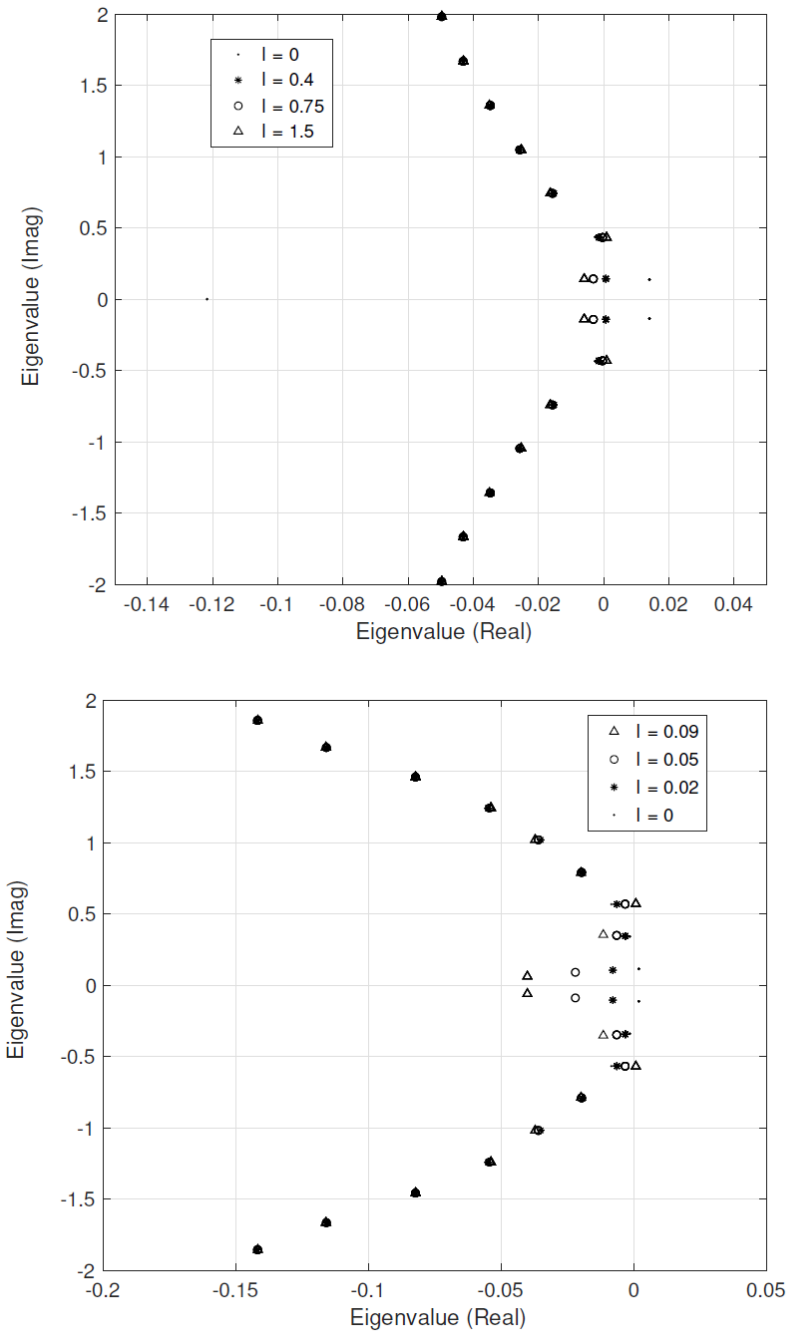

Figure 3.7: Calculated eigenvalues of the observer for different values of the observer gain ℓ: (Top) counter current configuration; (Bottom) parallel configuration.

The same procedure is done with the parallel configurations using the

boundary conditions given by Eq.(3.24) and the $\phi(\zeta = 0)$ is given as:

$$\phi(\zeta = 0) = \begin{bmatrix} 0 \\ -k\phi_2(\zeta = \zeta_m)\dfrac{[B_3^*(\zeta = 1) + M_{3,3}(\zeta = 1)B_1^*(\zeta = 1)]}{1 + M_{1,2}(\zeta = 1)M_{3,3}(\zeta = 1)k} \\ \phi_2(\zeta = \zeta_m)\dfrac{[B_1^*(\zeta = 1) - kB_3^*(\zeta = 1)M_{1,2}(\zeta = 1)]}{1 + M_{1,2}(\zeta = 1)M_{3,3}(\zeta = 1)k} \end{bmatrix} \tag{3.52}$$

Evaluating the solution at $\zeta = \zeta_m$ the following result is obtained:

$$1 + kM_{2,2}(\zeta = \zeta_m)\frac{[B_3^*(\zeta = 1) + M_{3,3}(\zeta = 1)B_1^*(\zeta = 1)]}{1 + M_{1,2}(\zeta = 1)M_{3,3}(\zeta = 1)k} - B_2^*(\zeta = \zeta_m) = 0 \tag{3.53}$$

and if λ is set as $\lambda = 0 + \alpha j$, it is possible to find the the stability region for the observer gains by numerically solving above non-linear equation. Figure3.7 (Bottom) shows the eigenvalues behaviour for changes in ℓ using the parallel configuration. Similarly to the counter current configuration, as the value of ℓ is increased, the unstable pair of eigenvalues is shifted to the the left side of the complex plain, while at the same time with the gain increase one stable pair is shifted to the right side of the plain, making the system unstable again. These values of ℓ which makes the system marginally stable are calculated using Eq.(3.53).

3.3.4 Full-state observer based control

Considering that the observer from the previous section is used to reconstruct the state variables based on the system output, the closed-loop realization is represented by Figure 3.8. The regulator only admits as inputs the system output (or the measured output) and the exosystem states as information. In this case, the reconstructed states of the system are used in the control law instead of the system real states, as this information is not available:

$$u(t) = -\bar{K}(\hat{x}(t)) \tag{3.54}$$

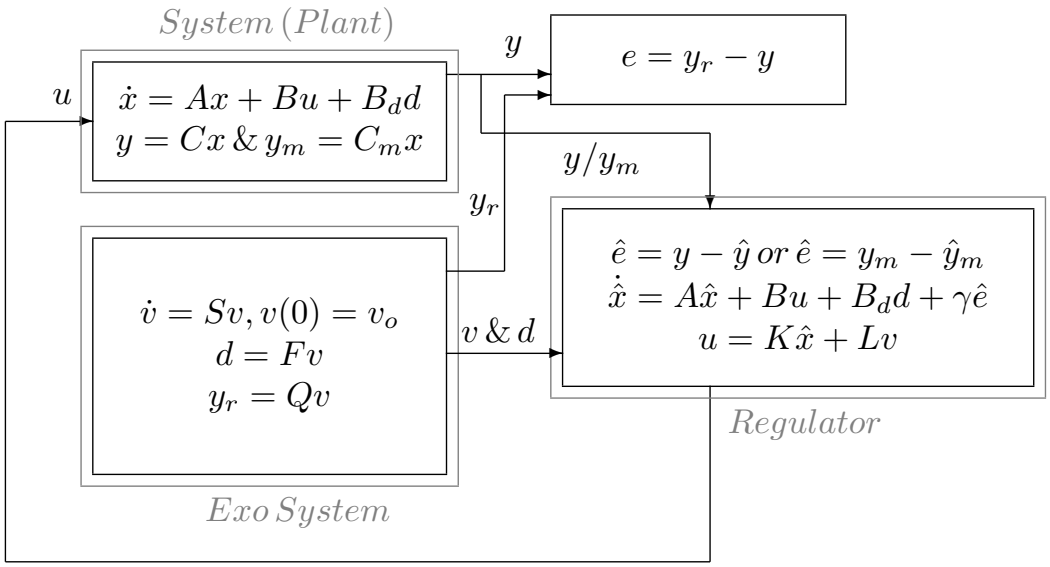

Figure 3.8: Closed system representation using a observer to reconstruct the state variables.

The design of the output regulator is based on the assumption that the reconstructed states $\hat{x}$ dynamic are the same as the system model (observer part of the regulator), augmented by the information from the controlled output, measured output or one can considered also the error signal. If the measured output or the controlled output are given, the output regulator takes the following form:

$$\dot{\hat{x}}(t) = A\hat{x}(t) + Bu(t) + B_d d(t) + \gamma\hat{e}(t) \tag{3.55a}$$

$$\hat{y}(t) = C_\Lambda \hat{x}(t) \tag{3.55b}$$

$$\hat{y}_m(t) = C_{m,\Lambda}\hat{x}(t) \tag{3.55c}$$

where $\hat{e}(t)$ represents the error between the given output ($y(t)$ or $y_m(t)$) and the reconstructed output ($\hat{y}$ or $\hat{y}_m$):

$$\hat{e}(t) = y(t) - \hat{y}(t) \tag{3.56a}$$

$$\hat{e}(t) = y_m(t) - \hat{y}_m(t) \tag{3.56b}$$

When the controlled output is considered, the error defined in (3.56a) is utilized while if the some other output measurement is utilized and does not coincide with the controlled output the error signal given by Eq.(3.56b) is used.

Given that converging observer gain is designed and deployed, the error between the reconstructed output and the actual output decreases, and the reconstructed states are able to properly describe the system states evolution. As the reconstructed states are used in the control law, it is also desired that the observer states converge rapidly to the real states (although a slower convergence will not affect the system stability).

In addition to the design given in Figure 3.8, frequently in the practice one can measure just difference among desired and controlled output and not directly the output signal. Hence, in this case only the error signal is given for the controller design. In this case, the caveat is that not only the system states need to be reconstructed, but also the exosystem states, as shown in Figure 3.9:

$$\dot{\hat{x}} = A\hat{x} + Bu + B_d F\hat{v} + \gamma_1 \begin{bmatrix} \hat{e} \\ e \end{bmatrix} \tag{3.57a}$$

$$\dot{\hat{v}} = S\hat{v} + \gamma_2 \begin{bmatrix} \hat{e} \\ e \end{bmatrix} \tag{3.57b}$$

$$\hat{y} = C_\Lambda \hat{x} \tag{3.57c}$$

$$\hat{y}_m = C_{m,\Lambda}\hat{x} \tag{3.57d}$$

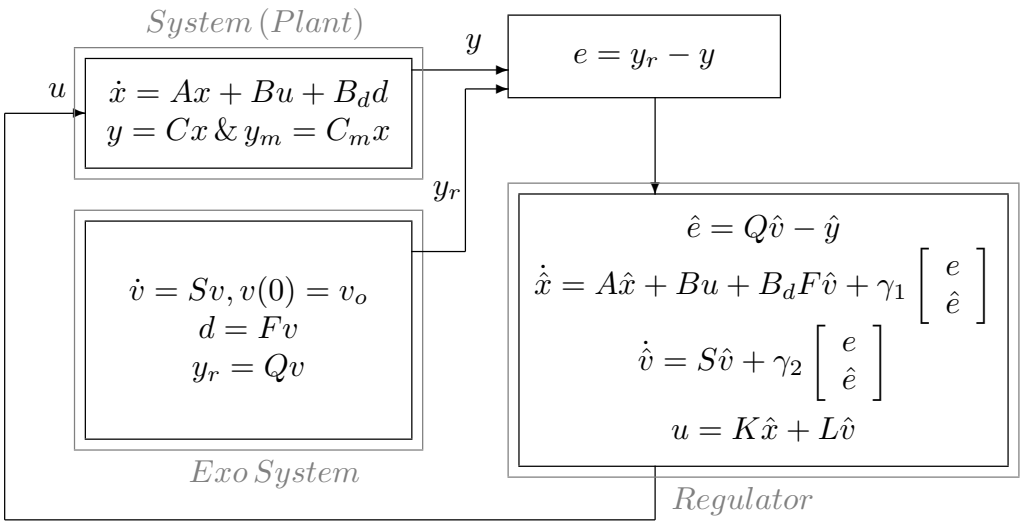

Figure 3.9: Closed system representation using a observer to reconstruct the state variables with the output error.

In this case, as there is no output utilized as the input signal to the observer, and only difference between the tracking error $e(t)$ and the reconstructed error $\hat{e}(t)$ can be used. Again, as in the above analysis, the observer design needs to ensure convergence of the observer error which induces properly reconstruction of the system states that is used in the stabilization by full state feedback.

3.3.5 Output Tracking

The servomechanism design philosophy which is embedded in the output regulator design is to configure control system to achieve that the tracking error evolution $e(t)$ decays to zero and guarantees the system closed-loop stability. If the system is inherently stable and the exosystem states are known, the control law becomes:

$$u(t) = Lv(t) \tag{3.58}$$

and it is only necessary to find a feedforward gain L that drives the tracking error to zero as $t \to \infty$ and guarantees the stability of the closed-loop system. Given that the system is already stable, one can find L as the solution for the following constrained linear Sylvester equations [14] associated with the closed loop system dynamics:

$$\Pi S = A\Pi + BL + B_d F \tag{3.59a}$$

$$C_\Lambda \Pi - Q = 0 \tag{3.59b}$$

where Π is a spatially varying operator ($\Pi = \Pi(\zeta)$), $\Pi \in \mathfrak{L}(\Re, H)$ and the solution of the Sylvester equations exists if Π and L exist. If there exists a bounded linear operator Π such that the Sylvester operator equation (3.59) holds, then the system ($x(t)$) and the exosystem ($v(t)$) are related by the expression $\Pi v(t) = x(t)$. Generally, the initial condition of the system and the exosystem do not satisfy the relation $\Pi v(t) = x(t)$, however, if the tracking error given by Eq.(3.16) decays, then the stabilizing dynamics can be obtained such that the relation holds [14]. If the system is intrinsically unstable, but stabilizable (as shown in 3.3.2), the control law must account for the stabilization:

$$u(t) = -\bar{K}(X(t)) + Lv(t) \tag{3.60}$$

Therefore, one needs to find L that decreases the tracking error and guarantees the stability of the closed-loop system. With the assumption of approximate controllability in the distributed parameter setting, and Theorem 3.1 holds, the $(\bar{A}_U, \bar{B}_U)$ is exponentially stabilizable (K is chosen in 3.3.2 to make $(\bar{A}_U - \bar{B}_U\bar{K})$ stable), then we can find L that satisfies the constrained Sylvester equations [14]:

$$\Pi S = (A - B\bar{K})\Pi + BL + B_d F \tag{3.61a}$$

$$C_\Lambda \Pi - Q = 0 \tag{3.61b}$$

If the reconstructed state is used, then the following control laws are utilized:

$$u(t) = -\bar{K}(\hat{x}(t)) + Lv(t) + \hat{K}\hat{e}(t) \tag{3.62a}$$

$$u(t) = -\bar{K}(\hat{x}(t)) + L\hat{v}(t) + \hat{K}\begin{bmatrix} \hat{e}(t) \\ e(t) \end{bmatrix} \tag{3.62b}$$

where (3.62a) represents the control law when the output or measured output are given, and $\hat{K}$ is a gain based on the error of the reconstructed state and the actual output measurement. Similarly, Eq.(3.62b) defines the control law when there is no output and just the error is given, with $\hat{K}$ as a gain based on the reconstructed error and the actual error signals.

3.4 Results

In this section, we provide the simulation findings associated with the proposed designs.

3.4.1 Output Tracking - Stable System

For a condition where the system is stable and the exosystem state is known, it is necessary to find an appropriate feedforward gain L that drives the tracking error to zero. Figure 3.10 and Figure 3.11 show the results for the stable system in countercurrent and parallel configuration, respectively.

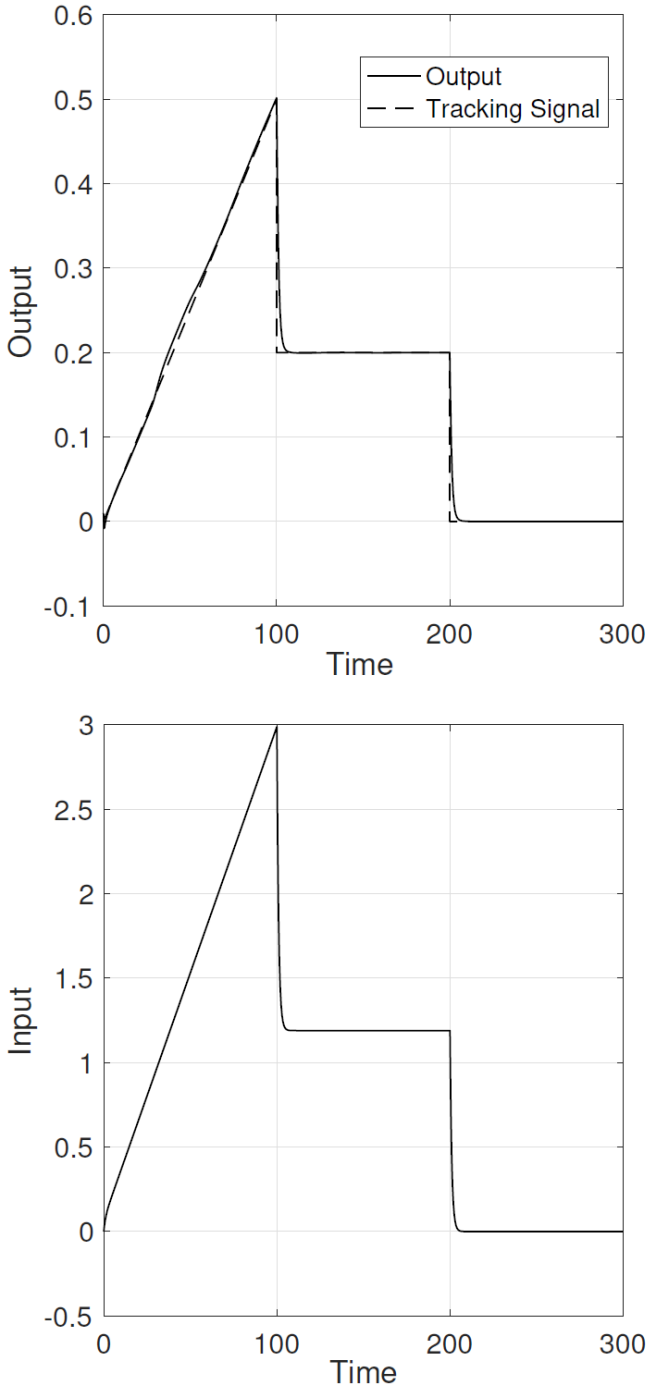

Figure 3.10: Simulation results for the stabilized counter current operating configuration: (Top) output and reference signal; (Bottom) system input.

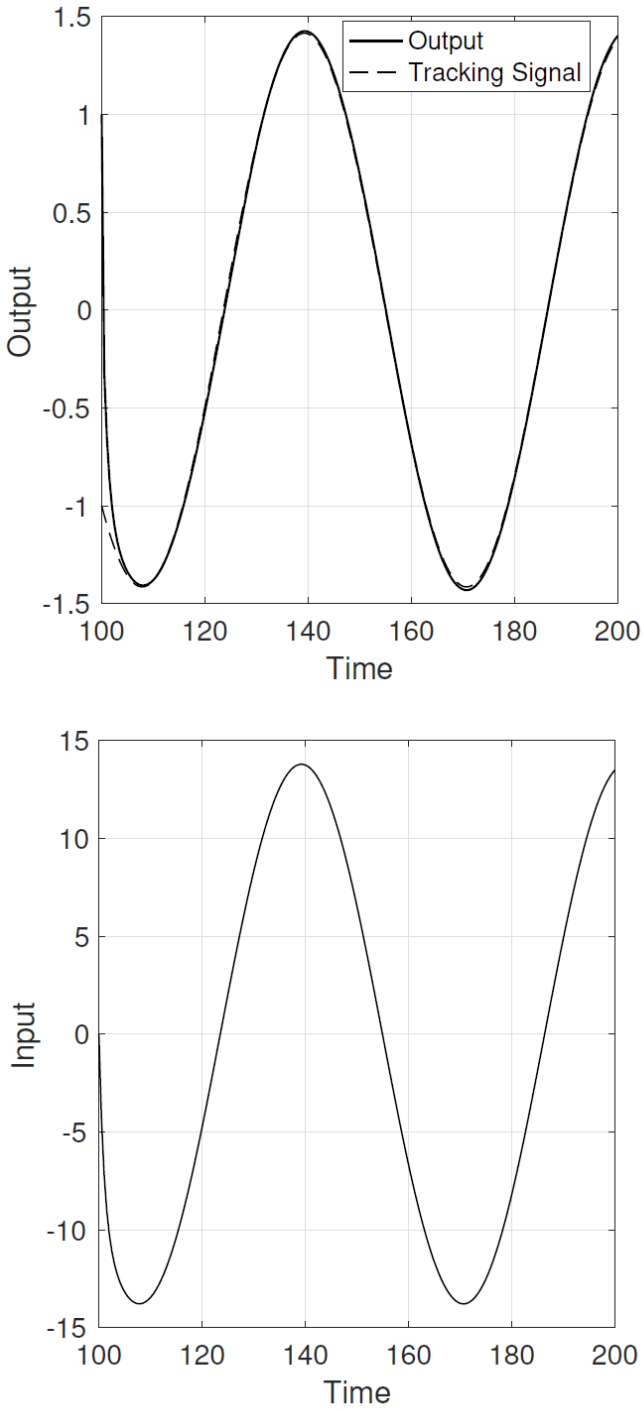

Figure 3.11: Simulation results for the stabilized parallel operating configuration: (Top) output and reference signal; (Bottom) system input.

Figure 3.10 shows the simulation results for the counter current system

when different kinds of tracking signals are used. First, the system starts tracking a ramp, then it is followed by two decreasing steps. The results for the parallel configuration tracking a periodic function is showed in Figure 3.11. As both system are stable, it is expected that the output is able to track the desired signal, as long as a adequate gain L has been used.

3.4.2 Output Tracking - Full-state feedback

As it is demonstrated in previous section given that information of all states is available, it is possible to use full-state feedback to stabilize the system and achieve proper tracking. Figure 3.12 shows the output and input profiles when the tracking function is given by $y_r(t) = 1 + 0.005t + cos(0.1t)$. The spatial profiles of heat exchanger temperatures, θ_1 and θ_2 are also shown in Figure 3.12. The system takes some time to stabilize due to the transients associated with initial conditions and the input on the first heat exchanger needs to take into account the negative feedback of the delayed boundary, which means that the input needs to compensate for the temperature change that is going to happen when the fluid enters the heat exchanger shell after the delayed feedback.

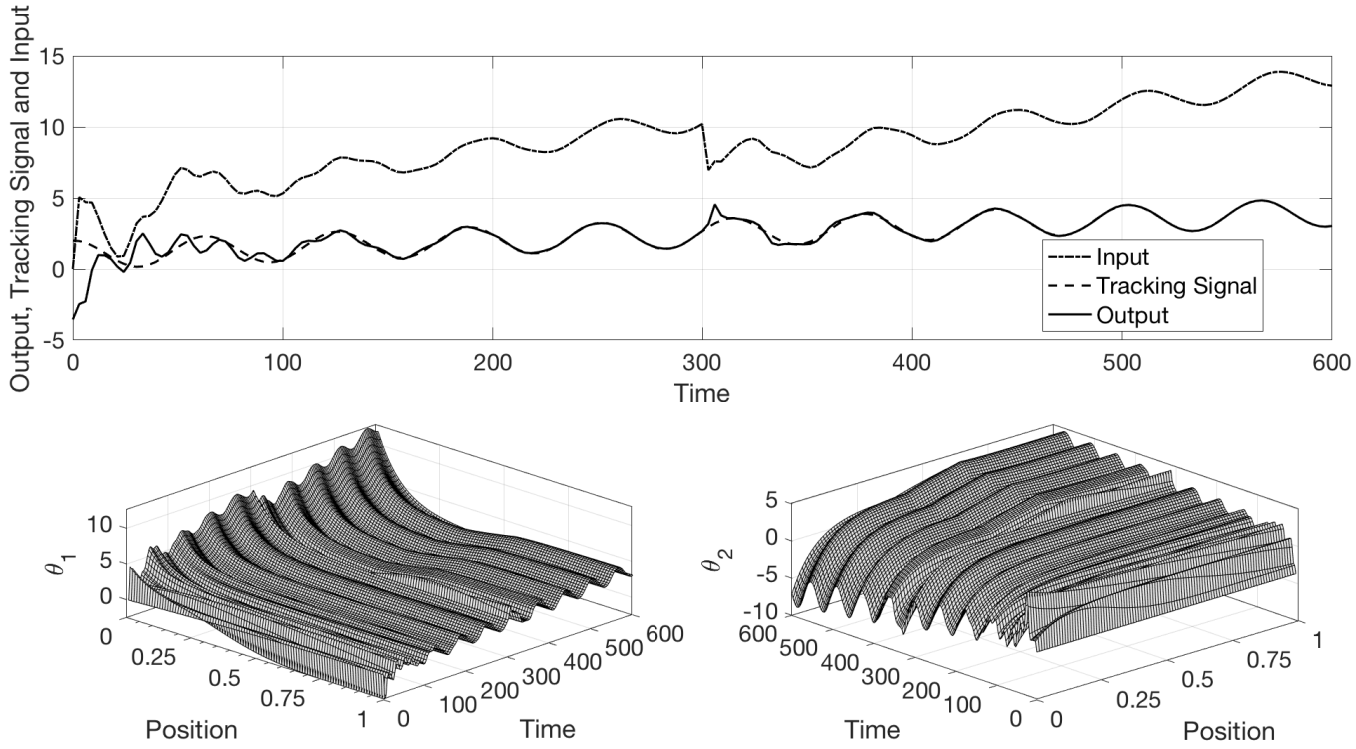

Figure 3.12: Fullstate feedback tracking using the parallel configuration: (Top) System output and input profiles; (Left) θ_1 time-space profile; (Right) θ_2 time-space profile.

Although there are some oscillations at the beginning, the controller is able to maintain stability of the closed-loop system and achieves proper tracking of the reference signal. In the simulation scenario, we consider that at $t = 300$, a step disturbance is applied to the system. This causes a sudden increase in both variables, as it can be seen on the spatial profiles in Figure 3.12, due to the energy added to the middle section of both heat exchangers by the disturbance. As expected, this increase in the system energy also makes the required input to decrease after the disturbance is applied, shown in the input profile.

3.4.3 Output Tracking - Observer based

Given that in realistic heat exchanger realizations and settings just the output or the tracking error information are given, an observer is used to estimate the states in order to stabilize the system and achieve proper tracking of a reference signal. First, the measured output is considered to be known and the output is estimated ($y(t) \neq y_m(t)$). The results for a tracking signal $y_r(t) = 0.005t$ using the counter current configuration are shown in Figure 3.13. The measured output is given by $y_m = \theta_2(\zeta = 0.5)$. It is possible to see that the actions taken in the beginning are higher than expected, as the controller is only using the observer states and the system has not been stabilized. As soon as the reconstructed states are close to the real states, the controller is able to stabilize the system and achieve proper tracking of the reference signal. The L_2 norm of the observer error for θ_1, θ_2 and ω are also shown in Figure 3.13. One can see that the system stabilizes as the observer error decreases, which demonstrates importance of designing observer with higher observer convergence rate than the convergence rate of stabilized system dynamics. As considered in the previous case, the disturbance happens in the system when $t = 700$. This increases the system energy, decreasing the required input necessary to achieve proper tracking. As the observer has already converged to the system states when the disturbance is made, there is no visible effects of the disturbance in the observer error, hence the robustness is achieved as well.

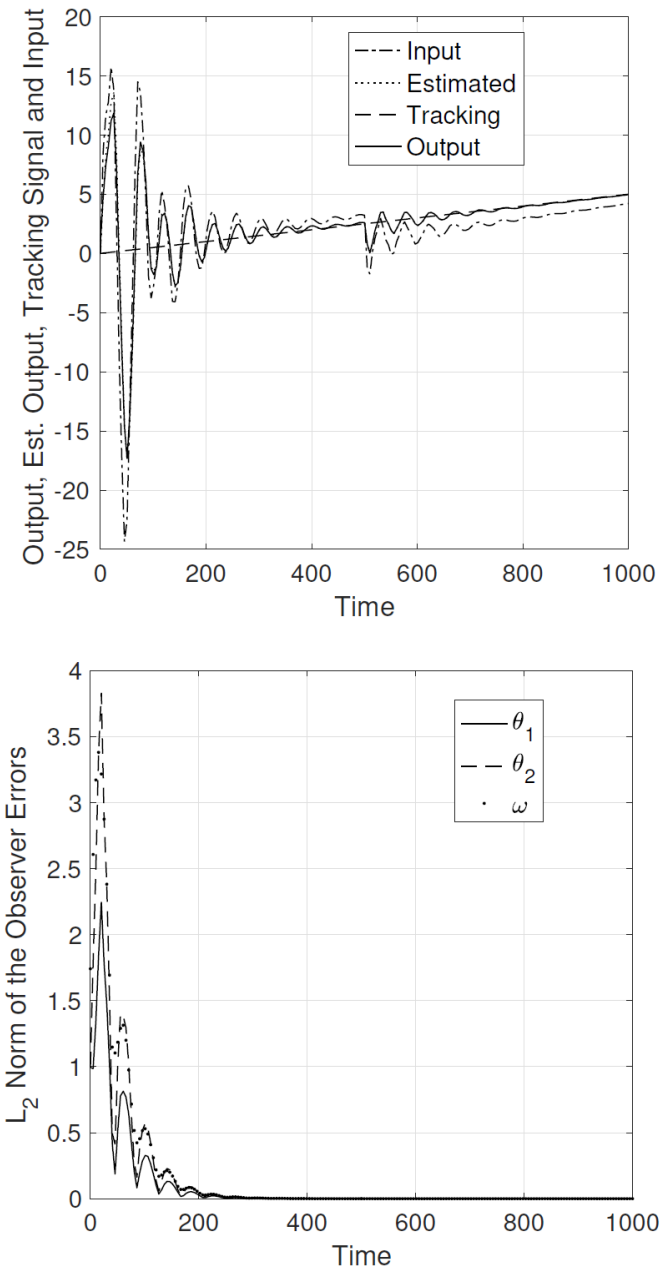

Figure 3.13: Counter current configuration when a observer based controller is used ($y_m \neq y$): (Top) System output and input profiles; (Bottom) L_2 norm of the observer errors.

The same tracking signal used in 3.4.2 for the full-state feedback ($y_r(t) = 1 + 0.005t + cos(0.1t)$) was used also in the parallel configuration, but this time considering that only the output is given (and not the full-state feedback

realization as considered previously). This require the use of the observer to properly estimate the system variables. The system output and input profiles for this case are shown in Figure 3.14. As expected, in the beginning the reconstructed states are different from the actual system states, which causes the oscillations to be higher than what was shown in Figure 3.12 when the full-state feedback was realized. Figure 3.14 also shows the L_2 norm of the observer error for θ_1, θ_2 and ω. As the observer error decreases, the controller is able to keep the system under control and track the desired signal. When the disturbance happens at $t = 300$, the system states have already been properly estimated and there are no noticeable effects of the disturbance on the observer error. This also produces a quick response of the regulator against the disturbance and proper tracking is again rapidly established. As in the previous cases, the energy increase caused by the disturbance reduces the necessary input required by the system.

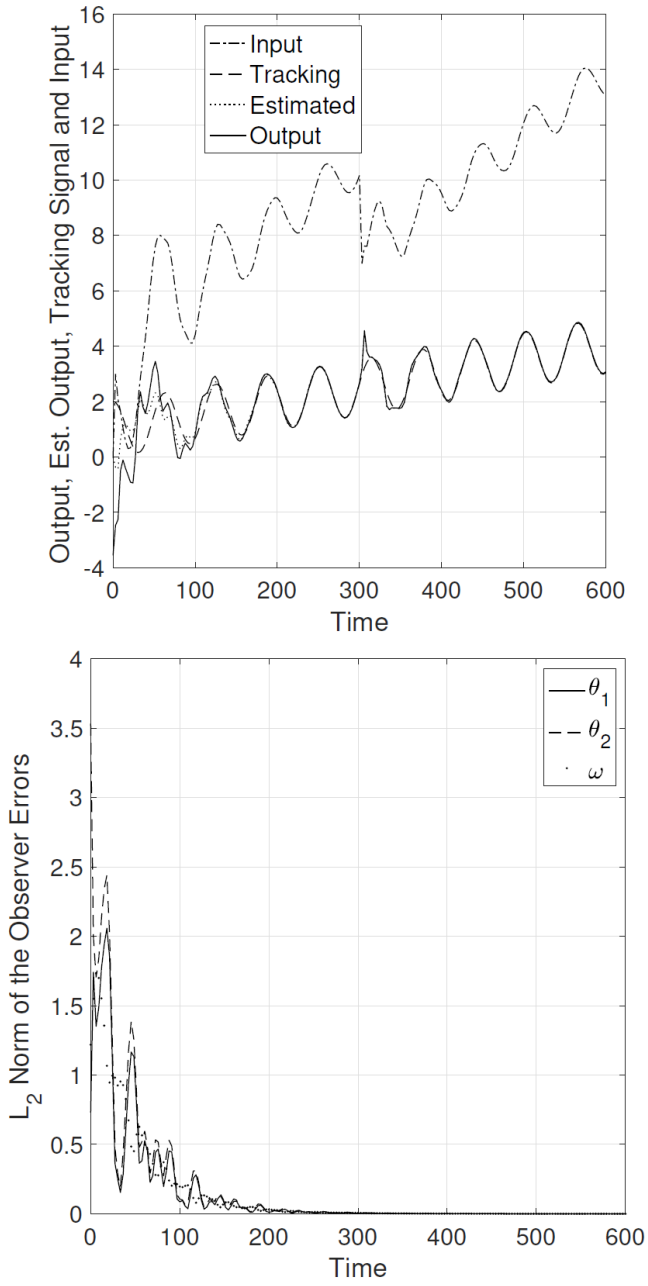

Figure 3.14: Parallel configuration when a observer based controller is used ($y_m = y$): (Top) System output and input profiles; (Bottom) L_2 norm of the observer errors.

The last case considered, only the tracking error defined in (3.16) is available. The desired tracking signal $y_r(t) = 0.005t$ is used and the counter-current configuration is considered, as in the previous case when information of the

measured output was available. Again, it is necessary to use an observer to estimate the system states and provide the necessary information to the controller to achieve stabilization and proper output tracking. The system output and input profiles and the L_2 norm of the observer error for θ_1, θ_2 and ω for this case are shown in Figure 3.15. As only the error is given and the observer needs to reconstruct the system and exosystem states, there are more oscillations at the beginning. When the observer error decreases, the system stabilizes and proper tracking is achieved. Compared to results from Figure 3.13, the observer takes longer to properly estimate the system and exosystem states, which also leads the slower controller convergence compered to the previous cases. When the disturbance happens at $t = 500$, the observer has already estimated the system states, thus, the controller is able to rapidly achieve proper tracking again.

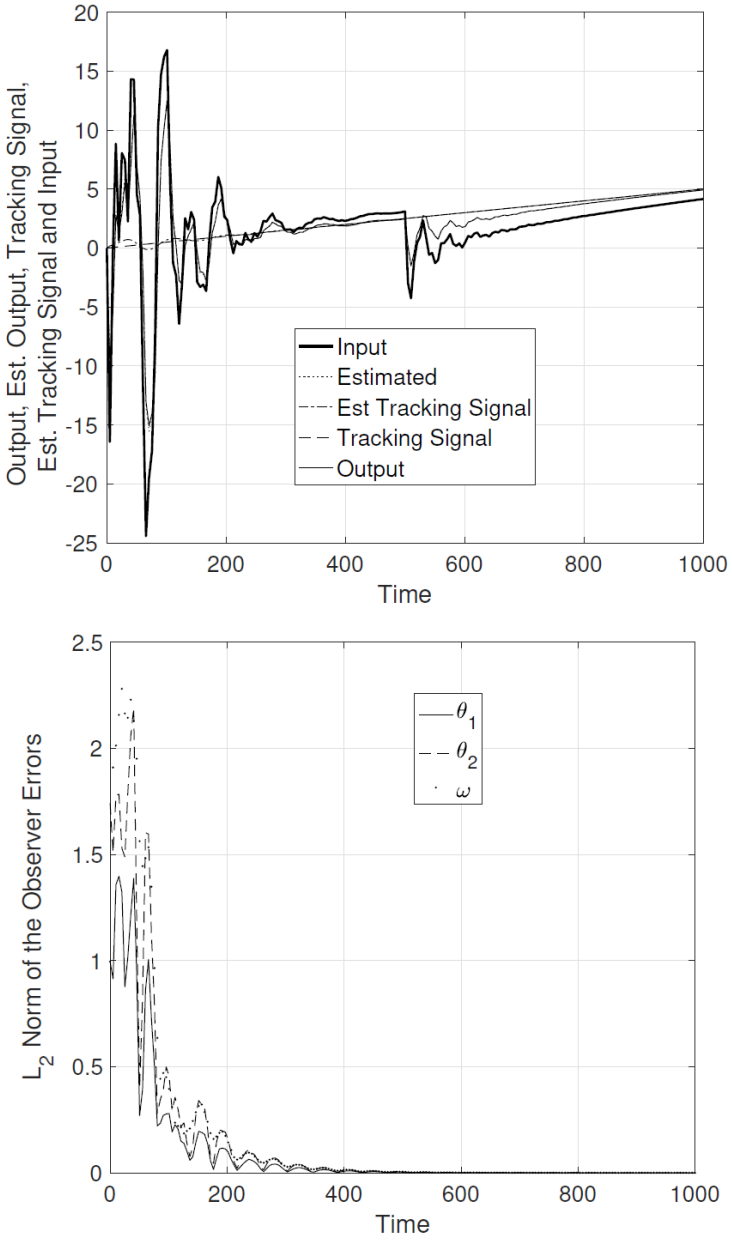

Figure 3.15: Counter current configuration when a observer based controller is used (only $e(t)$ is known): (Top) System output and input profiles; (Bottom) L_2 norm of the observer errors.

3.5 Summary and Future Work

In this chapter, the mathematical models of two different configurations of a heat exchanger system were studied. Both configurations considered a delayed

boundary feedback between the heat exchangers and the manipulated variable of the system was applied at the boundary. To deal with these conditions, the system was transformed. A corresponding in-domain input was used instead of the boundary input and the transport delay was transformed into a equivalent transport equation. When the unstable system is considered, it was shown that a output feedback is not sufficient to stabilize the system. For this reason, a full-state feedback was used in the control law. Unfortunately, information for all states of a distributed parameter system is hardly available, and the observer is designed to reconstruct the system states with the information from the measured output or the error signal. Finally, the computer simulations for all cases considered were presented and discussed showing the controller capability to stabilize the system and achieve output tracking of the desired signal even with disturbances present in the system.

The regulator design considered guarantees the system stability, proper tracking and disturbance rejection, but does not account for any optimal conditions when it comes to performance, which is an interesting extension to be considered in future studies.

3.6 Acknowledgements

The support for this work is provided by CAPES - 88881.128514/2016-01 (Brazil) and support for Guilherme Ozorio Cassol is gratefully acknowledged.

Chapter 4

Discrete Output Regulator Design for the Linearized *Saint–Venant–Exner* Model

4.1 Introduction

In many chemical, hydro-geological, petrochemical, and manufacturing processes the dynamic models take the mathematical form of partial differential equations (PDEs). One of these types of models is the Saint–Venant–Exner (SVE) equations, which consist of non-linear PDEs and are used to model the dynamics of a sediment-filled water canal with arbitrary values of the bottom slope, friction, porosity, and water-sediment interaction. Due to their nature, one of the crucial aspects of these distributed parameter systems is the complexity given by the infinite-dimensional system representation [16], [17], which is a challenging factor when it comes to the controller/regulator design and realization.

The primary goal of a regulator is to drive the desired output of a system to behave exactly as demanded, and at the same time it needs to assure the stability of the closed-loop system. Using early lumping methods is the simplest way to design the controller for distributed parameter systems. In these methods, the PDEs are generally converted to sets of ordinary differential equations (ODEs), which allows the use of standard control methodology applicable to ODE systems. But, this also results in some mismatch between the dynamical properties of the original distributed parameter and the lumped parameter

models, thus, affecting the controller [11].

Another way to deal with distributed parameter processes is to exploit the infinite-dimensional characteristic of the system, and there are significant research efforts made to solve the regulator design problem for infinite-dimensional systems [13], [80]. In [14], the generalized geometric methods were introduced in the regulator design for the first-order hyperbolic PDEs, and the robust output regulation problems were considered in [84]–[86], while taking into account infinite-dimensional exogenous systems (an independent system responsible for the generation of the tracking signal and/or disturbance). Specifically for the SVE model, there are several contributions that take into account the characteristics of the model. In [87], the proportional and integral output feedback controllers were proposed by using the semigroup theory. The H_∞ optimization framework was applied in [88] to design a controller considers the both water resource management and performance with respect to the users. And in [89], a Lyapunov approach was used to obtain the control laws that stabilize the system considering full-state and output feedback.

More recently, in [90], the exponential stabilization of this model was achieved by the backstepping design, also considering full-state and output feedback, where the design of an exponentially stable Luenberger observer was considered for state reconstruction. The PDE backstepping design has proved to be of valuable for the boundary stabilization of distributed parameter systems. Essentially, the technique consists of finding a suitable transformation that maps the closed-loop system into a stable target system. Due to the invertibility of the transformation, the original and the target system have equivalent stability [91], [92]. Other applications and developments along this line include, for instance, the boundary observer based-control design for a hyperbolic PDE [93], the boundary observer for a class of time-varying linear hyperbolic partial integral-differential equations (PIDEs) [94], and control of general linear heterodirectional hyperbolic ODE–PDE–ODE systems [95].

All the contributions mentioned above were developed in the continuous-time domain, but, as most modern and state-of-the-art controller realizations

are digital and discrete, time discretization realizations need to be taken into account at the final design stage. Although some contributions addressed the stabilization of PDEs using backstepping with time sampled-data [96], [97], these were made considering specific scalar equations and the design of a controller in the discrete-time setting was not the objective of these works. Traditional time discretization schemes (for instance, explicit or implicit Euler) could be used to obtain a discrete-time representation, but they have the disadvantage of reducing the accuracy of the discrete system representation as the sampling period increases [26]. Moreover, the sampling may impact the overall model and closed-loop stability when the controller is implemented. Therefore, a different type of time discretization scheme, that provides a reliable transformation of a continuous linear infinite-dimensional system representation to a linear discrete-time infinite-dimensional needs to be considered. A discretization scheme that accounts for this design criteria is the Crank-Nicolson midpoint integration rule, which can be easily applied to infinite-dimensional systems [28]. This type of discretization is also known as Cayley-Tustin time discretization, and it has been shown to preserve the intrinsic energy and dynamical characteristics of the linear distributed parameter system [29] without the application of spatial discretization or/and model reduction.

The unstable linearized SVE model is considered in this manuscript. The PDE system is given as a system of first-order transport hyperbolic PDE equations, with in-domain and boundary coupling. Based on this system, a discrete-time output regulator design is presented and attains the following objectives: (1) ensures the stability by output feedback; (2) considers the stabilization of the problem in the discrete-time setting, obtained by the application of the Caley-Tustin time discretization; (3) achieves tracking of periodic and polynomial signals generated by an exosystem, which is ensured by the solution of the corresponding Sylvester output regulation equations. To properly design the discrete-time regulator, the relation between the discrete-time and continuous-time control is developed, such that the closed-loop stability and proper tracking of the discrete-time representation is assured if the controller design is known in the continuous-time.

The chapter is organized as follows: in Section 4.2, the SVE system model and its properties are introduced together with the exosystem and control objectives. In Section 4.3, the system stabilization, observer design, and output regulation in the continuous-time setting are developed. In Section 4.4, the Caley-Tustin time discretization is applied to the system, and the discrete regulator design is developed. The stability of the closed-loop system is shown. In Section 4.5, the simulations results are presented and the regulator performance is discussed. Lastly, in Section 4.6, the final remarks are made.

4.2 Problem Formulation

The Saint–Venant and Exner equations are used to describe the dynamics in a sediment-filled open channel with rectangular cross-section [90]. Considering $H(t,\zeta)$ to be the water depth, $V(t,\zeta)$ as the water velocity and $B(t,\zeta)$ as the depth of the sediment layer above the channel bottom, the dynamics of the system can be described as the equations below:

$$\begin{aligned}
&\frac{\partial H}{\partial t} + V\frac{\partial H}{\partial \zeta} + H\frac{\partial V}{\partial \zeta} = 0 \\
&\frac{\partial V}{\partial t} + V\frac{\partial V}{\partial \zeta} + g\frac{\partial H}{\partial \zeta} + g\frac{\partial B}{\partial \zeta} = gS_b - C_f\frac{V^2}{H} \\
&\frac{\partial B}{\partial t} + aV^2\frac{\partial V}{\partial \zeta} = 0
\end{aligned} \tag{4.1}$$

As shown in [90], this system can be linearized around a steady-state and the Cardano-Vieta method can be applied to rewrite it in the characteristic form, which can be llustrated in Figure 4.1.

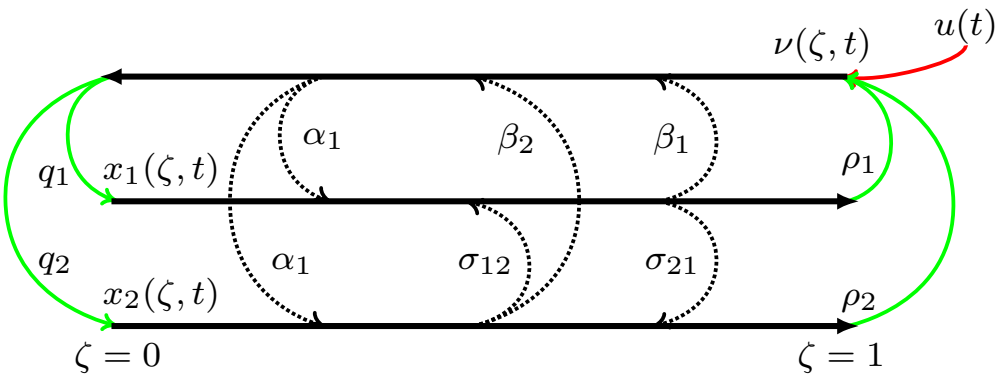

Figure 4.1: PDE system (Equation (4.2)) representation.

This linearized system is given by the following coupled system of first-order hyperbolic partial differential equations, in the domain $\{t \in \Re^+, \zeta \in [0,1]\}$, with t representing time and ζ representing the dimensionless spatial variable:

$$\begin{aligned}
\frac{\partial \nu}{\partial t} &= \mu\frac{\partial \nu}{\partial \zeta} + \alpha_1\nu + \beta_1 x_1 + \beta_2 x_2 \\
\frac{\partial x_1}{\partial t} &= -\gamma_1\frac{\partial x_1}{\partial \zeta} + \alpha_1\nu + \sigma_{11}x_1 + \sigma_{12}x_2 \\
\frac{\partial x_2}{\partial t} &= -\gamma_2\frac{\partial x_2}{\partial \zeta} + \alpha_1\nu + \sigma_{21}x_1 + \sigma_{22}x_2 \\
y_m(t) &= \nu(0,t) \\
y(t) &= x_1(1,t)
\end{aligned} \tag{4.2}$$

With the following algebraic boundary conditions:

$$\begin{aligned}
\nu(1,t) &= \rho_1 x_1(1,t) + \rho_2 x_2(\zeta=1,t) + u(t) \\
x_1(0,t) &= q_1\nu(0,t) \\
x_2(0,t) &= q_2\nu(0,t)
\end{aligned} \tag{4.3}$$

These linear hyperbolic PDEs represent the transport of $x(\zeta,t) = [\nu, x_1, x_2]^T \in L^2(0,1)$ (a real Hilbert space); γ_1, γ_2 and μ are the system's characteristics velocities; σ_{ij} for $i = 1,2$ and $j = 1,2$, α_1, β_1 and β_2 are the parameters representing the in-domain interaction between the state variables; and ρ_1, ρ_2, q_1 and q_2 are parameters representing the interaction on the boundaries. All these parameters are obtained from the characteristic form of the SVE model [90].

Usually, the openings of the gates located at the ends of the channel can be controlled to achieve the stabilization of the water level and flow rate. Thus, $u(t) \in \Re$ (a real finite space), the system input, is considered to be control of the downstream gate, represented by the boundary actuation at $\zeta = 1$, shown in (4.3). Measurements at the upstream ($\zeta = 0$) are considered to be the system measured output $y_m(t) \in \Re$ and are used to reconstruct the states with a Luenberger observer. The system desired system output $y(t) \in \Re$ is related to the properties of the water downstream. There are no direct measurements of this output and the regulator aim is to control it as desired. Thus, this system output should properly follow a predetermined pattern if the regulator is properly designed.

This system can be represented as an abstract differential equation:

$$\begin{aligned} \dot{x}(t) &= Ax(t) + Bu(t) \\ y_m(t) &= C_m x(t) \\ y(t) &= Cx(t) \end{aligned} \tag{4.4}$$

where A is a linear operator $\mathfrak{L}(L^2(0,1), L^2(0,1))$, B is the linear input operator $\mathfrak{L}(\Re, L^2(0,1))$, C_m is the measured output operator $\mathfrak{L}(L^2(0,1), \Re)$ and C is the desired output operator $\mathfrak{L}(L^2(0,1), \Re)$.

In this contribution, the goal is to achieve proper tracking of a reference signal, while maintaining the system stability. It is considered that the reference signal $y_r(t) \in \Re$ to be tracked by the system output $y(t)$ is generated as the output of a known finite-dimensional exogenous system (also called exosystem), which is independent from the system (the exosystem affects the system dynamics, but not the other way around) and is defined as the following throughout this work:

$$\dot{z}(t) = Sz(t), t > 0, z(0) \in \mathbb{R}^e \tag{4.5a}$$

$$y_r(t) = Qz(t), t \geq 0 \tag{4.5b}$$

where the matrix $S : D(S) : \mathbb{R}^e \to \mathbb{R}^e$ gives the dynamics of the exosystem states and Q is a matrix that gives the desired output tracking signal $y_r(t)$.

Assumption 4.1 *: The reference signal consists of periodic and polynomial functions, such that the exosystem dynamics can be represented in the following*

form:

$$S = \left[\begin{array}{c|c} J_1 & 0 \\ \hline 0 & J_2 \end{array}\right], J_1 = \begin{bmatrix} 0 & 1 & 0 & \dots & 0 \\ 0 & 0 & 1 & \dots & 0 \\ 0 & 0 & 0 & \dots & 0 \\ \vdots & \vdots & \vdots & \ddots & \vdots \\ 0 & 0 & 0 & \dots & 0 \end{bmatrix}, J_2 = \begin{bmatrix} 0 & f_1 & 0 & 0 & \dots \\ -f_1 & 0 & 0 & 0 & \dots \\ 0 & 0 & 0 & f_2 & \dots \\ 0 & 0 & -f_2 & 0 & \dots \\ \vdots & \vdots & \vdots & \vdots & \ddots \end{bmatrix} \tag{4.6}$$

notice that J_1 and J_2 are decoupled block matrices and it is assumed that each f_i is unique. J_1 generates a polynomial signal and the size of J_1 (n_1) determines the polynomial degree. J_2 generates a linear combination of periodic function, where each f_i is responsible for a function with different periodicity. Therefore, the size of J_2 will be n_2, and it is an even number.

Remark 4.1 *: The block matrix J_1 has all eigenvalues equal zero (i.e., $\sigma(J_1) = 0$) with multiplicity equal to the size of the matrix. J_2 on the other hand has conjugated complex eigenvalues $\sigma(J_2) = \{\pm f_i\mathbf{j}\}$. Therefore, the spectra of S in Equation (4.5) is $\sigma(S) = \sigma(J_1) \cup \sigma(J_2) = \{0, \pm f_i\mathbf{j}\}$. Due to their structures, J_1 is a Jordan block, while J_2 is a diagonal block matrix and its eigenvectors are filled with zeros in all rows except in the ones that correspond to each f_i. The elements in these rows will be $[1, -\mathbf{j}]^T$ and $[1, +\mathbf{j}]^T$ for the corresponding $\pm f_i\mathbf{j}$ eigenvalues.*

This exosystem will generate a linear combination of a polynomial ($\sum_{i=0}^{n_1} a_i t^i$ from J_1) and periodic functions with frequencies f_i ($\sum_{i=0}^{n_2/2} b_i \sin(f_i t) + c_i \cos(f_i t)$ from J_2), and $Q = [Q_1, Q_2] = [Q_{1,1}, \dots, Q_{1,n_1}, Q_{2,1}, \dots, Q_{2,n_2}]$ and the initial conditions $z(0)$ are defined accordingly to match the desired tracking signal. Without loss of generality, one can extend the ensuing design to the case when the exosystem is infinite dimensional [86].

In this contribution, an exosystem that generates a first-order polynomial in combination a periodic signal with one frequency is considered. Therefore, the desired reference signal ($y_r(t)$) has a general form given by:

$$\begin{aligned} y_r(t) = \underbrace{Q_{1,1} z_1(0) + (Q_{1,2} + Q_1 t) z_2(0)}_{J_1} + \\ \underbrace{\left[Q_{2,1}\cos(ft) - Q_{2,2}\sin(ft)\right] z_3(0) + \left[Q_{2,2}\cos(ft) + Q_{2,1}\sin(ft)\right] z_4(0)}_{J_2} \end{aligned} \tag{4.7}$$

with:

$$J_1 = \begin{bmatrix} 0 & 1 \\ 0 & 0 \end{bmatrix}, \quad J_2 = \begin{bmatrix} 0 & f \\ -f & 0 \end{bmatrix} \tag{4.8}$$

The tracking error $e(t)$ is defined as the difference between the system output and the tracking signal:

$$e(t) = y(t) - y_r(t) \tag{4.9}$$

In the continuous-time setting the regulation problem can be defined as finding a regulator of the form:

$$u(t) = K[x(t)] + Lz(t) \tag{4.10}$$

where $K(\cdot)$ is the linear feedback gain operator $\mathfrak{L}(L^2(0,1), \Re)$ that is used to stabilize the system and L is the feedforward gain $\mathfrak{L}(\mathbb{R}^e, \Re)$ that guarantees proper tracking of the desired signal. Therefore, the regulator should guarantee the following conditions:

- The closed-loop system is exponentially stable;
- For the closed-loop system, the tracking error $e(t \to \infty) = 0, \forall x(0) \in X, z(0) \in \Re^e$;

4.2.1 System Properties

Linearized System Stability

The system stability can be determined by the analysis of the eigenvalue problem $A\psi(\zeta) = \lambda\psi(\zeta)$, where $\psi(\zeta)$ are the eigenvector of the system, in this case given by $\psi(\zeta) = \Big[\psi_1(\zeta),\, \psi_2(\zeta),\, \psi_3(\zeta)\Big]^T$, where $\psi_i(\zeta)$ are the eigenfunctions, and λ is the system eigenvalues.

Lemma 4.1 *: The eigenvalues of the system given by Eq. 4.2 are the solution of the following non-linear equation:*

$$\begin{aligned} c(\lambda) = q_1 &\left[M_{31}(1,\lambda) - \rho_1 M_{11}(1,\lambda) - \rho_2 M_{21}(1,\lambda)\right] \\ +q_2 &\left[M_{32}(1,\lambda) - \rho_1 M_{12}(1,\lambda) - \rho_2 M_{22}(1,\lambda)\right] \\ + &\left[M_{33}(1,\lambda) - \rho_1 M_{13}(1,\lambda) - \rho_2 M_{23}(1,\lambda)\right] = 0 \end{aligned} \tag{4.11}$$

where M_{ij} are the elements of the exponential matrix given by $\mathrm{e}^{V^{-1}(A^* - \lambda I)\zeta}$, where V is a matrix with the system velocities and A^* is the matrix with the in-domain coupling coefficients.

Proof: The operator A can be written as $A = -V\partial_\zeta + A^*$, where V is a matrix with the system velocities and A^* is a matrix with the in-domain coupling coefficients. For the particular system considered (given in Equation (4.2)):

$$V = \begin{bmatrix} -\mu & 0 & 0 \\ 0 & \gamma_1 & 0 \\ 0 & 0 & \gamma_2 \end{bmatrix}; A^* = \begin{bmatrix} \alpha_1 & \beta_1 & \beta_2 \\ \alpha_1 & \sigma_{11} & \sigma_{12} \\ \alpha_1 & \sigma_{21} & \sigma_{22} \end{bmatrix} \tag{4.12}$$

Therefore, the eigenvalue problem can be written as:

$$-V\partial_\zeta\psi(\zeta) + A^*\psi(\zeta) = \lambda\psi(\zeta) \implies \partial_\zeta\psi(\zeta) = V^{-1}(A^* - \lambda I)\psi(\zeta) \tag{4.13}$$

which has the following general solution:

$$\psi(\zeta) = \mathrm{e}^{V^{-1}(A^* - \lambda I)\zeta}\psi(\zeta = 0) \tag{4.14}$$

with:

$$\mathrm{e}^{V^{-1}(A^* - \lambda I)\zeta} = \begin{bmatrix} M_{11}(\zeta,\lambda) & M_{12}(\zeta,\lambda) & M_{13}(\zeta,\lambda) \\ M_{21}(\zeta,\lambda) & M_{22}(\zeta,\lambda) & M_{23}(\zeta,\lambda) \\ M_{31}(\zeta,\lambda) & M_{32}(\zeta,\lambda) & M_{33}(\zeta,\lambda) \end{bmatrix} \tag{4.15}$$

Finally, applying the boundary conditions of Equations (4.3)–(4.14) with the definition given in Equation (4.15), the non-linear equation shown in Equation (4.11) is obtained.

In this contribution, the system parameters as shown in Table 4.1 are considered. For these values, the eigenvalue distribution is shown in Figure 4.2. With the values considered, it is possible to conclude that the steady-state considered generates an unstable linearized system. Furthermore, it has an infinity number of unstable eigenvalues, which would not be easily stabilized with techniques generally used for linear finite systems, such as pole-placement.

Table 4.1: Values of the parameters considered.

Parameter	**Value**	**Parameter**	**Value**
$q_1 = q_2$	1	$\rho_1 = \rho_2$	0.5
$\sigma_{11} = \sigma_{21} = \beta_1$	0.2	$\sigma_{12} = \sigma_{22} = \beta_2$	0.05
α_1	0.1	μ	2
γ_1	0.5	γ_2	1

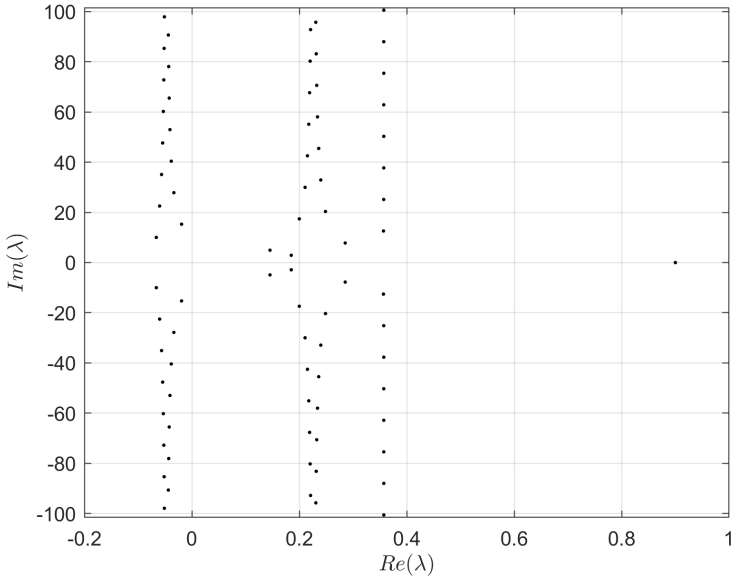

Figure 4.2: System eigenvalue distribution for the parameters given in Table 4.1.

Resolvent and Transfer Function

In this section, the system's resolvent and transfer function are derived, as they will be used in the following sections. The resolvent is used to generate the discrete representation of the system, shown in Section 4.4.1. The transfer function and the resolvent are also necessary to solve the Sylvester equations related to the output regulation problem, defined in Section 4.3.2.

Lemma 4.2 *: The system resolvent is given by:*

$$X(\zeta, s) = \underbrace{\mathrm{e}^{V^{-1}(A^*-sI)\zeta}\left\{\begin{bmatrix} q_1 \\ q_2 \\ 1 \end{bmatrix}\frac{1}{c(s)}\int_0^1 \left[g_1(1-\eta,s)\, g_2(1-\eta,s)\, g_3(1-\eta,s)\right]\bar{x}_0(\eta)d\eta + \int_0^\zeta \mathrm{e}^{-V^{-1}(A^*-sI)\eta}V^{-1}\bar{x}_0(\eta)\right\}}_{(sI-A)^{-1}\bar{x}_0} \tag{4.16}$$

with $g_i(1-\eta,s) = \rho_1 M_{1,i}(1-\eta,s) + \rho_2 M_{2,i}(1-\eta,s) - M_{3,i}(1-\eta,s)$*, with* $M_{j,i}$ *defined as in Equation (4.14) and* $c(s)$ *is the same function given in Equation (4.11) (as expected, if* $s = \lambda$*,* $(sI-A)^{-1}$ *does not exist).* $(sI-A)^{-1}B$

and the system transfer function are:

$$X(\zeta, s) = \underbrace{\mathrm{e}^{V^{-1}(A^*-sI)\zeta} \begin{bmatrix} q_1 \\ q_2 \\ 1 \end{bmatrix} \frac{1}{c(s)}}_{(sI-A)^{-1}B} U(s); \tag{4.17}$$

$$G(s) = \frac{Y(s)}{U(s)} = C(sI - A)^{-1}B = \tfrac{1}{c(s)}$$

Pooof: By applying Laplace Transform in the system defined by Equation (4.4), the following system is obtained:

$$\begin{cases} X(s) - x_0 = AX(s) + BU(s) \\ Y(s) = CX(s) \end{cases} \tag{4.18}$$

Using the fact that $A(\cdot) = -V\partial_\zeta(\cdot) + A^*(\cdot)$ gives the general solution as:

$$X(\zeta, s) = \mathrm{e}^{V^{-1}(A^*-\lambda s)\zeta} X(s, \zeta = 0) + \int_0^\zeta V^{-1}\mathrm{e}^{V^{-1}(A^*-\lambda s)(\zeta-\eta)} x_0(\eta) d\eta \tag{4.19}$$

By applying the boundary conditions shown in Equation (4.3), the general solution can be written as $X(\zeta, s) = (sI - A)^{-1}x_0 + (sI - A)^{-1}BU(s)$ where the operator $(sI - A)^{-1}$ and the function $(sI - A)^{-1}B$ are the ones shown in Equations (4.16) and (4.17), respectively.

4.3 Continuous Time Regulator Design

First, the regulator in the continuous time setting is considered, as represented in Figure 4.3. It is necessary to find a control law that guarantees the closed-loop stability and proper output tracking using only the measured output information provided by the plant.

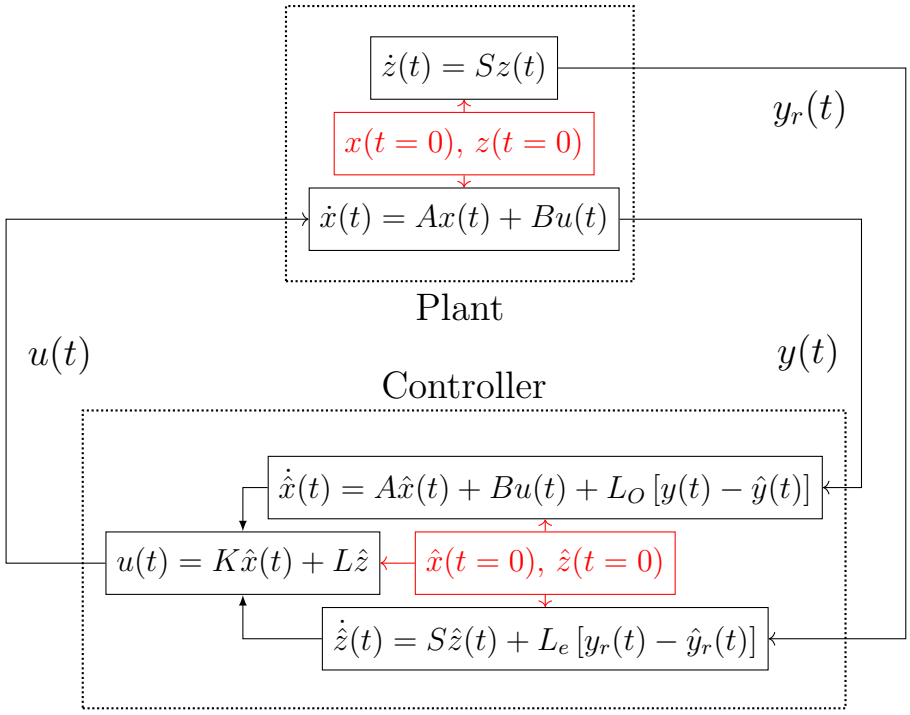

Figure 4.3: Continuous closed-loop representation.

4.3.1 System Stabilization

The first part of the controller is designed to guarantee the closed-loop stability of the system given by Equation (4.2) or, in a general form, by Equation (4.4), such that:

$$u(t) = Kx(t) + r(t) \tag{4.20}$$

Which leads to a stable closed-loop system:

$$\begin{aligned} \dot{x}(t) &= (A + BK)x(t) + Br(t) = \bar{A}x(t) + Br(t) \\ y(t) &= Cx(t) \end{aligned} \tag{4.21}$$

Thus, it is desired to find a proper operator $K(\cdot)$ that achieves closed-loop stabilization ($\bar{A} = A + BK$ is stable). To obtain closed-loop stability for the PDE system, backstepping is applied, as it was developed in [90] for continuous-time setting and it is shown in Appendix 4.A. Although other methods could be applied to ensure the closed-loop stability [87]–[89], the backstepping methodology has been used for boundary control, as it maps the

closed-loop system to a stable desired target system. Specifically for systems of hyperbolic PDEs, finite-time stabilization of the closed-loop system can be achieved by choosing a target system with this type of stability [95]. The following control law is able to map the closed-loop system into the stable target system (given by Equation (4.86)):

$$u(t) = K[x(t)] + r(t) = -\rho_1 x_1(t, \zeta = 1) - \rho_2 x_2(t, \zeta = 1)$$
$$+\mathrm{e}^{-\frac{\alpha_1}{\mu}} \int_0^1 \left[K_1(1,\eta)\mathrm{e}^{\frac{\alpha_1}{\mu}\eta}\nu(\eta,t) + K_2(1,\eta)x_1(\eta,t) + K_3(1,\eta)x_2(\eta,t) \right] d\eta + r(t) \tag{4.22}$$

where the integral kernels ($K_i(\zeta,\eta)$) need to satisfy the system of hyperbolic PDEs given by Equation (4.85).

Remark 4.2 *: The target system shown in Equation (4.86) can be represented in a general form as:*

$$\begin{aligned} \dot{\tilde{x}}(t) &= \tilde{A}\tilde{x}(t) + \tilde{B}r'(t) \\ y(t) &= \tilde{C}\tilde{x}(t) \end{aligned} \tag{4.23}$$

If the transformation T shown in Equation (4.84) exists, then the closed loop system $(A + BK)$ can be transformed in the target system. Therefore, the transformation is such that $\tilde{x}(t) = Tx(t)$ and $x(t) = T^{-1}\tilde{x}(t)$, and, finally, $T(A + BK)T^{-1} = \tilde{A}$. From linear algebra, the following properties of the transformation of a linear system are guaranteed:

$$\sigma(A + BK) = \sigma(\tilde{A}) \tag{4.24a}$$

$$[sI - (A + BK)]^{-1}(\cdot) = T^{-1}\left[(sI - \tilde{A})^{-1}\right] T(\cdot) \tag{4.24b}$$

$$[sI - (A + BK)]^{-1} B = T^{-1}\left[(sI - \tilde{A})^{-1}\right] TB = T^{-1}\left[(sI - \tilde{A})^{-1}\right] \tilde{B} \tag{4.24c}$$

$$\begin{aligned} G_{CL}(s) = C\left[sI - (A + BK)\right]^{-1} B = CT^{-1}\left[(sI - \tilde{A})^{-1}\right] TB = \\ \tilde{C}\left[(sI - \tilde{A})^{-1}\right] \tilde{B} = \tilde{G}(s) \end{aligned} \tag{4.24d}$$

Therefore, the closed-loop will be stable if the target system is stable (and the transformation T and its inverse exist).

Lemma 4.3 *: The closed-loop system will reach the origin in a finite-time of $t = t_s = \phi_1 + \phi_2$, with $\phi_1 = \frac{1}{\mu}$ and $\phi_2 = max\left\{\frac{1}{\gamma_1}, \frac{1}{\gamma_2}\right\}$ and $r(t) = 0$.*

Proof: From the linear properties shown in Remark 4.2, it is important to notice that the closed-loop dynamics will not necessarily be exactly the same as the target system. But, due to the structure of the target system shown in Equation (4.86), it is easy to see that if $r(t) = 0$, then $r'(t) = 0$ and $W(\zeta, t > \phi_1) = 0, \forall\zeta \in [0,1]$, with $\phi_1 = \frac{1}{\mu}$. This also implies that $X_1(0, t > \phi_1) = X_2(0, t > \phi_1) = 0$ due to the boundary conditions, which finally leads to $X_1(\zeta, t > \phi_1 + \phi_2) = X_2(\zeta, t > \phi_1 + \phi_2) = 0, \forall\zeta \in [0,1]$, where $\phi_2 = \max\left\{\frac{1}{\gamma_1}, \frac{1}{\gamma_2}\right\}$. Therefore, the target system will reach steady-state ($\tilde{x}(\zeta, t) = 0$) in a finite-time of $t = t_s = \phi_1 + \phi_2$. Due the transformation T, the closed-loop states will be $x(t) = T^{-1}\tilde{x}(t))$, thus $x(\zeta, t) = 0, \forall\zeta \in [0,1]$ for $t \geq t_s$.

Thus, the control law given in Equation (4.22) will stabilize the PDE system in a finite-time t_s. With the system stabilized, it is expected that system's properties (such as the resolvent, and consequently, the transfer function) will change in the closed-loop.

Lemma 4.4 *: The closed-loop resolvent is given by:*

$$\begin{aligned}(sI - \bar{A})^{-1}(\cdot) = \Big\{&(sI - A)^{-1} + \\ &(sI - A)^{-1}B\left[I - K(sI - A)^{-1}B\right]^{-1}K(sI - A)^{-1}\Big\}(\cdot)\end{aligned} \tag{4.25}$$

which leads to the closed-loop transfer function as:

$$\begin{aligned}\bar{G}(s) = C(sI - \bar{A})^{-1}B = \\ G(s)\left\{I + \left[I - K(sI - A)^{-1}B\right]^{-1}K(sI - A)^{-1}B\right\}\end{aligned} \tag{4.26}$$

Proof: The closed-loop resolvent is obtained as follows:

$$(sI - \bar{A})^{-1}(\cdot) = (sI - A - BK)^{-1}(\cdot) = (sI - A)^{-1}\left[I - BK(sI - A)^{-1}\right]^{-1} \tag{4.27}$$

And applying Woodbury identity to the term in brackets gives the resolvent shown in Equation (4.25). By using the definition of the open-loop transfer function ($G(s) = C(sI - A)^{-1}B$), Equation (4.26) is easily obtained.

Therefore, by knowing $(sI - A)^{-1}B$ and the feedback control gain K, it is possible to easily calculate the closed-loop properties. Although Equations (4.25) and (4.26) might seem to increase the complexity on finding the

closed-loop properties, control laws as given in Equation (4.22) will result in a integral equation if one tries to calculate these properties directly.

4.3.2 Output Regulation

The last step in the design of the regulator in the continuous-time setting is finding the feedforward gain L that achieves proper tracking of the signal generated by the exosystem states ($z(t)$) given by Equations (4.5) and (4.6). The control law obtained after taking the feedforward gain L into account is given by Equation (4.10)

$$u(t) = Kx(t) + Lz(t) \tag{4.28}$$

Lemma 4.5 *: The proper output regulation can be easily achieved by solving the following Sylvester equation:*

$$\begin{aligned} &\Pi S = \bar{A}\Pi + BL = (A + BK)\Pi + BL \\ &C\Pi = Q \end{aligned} \tag{4.29}$$

Proof: First, the error $e_r(t) = x(t) - \Pi z(t)$ is defined, and, considering that $u(t) = K\left[x(t)\right] + r(t)$, taking the time derivative gives :

$$\dot{e}_r(t) = \dot{x}(t) - \Pi\dot{z}(t) = (A + BK)x(t) - \Pi S z(t) + Br(t) \tag{4.30}$$

If we consider that there is a feedforward gain L, such that $r(t) = Lz(t)$, and by adding and subtracting $(A + BK)\Pi z(t)$:

$$\dot{e}_r(t) = (A + BK)\left[x(t) - \Pi z(t)\right] + \left[(A + BK)\Pi z(t) - \Pi S z(t) + BLz(t)\right] \tag{4.31}$$

And by making the term in the second bracket equal zero:

$$\dot{e}_r(t) = (A + BK)e_r(t) \tag{4.32}$$

which generates a stable system if Equation (4.29) holds. Notice that the tracking error $e(t)$, defined in Equation (4.9), will be:

$$Ce_r(t) = Cx(t) + C\Pi z(t) = y(t) - y_r(t) + \left[C\Pi z(t) - Qz(t)\right] \tag{4.33}$$

Therefore, if $C\Pi = Q$, then $Ce_r(t) = e(t)$, and, as $e_r(t)$ is stable, $e(t)$ will decrease and proper tracking is achieved.

Remark 4.3 *: From Remark 4.2 and Lemma 4.3, it is possible to say that $e_r(t)$ is going to reach the origin at a finite time t_s. Thus, $y(t) = y_r(t)$ for $t > t_s$, as $e(t) = Ce_r(t) = 0$ for $t > t_s$. Also, as $e_r(t) = 0$ for $t > t_s$, $x(t) = \Pi z(t)$ and Π can be recognized as a mapping between the system states and the exosystem states when proper tracking is achieved.*

Remark 4.4 *: Due to the exosystem structure defined in Assumption 4.1, the Sylvester equation shown in Equation 4.29 can be separated in two different sets of equations and solved separately.*

Lemma 4.6 *: Considering the same number of inputs as of outputs, the solution for the first set of Sylvester equations will be:*

$$\begin{aligned} L_{1,i} &= \left[\bar{G}_1(0)\right]^{-1}\left[Q_{1,i} + \sum_{j=1}^{i-1}(-1)^{i-(j-1)}\bar{G}_{i-(j-1)}(0)L_{1,j}\right] \\ \Pi_{1,i} &= \sum_{j=1}^{i}(-1)^{i-j}\left[(0-\bar{A})^{-1}\right]^{i-(j-1)}BL_{1,j} \end{aligned} \tag{4.34}$$

for $i = 1, ..., n_1$, where $L_1 = [L_{1,1}, \ldots, L_{1,n_1}]$, $\Pi_1 = [\Pi_{1,1}, \ldots, \Pi_{1,n_1}]$ and $\bar{G}_k(0) = C\left[(0-\bar{A})^{-1}\right]^k B$, such that $\bar{G}_1(0) = C\left[(0-\bar{A})^{-1}\right]B = \bar{G}(0)$. And for the second set of equations, the solution will be:

$$\begin{aligned} L_{2,2i-1} &= Re\left[\bar{G}(f_i\mathbf{j})^{-1}\right]Q_{2,2i-1} - Im\left[\bar{G}(f_i\mathbf{j})^{-1}\right]Q_{2,2i} \\ L_{2,2i} &= Re\left[\bar{G}(f_i\mathbf{j})^{-1}\right]Q_{2,2i} + Im\left[\bar{G}(f_i\mathbf{j})^{-1}\right]Q_{2,2i-1} \\ \Pi_{2,2i-1}(\zeta) &= Re\left[\left(f_i\mathbf{j}I - \bar{A}\right)^{-1}B\right]L_{2,2i-1} - Im\left[\left(f_i\mathbf{j}I - \bar{A}\right)^{-1}B\right]L_{2,2i} \\ \Pi_{2,2i}(\zeta) &= Re\left[\left(f_i\mathbf{j}I - \bar{A}\right)^{-1}B\right]L_{2,2i} + Im\left[\left(f_i\mathbf{j}I - \bar{A}\right)^{-1}B\right]L_{2,2i-1} \end{aligned} \tag{4.35}$$

for $i = 1, ..., n_2/2$, where $L_2 = [L_{2,1}, \ldots, L_{2,n_2}]$ and $\Pi_2 = [\Pi_{2,1}, \ldots, \Pi_{2,n_2}]$.

Proof: For the first set of Sylvester equation it is easy to see that due to the structure of J_1 considered in Assumption 4.1, the following relation must hold:

$$\Pi_{1,i} = \bar{A}\Pi_{1,i+1} + BL_{1,i+1} \tag{4.36}$$

for $i = 1, ..., n_1 - 1$ and with $0 = \bar{A}\Pi_{1,1} + BL_{1,1}$. Applying $(0-\bar{A})^{-1}$ on both sides and isolating Π leads to:

$$\Pi_{1,i+1} = -(0-\bar{A})^{-1}\Pi_{1,i} + (0-\bar{A})^{-1}BL_{1,i+1} \tag{4.37}$$

with $\Pi_{1,1} = (0 - \bar{A})^{-1} B L_{1,1}$, which recursively leads to $\Pi_{1,i}$ in Equation (4.34). Applying C in both sides of this last equation, taking into account that $C\Pi_{1,i} = Q_{1,i}$ and isolating for $L_{1,i}$ leads to the result shown in (4.34).

For the second set of Sylvester equations, first, both sides of the equation are multiplied by the eigenvector of J_2, and taking into account that $J_2\phi_{J_2} = \lambda_{J_2}\phi_{J_2}$ leads to:

$$\Pi_2 J_2 \phi_{J_2} = \Pi_2 \lambda_{J_2} \phi_{J_2} = \bar{A}\Pi_2\phi_{J_2} + BL_2\phi_{J_2} \tag{4.38}$$

From Remark 4.1, the eigenvectors of J_2 are all null except at the corresponding row of $\pm f_i\mathbf{j}$, with $i = 1, ..., n_2/2$. Therefore:

$$\begin{aligned} \Pi_2\phi_{J_2} &= \left(\lambda_{J_2} I - \bar{A}\right)^{-1} BL_2\phi_{J_2} \\ \left[\Pi_{2,2i-1}\ \Pi_{2,2i}\right]\left[1\ \mathbf{j}\right]^T &= \left(f_i\mathbf{j}I - \bar{A}\right)^{-1} B\left[L_{2,2i-1}\ L_{2,2i}\right]\left[1\ \mathbf{j}\right]^T \end{aligned} \tag{4.39}$$

and the equivalence of the complex numbers from both sides of the equations gives the solution for $\Pi_{2,2i-1}$ and $\Pi_{2,2i}$. Applying C in both sides, knowing that $C\Pi_{2,i} = Q_{2,i}$ gives the results shown in Equation (4.35).

Remark 4.5 *: From the solution shown in Lemma 4.6, it is possible to conclude that the solutions of the Sylvester equations* Π *exist if* $\sigma(\bar{A}) \neq \sigma(S) = \sigma(J_1) \cup \sigma(J_2)$*, such that* $\bar{G}(\lambda_S) \neq \infty$*. In a similar way, for the feedforward gains* L *to exist the eigenvalues* S *must not be a zero of the transfer function, as the inverse of the transfer function must exist (which means that* $\bar{G}(\lambda_S) \neq 0$*, such that* L *exist in Equations (4.34) and (4.35)).*

For the exosystem shown in Equation (4.8), the solution of the Sylvester equations will be $L = [L_{1,1}\, L_{1,2}\, L_{2,1}\, L_{2,2}]$ and $\Pi = [\Pi_{1,1}\, \Pi_{1,2}\, \Pi_{2,1}\, \Pi_{2,2}]$, given by:

$$\begin{aligned} L_{1,1} &= \bar{G}(0)^{-1} Q_{1,1} \\ \Pi_{1,1}(\zeta) &= \left(0 - \bar{A}\right)^{-1} BL_{1,1} \\ L_{1,2} &= \bar{G}(0)^{-1}\left[Q_{1,2} + \bar{G}_2(0)L_{1,1}\right] \\ \Pi_{1,2}(\zeta) &= -\left(0 - \bar{A}\right)^{-1}\left(0 - \bar{A}\right)^{-1} BL_{1,1} + \left(0 - \bar{A}\right)^{-1} BL_{1,2} \end{aligned} \tag{4.40}$$

and:

$$\begin{aligned} L_{2,1} &= Re\left[\bar{G}(f\mathbf{j})^{-1}\right] Q_{2,1} - Im\left[\bar{G}(f\mathbf{j})^{-1}\right] Q_{2,2} \\ L_{2,2} &= Re\left[\bar{G}(f\mathbf{j})^{-1}\right] Q_{2,2} + Im\left[\bar{G}(f\mathbf{j})^{-1}\right] Q_{2,1} \\ \Pi_{2,1}(\zeta) &= Re\left[\left(f\mathbf{j}I - \bar{A}\right)^{-1} B\right] L_{2,1} - Im\left[\left(f\mathbf{j}I - \bar{A}\right)^{-1} B\right] L_{2,2} \\ \Pi_{2,2}(\zeta) &= Re\left[\left(f\mathbf{j}I - \bar{A}\right)^{-1} B\right] L_{2,2} + Im\left[\left(f\mathbf{j}I - \bar{A}\right)^{-1} B\right] L_{2,1} \end{aligned} \tag{4.41}$$

4.3.3 System Observer Design

The control law defined in Equation (4.22) needs a fullstate feedback measurement across the whole domain. As this is generally not practical or viable, in this section the observer design for thesystem shown in Equations (4.2) and (4.3) is considered. The observer dynamics will be given by the following set of PDE's:

$$\begin{cases} \dfrac{\partial \hat{\nu}}{\partial t} = \mu \dfrac{\partial \hat{\nu}}{\partial \zeta} + \alpha_1 \hat{\nu} + \beta_1 \hat{x}_1 + \beta_2 \hat{x}_2 + \mathrm{e}^{-\frac{\alpha_1}{\mu}\zeta} l_1(\zeta) \left[y_m(t) - \hat{\nu}(\zeta = 0) \right] \\ \dfrac{\partial \hat{x}_1}{\partial t} = -\gamma_1 \dfrac{\partial \hat{x}_1}{\partial \zeta} + \alpha_1 \hat{\nu} + \sigma_{11} \hat{x}_1 + \sigma_{12} \hat{x}_2 + l_2(\zeta) \left[y_m(t) - \hat{\nu}(\zeta = 0) \right] \\ \dfrac{\partial \hat{x}_2}{\partial t} = -\gamma_2 \dfrac{\partial \hat{x}_2}{\partial \zeta} + \alpha_1 \hat{\nu} + \sigma_{21} \hat{x}_1 + \sigma_{22} \hat{x}_2 + l_3(\zeta) \left[y_m(t) - \hat{\nu}(\zeta = 0) \right] \\ \hat{\nu}(1,t) = \rho_1 \hat{x}_1(1,t) + \rho_2 \hat{x}_2(1,t) + u(t) \\ \hat{x}_1(0,t) = q_1 y_m(t) \\ \hat{x}_2(0,t) = q_2 y_m(t) \end{cases} \tag{4.42}$$

where $\hat{x}(\zeta, t) = \left[\hat{\nu}\, \hat{x}_1\, \hat{x}_2 \right]^T \in L^2(0,1)$ are the reconstructed states and $l_i(\zeta)$ are the in-domain observer gains. Similarly to the system stabilization shown in Section 4.3.1 and Appendix 4.A, the backstepping methodology is used once again to find the appropriate gains for the observer. Other techniques could be used, but, once again, the backstepping methodology can be used to ensure finite-time convergence of the observer states to the system states. The derivation of the observer gains are shown in Appendix 4.B.

The observer dynamics can be written in a general state-space representation as:

$$\begin{array}{l} \dot{\hat{x}}(t) = \hat{A}\hat{x}(t) + L_{o,1} \left[y(t) - C_m \hat{x}(t) \right] + L_{o,2} \left[y(t) \right] + Bu(t) = \\ \dot{\hat{x}}(t) = \hat{A}\hat{x}(t) + L_{o,1} C_m \left[\bar{x}(t) - \hat{x}(t) \right] + L_{o,2} C_m \left[\bar{x}(t) \right] + Bu(t) \end{array} \tag{4.43}$$

where $L_{o,1}$ is related to the in-domain observer gains and $L_{o,2}$ is related to the boundary observer gains shown in Equation (4.88). Although $\hat{A}$ has the same in-domain operators as A, it has different boundary conditions, such that $A = \hat{A} + L_{o,2} C_m$.

Lemma 4.7 *: The system observer error will reach the origin in a finite-time of* $t = t_o = \phi_2 + \phi_1$*, with* $\phi_2 = max\left\{ \frac{1}{\gamma_1}, \frac{1}{\gamma_2} \right\}$ *and* $\phi_1 = \frac{1}{\mu}$

Proof: Due to the structure of the target system shown in Equation (4.91), it is easy to see that $\tilde{e}_1(\zeta = 0, t > \phi_2) = \tilde{e}_2(\zeta = 0, t > \phi_2) = 0, \forall \zeta \in [0,1]$, with $\phi_2 = \max\left\{\frac{1}{\gamma_1}, \frac{1}{\gamma_2}\right\}$. This also implies that $\tilde{e}_3(\zeta = 0, t > \phi_2) = 0$ due to the boundary condition. Finally, $\tilde{e}_3(\zeta, t > \phi_1 + \phi_2) = 0, \forall \zeta \in [0,1]$, where $\phi_1 = \frac{1}{\mu}$. Therefore, the observer error target system will reach the origin ($\tilde{e}(\zeta, t) = 0$) in a finite-time of $t = t_o = \phi_2 + \phi_1$. As backstepping is just a linear transformation of the observer error, such that the original observer error is related to the target system by $\hat{e} = T^{-1}\tilde{e}(t)$, $\hat{e}(t) = 0, \forall \zeta \in [0,1]$ for $t \geq t_o$.

4.3.4 Exosystem Observer

If the exosystem dynamics is known, but its states are not available, it is possible to reconstruct the states using the reference signal $y_r(t)$. As the exosystem considered here is a finite system (as shown in Equations (4.5) and (4.6)), the following observer is considered:

$$\dot{\hat{z}}(t) = S\hat{z}(t) + L_e\left[y_r(t) - Q\hat{z}(t)\right] = S\hat{z}(t) + L_eQ\left[z(t) - \hat{z}(t)\right] \tag{4.44}$$

where $\hat{z}$ is the estimated exosystem state and L_e is the observer gain to be defined. The exosystem observer error is given by $\hat{e}_e(t) = z(t) - \hat{z}(t)$ and its dynamics will be:

$$\dot{\hat{e}}_e(t) = (S - L_eQ)\hat{e}_e(t) \tag{4.45}$$

If (S, Q) is detectable, then it is possible to guarantee the reconstruction of the significant exosystem states and stabilization can be achieved by using pole-placement.

Exosystem Finite-Time Observer

The observer design from the previous section attains stabilization in a exponential matter. Here, the finite-time observer is considered to obtain a faster estimation of the exosystem observer. This kind of stabilization was shown in [98] and used in [99]. For this design, two exosystem observers ($\hat{z}_1$ and $\hat{z}_2$) with different observer gains ($L_{e,1}$ and $L_{e,2}$) are considered and the redundant information from this two observers can be used in combination with previous

information to get the estimation to converge in a finite-time. This observer equations are given as:

$$\hat{z}_F(t) = \begin{bmatrix} I & 0 \end{bmatrix} \begin{bmatrix} I & \mathrm{e}^{(A-L_{e,1}Q)D_F} \\ I & \mathrm{e}^{(A-L_{e,2}Q)D_F} \end{bmatrix}^{-1} \left(\begin{bmatrix} \hat{z}_1(t) \\ \hat{z}_2(t) \end{bmatrix} - \begin{bmatrix} \mathrm{e}^{(A-L_{e,1}Q)D_F}\hat{z}_1(t-D_F) \\ \mathrm{e}^{(A-L_{e,2}Q)D_F}\hat{z}_2(t-D_F) \end{bmatrix} \right) \tag{4.46}$$

where $\hat{z}_F(t)$ is the estimation given by the finite-time observer, D_F is the time delay used, $\mathrm{e}^{(A-L_{e,i}Q)D_F}$ is the exponential matrix and I is the identity matrix. With this observer design, $\hat{z}_F(t)$ is guaranteed to converge to $z(t)$ when $t > D_F$ as shown in [98].

4.4 Discrete Time Regulator Design

The discrete regulator design is considered in this section. It is necessary to find a control law for the discrete system that guarantees the closed-loop stability and proper output tracking. Figure 4.4 represents the closed-loop controller for the discrete setting. The closed-loop begins at the controller, where the initial condition for the system and exosystem observers ($\hat{x}_{k=-1}$ and $\hat{z}_{k=-1}$) are used to calculate the first control action $u_{k=0}$. Then, the action is applied to the plant and the system measured output and the reference signal from the exosystem become available ($y_{k=0}$ and $y_{r,k=0}$). These output are used to estimate the system and exosystem states in the observer ($\hat{x}_{k=0}$ and $\hat{z}_{r,k=0}$). Finally, the estimates are used in the control law to calculate the next input (u_1) and the process is repeated.

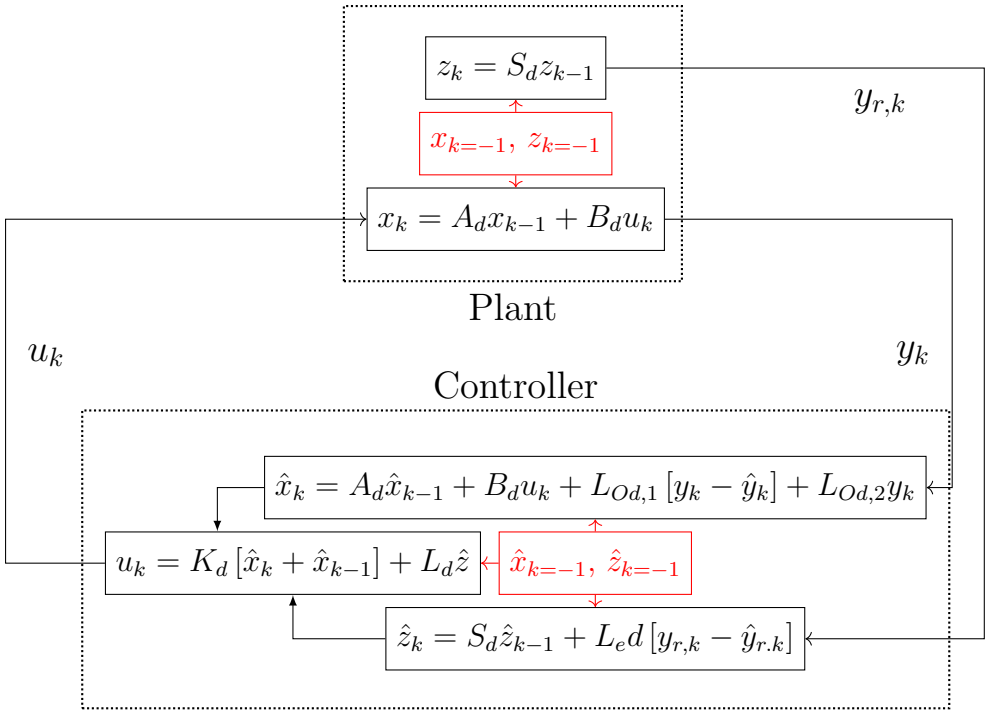

Figure 4.4: Discrete time closed-loop representation.

The control law used to ensure the system stability and proper signal tracking is similar to the regulator equation shown in Equation (4.10) for the continuous setting considering fullstate feedback:

$$u_k = K_d x_{k-1} + L_d z_{k-1} \tag{4.47}$$

where the first part of the right side of the control law represents the feedback control used to guarantee the system stability. The second part is responsible for the output tracking and L_d is a matrix that needs to be found to ensure proper output tracking.

The discrete output tracking error can be defined as:

$$e_k = y_k - y_{r,k} \tag{4.48}$$

Similar to the controller in the continuous time setting, the discrete regulator should guarantee:

- The closed-loop system is stable;

- For the closed-loop system, the tracking error $e_k(k \to \infty) = 0, \forall x_{k=0} \in X, z_{k=0} \in \mathbb{R}$;

Before addressing the discrete regulator design, first the proper discrete representation of the system is considered.

4.4.1 Discrete Representation

Given the system defined in Equation (4.4), one can apply a structure preserving time discretization of the dynamical system. By the application of the Crank-Nicolson midpoint integration rule, and with the assumption of piecewise constant input within the sampled intervals, the Cayley-Tustin time discretization transformation is achieved [28]. The obtained discrete system is represented as:

$$\begin{aligned} x_k &= A_d x_{k-1} + B_d u_k \\ y_k &= C_d x_{k-1} + D_d u_k \\ y_{m,k} &= C_{m,d} x_{k-1} + D_{m,d} u_k \end{aligned} \tag{4.49}$$

where $\delta = 2/\Delta t$, A_d, B_d, C_d, D_d, $C_{m,d}$ and $D_{m,d}$ are the discrete time system operators and are given by:

$$\begin{bmatrix} A_d(\cdot) & B_d \\ C_d(\cdot) & D_d \\ C_{m,d}(\cdot) & D_{m,d} \end{bmatrix} = \begin{bmatrix} -I + 2\delta \left(\delta I - A\right)^{-1}(\cdot) & \sqrt{2\delta}\left(\delta I - A\right)^{-1} B \\ \sqrt{2\delta} C \left(\delta I - A\right)^{-1}(\cdot) & C\left(\delta I - A\right)^{-1} B \\ \sqrt{2\delta} C_m \left(\delta I - A\right)^{-1}(\cdot) & C_m\left(\delta I - A\right)^{-1} B \end{bmatrix} \tag{4.50}$$

and $(\delta I - A)^{-1} = R(\delta, A)$ is defined as the resolvent operator of the operator A, which can be found in Equation (4.16), $(\delta I - A)^{-1} B$ and $G(\delta) = C\left(\delta I - A\right)^{-1} B$ were defined in Equation (4.17) for the specific system considered.

The operators given by Equation (4.50) are all compact and well-defined and the issue of boundary (point) actuation or/and observation does not induce mathematical difficulties which are associated with the continuous counterparts, usually leading to unboundness of the boundary (point) actuation and/or observation.

Assumption 4.2 *: A small enough value of Δt is used such that the discrete time representation of the system shown in Equation (4.49) is a good approximation of the open-loop system internal dynamics and input/output relation.*

Assumption 4.2 presumes there is a large enough δ (small enough Δt) such that the discretization can be applied to unstable systems as well [100] and is necessary for the development of the discrete regulator in the following sessions. For an unstable open-loop system, the following lemma gives an interval for which the discrete representation might be a good approximation of the system:

Lemma 4.8 *: In the case of an unstable system, the discrete system* (A_d, B_d, C_d, D_d) *will not be a good discrete approximation of the system* (A, B, C, D) *if* $\Delta t > \frac{2}{s(A)}$*, where* $s(A) = \sup\{Re\, z : z \in \sigma(A)\}$.

Proof: For a stable system, $s(A) < 0$ (all eigenvalues are negative), thus, as $\delta = \frac{2}{\Delta t}$ and $\Delta t > 0$, $(\delta I - A)^{-1}$ exists for any value of Δt. For an unstable system, $s(A) > 0$, there will be at least one unstable eigenvalue with a positive real part. If this eigenvalue is real, $\delta \to s(A)$ and $(\delta I - A)^{-1} \to \infty$, if $\Delta t \to \frac{2}{s(A)}$. As the discrete operators shown in Equation (4.49) depend on the resolvent, $\Delta t \geq \frac{2}{s(A)}$ will not result in a good discrete approximation. If the eigenvalue is complex, the Spectral Mapping Theorem can give an insight on the behavior of the discrete eigenvalue. If there exists a exact discrete representation of A, it's largest eigenvalue will be $\lambda_{d,E} = \mathrm{e}^{\frac{2}{\delta}\lambda_s}$, such that $\lambda_s = a + b\mathbf{j}$ and $Re\lambda_s = a = s(A)$. For the Cayley-Tustin transformation, this relation is given by $\lambda_{d,CT} = \frac{\delta+\lambda_s}{\delta-\lambda_s}$. If we calculate the modulus of these eigenvalues, we get:

$$||\lambda_{d,E}|| = \mathrm{e}^{\frac{2a}{\delta}};\ ||\lambda_{d,CT}|| = \sqrt{1 + \frac{4a\delta + ||\lambda_s||^2}{\delta^2 - 2a\delta + ||\lambda_s||^2}} \tag{4.51}$$

As expected, if $\Delta t \to 0$, $\delta \to \infty$ and $||\lambda_{d,CT}|| \to ||\lambda_{d,E}||$. Taking the derivative with respect to δ yields:

$$\frac{\partial||\lambda_{d,E}||}{\partial\delta} = \frac{-2a}{\delta^2}\mathrm{e}^{\frac{2a}{\delta}};\ \frac{\partial||\lambda_{d,CT}||}{\partial\delta} = \frac{2a(||\lambda_s||^2 - \delta^2)}{(||\lambda_s||^2 - 2a\delta + \delta^2)^2||\lambda_{d,CT}||} \tag{4.52}$$

For the exact representation, the value of the discrete eigenvalues will decrease as δ increases (i.e., Δt decreases). For the Cayley-Tustin transformation it is possible to see that the function will have an turning point at $(\delta)_{\text{Turn}} = ||\lambda_s||$ or $(\Delta t)_{\text{Turn}} = \frac{2}{||\lambda_s||}$. If $\delta = \frac{2}{\Delta t} = s(A) \leq ||\lambda_s||$, then

$\Delta t > (\Delta t)_{\text{Turn}}$ and the functions have different responses, i.e., $||\lambda_{d,E}||$ is increasing as Δt increases, but $||\lambda_{d,CT}||$ will decrease past the turning point. Thus, $\Delta t \geq \frac{2}{s(A)}$ will not generate a good discrete approximation of the system.

Similar to the controller design in the continuous time setting, first the stabilization of the system in the discrete time setting given by Equations (4.49) and (4.50) is addressed.

4.4.2 Discrete System Stabilization

The design of the discrete regulator is considered in this section. First, it is shown in Lemma 4.9 that the discrete system can be stabilized.

Lemma 4.9 *: If K in the continuous time setting is able to stabilize the system, then there is a corresponding $K_d(\cdot)$ in the discrete time setting that ensures the discrete system stability with the control law:*

$$u_k = K_d x_{k-1} \tag{4.53}$$

with:

$$K_d = \sqrt{2\delta}\left(I - K(\delta I - A)^{-1}B\right)^{-1} K(\delta I - A)^{-1} \tag{4.54}$$

Proof: With the control law considered, the closed-loop discrete system is given by:

$$x_k = \left(A_d + B_d K_d\right) x_{k-1} \tag{4.55}$$

By using the definitions of the operators, the following relation can be achieved:

$$\begin{array}{c} x_k = \Big[-I + 2\delta(\delta I - A)^{-1} \\ +2\delta(\delta I - A)^{-1}B\left(I - K(\delta I - A)^{-1}B\right)^{-1} K(\delta I - A)^{-1}\Big] x_{k-1} \\ = \left\{-I + 2\delta(\delta I - A)^{-1}\left[I - BK(\delta I - A)^{-1}\right]^{-1}\right\} x_{k-1} = \\ \left[-I + 2\delta\left(\delta I - A - BK\right)^{-1}\right] x_{k-1} \end{array} \tag{4.56}$$

where the Woodbury identity was used to properly manipulate the expressions. The resulting operator is equivalent to the discrete operator obtained by applying the Cayley-Tustin time discretization in the closed-loop system

obtained in Section 4.3.1. Using the Cayley-Tustin transformation, the closed-loop system can be represented in the discrete setting as:

$$x_k = \bar{A}_d x_{k-1} \implies \bar{A}_d = -I + 2\delta(\delta I - \bar{A})^{-1} = -I + 2\delta\left(\delta I - A - BK\right)^{-1} \tag{4.57}$$

From [6], [101], it was shown that a stable continuous operator generates a stable discrete operator, thus, if $(A+BK)$ is stable, then the discrete operator $\bar{A}_d = -I + 2\delta\left(\delta I - A - BK\right)^{-1}$ is stable as well. Finally, if the control law proposed in Equation (4.53) with K_d shown in Equation (4.54), is used, then the closed-loop discrete operator is equivalent to the operator shown above and the discrete closed-loop system is stable as well (i.e., $A_d + B_d K_d = \bar{A}_d$).

With the proposed control law, the discrete closed-loop system is given as:

$$\begin{aligned} x_k &= \bar{A}_d x_{k-1} + B_d r_k \\ y_k &= \bar{C}_d x_{k-1} + D_d r_k \end{aligned} \tag{4.58}$$

with:

$$\begin{bmatrix} \bar{A}_d & B_d \\ \bar{C}_d & D_d \end{bmatrix} = \begin{bmatrix} A_d + B_d K_d & B_d \\ C_d + D_d K_d & D_d \end{bmatrix} = \begin{bmatrix} \left[-I + 2\delta\left(\delta I - A - BK\right)^{-1}\right] & B_d \\ \sqrt{2\delta} C\left(I\delta - A - BK\right)^{-1} & D_d \end{bmatrix} \tag{4.59}$$

4.4.3 Discrete Output Regulation

After achieving the system stabilization, it is possible to accomplish proper output tracking. First, the Cayley-Tustin time discretization is applied to the exosystem, such that the discrete time exosystem is given as:

$$\begin{aligned} z_k &= S_d z_{k-1} \\ y_{r,k} &= Q_d z_{k-1} \end{aligned} \tag{4.60}$$

with:

$$S_d = -I + 2\delta(\delta - S)^{-1} =$$

$$\begin{bmatrix} 1 & \frac{2}{\delta} & 0 & 0 \\ 0 & 1 & 0 & 0 \\ 0 & 0 & \frac{\delta^2 - f^2}{\delta^2 + f^2} & \frac{2\delta f}{\delta^2 + f^2} \\ 0 & 0 & -\frac{2\delta f}{\delta^2 + f^2} & \frac{\delta^2 - f^2}{\delta^2 + f^2} \end{bmatrix}; \tag{4.61}$$

$$Q_d = \sqrt{2\delta} Q \left(\delta I - S\right)^{-1}$$

Then, it is necessary to find the discrete feedforward gain L_d that is able to guarantee the proper tracking of the reference signal $y_{r,k}$. This can be accomplished by solving the output regulator equations in the discrete-time setting.

Discrete Regulator Equations

In Section 4.3.2, the regulation equations were solved in the continuous setting. In this section, the output regulation equations for the discrete time setting are derived. The following Lemma summarizes the results for the output tracking if the Cayley-Tustin time discretization is applied.

Lemma 4.10 *: If the Cayley-Tustin time discretization is considered, then the solution of the regulation equation (Sylvester equations) in the discrete setting is the same as in the continuous setting, i.e.,* $\Pi_d = \Pi$*, such that* $x_k = \Pi_d(\zeta) z_k$ *when proper tracking is achieved and it is the solution of the following Sylvester equations in the discrete-time setting:*

$$\begin{aligned} \Pi_d S_d &= \bar{A}_d \Pi_d + B_d L_d \\ \bar{C}_d \Pi_d + D_d L_d &= Q_d \end{aligned} \tag{4.62}$$

with the following relation between L *and* L_d*:*

$$L_d = \sqrt{2\delta} \left(I - K(\delta I - A)^{-1} B\right)^{-1} L(\delta I - S)^{-1} \tag{4.63}$$

Proof: The discrete control law that stabilizes the system and ensures the proper tracking of the discrete signal is given by: with the following relation

between L and L_d:

$$u_k = K_d x_{k-1} + L_d z_{k-1} \tag{4.64}$$

The discrete error is defined as $e_{r,k} = x_k - \Pi_d z_k$, which leads to:

$$\begin{gathered} e_{r,k} = x_k - \Pi_d z_k = \bar{A}_d x_{k-1} + B_d L_d z_{k-1} - \Pi_d z_k = \\ \bar{A}_d \left[x_{k-1} - \Pi_d z_{k-1} \right] + \left[\bar{A}_d \Pi_d + B_d L_d - \Pi_d S_d \right] z_{k-1} \end{gathered} \tag{4.65}$$

and if the last term in brackets is equal zero, the error system becomes:

$$e_{r,k} = \bar{A}_d e_{r,k-1} \tag{4.66}$$

which is stable if $\bar{A}_d$ is stable. This yields the following Sylvester equation:

$$\Pi_d S_d = \bar{A}_d \Pi_d + \bar{B}_d L_d \tag{4.67}$$

And the tracking error will be:

$$\begin{gathered} e_k = y_k - y_{r,k} = \bar{C}_d x_{k-1} + D_d L_d z_{k-1} - Q_d z_{k-1} = \\ \bar{C}_d \left[x_{k-1} - \Pi_d z_{k-1} \right] + \\ \left[\bar{C}_d \Pi_d z_{k-1} + D_d L_d z_{k-1} - Q_d z_{k-1} \right] = \\ \bar{C}_d e_{k-1} + \left[\bar{C}_d \Pi_d + D_d L_d - Q_d \right] z_{k-1} \end{gathered} \tag{4.68}$$

which gives the condition:

$$\bar{C}_d \Pi_d + \bar{D}_d L_d = Q_d \tag{4.69}$$

Lastly, the proof that $\Pi_d(\zeta) = \Pi(\zeta)$ for the Cayley-Tustin time discretization is derived. First, the discrete Sylvester equation is considered and the definition of each operator is used:

$$\begin{gathered} \Pi_d S_d = \bar{A}_d \Pi_d + B_d L_d \implies \\ \Pi_d \left(\delta I - S \right)^{-1} = \left(\delta I - A - BK \right)^{-1} \Pi_d + \\ \left(\delta I - A \right)^{-1} B \left(I - K (\delta I - A)^{-1} B \right)^{-1} L \left(\delta I - S \right)^{-1} \implies \\ \Pi_d \left(\delta I - S \right)^{-1} = \left(\delta I - A - BK \right)^{-1} \Pi_d \\ + \left(\delta I - A - BK \right)^{-1} BL \left(\delta I - S \right)^{-1} \implies \\ \left(\delta I - A - BK \right) \Pi_d = \Pi_d \left(\delta I - S \right) + BL \implies \\ \Pi_d S = (A + BK) \Pi_d + BL \end{gathered} \tag{4.70}$$

And for the algebraic condition:

$$\begin{gathered}
\bar{C}_d\Pi_d + D_d L_d = Q_d \implies \\
C\left(\delta I - A\right)^{-1}\left[I + B\left(I - K\left(\delta I - A\right)^{-1}B\right)^{-1}K\left(\delta I - A\right)^{-1}\right]\Pi_d + \\
C\left(I - \left(\delta I - A\right)^{-1}BK\right)^{-1}\left(\delta I - A\right)^{-1}BL\left(\delta I - S\right)^{-1} = \\
Q\left(\delta I - S\right)^{-1} \implies \\
C\left(\delta I - A\right)^{-1}\left(I - BK\left(\delta I - A\right)^{-1}\right)^{-1}\Pi_d \\
+C\left(\delta I - A - BK\right)^{-1}BL\left(\delta I - S\right)^{-1} = Q\left(\delta I - S\right)^{-1} \implies \\
C\left[\left(\delta I - A - BK\right)^{-1}\Pi_d + \left(\delta I - A - BK\right)^{-1}BL\left(\delta I - S\right)^{-1}\right] = \\
Q\left(\delta I - S\right)^{-1} \implies C\Pi_d\left(\delta I - S\right)^{-1} = Q\left(\delta I - S\right)^{-1} \implies C\Pi_d = Q
\end{gathered} \tag{4.71}$$

which is the same Sylvester equation and algebraic condition shown in the continuous-time setting (Equation (4.29)), consequently, $\Pi_d = \Pi$.

4.4.4 Discrete System Observer Design

The discrete observer design is considered in this section, as it was developed in Section 4.3.3 in the continuous time setting. In the continuous setting (Equation (4.43)), the observer does not have the same operator as the system ($\hat{A}$ is different from A), thus, the discrete observer will also have different operators A_d, B_d, C_d and D_d when compared to the discrete system. Thus, the discrete system is observable as well and the discrete observer will take the following form:

$$\begin{aligned}
\hat{y}_{m,k} &= \hat{C}_{m,d}\hat{x}_{k-1} + \hat{D}_{m,d}u_k + (M_{od,1} + M_{od,2})y_k \\
\hat{x}_k &= \hat{A}_d\hat{x}_{k-1} + \hat{B}_d u_k + L_{od,1}\left[y_{m,k} - \hat{y}_{m,k}\right] + L_{od,2}\left[y_{m,k}\right]
\end{aligned} \tag{4.72}$$

where B_d and y_k have been defined previously. The other discrete operators are given as:

$$\begin{bmatrix} \hat{A}_d(\cdot) & \hat{B}_d \\ \hat{C}_{m,d}(\cdot) & \hat{D}_{m,d} \end{bmatrix} =$$
$$\begin{bmatrix} -I(\cdot) + 2\delta \left(\delta I - \hat{A}\right)^{-1} (\cdot) & \sqrt{2\delta} \left(\delta I - \hat{A}\right)^{-1} B \\ \sqrt{2\delta} \left[I + C_m \left(\delta I - \hat{A}\right) L_{o,1}\right]^{-1} C_m \left(\delta I - \hat{A}\right)^{-1} & \left[I + C_m \left(\delta I - \hat{A}\right) L_{o,1}\right]^{-1} C_m \left(\delta I - \hat{A}\right)^{-1} B \end{bmatrix} \tag{4.73}$$
$$M_{od,1} = \left[I + C_m \left(\delta I - \hat{A}\right) L_{o,1}\right]^{-1} C_m \left(\delta I - \hat{A}\right)^{-1} L_{o,1}$$
$$L_{od,1} = \sqrt{2\delta} \left(\delta I - \hat{A}\right)^{-1} L_{o,1}$$
$$M_{od,2} = \left[I + C_m \left(\delta I - \hat{A}\right) L_{o,1}\right]^{-1} C_m \left(\delta I - \hat{A}\right)^{-1} L_{o,2}$$
$$L_{od,2} = \sqrt{2\delta} \left(\delta I - \hat{A}\right)^{-1} L_{o,2}$$

Notice that $L_{od,1}$ and $L_{od,2}$ have similar structure to B_d, as the system measured output $y_{m,k}$ can be considered as an input to the observer as well.

Lemma 4.11 *: If the observer gains in the continuous time setting ($L_{o,1}$ and $L_{o,2}$) are chosen such that ($\hat{A} - L_{o,1}C_m$) is stable, then, the discrete observer given by Equation (4.72) and the operators defined in Equation (4.73) will be able to reconstruct the states of the discrete system (the discrete observer error - $\hat{e}_k$ - decreases with time and eventually reaches the origin).*

Proof: To prove the observer states convergence to the system states, it is necessary to analyze the discrete observer error:

$$\hat{e}_k = x_k - \hat{x}_k \tag{4.74}$$

After some algebraic manipulation (shown in Appendix 4.C), the discrete error can be written as:

$$\hat{e}_k = (\hat{A}_d - L_{od,1}\hat{C}_{m,d})\hat{e}_{k-1} = \left\{-I + 2\left[\delta I - \hat{A} + L_{o,1}C_m\right]^{-1}\right\} \hat{e}_{k-1} \tag{4.75}$$

which is the discrete operator generated by ($\hat{A} - L_{o,1}C_m$). Thus, if $L_{o,1}$ is chosen such that ($\hat{A} - L_{o,1}C_m$) is stable, the discrete observer will be stable as well, as the Cayley-Tustin time discretization cannot map a stable continuous system to a unstable discrete one.

4.4.5 Discrete Exosystem Observer Design

The discrete observer design for the exosystem is considered in this section using the discrete reference signal $y_{r,k}$. The following finite discrete observer is considered:

$$\begin{aligned} \hat{y}_{r,k} &= \hat{Q}_d \hat{z}_{k-1} + M_{ed} y_{r,k} \\ \hat{z}_k &= S_d \hat{z}_{k-1} + L_{ed}(y_{r,k} - \hat{y}_{r,k}) \end{aligned} \tag{4.76}$$

where $\hat{z}_k$ is the estimated exosystem state, S_d and Q_d have been defined in Section 4.4.3 (in Equation (4.60)). L_{ed} and M_{ed} are defined as:

$$\begin{aligned} L_{ed} &= \sqrt{2\delta}\left(\delta I - S\right)^{-1} L_e \\ \hat{Q}_d &= \left[I + Q\left(\delta I - S\right)^{-1} L_e\right]^{-1} \sqrt{2\delta} Q \left(\delta I - S\right)^{-1} \\ M_{ed} &= \left[I + Q\left(\delta I - S\right)^{-1} L_e\right]^{-1} Q \left(\delta I - S\right)^{-1} L_e \end{aligned} \tag{4.77}$$

Lemma 4.12 *: If the exosystem observer gain in the continuous time setting (L_e) is chosen such that $(S - L_e Q)$ is stable, then, the discrete observer given by Equation (4.76) and the operators defined in Equation (4.77) will be able to reconstruct the states of the discrete exosystem.*

Proof: To prove the exosystem observer convergence to the system states, the discrete error of the exosystem observer is analyzed:

$$\hat{e}_{r,k} = z_k - \hat{z}_k \tag{4.78}$$

After some algebraic manipulation (shown in Appendix 4.D), the discrete error can be written as:

$$\hat{e}_{r,k} = (S_d - L_{ed}\hat{Q}_d)\hat{e}_{r,k-1} = \left\{-I + 2\left[\delta I - S + L_e Q\right]^{-1}\right\} \hat{e}_{r,k-1} \tag{4.79}$$

which is the operator generated by the discrete representation of $(S - L_e Q)$. Thus, if L_e is chosen such that $(S - L_e Q)$ is stable, the discrete observer will be stable as well.

4.4.6 Finite-Time Discrete Exosystem Observer Design

The exosystem discrete dynamics is given by $z_k = S_d z_{k-1}$ and the reference signal is $y_{r,k} = Q_d z_{k-1}$. If the pair (S_d, Q_d) is observable (which can be proved

by the observability of (S, Q)), then the exosystem states can be estimated in the discrete setting using the observability matrix:

$$\begin{bmatrix} y_{r,k} \\ y_{r,k+1} \\ \vdots \\ y_{r,k+e-1} \end{bmatrix} = \begin{bmatrix} Q_d \\ Q_d S_d \\ \vdots \\ Q_d S_d^{e-1} \end{bmatrix} \hat{z}_{k-1} = \text{OBSV}_{Exo} \hat{z}_{k-1} \implies \hat{z}_k = S_d^{k+1} \hat{z}_{k-1} \tag{4.80}$$

where, OBSV_{Exo} is the exosystem observability matrix in the discrete-time setting. Therefore, after e time steps (and e samples of $y_{r,k}$) it is possible to properly estimate z_k. For any instance before that, the discrete observer from Section 4.4.5 can be used.

4.5 Results

In this section, the numerical simulations are shown to demonstrate the application of the regulator designed. The system parameters used in the following results are given in Table 4.1. For the given values the open-loop system is unstable, as shown in Section 4.2.1. The desired reference signal is given by the function:

$$y(t) = 1 + 0.1t + \frac{\sin\left(\frac{\pi}{2}t\right)}{2} \tag{4.81}$$

To generate this signal with the exosystem, the following conditions are chosen:

$$Q = \begin{bmatrix} 1 & 0 & 1 & 0 \end{bmatrix}; f = \frac{1}{2}; z(0) = \begin{bmatrix} 1 & 0.1 & 0 & 0.5 \end{bmatrix}^T \tag{4.82}$$

First, the simulations for the design of the regulator in the continuous-time setting are shown.

4.5.1 Continuous Time Regulation

Using the values given in Table 4.1, a numerical simulation was performed in the continuous time setting to show the system stabilization with the control law shown in Equation (4.22), in Section 4.3.1. The result is shown in Figure 4.5 and it is possible to see that the system is stabilized at a time close to $t = \phi_1 + \phi_2 = \frac{1}{\mu} + \max\left\{\frac{1}{\gamma_1}, \frac{1}{\gamma_2}\right\} = \frac{1}{2} + \max\left\{\frac{1}{0.5}, \frac{1}{1}\right\} = 2.5$, as expected from the relation between the target and the closed-loop system.

Next, the results for the output tracking are presented. The result is shown in Figure 4.6 and the control law from Equation (4.10) is used. As expected from the finite time stabilization obtained due to the desired target system, the system output starts to perfectly track the reference signal for a time close to $t = 2.5$. The results from Figures 4.5 and 4.6 consider that all the system states and exosystem states are available.

The measurement of all states is generally not feasible, specially when a DPS is considered. Thus, the control law shown in Equations (4.22) and (4.10) might not be used directly. Taking that into account, the observer design for the system states and the exosystem were considered in Sections 4.3.3 and 4.3.4, respectively. First, the results for the system observer are examined. Figure 4.7 shows the results for this simulation. As expected, the observer states are able to reconstruct the system states at a finite time close to $t = 2.5$ (i.e., the observer error reaches the origin for a time close to $t = 2.5$).

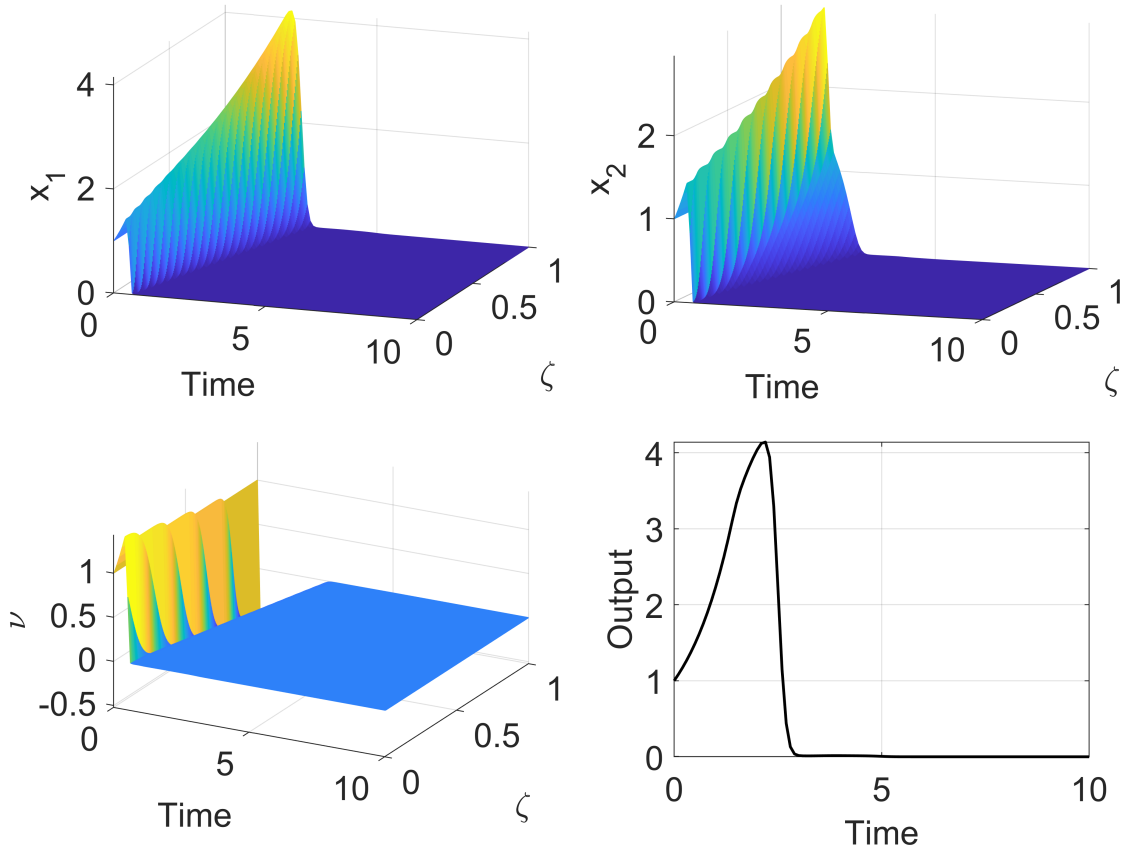

Figure 4.5: System stabilization with the control law given in Equation (4.22).

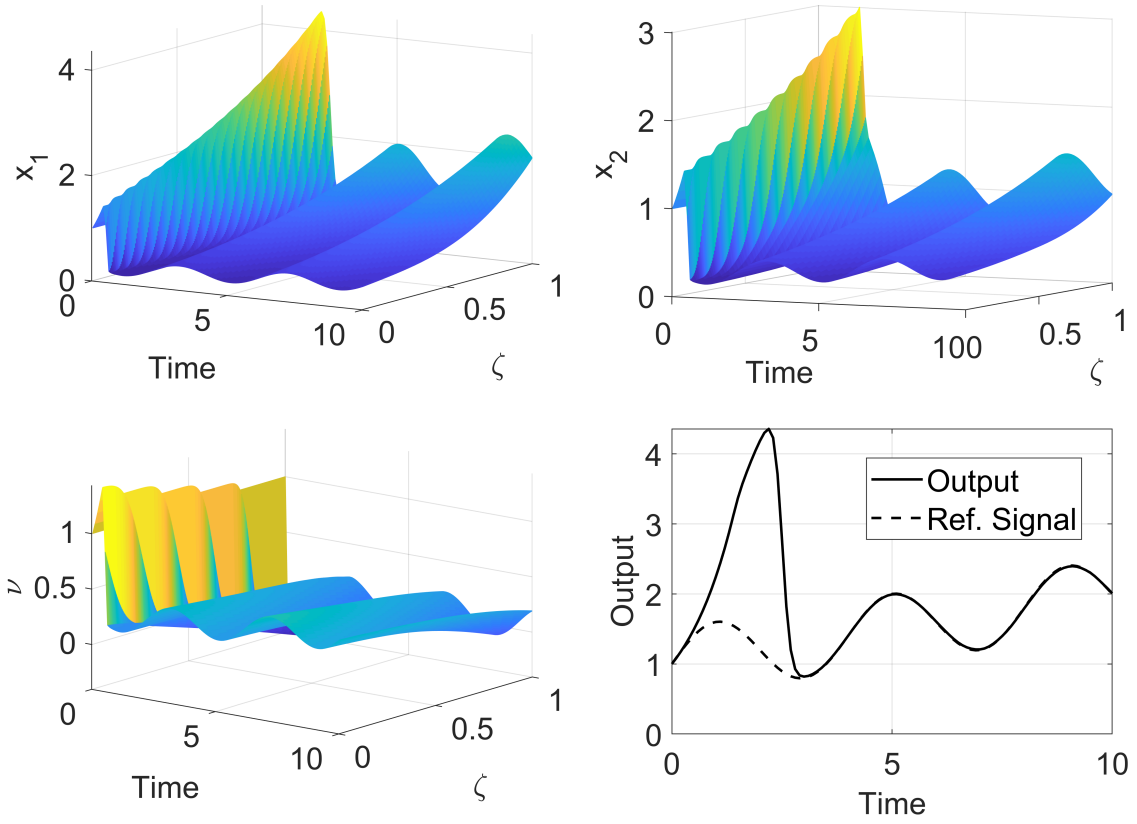

Figure 4.6: System stabilization and output regulation with the control law given in Equation (4.10).

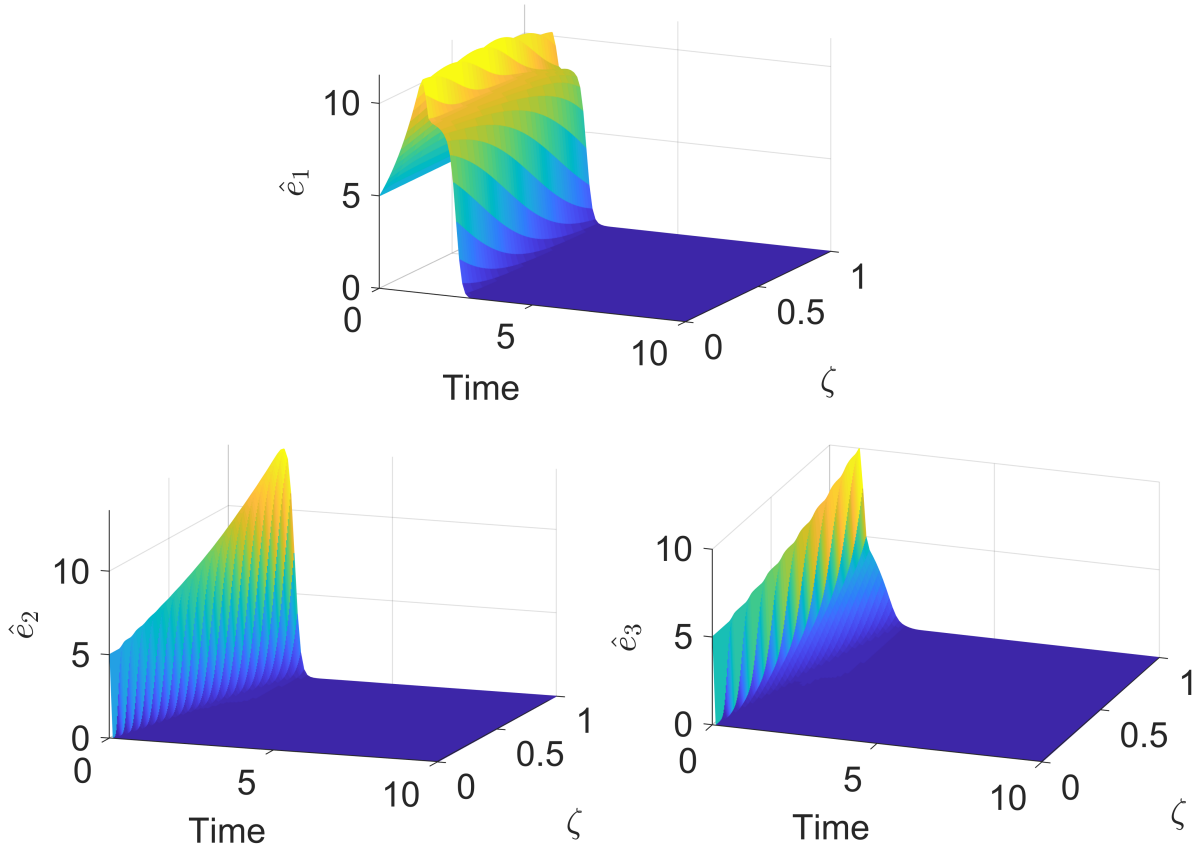

Figure 4.7: System observer error, using the observer developed in Section 4.3.3.

Next, the performance of the system observer with the Equation (4.10) is examined. Instead of using the system states in the control law, the observer states are used and the result is shown in Figure 4.8. As the observer is able to properly reconstruct the system states for $t > t_o = 2.5$, the controller can just properly stabilize and achieve proper tracking after that. Thus, the system is stabilized and the output properly tracks the reference signal at $t = t_o + t_s = 5$.

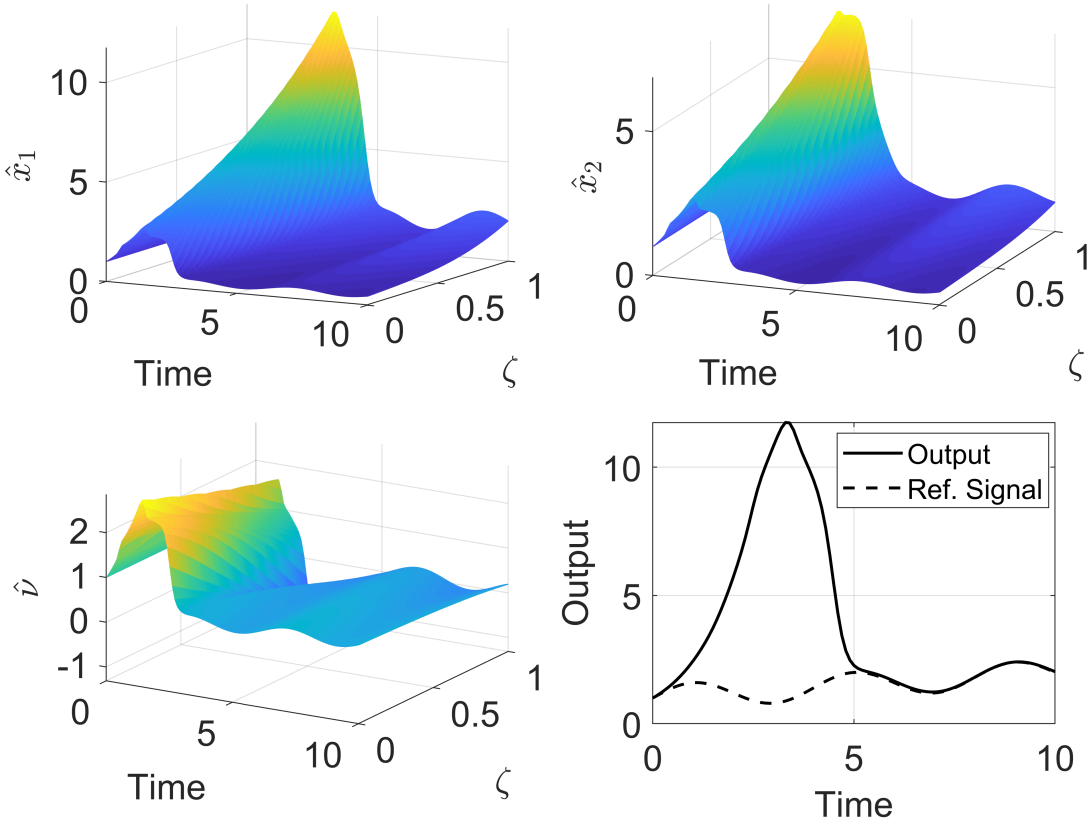

Figure 4.8: System closed-loop response, using the observer developed in Section 4.3.3 and the control law given in Equation (4.10).

The simulation results shown before still considered that the exosystem states were available. Next, the results with the exosystem observer, shown in Section 4.3.4, are explored. Figure 4.9 shows the closed-loop system response considering that the exosystem observer will have the poles placed at $\sigma(S - L_e Q) = \{-1, -2, -3, -4\}$. The finite stabilization and system observer convergence are still achieved, but, as the exosystem observer, in this case, does not have a finite time convergence, the proper output tracking takes longer to be obtained (it exponentially converges).

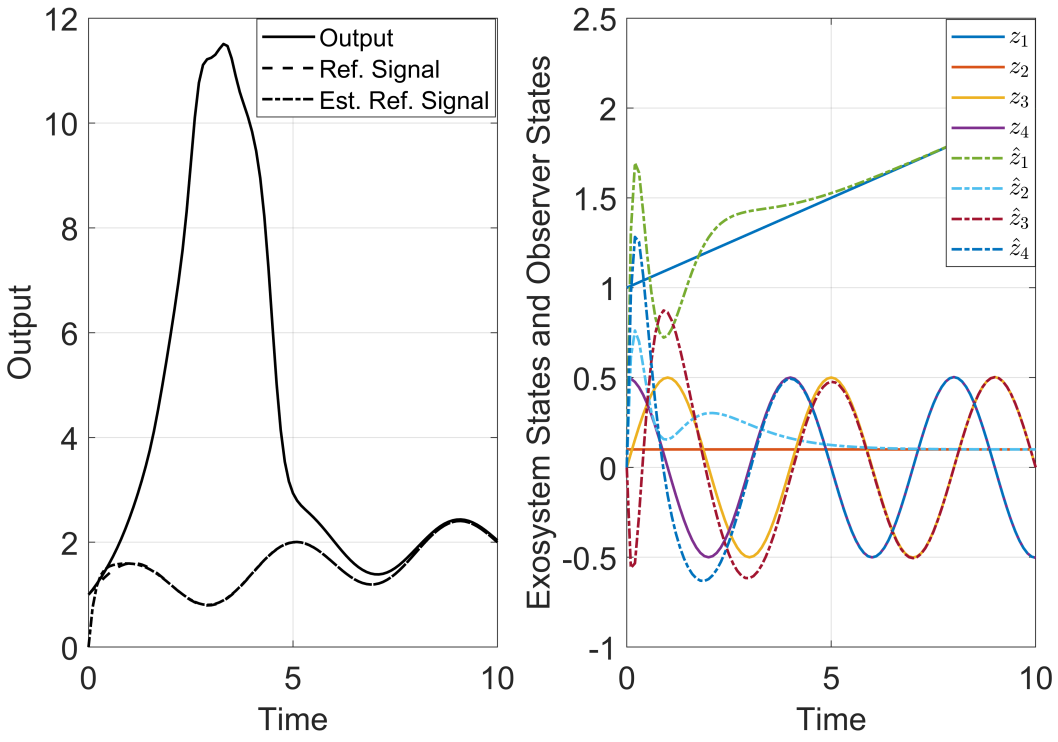

Figure 4.9: System closed-loop response (on the left), using the system and exosystem observers and the control law given in Equation (4.10). On the right, the exosystem states and its observer states.

The last case considered in the continuous-time setting is the use of the finite-time observer to reconstruct the exosystem states. The simulation results are presented in Figure 4.10. As two observer are necessary to obtain the finite-time convergence, one observer was designed such that $\sigma(S - L_{e,1} Q) = \{-1, -1.5, -2, -2.5\}$ and the other such that $\sigma(S - L_{e,2} Q) = \{-3, -3.5, -4, -4.5\}$.

The desired convergence time was set to $D_F = t_o + t_s = 5$. Thus the system stability and proper tracking, plus the system and exosystem states reconstruction should be guaranteed for a time close to $t = 5$. As results show, although this observer convergence is guaranteed for time close to $t = 5$, the drawback is the higher error for the estimation in the beginning, which leads to excessive control actions and an increase in the output, which might not be desirable or physically possible.

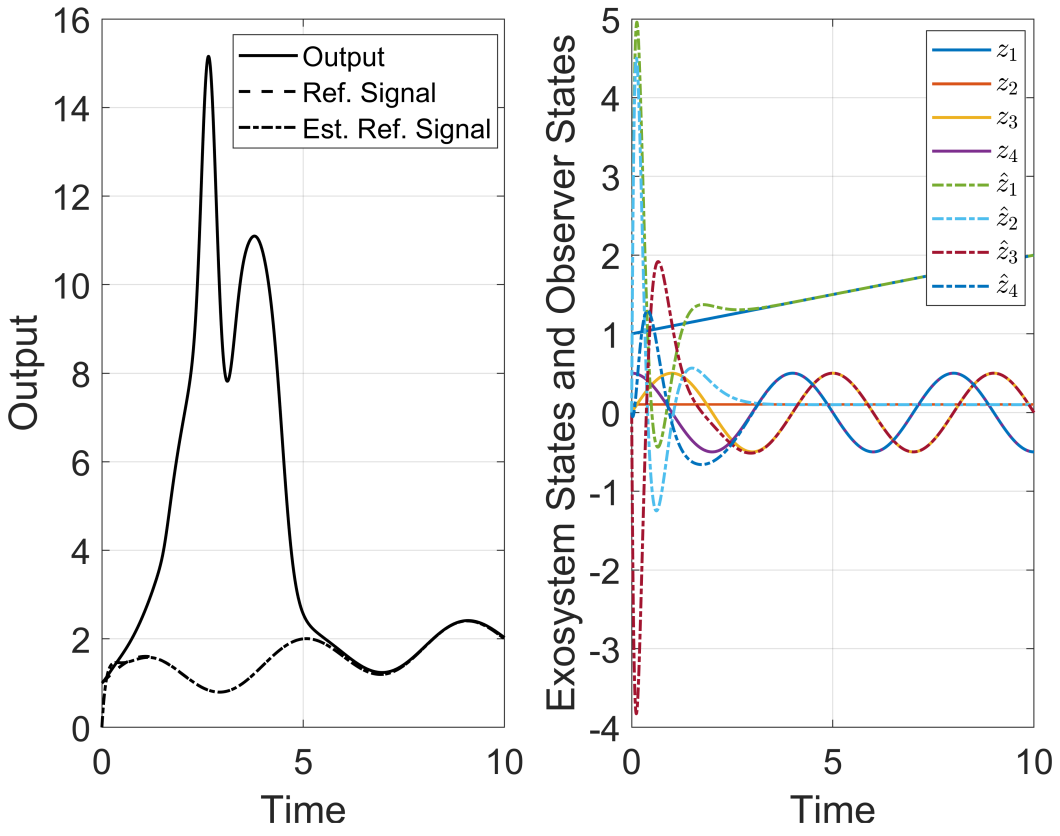

Figure 4.10: System closed-loop response (on the left), using the system observer, finite-time exosystem observer and the control law given in Equation (4.10). On the right, the exosystem states and its observer states.

4.5.2 Discrete Time Regulation

After the design of the regulator in the continuous-time setting has been achieved, the results for the discrete-time settings are considered, using the design developed in Section 4.4. A sampling time of $\Delta t = 0.1$ is used. First,

the system stabilization with the control law shown in Equation (4.53), developed in Section 4.4.2, is shown. The result is presented in Figure 4.11 and it is possible to see that the system is stabilized, as expected from the relation between the closed-loop of the discrete representation and the continuous closed-loop system.

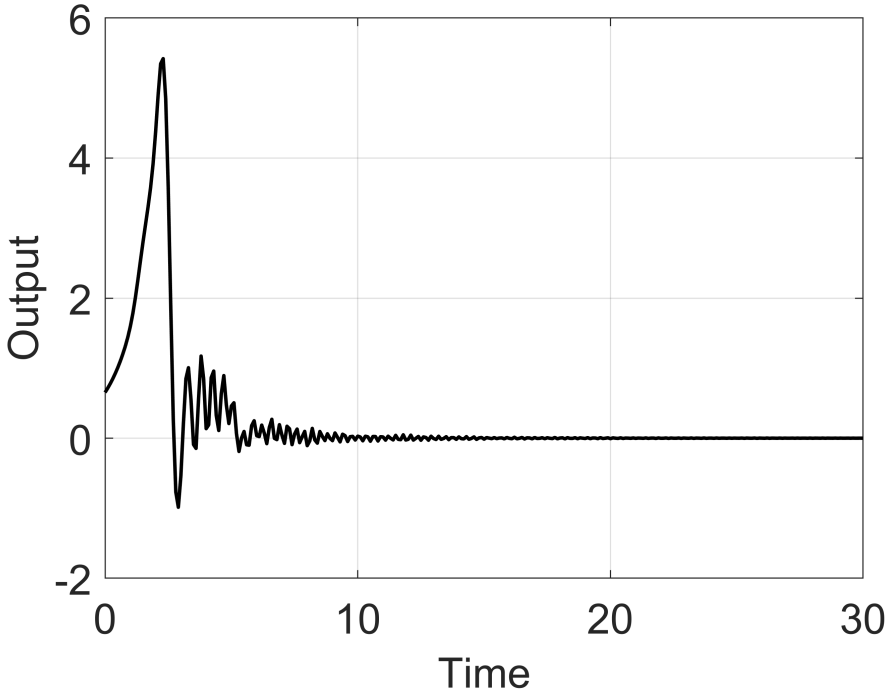

Figure 4.11: Discrete system stabilization with the control law given in Equation (4.53), considering $z_k = 0$.

Next, the results for the output tracking in the discrete time setting are considered. The result is shown in Figure 4.12 and the control law from Equation (4.53), developed in Section 4.4.3, is used. It is assumed that the system and exosystem states are known. As expected, the system stabilization is obtained and the system output is able to perfectly track the reference signal.

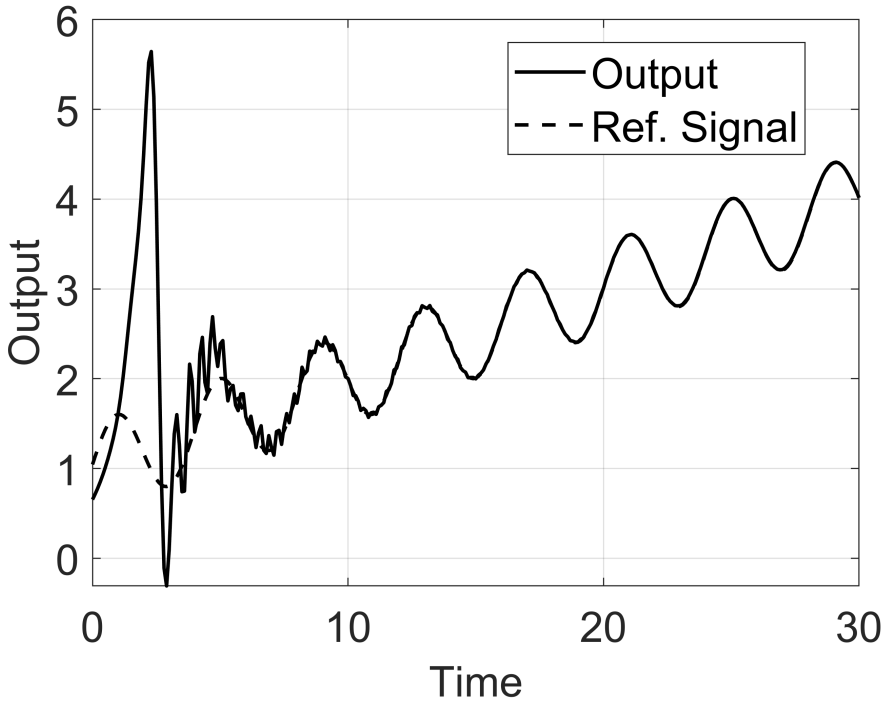

Figure 4.12: Discrete system stabilization and output regulation with the control law given in Equation (4.53), assuming that z_k are known states.

As in the continuous-time setting, the system observer and exosystem observer designs in the discrete-time setting are considered next, using the developed discrete observers designs shown in Section 4.4.4 and Section 4.4.5, respectively. The results for the system observer are considered first in Figure 4.13. As expected, the observer is able to reconstruct the system states and using the observer states in the control law shown in Equation (4.53), the closed-loop of the discrete-time system is stable, achieving proper tracking of the reference signal.

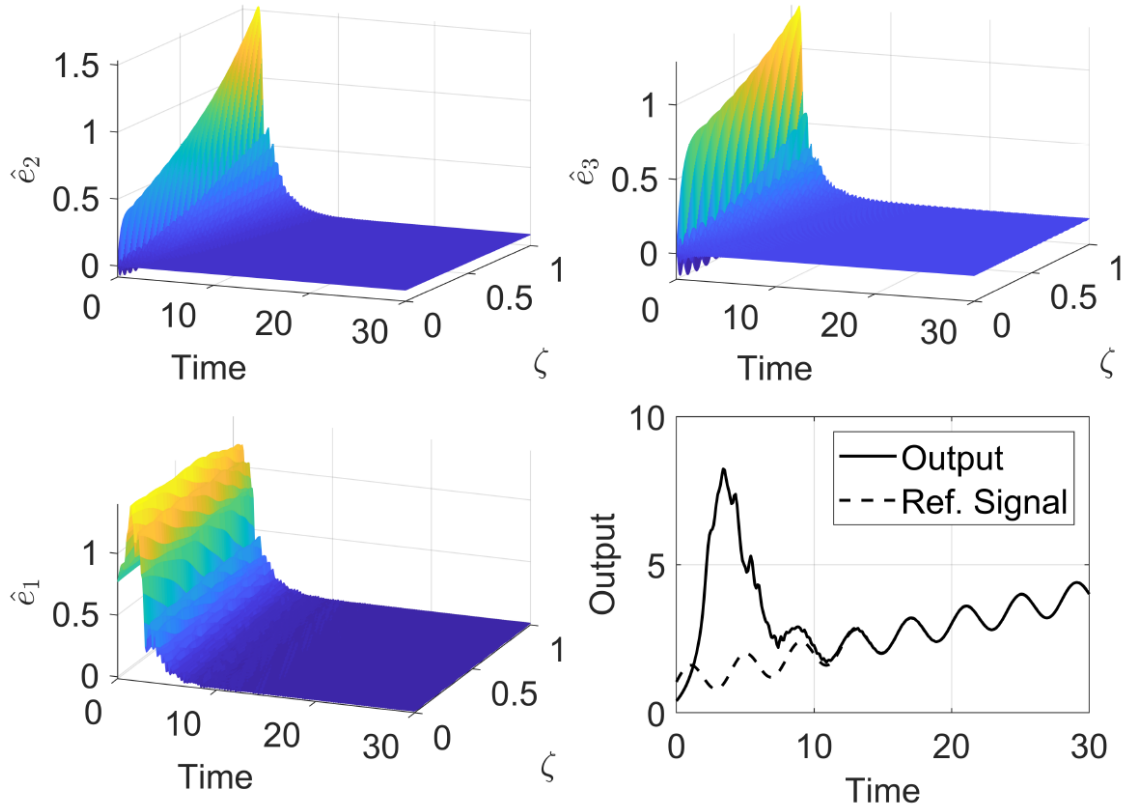

Figure 4.13: Discrete system closed-loop response, using the observer developed in Section 4.4.4 and the control law given in Equation (4.53).

Finally, the exosystem observer design in the discrete-time setting is considered, as shown in Section 4.4.5. Figure 4.14 shows the closed-loop response of the discrete system using the observer gain of the continuous-time setting to guarantee the stability of the observer in the discrete-time. As it is possible to notice, the system stabilization, the system and exosystem observer convergence are achieved, yielding to the proper tracking of the closed-loop system response.

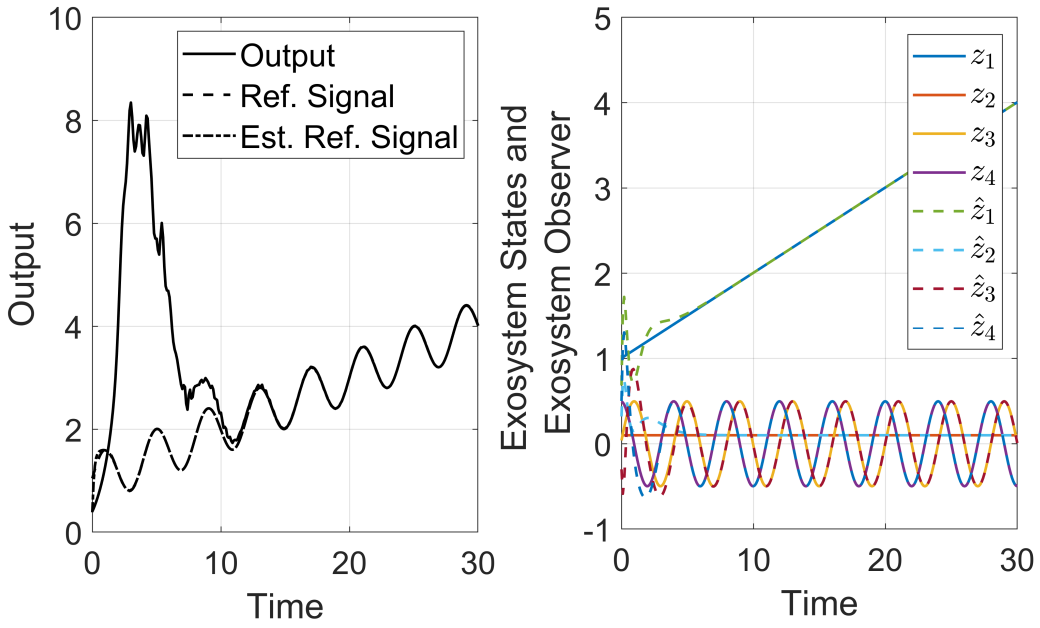

Figure 4.14: Discrete system closed-loop response (on the left), using the system and exosystem observers and the control law given in Equation (4.53). On the right, the discrete exosystem states and its observer states.

Lastly, the closed-loop response using a finite-time observer design in the discrete time setting based in the observability matrix is considered, as examined in Section 4.4.6. The result is shown in Figure 4.15 and, as expected, the exosystem states are properly reconstructed after four sampling times, as there are 4 states in the exosystem, which makes the closed-loop system response better.

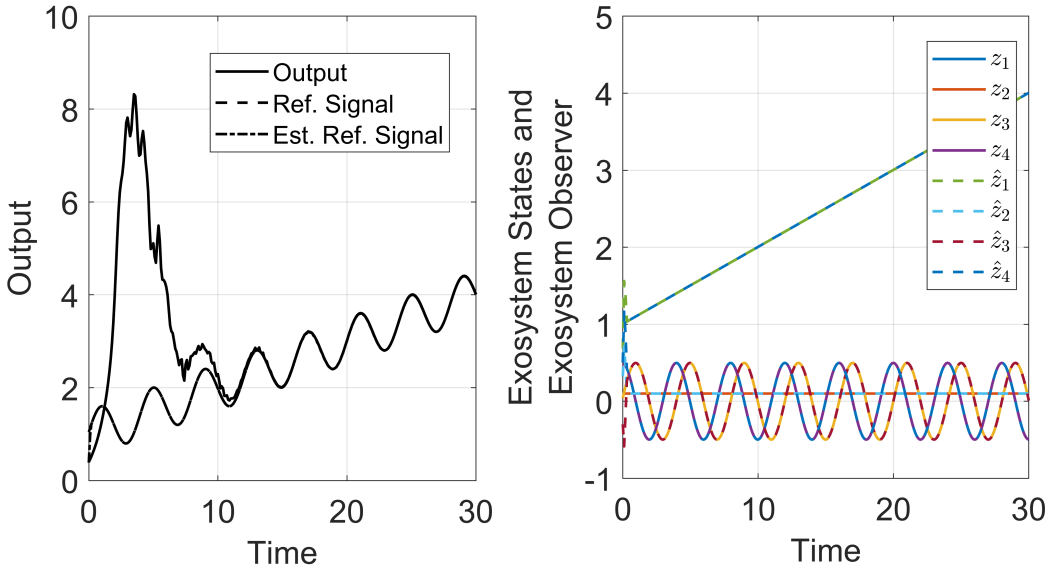

Figure 4.15: Discrete system closed-loop response (on the left), using the observability matrix to reconstruct the exosystem states. On the right, the discrete exosystem states and the observer states.

4.6 Conclusions

In this chapter, the regulator design for the Saint–Venant–Exner model was developed so it would achieve proper closed-loop stability and output tracking of a reference signal in both continuous and discrete-time setting. The backstepping methodology was used in the continuous-time setting to map the closed-loop system to a stable target system, thus guaranteeing the system stability. Furthermore, the same method was used to design the observer, allowing for the reconstruction of the system states by using just the output. Considering a reference signal generated by an exosystem, the output tracking problem was solved. Next, with the stabilization and proper tracking achieved in the continuous-time setting, the discrete regulator was explored. The closed-loop stability, observer design and the regulator equations were shown to be directly related to their construction in the continuous-time, thus ensuring the proper performance of the regulator, as it was possible to observe in the simulations.

For future work, the constrained optimal stabilization and tracking problem

could be considered, as the regulator designed here did not take into account any physical limitations, neither in the states nor the input.

4.A System Stabilization: Backstepping

First, the state transformation $\omega(\zeta,t)=\nu(\zeta,t)\mathrm{e}^{\frac{\alpha_1}{\mu}\zeta}$ is used:

$$\begin{aligned}
\frac{\partial\omega}{\partial t} &= \mu\frac{\partial\omega}{\partial\zeta} &&+\theta_1(\zeta)x_1+\theta_2(\zeta)x_2\\
\frac{\partial x_1}{\partial t} &= -\gamma_1\frac{\partial x_1}{\partial\zeta}+\alpha(\zeta)\omega &&+\sigma_{11}x_1 \quad +\sigma_{12}x_2\\
\frac{\partial x_2}{\partial t} &= -\gamma_2\frac{\partial x_2}{\partial\zeta}+\alpha(\zeta)\omega &&+\sigma_{21}x_1 \quad +\sigma_{22}x_2\\
\omega(1,t) &= \rho_1'x_1(1,t)+\rho_2'x_2(1,t)+u'(t)\\
x_1(0,t) &= q_1\omega(0,t)\\
x_2(0,t) &= q_2\omega(0,t)\\
y_m(t) &= \nu(0,t)=\omega(0,t)\\
y(t) &= x_1(1,t)
\end{aligned} \tag{4.83}$$

where $\theta_1(\zeta)=\beta_1\mathrm{e}^{\frac{\alpha_1}{\mu}\zeta}$, $\theta_2(\zeta)=\beta_2\mathrm{e}^{\frac{\alpha_1}{\mu}\zeta}$, $\alpha(\zeta)=\alpha_1\mathrm{e}^{-\frac{\alpha_1}{\mu}\zeta}$, $\rho_1'=\rho_1\mathrm{e}^{\frac{\alpha_1}{\mu}\zeta}$, $\rho_2'=\rho_2\mathrm{e}^{\frac{\alpha_1}{\mu}\zeta}$ and $u'(t)=u(t)\mathrm{e}^{\frac{\alpha_1}{\mu}\zeta}$.

The stabilization in the continuous-time setting was developed in [90] and assumes that the following Volterra transformation exists:

$$\begin{aligned}
&W(\zeta,t)=\omega(\zeta,t)\\
&-\textstyle\int_0^\zeta\left[K_1(\zeta,\eta)\omega(\eta,t)+K_2(\zeta,\eta)x_1(\eta,t)+K_3(\zeta,\eta)x_2(\eta,t)\right]d\eta\\
&X_1(\zeta,t)=x_1(\zeta,t)\\
&X_2(\zeta,t)=x_2(\zeta,t)
\end{aligned} \tag{4.84}$$

$$\begin{cases}
\mu\dfrac{\partial K_1}{\partial\zeta}+\mu\dfrac{\partial K_1}{\partial\eta} = \alpha(\eta)K_2+\alpha(\eta)K_3\\
\mu\dfrac{\partial K_2}{\partial\zeta}-\gamma_1\dfrac{\partial K_2}{\partial\eta} = \theta_1(\eta)K_1+\sigma_{11}K_2+\sigma_{21}K_3\\
\mu\dfrac{\partial K_3}{\partial\zeta}-\gamma_2\dfrac{\partial K_3}{\partial\eta} = \theta_2(\eta)K_1+\sigma_{12}K_2+\sigma_{22}K_3\\
\mu K_1(\zeta,0)=q_1\gamma_1K_2(\zeta,0)+q_2\gamma_2K_3(\zeta,0)\\
K_2(\zeta,\zeta)=-\dfrac{\theta_1(\zeta)}{\gamma_1+\mu}\\
K_3(\zeta,\zeta)=-\dfrac{\theta_2(\zeta)}{\gamma_2+\mu}
\end{cases} \tag{4.85}$$

The PDE system given in Equation (4.85) can be solved numerically [102], [103]. The control law and the Volterra transformation shown in (4.84) map the system to the following target system:

$$\begin{cases} \dfrac{\partial W}{\partial t} = \mu \dfrac{\partial W}{\partial \zeta} \\ \dfrac{\partial X_1}{\partial t} = -\gamma_1 \dfrac{\partial X_1}{\partial \zeta} \\ + \int_0^\zeta \left[\kappa_1(\zeta,\eta)W(\eta,t) + c_{11}(\zeta,\eta)X_1(\eta,t) + c_{12}(\zeta,\eta)X_2(\eta,t)\right] d\eta \\ \dfrac{\partial X_2}{\partial t} = -\gamma_2 \dfrac{\partial X_2}{\partial \zeta} \\ - \int_0^\zeta \left[\kappa_2(\zeta,\eta)W(\eta,t) + c_{21}(\zeta,\eta)X_1(\eta,t) + c_{22}(\zeta,\eta)X_2(\eta,t)\right] d\eta \\ W(1,t) = r'(t) \\ X_1(0,t) = q_1 W(0,t) \\ X_2(0,t) = q_2 W(0,t) \end{cases} \tag{4.86}$$

where $r'(t) = r(t)\mathrm{e}^{\frac{\alpha_1}{\mu}\zeta}$ and the coefficients are defined as:

$$\begin{aligned} c_{ij}(\zeta,\eta) &= \alpha(\zeta)K_j(\zeta,\eta) + \int_\eta^\zeta \kappa_i(\zeta,\phi)K_j(\phi,\eta)d\phi \\ \kappa_i(\zeta,\eta) &= \alpha(\zeta)K_3(\zeta,\eta) + \int_\eta^\zeta \kappa_i(\zeta,\phi)K_3(\phi,\eta)d\phi \end{aligned} \tag{4.87}$$

4.B Observer Design: Backstepping

The state transformation $\hat{\omega}(\zeta,t) = \hat{\nu}(\zeta,t)\mathrm{e}^{\frac{\alpha_1}{\mu}\zeta}$ is used:

$$\begin{cases} \dfrac{\partial \hat{\omega}}{\partial t} = & \mu \dfrac{\partial \hat{\omega}}{\partial \zeta} + \theta_1(\zeta)\hat{x}_1 + \theta_2(\zeta)\hat{x}_2 - l_1(\zeta)\left[y_m(t) - \hat{\omega}(\zeta=0)\right] \\ \dfrac{\partial \hat{x}_1}{\partial t} = & -\gamma_1 \dfrac{\partial \hat{x}_1}{\partial \zeta} + \alpha(\zeta)\omega + \sigma_{11}\hat{x}_1 + \sigma_{12}\hat{x}_2 - l_2(\zeta)\left[y_m(t) - \hat{\omega}(\zeta=0)\right] \\ \dfrac{\partial \hat{x}_2}{\partial t} = & -\gamma_2 \dfrac{\partial \hat{x}_2}{\partial \zeta} + \alpha(\zeta)\omega + \sigma_{21}\hat{x}_1 + \sigma_{22}\hat{x}_2 - l_3(\zeta)\left[y_m(t) - \hat{\omega}(\zeta=0)\right] \\ \hat{\omega}(1,t) = & \rho_1'\hat{x}_1(1,t) + \rho_2'\hat{x}_2(1,t) + u'(t) \\ \hat{x}_1(0,t) = & q_1 y_m(t) \\ \hat{x}_2(0,t) = & q_2 y_m(t) \end{cases} \tag{4.88}$$

where $\hat{x}(\zeta,t) = \left[\hat{\omega}\ \hat{x}_1\ \hat{x}_2\right]^T$ are the transformed observer states. The observer error $(\hat{e})$ is defined as $\hat{e}(\zeta,t) = \left[\hat{e}_1\ \hat{e}_2\ \hat{e}_3\right] = \left[\omega - \hat{\omega}, x_1 - \hat{x}_1, x_2 - \hat{x}_2\right]^T \in L^2(0,1)$, and the observer error dynamics is given as:

$$\begin{cases} \dfrac{\partial \hat{e}_1}{\partial t} = \mu \dfrac{\partial \hat{e}_1}{\partial \zeta} + \theta_1(\zeta)\hat{e}_2 + \theta_2(\zeta)\hat{e}_3 - l_1(\zeta)\hat{e}_1(\zeta = 0) \\ \dfrac{\partial \hat{e}_2}{\partial t} = -\gamma_1 \dfrac{\partial \hat{e}_2}{\partial \zeta} + \alpha(\zeta)\hat{e}_1 + \sigma_{11}\hat{e}_2 + \sigma_{12}\hat{e}_3 - l_2(\zeta)\hat{e}_1(\zeta = 0) \\ \dfrac{\partial \hat{e}_3}{\partial t} = -\gamma_2 \dfrac{\partial \hat{e}_3}{\partial \zeta} + \alpha(\zeta)\hat{e}_1 + \sigma_{21}\hat{e}_2 + \sigma_{22}\hat{e}_3 - l_3(\zeta)\hat{e}_1(\zeta = 0) \\ \hat{e}_1(1,t) = \rho_1'\hat{e}_2(1,t) + \rho_2'\hat{e}_3(1,t) \\ \hat{e}_2(0,t) = 0 \\ \hat{e}_3(0,t) = 0 \end{cases} \tag{4.89}$$

which can be represented in a general form as:

$$\dot{\hat{e}}(t) = (\hat{A} - L_{o,1}C_m)\hat{e}(t) \tag{4.90}$$

Therefore, to design the observer it is necessary to find an appropriate set of gains L_1 that makes $\hat{A} - L_{o,1}C_m$ stable. Considering the error system shown in Equation (4.89), the following stable target system is desired:

$$\begin{cases} \dfrac{\partial \tilde{e}_1}{\partial t} = \mu \dfrac{\partial \tilde{e}_1}{\partial \zeta} + \theta_1(\zeta)\tilde{e}_2 + \theta_2(\zeta)\tilde{e}_3 + \int_0^\zeta \hat{g}_{12}(\zeta,\eta)\tilde{e}_2(\eta)d\eta + \int_0^\zeta \hat{g}_{13}(\zeta,\eta)\tilde{e}_3(\eta)d\eta \\ \dfrac{\partial \tilde{e}_2}{\partial t} = -\gamma_1 \dfrac{\partial \tilde{e}_2}{\partial \zeta} + \sigma_{11}\tilde{e}_2 + \sigma_{12}\tilde{e}_3 + \int_0^\zeta \hat{g}_{22}(\zeta,\eta)\tilde{e}_2(\eta)d\eta + \int_0^\zeta \hat{g}_{23}(\zeta,\eta)\tilde{e}_3(\eta)d\eta \\ \dfrac{\partial \tilde{e}_3}{\partial t} = -\gamma_2 \dfrac{\partial \tilde{e}_3}{\partial \zeta} + \sigma_{21}\tilde{e}_2 + \sigma_{22}\tilde{e}_3 + \int_0^\zeta \hat{g}_{32}(\zeta,\eta)\tilde{e}_2(\eta)d\eta + \int_0^\zeta \hat{g}_{33}(\zeta,\eta)\tilde{e}_3(\eta)d\eta \\ \tilde{e}_1(1,t) = \rho_1'\tilde{e}_e(1,t) + \rho_2'\tilde{e}_3(1,t) \\ \tilde{e}_2(0,t) = 0 \\ \tilde{e}_3(0,t) = 0 \end{cases} \tag{4.91}$$

To achieve the target system, the following backstepping transformation is used:

$$\tilde{e}_i(\zeta,t) = \hat{e}_i(\zeta,t) + \int_0^\zeta m_i(\zeta,\eta)\hat{e}_1(\zeta,t)d\eta \tag{4.92}$$

For $i = 1, 2, 3$, where $m_i(\zeta,\eta)$ are the transformation kernels, which can be found by solving the following set of equations:

$$\begin{cases} \mu\dfrac{\partial m_1}{\partial \zeta} + \mu\dfrac{\partial m_1}{\partial \eta} = -\theta_1(\zeta)K_2 - \theta_2(\zeta)K_3 \\ \gamma_1\dfrac{\partial m_2}{\partial \zeta} - \mu\dfrac{\partial m_2}{\partial \eta} = \alpha(\zeta)m_1 + \sigma_{11}m_2 + \sigma_{21}m_3 \\ \gamma_2\dfrac{\partial m_3}{\partial \zeta} - \mu\dfrac{\partial m_3}{\partial \eta} = \alpha(\zeta)m_1 + \sigma_{12}m_2 + \sigma_{22}m_3 \\ m_1(1,\eta) = \rho_1 m_2(1,\eta) + \rho_2 m_3(1,\eta) \\ m_2(\zeta,\zeta) = \dfrac{\alpha(\zeta)}{\gamma_1 + \mu} \\ m_3(\zeta,\zeta) = \dfrac{\alpha(\zeta)}{\gamma_2 + \mu} \end{cases} \tag{4.93}$$

This system can be solved numerically in the domain $0 \leq \eta \leq \zeta \leq 1$, and result in the following equations for the functions $\hat{g}_{i,j}$, for $i = 1, 2, 3$ and $j = 2, 3$ in Equation (4.91):

$$\hat{g}_{i,j} = -\theta_j(\zeta)m_i(\zeta,\eta) - \int_{\eta}^{\zeta} m_i(\zeta,\phi)\hat{g}_{1,j}(\phi,\eta)d\phi \tag{4.94}$$

And the observer gains $l_i(\zeta)$ will be given as:

$$l_i(\zeta) = -\mu m_i(\zeta, \eta = 0) \tag{4.95}$$

4.C Discrete System Observer Stability

It is necessary to show that the observer error can be written as:

$$\hat{e}_k = x_k - \hat{x}_k = (\hat{A}_d - L_{od,1}\hat{C}_{m,d})\hat{e}_{k-1} \tag{4.96}$$

First, the relation between the system discrete operators and the observer operators is defined. As $A = \hat{A} + L_{o,2}C_m$ the following relation between $(\delta I - A)^{-1}$ and $\left(\delta I - \hat{A}\right)^{-1}$ holds:

$$\begin{aligned} (\delta I - A)^{-1} &= \left(\delta I - \hat{A} - L_{o,2}C_m\right)^{-1} = \left(\delta I - \hat{A}\right)^{-1} \\ &+ \left(\delta I - \hat{A}\right)^{-1} L_{o,2}\left[I - C_m\left(\delta I - \hat{A}\right)^{-1} L_{o,2}\right]^{-1} C_m\left(\delta I - \hat{A}\right)^{-1} \end{aligned} \tag{4.97}$$

Thus, the following relations between the system discrete operators and

the observer operators will hold as well:

$$
\begin{aligned}
A_d &= \hat{A}_d + L_{od,2}\left[I - C_m\left(\delta I - \hat{A}\right)^{-1} L_{o,2}\right]^{-1}\sqrt{2\delta}C_m\left(\delta I - \hat{A}\right)^{-1} \\
B_d &= \hat{B}_d + L_{od,2}\left[I - C_m\left(\delta I - \hat{A}\right)^{-1} L_{o,2}\right]^{-1} C_m\left(\delta I - \hat{A}\right)^{-1} B \\
C_{m,d} &= \left[I - C_m\left(\delta I - \hat{A}\right)^{-1} L_{o,2}\right]^{-1}\sqrt{2\delta}C_m\left(\delta I - \hat{A}\right)^{-1} \\
&= \left[I - C_m\left(\delta I - \hat{A}\right)^{-1} L_{o,2}\right]^{-1}\left[I + C_m\left(\delta I - \hat{A}\right)^{-1} L_{o,1}\right]\hat{C}_{m,d} \\
D_{m,d} &= \left[I - C_m\left(\delta I - \hat{A}\right)^{-1} L_{o,2}\right]^{-1} C_m\left(\delta I - \hat{A}\right)^{-1} B = \\
&\left[I - C_m\left(\delta I - \hat{A}\right)^{-1} L_{o,2}\right]^{-1}\left[I + C_m\left(\delta I - \hat{A}\right)^{-1} L_{o,1}\right]\hat{D}_{m,d}
\end{aligned}
\tag{4.98}
$$

And the discrete observer error can be written as:

$$
\begin{aligned}
\hat{e}_k = x_k - \hat{x}_k = A_d x_{k-1} + B_d u_k \\
-\left(\hat{A}_d\hat{x}_{k-1} + \hat{B}_d u_k + L_{od,1}\left[y_{m,k} - \hat{y}_{m,k}\right] + L_{od,2}\left[y_{m,k}\right]\right) = \\
\hat{A}_d(x_{k-1} - \hat{x}_{k-1}) \\
+L_{od,2}\left[I - C_m\left(\delta I - \hat{A}\right)^{-1} L_{o,2}\right]^{-1}\sqrt{2\delta}C_m\left(\delta I - \hat{A}\right)^{-1} x_{k-1} \\
+L_{od,2}\left[I - C_m\left(\delta I - \hat{A}\right)^{-1} L_{o,2}\right]^{-1} C_m\left(\delta I - \hat{A}\right)^{-1} B u_k \\
-\left(L_{od,1}\left[y_{m,k} - \hat{y}_{m,k}\right] + L_{od,2}\left[y_{m,k}\right]\right)
\end{aligned}
\tag{4.99}
$$

By the definition of the operators, it is possible to write:

$$
\begin{aligned}
y_{m,k} = C_{m,d}x_{k-1} - D_{m,d}u_k = \left[I - C_m\left(\delta I - \hat{A}\right)^{-1} L_{o,2}\right]^{-1} \\
\left[\sqrt{2\delta}C_m\left(\delta I - \hat{A}\right)^{-1} x_{k-1} + C_m\left(\delta I - \hat{A}\right)^{-1} B u_k\right]
\end{aligned}
\tag{4.100}
$$

and:

$$
\begin{gathered}
[y_{m,k} - \hat{y}_{m,k}] = \\
-\hat{C}_{m,d}\hat{x}_{k-1} - \hat{D}_{m,d}u_k + (I - M_{od,1} - M_{od,2})y_k = \\
-\hat{C}_{m,d}\hat{x}_{k-1} - \hat{D}_{m,d}u_k + (I - M_{od,1} - M_{od,2})\left[I - C_m\left(\delta I - \hat{A}\right)^{-1} L_{o,2}\right]^{-1} \\
\left[I + C_m\left(\delta I - \hat{A}\right)^{-1} L_{o,1}\right](\hat{C}_{m,d}x_{k-1} + \hat{D}_{m,d}u_k) \implies \\
(I - M_{od,1} - M_{od,2}) = \left[I + C_m\left(\delta I - \hat{A}\right) L_{o,1}\right]^{-1} \\
\left[I + C_m\left(\delta I - \hat{A}\right) L_{o,1} - C_m\left(\delta I - \hat{A}\right)^{-1} L_{o,1} - C_m\left(\delta I - \hat{A}\right)^{-1} L_{o,2}\right] \\
= \left[I + C_m\left(\delta I - \hat{A}\right) L_{o,1}\right]^{-1}\left[I - C_m\left(\delta I - \hat{A}\right)^{-1} L_{o,2}\right] \implies \\
(I - M_{od,1} - M_{od,2})\left[I - C_m\left(\delta I - \hat{A}\right)^{-1} L_{o,2}\right]^{-1} = \left[I + C_m\left(\delta I - \hat{A}\right) L_{o,1}\right]^{-1} \\
\implies [y_{m,k} - \hat{y}_{m,k}] = -\hat{C}_{m,d}\hat{x}_{k-1} - \hat{D}_{m,d}u_k + \\
\left[I + C_m\left(\delta I - \hat{A}\right) L_{o,1}\right]^{-1}\left[I + C_m\left(\delta I - \hat{A}\right)^{-1} L_{o,1}\right](\hat{C}_{m,d}x_{k-1} + \hat{D}_{m,d}u_k) \\
= \hat{C}_{m,d}(x_{k-1} - \hat{x}_{k-1})
\end{gathered}
\tag{4.101}
$$

Finally, the discrete observer error can be written as:

$$
\hat{e}_k = \hat{A}_d(x_{k-1} - \hat{x}_{k-1}) - L_{od,1}\hat{C}_{m,d}(x_{k-1} - \hat{x}_{k-1}) = (\hat{A}_d - L_{od,1}\hat{C}_{m,d})\hat{e}_{k-1} \tag{4.102}
$$

And this can be linked to the operators in the continuous time setting by:

$$
\begin{gathered}
\hat{A}_d - L_{od,1}\hat{C}_{m,d} = \\
-I + 2\delta\left(\delta I - \hat{A}\right)^{-1} - 2\delta\left\{I - \left[I + \left(\delta I + \hat{A}\right)^{-1} L_{o,1}C_m\right]^{-1}\right\}\left(\delta I - \hat{A}\right)^{-1} \\
= -I + 2\delta\left[I + \left(\delta I - \hat{A}\right)^{-1} L_{o,1}C_m\right]^{-1}\left(\delta I - \hat{A}\right)^{-1} = \\
-I + 2\left[\delta I - \hat{A} + L_{o,1}C_m\right]^{-1}
\end{gathered}
\tag{4.103}
$$

which would be the discrete operator generated by $(\hat{A} - L_{o,1}C_m)$. Thus, if $L_{o,1}$ is chosen such that $(\hat{A} - L_{o,1}C_m)$ is stable, the discrete observer will be stable as well, as the Cayley-Tustin time discretization cannot map a stable continuous system to a unstable discrete one.

4.D Discrete Exosystem Observer Stability

Similarly to the system observer, it is necessary to show that the exosystem observer error can be written as:

$$\hat{e}_{r,k} = z_k - \hat{z}_k = (S_d - L_{ed}Q_d)\hat{e}_{r,k-1} \tag{4.104}$$

$$\begin{aligned} \hat{y}_{r,k} &= \hat{Q}_d\hat{z}_{k-1} + M_{ed}y_{r,k} \\ \hat{z}_k &= S_d\hat{z}_{k-1} - L_{ed}(y_{r,k} - \hat{y}_{r,k}) \end{aligned} \tag{4.105}$$

where $\hat{z}_k$ is the estimated exosystem state, S_d and Q_d have been defined in Section 4.4.3 (in Equation (4.60)). L_{ed} and M_{ed} are defined as:

$$\begin{aligned} L_{ed} &= \sqrt{2\delta}\left(\delta I - S\right)^{-1} L_e \\ M_{ed} &= \left[I + Q\left(\delta I - S\right)^{-1} L_e\right]^{-1} Q\left(\delta I - S\right)^{-1} L_e \end{aligned} \tag{4.106}$$

Lemma 4.13 *: If the exosystem observer gain in the continuous time setting (L_e) is chosen such that $(S - L_eQ)$ is stable, then, the discrete observer given by Equation (4.105) and the operators defined in Equation (4.106) will be able to reconstruct the states of the discrete exosystem.*

Proof: To prove the exosystem observer convergence to the system states, the discrete error of the exosystem observer is analyzed:

$$\hat{e}_{r,k} = z_k - \hat{z}_k \tag{4.107}$$

After some algebraic manipulation (shown in Appendix 4.D), the discrete error can be written as:

$$\hat{e}_{r,k} = (S_d - L_{ed}\hat{Q}_d)\hat{e}_{r,k-1} = \left\{-I + 2\left[\delta I - S + L_eQ\right]^{-1}\right\}\hat{e}_{r,k-1} \tag{4.108}$$

which is the discrete operator generated by $(S - L_eQ)$. Thus, if L_e is chosen such that $(S - L_eQ)$ is stable, the discrete observer will be stable as well.

First, the discrete observer error can be written as:

$$\begin{gathered}
\hat{e}_{r,k} = z_k - \hat{z}_k = S_d z_{k-1} - S_d \hat{z}_{k-1} - L_{ed}(y_{r,k} - \hat{y}_{r,k}) \\
= S_d(z_{k-1} - \hat{z}_{k-1}) - L_{ed}((I - M_{ed})Q_d z_{k-1} - \hat{Q}_d \hat{z}_{k-1}) \implies \\
(I - M_{ed})Q_d = \\
\left[I + Q\left(\delta I - S\right)^{-1} L_e\right]^{-1} \left[I + Q\left(\delta I - S\right)^{-1} L_e - Q\left(\delta I - S\right)^{-1} L_e\right] Q_d \\
= \left[I + Q\left(\delta I - S\right)^{-1} L_e\right]^{-1} Q_d = \hat{Q}_d \implies \\
= S_d(z_{k-1} - \hat{z}_{k-1}) - L_{ed}(\hat{Q}_d z_{k-1} - \hat{Q}_d \hat{z}_{k-1}) = (S_d - L_{ed}\hat{Q}_d)\hat{e}_{r,k-1}
\end{gathered} \tag{4.109}$$

And this can be linked to the operators in the continuous time setting by:

$$\begin{gathered}
S_d - L_{ed}\hat{Q}_d = \\
-I + 2\delta\left(\delta I - S\right)^{-1} - 2\delta\left\{I - \left[I + \left(\delta I + S\right)^{-1} L_e Q\right]^{-1}\right\}\left(\delta I - S\right)^{-1} = \\
-I + 2\delta\left[I + \left(\delta I - S\right)^{-1} L_e Q\right]^{-1}\left(\delta I - S\right)^{-1} = -I + 2\left[\delta I - S + L_e Q\right]^{-1}
\end{gathered} \tag{4.110}$$

which would be the discrete operator generated by $(S - L_e Q)$. Choosing L_e such that $(S - L_e Q)$ is stable will make the discrete exosystem observer stable as well if the exosystem observer shown in Section 4.3.4 is used.

Chapter 5

Dynamical Analysis and Model Predictive Control of an Auto-Thermal Reactor

5.1 Introduction

Transport-reaction distributed parameter system (DPS) models present in chemical, petrochemical, manufacturing and process industry take the mathematical form given by hyperbolic partial differential equations (PDEs). The main conservation laws are embedded in a modelling variety provided by the hyperbolicity of the transport systems which is physically relevant and desired property as action at distance is precluded and physically meaningful finite speed of phenomena propagation is ensured. On the other hand, a hyperbolicity mathematically ensures well-posedness of local Cauchy problems [44]. Along the same line of mathematical representation and analysis, when it comes to the mathematical setting of transport-reaction distributed parameter systems, the inevitable difficulty comes from the infinite dimensional nature of their representation [16], [17] which is a limiting factor when controller designs and monitoring realizations are considered.

The class of transport-reaction hyperbolic PDEs considered in this work is given by the model of auto-thermal reactor with internal counter-current heat exchanger (ARICHE) which is industrially important and energy saving reactor commonly used for the ammonia synthesis at commercial scale, see the contributions by Bonvin et. al. [81] The underlying dynamical complexity ar-

rises from the fact that dynamical instabilities may arise from both microscopic effects (represented by axial mass and energy dispersion) and macroscopic effects (heat transfer between the reaction system and the feed stream) coupled through the feedback transport mechanism. In particular, the ARICHE and tubular reactor with recycle are only two commonly used reactors which exhibit the macroscopic feedback mechanism. Hence, the issue of stability of operating these reactors is of permanent interest to the engineering control community and industrial practitioners. In particular, there were studies on stability of operating ARICHE [81], [83] and tubular reactor with recycle [104]. Due to intrinsic complexity to some extent the stability of ARCHE has not been rigorously investigated, while Sano [105] analyzed the important property of exponential stabilization of the mono-tubular heat exchanger equation with static output feedback, and the same property was explored by time-delayed boundary observation utilized in stabilizing control law design [106].

When it comes to the control of distributed parameter systems within a constrained optimal control setting, there have been several seminal contributions which address the transport-reaction system setting primarily in Harmon Ray [107] and Curtain and Zwart [16]. In particular, for transport systems modelled by a first order hyperbolic systems, there are several contributions regarding the dynamical analysis and control of these systems, for instance, the design of an optimal linear quadratic feedback controller [108] and a linear quadratic controller design for a fixed-bed reactor [109]. Furthermore, there are contributions related to the model predictive control of hyperbolic systems using finite dimensional approximation [31] or based on the method of characteristics to help predict the future output for quasilinear hyperbolic systems [110]. Similarly, the optimal and model predictive control design are extended to the class of Riesz spectral systems with a separable eigenspectrum, allowing for successful application of algorithms that account for the input and state constraints [35], [37], [111], [112]. Regarding nonlinear model predictive control for distributed parameter systems, there are contributions in the area, for instance, a combination of on-line model reduction and successive linearizations have been used [113] and data-based modellng was used

to design a model predictive control framework [114].

The current trend of digitalization and computer applications in all engineering disciplines motivate to explore modern control designs and the state-of-the-art controller realizations which are ultimately digital and therefore discrete in their nature. Therefore, the traditional numerical time discretization schemes are frequently utilized to transform models and/or controllers in the form suitable for the implementation with the understanding that that the accuracy of the discrete system representation may be impacted as the sampling period is increasing which adversely may impact the overall model and closed-loop stability [26]. In addition, it is well known from the linear systems theory that simple explicit and implicit Euler time discretization of linear dynamics may impact the systems stability by mapping stable continuous to possible unstable discrete counterpart system and vice versa [27]. This issue becomes even more prominent in the case of controller design and/or realizations in the setting of distributed parameter systems usually represented in the infinite dimensional state space settings. Hence, motivated by this, we explore the time discretization schemes which provide an accurate and reliable transformation of continuous linear infinite dimensional system to the linear discrete time infinite dimensional one, by application of Crank-Nicolson mid point integration rule [28]. This type of discretization in the systems science is also known as Cayley-Tustin time discretization, and it has been shown that it preserves the intrinsic energy and dynamical characteristics of the linear distributed parameter system [29], so that no spatial discretization or/and spatial model reduction needs to be applied.

Motivated by the modern and well established developments in finite dimensional model predictive (MPC) theory applied to linear systems [115], [116], we extend the finite dimensional MPC setting to the case of distributed parameter systems modelled by the system of hyperbolic PDEs, and in particular the structure preserving discretization of continuous hyperbolic PDE model representation is realized [28], [29], and utilized in the linear MPC controller design which accounts for constrained stabilization of unstable hyperbolic PDEs model and which does ensure the input and state constraints

feasibility under the assumption of successive feasibility of the formulated finite dimensional quadratic optimization problem [117].

The chapter is organized as follows: In the System Description Section the ARICHE model is presented and it is followed by the Nonlinear Analysis section where parametric studies provided the insight in the rich behaviours of ARICHE internal dynamics. This is followed by the System Linearization and Linear System Stability section where insight is provided in linear model features and stability characterization. Finally, in Model Predictive Control Design section the linear MPC design is realized and it is followed by simulation studies which demonstrate the successful realization of the constrained optimization based control design to important industrial reactor example.

5.2 System Description

The feed to an ARICHE, which also serves as the coolant, flows countercurrent to the effluent stream and is pre-heated by the energy released by the exothermic reaction. The feed turns around at the top of the reaction section and is introduced into the catalyst bed. It is considered that the reactions happen just inside the catalyst packed bed. The representation of an auto-thermal reactor is shown in Fig. 5.1 below:

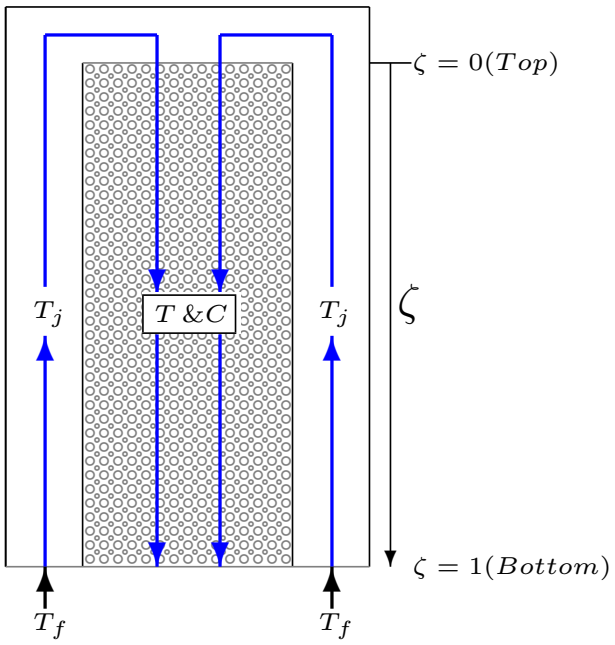

Figure 5.1: Autothermal Reactor Representation

This autothermal reactor can be described by the following set of non-linear dimensionless hyperbolic PDE's [81]:

$$\begin{aligned}
\frac{\partial T_j(\zeta,t)}{\partial t} &= \rho\frac{\partial T_j(\zeta,t)}{\partial \zeta} + \omega(T(\zeta,t) - T_j(\zeta,t)) \\
\frac{\partial T(\zeta,t)}{\partial t} &= -\delta\frac{\partial T(\zeta,t)}{\partial \zeta} - \lambda(T(\zeta,t) - T_j(\zeta,t)) + \beta\psi C(\zeta,t)\mathrm{e}^{-\frac{\gamma}{T(\zeta,t)}} \\
\frac{\partial C(\zeta,t)}{\partial t} &= -\frac{1}{\epsilon}\frac{\partial C(\zeta,t)}{\partial \zeta} - \frac{1}{\epsilon}\psi C(\zeta,t)\mathrm{e}^{-\frac{\gamma}{T(\zeta,t)}}
\end{aligned} \tag{5.1}$$

where $T_j(\zeta,t)$ is the dimensionless temperature of the fluid through the cooling jacket, T is the dimensionless temperature of the fluid through the catalyst bed and C is the dimensionless concentration inside the catalyst bed. Low dimensional models have been validated in the previous contributions and they can capture the relevant physical and dynamical characteristics of the system [81]–[83], [118]–[121]. The following boundary conditions are considered:

$$\begin{aligned}
T_j(\zeta = 1,t) &= T_f(t) = u(t) \\
T(\zeta = 0,t) &= T_j(\zeta = 0,t) \\
C(\zeta = 0,t) &= 1
\end{aligned} \tag{5.2}$$

Therefore, the temperature of the fluid at the jacket at the bottom (at $\zeta = 1$) is given by a feed temperature, which also is the manipulated variable considered

in this manuscript, the temperature at the inlet of the catalyst bed (at $\zeta = 0$) is equal to the jacket fluid at the same point (as the jacket fluid is fed into the catalyst bed) and the dimensionless inlet concentration (at $\zeta = 0$) in the catalyst bed is considered to be constant. The steady-state for this system is given by the solution of a system of non-linear ordinary differential equations:

$$\begin{aligned} \frac{\partial T_{j,ss}(\zeta)}{\partial \zeta} &= -\frac{\omega}{\rho}(T_{ss}(\zeta) - T_{j,ss}(\zeta)) \\ \frac{\partial T_{ss}(\zeta)}{\partial \zeta} &= -\frac{\lambda}{\delta}(T_{ss}(\zeta) - T_{j,ss}(\zeta)) + \frac{\beta\psi}{\delta} C_{ss}(\zeta) \mathrm{e}^{-\frac{\gamma}{T_{ss}(\zeta)}} \\ \frac{\partial C_{ss}(\zeta)}{\partial \zeta} &= -\psi C_{ss}(\zeta) \mathrm{e}^{-\frac{\gamma}{T_{ss}(\zeta)}} \end{aligned} \tag{5.3}$$

and the boundary conditions previously specified as:

$$\begin{aligned} T_j(\zeta = 1) &= T_f \\ T(\zeta = 0) &= T_j(\zeta = 0) \\ C(\zeta = 0) &= 1 \end{aligned} \tag{5.4}$$

This model shows that steady-state solution is dependent on the feed temperature (T_f). Therefore, in order to obtain the steady-state profiles, a finite-difference numerical scheme was used with the same set of parameters as in Bonvin et. al [81]., shown in Table 4.1. In the work of Bonvin et al. [81], it was shown that the same value of T_f can yield a different steady-states profiles, and this multiplicity of steady-states generally has one unstable steady-state. This behaviour can be seen in Fig. 5.2, where there is a range of feed temperature values that can yield a different top temperature steady-states (reactor temperature at $\zeta = 0$) and bottom conversions (defined as $1 - C(\zeta = 1, t)$).

The different spatial profiles for the variables at each possible steady-state when the same value of the feed temperature is used can be seen in Fig. 5.3. For $T_f = 550$ K, three distinctly different dynamic behaviours can be observed. The long and short dashes line represents the steady-state with low conversion (SS3). At this equilibrium state, the initial energy is not substantial enough to start the reaction and the reactor and jacket have the same temperature as the feed. The solid line represents the steady-state with high conversion (SS1). In this case, the initial energy is high enough to start the reaction and due to the counter-flow between the jacket and the reactor part of this energy

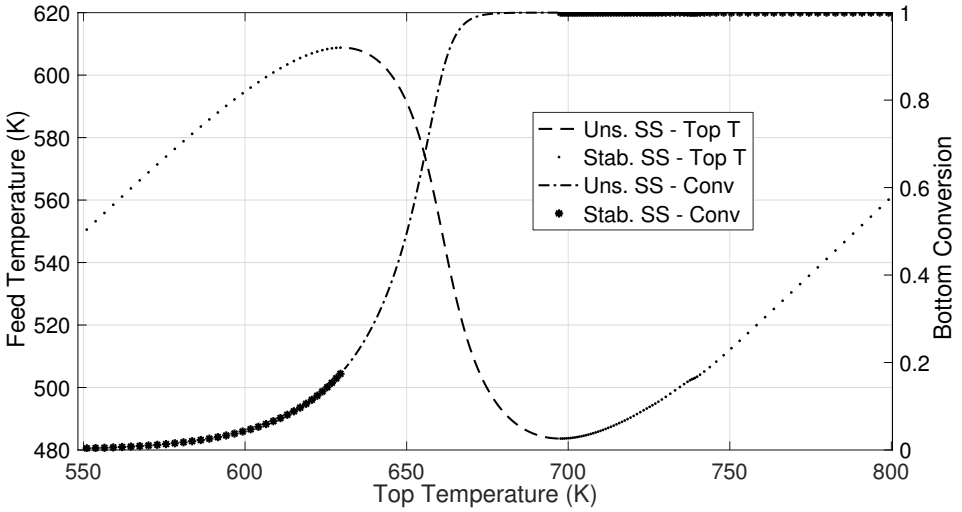

Figure 5.2: Steady states of reactor temperature at the top and conversion at the bottom obtained for different values of the input T_f.

goes back to the reactor inlet, increasing reaction extent up to the point where the reactant is completely consumed in the first portion of the reactor. This also may cause some concern regarding the safe reactor operations, as there is a region where the temperature inside is almost 400 K greater than the feed temperature.

The steady-state of interest is a intermediate between the high conversion and low conversion profiles (represented by the long dash line - SS2). It presents a reactor temperature that is not as high as the state with high conversion, while also offering a reasonably high conversion. Unfortunately, this is an unstable point of operation, and it can be seen as a transition between the low and high conversion states and without any control action it is not possible to keep the reactor operating at this condition. Therefore, it is of interest to implement controller to keep the reactor working at this unstable operating point.

5.3 Non-linear behaviour analysis

In order to access how variations of the parameters shown in Table 4.1 affect the system behaviour, a pseudo arclength continuation method is used [122].

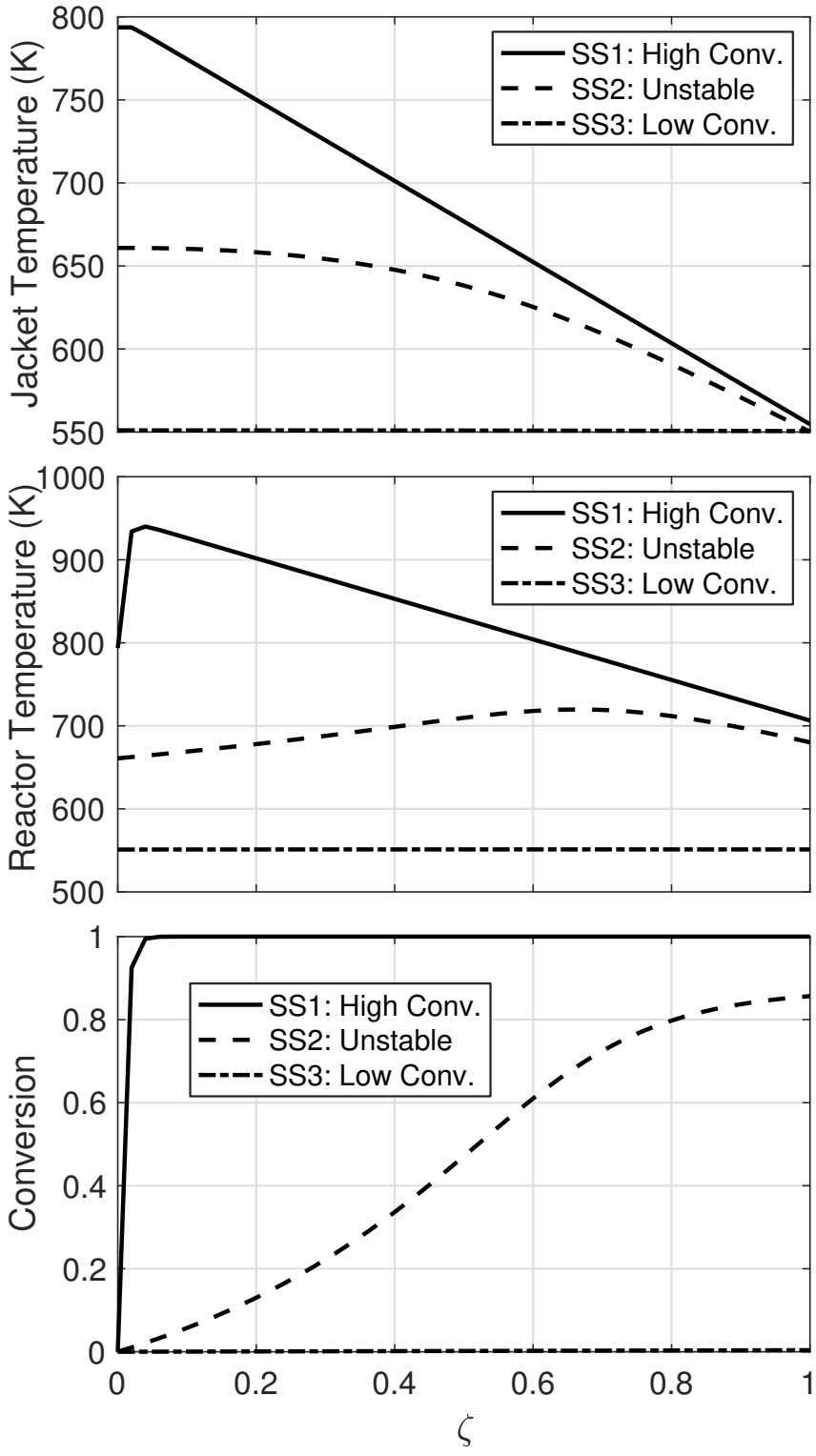

Figure 5.3: Different Steady-States profiles for the same value of $T_f = 550$ K.

In Fig. 5.4 is given the pictorial representation how this method provides the construction of steady state of interest. In the pseudo arclength continuation method everything is parameterized with respect to the arclength and is based on the tangent with respect to this arclength at a given initial point. As a fixed step of the arclength is taken, and with an approximation of the tangent, a new initial guess of the solution is obtained. This new guess is then used to solve the system of equations.

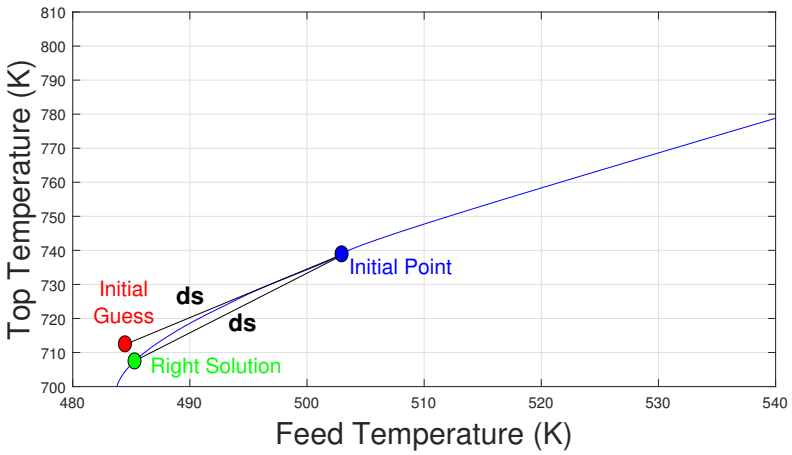

Figure 5.4: Representation of the Pseudo arclength method

Specifically, first it is necessary to solve the following system of equations to find the value of the tangents of the state variables (x) and the chosen parameter (μ) in respect to the arclength (s) at a the step (k), as shown in Equation (5.5):

$$\begin{cases} J_k \left(\frac{dx}{ds}\right)_k + f_{\mu,k} \left(\frac{d\mu}{ds}\right)_k = 0 \\ \left(\frac{dx}{ds}\right)_k^T \left(\frac{dx}{ds}\right)_k + \left(\frac{d\mu}{ds}\right)_k^2 = 1 \end{cases} \tag{5.5}$$

where J_k is the jacobian matrix (derivatives of the functions in respect to the states) in the step k and $f_{\mu,k}$ is a vector with the derivatives of the equations to the chosen parameter. In the Eqn. (5.6), it is shown that the approximation

used to calculate the value of the initial guess for the next step.

$$\begin{aligned}\left(\frac{dx}{ds}\right)_k &\approx \frac{x_{k+1}-x_k}{\Delta s} \rightarrow x_{k+1} = x_k + \left(\frac{dx}{ds}\right)_k \Delta s \\ \left(\frac{d\mu}{ds}\right)_k &\approx \frac{\mu_{k+1}-\mu_k}{\Delta s} \rightarrow \mu_{k+1} = \mu_k + \left(\frac{d\mu}{ds}\right)_k \Delta s\end{aligned} \tag{5.6}$$

where Δs is the arclength variation used and is a value that must be chosen. Finally, the new initial guess for the state variables (x_{k+1}) and for the system parameter (μ_{k+1}) is used in the system of equations that needs to be solved. If the value of Δs is appropriate, the values found for x_{k+1} and μ_{k+1} are a good guess. Furthermore, one extra equation needs to be solved simultaneously with the system of equations, to guarantee that the solution in the next step does not overstep with the chosen variation of the arclength. These conditions are represented in Equation 5.7.

$$\begin{cases} f(x_{k+1}, \mu_{k+1}) = 0 \\ (x_{k+1}-x_k)\left(\dfrac{dx}{ds}\right)_k + (\mu_{k+1}-\mu_k)\left(\dfrac{d\mu}{ds}\right)_k = \Delta s \end{cases} \tag{5.7}$$

For the autothermal reactor, the system of equations that needs to be solved are given by the steady-states ordinary differential equations (ODE's) shown in Eqn.(5.3) when a spatial discretization is applied (in this manuscript, finite differences were used). This transform the system of ODE's in a system of algebraic equations, where the state variables (x) are $T_j(\zeta)$, $T(\zeta)$ and $C(\zeta)$ and the continuation parameter is the feed temperature (T_f). For a initial value of T_f (μ_k), the partial differential equations shown in Eqn.(5.1) are solved with spatial discretization until a steady-state is reached in order to obtain an initial solution of the system of algebraic equation (x_k). Then, the arclength continuation method is applied to get the new initial guesses to the state variables (x_{k+1}) and the continuation parameter (μ_{k+1}). It is possible to solve the system of algebraic equation without the use of a continuation method, but the computational cost may not be worth, as it is necessary to find the steady-state for the three spatially dependent variables. If N discretization points are used, then there are $3N$ non-linear equations to be solved. With

a continuation method, a good initial guess for the solution of this system of equations can be found.

To investigate how the system parameters shown in Table 4.1 influence the non-linear behaviour of the autothermal reactor, the continuation method is utilized with different values of table parameters. The results for variations in each of these parameters are shown in ensuing section with assumption that the variations of the parameters are taken around the nominal values given in Table 4.1.

- Variations in β: this parameter represents the dimensionless heat of reaction and is given by the ratio of the heat of reaction (ΔH_r), mole fraction in the feed (Y_o) and total pressure (P) by the reference temperature (T_{ref}), density of the bed (ρ_b), bed specific heat capacity (c_p), gas constant (R_g) and the average dimensionless temperature in the reactor (T_{av}). The result of the parameter continuation method applied for different values of β ($0.1\beta_0 \leq \beta \leq 1.5\beta_0$, with β_0 as the nominal value given in Table 4.1) is given in Fig.5.5 (Left). The dimensionless heat of reaction is important for the non-linear behaviour of the autothermal reactor. A higher value of this parameter increases the the region of non-linear behaviour and a minimum value is necessary for the system to exhibits multiplicity of steady-states. This is expected, as an increase in this parameter would increase the thermal feedback in the system, which is fundamentally responsible for the reactor instability as shown in [50], [81].

- Variations in ψ: this parameter is the Damkohler number and is given by the ratio of the Arrhenius pre-exponential factor (k_o) and reactor length (L) by the reactor bed void fraction (ϵ) and the fluid velocity inside the packed bed (v). The result of the parameter continuation method applied for different values of ψ ($0.1\psi_0 \leq \psi \leq 1.5\psi_0$, with ψ_0 as the nominal value given in Table 4.1) is given in Figure 5.5 (Right). The Damkohler number also has some influence on the non-linear behaviour, as with the dimensionless heat of reaction, a higher parameter values also

increase the region of non-linear behaviour characterized with steady set multiplicity and a minimum value is necessary for the system to exhibit multiplicity of steady-states. As the Damkohler number can be interpreted as the ratio between the reaction rate to the transport phenomena rate occurring in a system, a higher value of this parameter can be seen as a longer reaction timescale (higher conversion), which increases the amount of energy released in the system and, consequently, a higher thermal feedback.

- Variations in γ: this parameter is the dimensionless activation energy corresponding to the ratio of activation energy (E_a) by the gas constant (R_g) and the reference temperature(T_{ref}). The result of the parameter continuation method applied for different values of γ ($\gamma_0 \leq \gamma \leq 1.2\gamma_0$, with γ_0 as the nominal value given in Table 4.1) is given in Fig.5.6 (Left). The dimensionless activation energy is very important for the on-linear behaviour, as it shifts the feed temperature values where the steady-states multiplicity occurs and as a result also changes the reactor bed temperature profile. Furthermore, if it is set as zero, the non-linearity of the system disappears and it becomes a linear system with a first order reaction. The steady-state profile for this special case is shown in Fig.5.6 (Right). The full conversion is always obtained in the exit of the reactor and the temperature increases linearly with the feed temperature.

- Variations in λ: this parameter is the reactor bed dimensionless heat transfer coefficient and is defined as the ratio of the overall heat transfer coefficient (U), the heat transfer area (a) and the reactor length (L) by the reaction section volume (V_c), reactor bed void fraction, fluid velocity inside the packed bed (v), density of the bed (ρ_b) and the bed specific heat capacity (c_p). The result of the parameter continuation method applied for different values of λ ($0.1\lambda_0 \leq \lambda \leq 1.5\lambda_0$, with λ_0 as the nominal value given in Table 4.1) is given in Fig.5.7 (Left). Different from the previous parameters, an increase in the reactor bed dimensionless heat transfer coefficient reduces the region of non-linearity. As this parameter

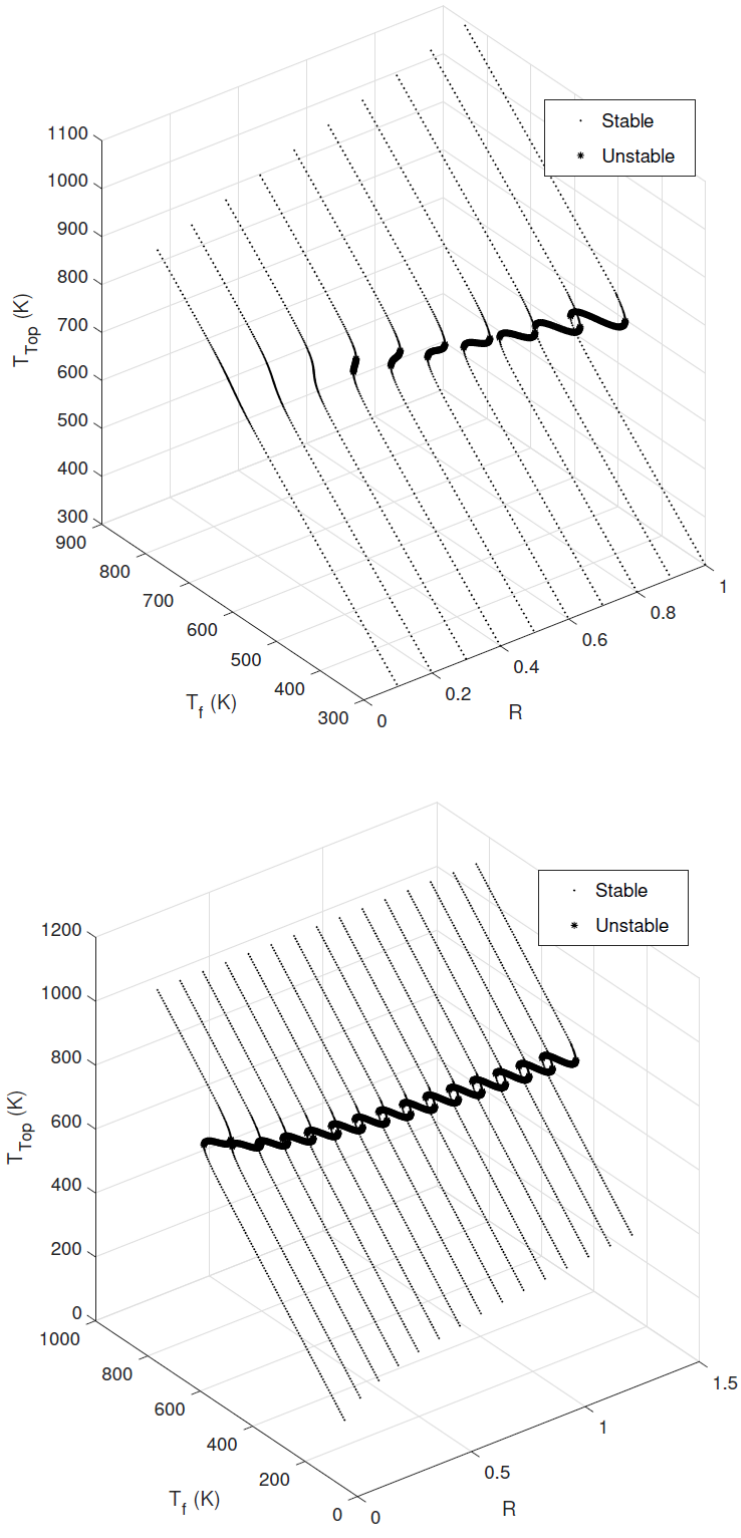

Figure 5.5: Parameter continuation results for: (Top) $\beta = R\beta_0 \rightarrow 0.1\beta_0 \leq \beta \leq 1\beta_0$; (Bottom) $\psi = R\psi_0 \rightarrow 0.1\psi_0 \leq \psi \leq 1.5\psi_0$

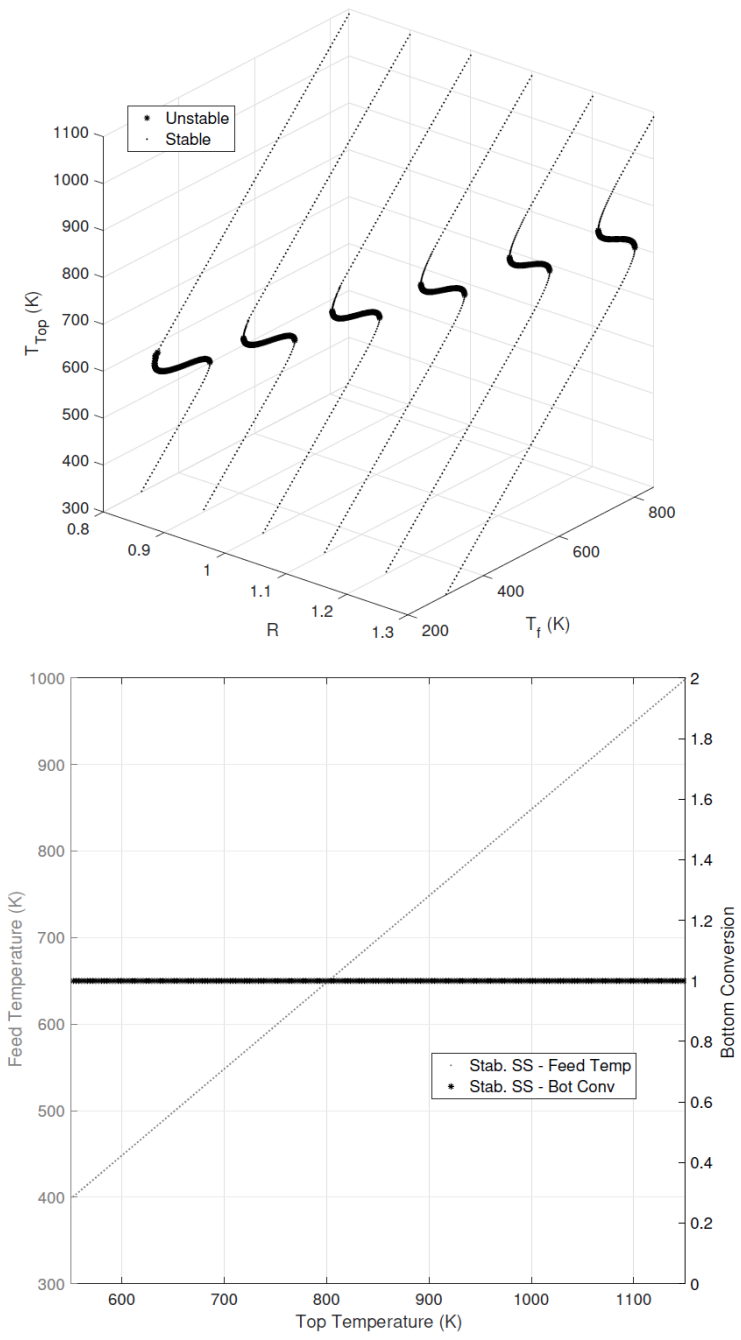

Figure 5.6: Parameter continuation results for: (Top) $\gamma = R\gamma_0 \rightarrow 0.8\gamma_0 \leq \gamma \leq 1.2\gamma_0$; (Bottom) A system with no temperature dependence on the reaction rate

is increased, the higher will be the effect of the heat transfer with the cooling section, which means a higher cooling effect (as the reactor bed temperature is generally higher than the jacket temperature). Therefore, the temperature in the bed reactor is cooled down faster and the temperature feedback decreases, reducing the instability region.

- Variations in ρ: this parameter is the ratio of velocities given by the quotient of the coolant velocity (v_c) by the reactor bed void fraction (ϵ) and the fluid velocity inside the packed bed (v). The result of the parameter continuation method applied for different values of ρ ($0.6\rho_0 \leq \rho \leq 1.5\rho_0$, with ρ_0 as the nominal value given in Table 4.1) is given in Fig.5.7 (Right). Similarly to the λ variations, a decrease in the ratio of velocities causes an increase in the instability region. This happens due to the decrease in ρ which increases the residence time of the cooling fluid, and also increases the overall heat exchange between the reactor and bed. This increases the magnitude of the thermal feedback in the system, which yields increase in the operating region characterized by the unstable dynamics.

- Variations in ω: this parameter is the cooling jacket dimensionless heat transfer coefficient given by the ratio of the overall heat transfer coefficient (U), the heat transfer area (a) and the reactor length (L) by the coolant section volume (V_c), reactor bed void fraction, fluid velocity inside the packed bed (v), density of the fluid (ρ_f) and specific heat capacity of the fluid (c_{pf}). The result of the parameter continuation method applied for different values of ω ($0.1\omega_0 \leq \omega \leq 1.2\omega_0$, with ω_0 as the nominal value given in Table 4.1) is given in Fig.5.8 (Left). In the same way as ρ, as the cooling jacket dimensionless heat transfer coefficient is increased, the higher is going to be the effect of the reactor bed temperature in the coolant temperature, resulting in a higher thermal feedback and an increase in the instability region.

- Variations in δ: this parameter is the ratio of thermal capacitances de-

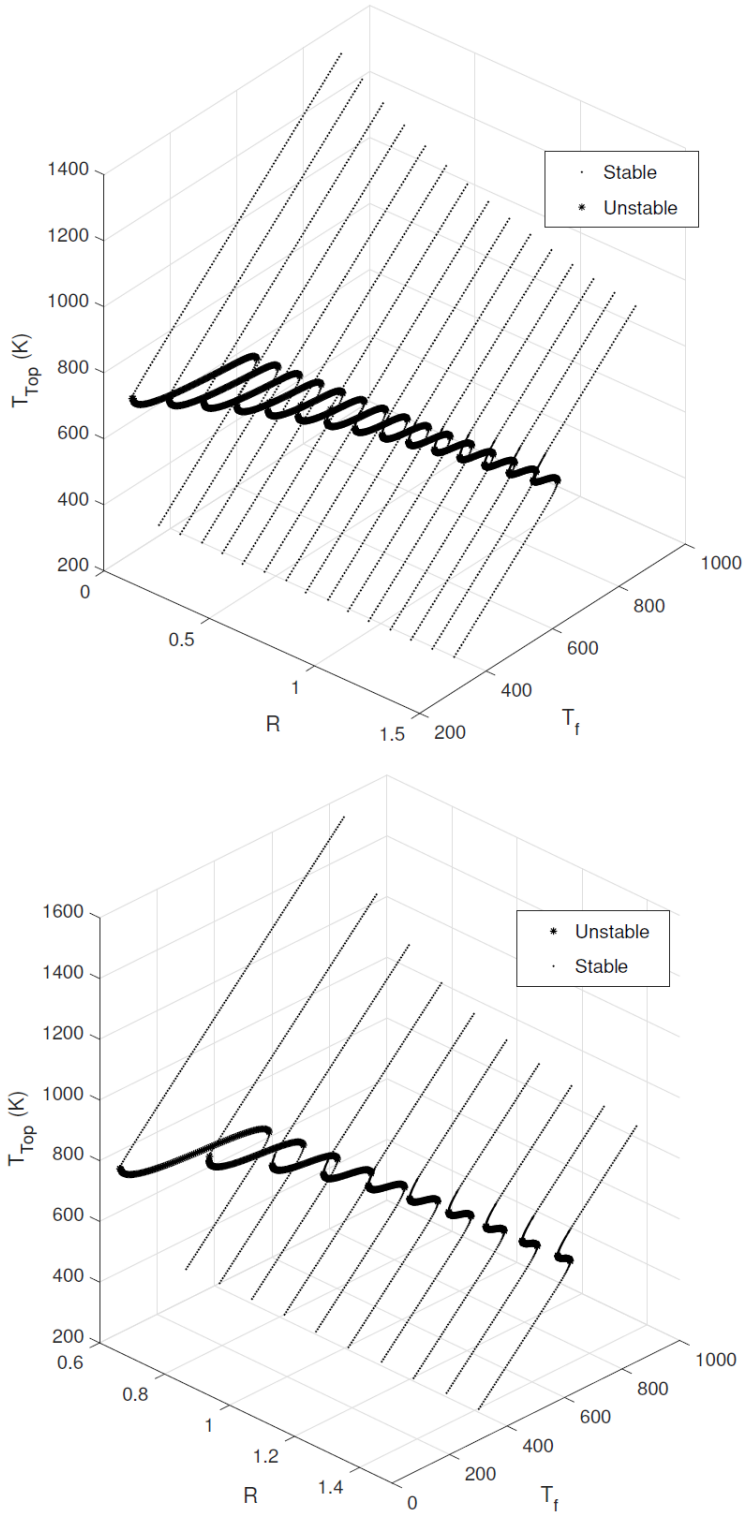

Figure 5.7: Parameter continuation results for: (Top) $\lambda = R\lambda_0 \rightarrow 0.1\lambda_0 \leq \lambda \leq 1.5\lambda_0$; (Bottom) $\rho = R\rho_0 \rightarrow 0.6\rho_0 \leq \rho \leq 1.5\rho_0$

fined as the quotient of the density of the fluid (ρ_f) and specific heat capacity of the fluid (c_{pf}) by the density of the bed (ρ_b) and the bed specific heat capacity (c_p). The result of the parameter continuation method applied for different values of δ ($0.7\delta_0 \leq \delta \leq 1.5\delta_0$, with δ_0 as the nominal value given in Table 4.1) is given in Fig.5.8 (Right). As δ decreases, the lower is the ratio between the energy necessary to heat the cooling jacket and the energy removed from reactor bed, increasing the overall thermal feedback, thus, increasing the instability region.

- One last case in considered in Fig.5.9, which represents the parameter continuation results when no cooling jacket is considered. An increase in the feed temperature increases the conversion in the reactor, which also induces the temperature to increase in the reactor outlet as well up to a point where total conversion is achieved. However, as there is no thermal feedback in the system present, there is no region characterized by the multiplicity of steady-states. In Dochain (2016) [50], the multiplicity of equilibrium profiles in tubular reactors was studied, and it was demonstrated that the multiplicity can happen in a simple tubular reactor as long as diffusive effects are present (which are responsible for the back mixing). As this model just considers a convective transport setting and, in this case, no cooling jacket is used, the thermal feedback is not possible, hence he multiplicity of steady-states is not seen.

5.4 System Linearization

In order to implement the model predictive controller (MPC) design, a discrete model representation of the system is required. In this work, a Cayley-Tustin time discretization is applied to the distributed parameter system, and a linear representation of the coupled hyperbolic PDEs system needs to be considered. Therefore, the first step to obtain the discrete representation is the linearization of the model presented in Eq.(5.1). Specifically, the reaction rate is linearized as it depends on the dimensionless reactor temperature and

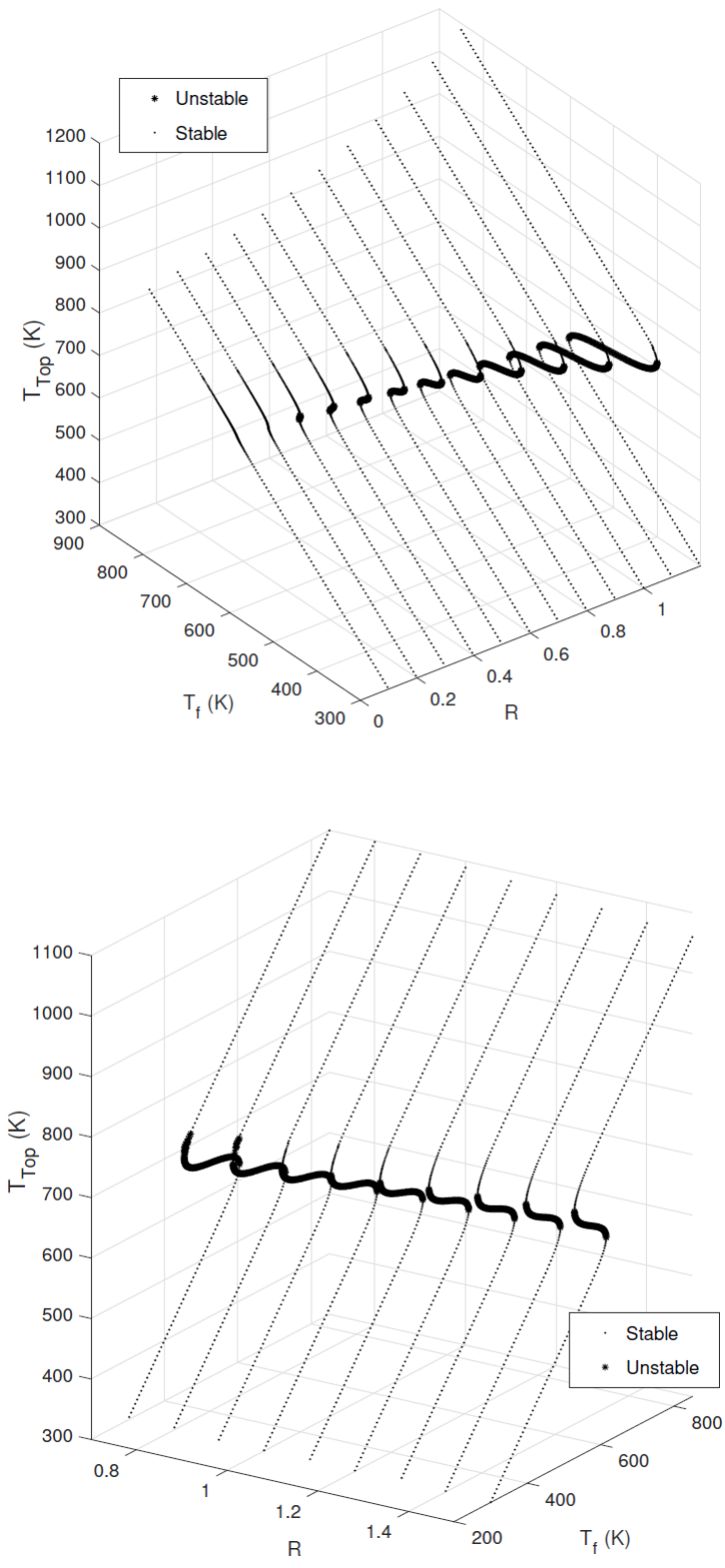

Figure 5.8: Parameter continuation results for: (Top) $\omega = R\omega_0 \rightarrow 0.1\omega_0 \leq \omega \leq 1.2\omega_0$; (Bottom) $\delta = R\delta_0 \rightarrow 0.7\delta_0 \leq \delta \leq 1.5\delta_0$

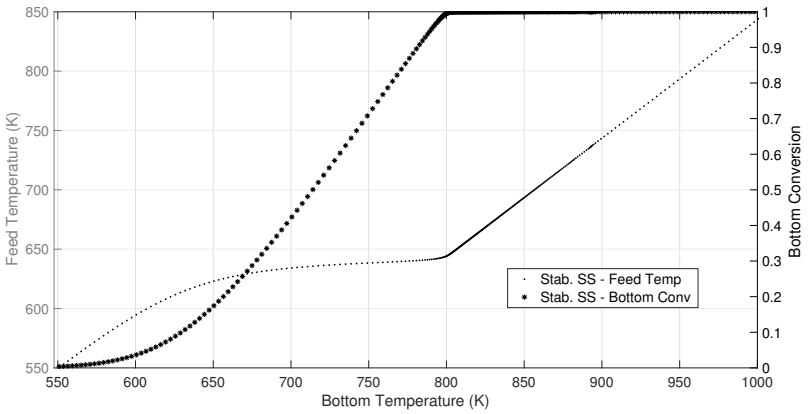

Figure 5.9: Parameter continuation results for a system without cooling jacket

concentration:

$$\begin{aligned} f_{NL}(C,T) &= C\mathrm{e}^{-\frac{\gamma}{T}} \approx f_{NL}(C_{ss},T_{ss}) \\ &\quad +a_T(T-T_{ss})+a_C(C-C_{ss}) \end{aligned} \tag{5.8}$$

where T_{ss}, C_{ss} represents the dimensionless reactor temperature and concentration at a steady-state of interest, and the linearized coefficients are given as follow:

$$\begin{cases} a_T &= \frac{\partial f_{NL}}{\partial T}\big|_{ss} = \left(\frac{C\gamma \mathrm{e}^{-\frac{\gamma}{T}}}{T^2}\right)\Big|_{ss} \\ a_C &= \frac{\partial f_{NL}}{\partial C}\big|_{ss} = \left(\mathrm{e}^{-\frac{\gamma}{T}}\right)\big|_{ss} \end{cases} \tag{5.9}$$

Thus, a linear representation of the original model is obtained and the a_T and a_C coefficients are averaged over the space. Furthermore, the following deviation variables are defined:

$$\begin{cases} \bar{T}_j = T_j - T_{j,ss} \\ \bar{T} = T - T_{ss} \\ \bar{C} = C - C_{ss} \end{cases} \tag{5.10}$$

Then, it is straightforward to obtain the linearized representation of the original system:

$$\frac{\partial}{\partial t}\begin{bmatrix} \bar{T}_j \\ \bar{T} \\ \bar{C} \end{bmatrix} = \underbrace{\begin{bmatrix} \rho\partial_\zeta - \omega & \omega & 0 \\ \lambda & -\lambda - \delta\partial_\zeta + \beta\psi\bar{a}_T & +\beta\psi\bar{a}_C \\ 0 & -\frac{\psi\bar{a}_T}{\epsilon} & -\frac{1}{\epsilon}\partial_\zeta - \frac{\psi\bar{a}_C}{\epsilon} \end{bmatrix}}_{\mathfrak{A}} \begin{bmatrix} \bar{T}_j \\ \bar{T} \\ \bar{C} \end{bmatrix} \tag{5.11}$$

where $\bar{a}_T$ and $\bar{a}_C$ are the spatial averages of the coefficients defined in Eq. (5.9):

$$\begin{cases} \bar{a}_T &= \dfrac{\int_0^1 a_T(\zeta)d\zeta}{\int_0^1 d\zeta} \\ \\ \bar{a}_C &= \dfrac{\int_0^1 a_C(\zeta)d\zeta}{\int_0^1 d\zeta} \end{cases} \tag{5.12}$$

And the boundary conditions represented in deviation variables are:

$$\begin{array}{rcl} \bar{T}_j(\zeta=1,t) &=& \bar{T}_f(t) = T_f(t) - T_{f,ss} = u(t) \\ \bar{T}(\zeta=0,t) &=& \bar{T}_j(\zeta=0,t) \\ \bar{C}(\zeta=0,t) &=& 0 \end{array} \tag{5.13}$$

5.5 Linear System Stability Analysis

From the linear system representation, it is also possible to access the internal stability of the operator $\mathfrak{A}$ by solving the eigenvalue problem associated with the system:

$$\mathfrak{A}\phi(\zeta) = \lambda\phi(\zeta) \tag{5.14}$$

The operator $\mathfrak{A}$ is defined in Eq.(5.11) with its boundary conditions in Eq.(5.13). If $\mathfrak{A}$ is written as $\mathfrak{A} = \bar{A} + V\partial_\zeta$, where $\bar{A}$ is a matrix with the constant coefficients of Eq.(5.11) and V is the matrix with system's velocities and are given by:

$$\bar{A} = \begin{bmatrix} -\omega & \omega & 0 \\ \lambda & -\lambda + \beta\psi\bar{a}_T & +\beta\psi\bar{a}_C \\ 0 & -\frac{\psi\bar{a}_T}{\epsilon} & -\frac{\psi\bar{a}_C}{\epsilon} \end{bmatrix}; \quad V = \begin{bmatrix} \rho & 0 & 0 \\ 0 & -\delta & 0 \\ 0 & 0 & -\frac{1}{\epsilon} \end{bmatrix} \tag{5.15}$$

Thus, the eigenvalue problem can be written as $\mathfrak{A}\phi(\zeta) = \bar{A}\phi(\zeta) + V\partial_\zeta\phi(\zeta) = \lambda\phi(\zeta)$ and has a general solution given by:

$$\phi(\zeta) = \mathrm{e}^{V^{-1}(\lambda-\bar{A})\zeta}\phi(\zeta=0) = M(\zeta)\phi(\zeta=0) \tag{5.16}$$

where $M(\zeta) = \mathrm{e}^{V^{-1}(\lambda-\bar{A})\zeta}$ is the exponential matrix of $V^{-1}(\lambda - \bar{A})\zeta$, for this system it is a 3x3 matrix with components given as $M_{i,j}(\zeta)$, and $\phi(\zeta =$

$0) = \left[\ \phi_1(\zeta = 0) \quad \phi_2(\zeta = 0) \quad \phi_3(\zeta = 0)\ \right]^T$. The solution also needs to satisfy the boundary conditions:

$$\begin{aligned} \phi_1(\zeta = 1) &= 0 \\ \phi_2(\zeta = 0) &= \phi_1(\zeta = 0) \\ \phi_3(\zeta = 0) &= 0 \end{aligned} \tag{5.17}$$

By applying these boundary conditions to the general solution, the following condition is obtained:

$$0 = \phi_1(\zeta = 0)\left[M_{1,1}(\zeta = 1) + M_{1,2}(\zeta = 1)\right] \tag{5.18}$$

Therefore, if the system has a non-trivial solution to the eigenvalue problem, there exists a value for λ such that $M_{1,1}(\zeta = 1) + M_{1,2}(\zeta = 1) = 0$. This is a non-linear equation that is numerically solvable to find the value of λ that satisfy the previous condition. The solution for the eigenvalue problem generates two sets of solutions: stable eigenvalues ($\lambda_S \leq 0$,) associated with a set of eigenfunctions (ϕ_S) spanning the stable eigenspace, and unstable eigenvalues ($\lambda_U \geq 0$) associated with a set of eigenfunctions (ϕ_U).

Considering the steady-states obtained when $T_f = 550$ K (the three possible profiles presented in Fig.5.3), the eigenvalue distributions shown in Fig.5.10 are obtained. As expected, the distribution from the linearized system that is originated from a stable steady-state has all the eigenvalues in the left side of the complex plan (in Fig.5.10 there are two stable steady-states, one is the stable steady-state with high conversion and the other with low conversion), therefore the set of unstable eigenvalues and eigenfunctions is empty ($\lambda_U = \{\emptyset\}$ and $\phi_U = \{\emptyset\}$).

The unstable steady-state has one real eigenvalue on the right side of the complex plan, which is responsible for the system instability and the set of unstable eigenvalues and eigenfunctions ($\lambda_U = \{\lambda_1\}$ and $\phi_U = \{\phi_1\}$).

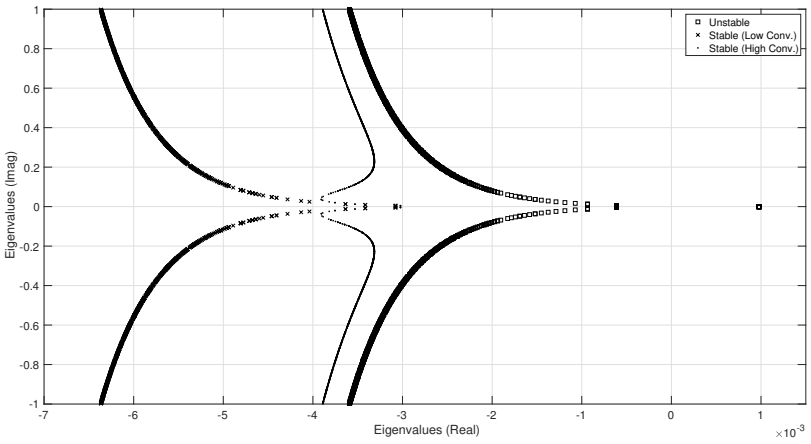

Figure 5.10: Eigenvalue distribution for the three possible steady-states at $T_f = 550$ K.

A results of the stability analysis are shown in Table 5.1. This analysis just takes into account the unstable steady-states found in a inlet temperature between 500 K $\leq T_f \leq$ 600 K. In Bonvin et. al [81], the stability analysis was made using the model obtained from spatial discretization (orthogonal colocation was used) of the set of partial differential equations into a set of ordinary differential equations. It was shown that the eigenvalues converged as the number of discretization points was increased. In this manuscript, all the eigenvalues obtained by the stability analysis of the linearized system have the same order of magnitude as the ones found in Bonvin et. al [81]. As expected, all the eigenvalues have a negative real part except the unstable one ($\lambda > 0$), which is also the only real eigenvalue in the eigenvalue spectrum. The difference among results found in this manuscript and in previous contributions increases when the inlet temperature is close to the blow-off temperature (close to 475 K). In Bonvin et. al [81], it was mentioned that for temperatures close to the blow-off temperatures the value of the eigenvalues presented had not converged for the number of discretization points used, as this is a region that is difficult to dynamically model. For the other values of the inlet temperature, the real and imaginary parts of the shown eigenvalues are very close to the previous work.

T_f (K)	600	575	550	540	520	500
λ_1	0.000573	0.001016	0.000977	0.000873	0.000552	0.000158
$\lambda_{2,3}$ (Real)	-0.0017	-0.000952	-0.000612	-0.000594	-0.000759	-0.0012
$\lambda_{2,3}$ (Imag.)	± 0.0043	± 0.0041	± 0.0039	± 0.0038	± 0.0036	± 0.0035
$\lambda_{4,5}$ (Real)	-0.0021	-0.001214	-0.000776	-0.000709	-0.00082	-0.0011
$\lambda_{4,5}$ (Imag.)	± 0.0086	± 0.0084	± 0.0083	± 0.0082	± 0.0122	± 0.0078

Table 5.1: Eigenvalues obtained with the linearized system stability analysis

5.6 Boundary transformation and system discretization

In order to obtain the discrete representation of the system, a linear system in the following form is considered:

$$\begin{aligned} \dot{x}(t) &= Ax(t) + Bu(t) \\ y(t) &= Cx(t) + Du(t) \end{aligned} \tag{5.19}$$

Although the system shown in Eq. (5.11) is linear, its input is applied at the system's boundary. A boundary transformation is applied to change this boundary controlled system into a corresponding in-domain respresentation:

$$p(t,\zeta) = x(t,\zeta) + \beta(\zeta)u(t) \tag{5.20}$$

where $x(t,\zeta)$ are the original variables ($\bar{T}_j$, $\bar{T}$ and $\bar{C}$ in this case) $\beta(\zeta)$ can be found by solving $\mathfrak{A}\beta(\zeta) = 0$. The new system representation is given as:

$$\begin{bmatrix} \dot{u}(t) \\ \dot{p}(t) \end{bmatrix} = \underbrace{\begin{bmatrix} 0 & 0 \\ 0 & A^* \end{bmatrix}}_{A} \begin{bmatrix} u(t) \\ p(t) \end{bmatrix} + \underbrace{\begin{bmatrix} 1 \\ \beta(\zeta) \end{bmatrix}}_{B} \dot{u}(t) \tag{5.21}$$

notice that the new manipulated variable is $\dot{u}(t)$ and $u(t)$ is now a state of the system. The operator A^* is defined as $\mathfrak{A}$ shown in (5.11), except for its boundary conditions:

$$A^*p(t) \rightarrow \begin{cases} p_1(\zeta = 1, t) = 0 \\ p_2(\zeta = 0, t) = p_1(\zeta = 0, t) \\ p_3(\zeta = 0, t) = 0 \end{cases} \tag{5.22}$$

Given that the system is represented as in Eqn. (5.19), it is possible to apply the Cayley-Tustin time discretization to obtain the discrete representation as follows:

$$\begin{aligned} x_k &= A_d x_{k-1} + B_d u_k \\ y_k &= C_d x_{k-1} + D_d u_k \end{aligned} \tag{5.23}$$

where A_d, B_d, C_d and D_d are the discrete time system operators and are given by:

$$\begin{bmatrix} A_d & B_d \\ C_d & D_d \end{bmatrix} = \begin{bmatrix} -I + 2\theta\left[\theta - A\right]^{-1} & \sqrt{2\theta}\left[\theta - A\right]^{-1} B \\ \sqrt{2\theta}C\left[\theta - A\right]^{-1} & C\left[\theta - A\right]^{-1} B \end{bmatrix} \tag{5.24}$$

and $\theta = 2/\Delta t$, $\left[\theta - A\right]^{-1} = R(\theta, A)$ is the resolvent operator of A. The resolvent operator is obtained by applying the Laplace transform to unforced (zero

input) representation of Eq. (5.21), then by applying integration in space and by implementation of the boundary conditions so that $(sI - A)^{-1} = R(s, A)$ is obtained and evaluated at $s = \delta$. For the A operator shown in Eq. (5.21), the resolvent is given by:

$$R(s, A)(\cdot) = \begin{bmatrix} (\cdot)/s & 0 \\ 0 & R(s, A^*)(\cdot) \end{bmatrix} \tag{5.25}$$

The operator A^* can be written as $A^* = \bar{A} + V\partial_\zeta$, with $\bar{A}$ and V defined the same way as in Eq. (5.15) and the resolvent for this operator ($R(s, A^*)$) is given by:

$$\begin{aligned} &R(s, A^*)(\cdot) = \\ &M(\zeta) \begin{bmatrix} 1 \\ 1 \\ 0 \end{bmatrix} \frac{\displaystyle\int_0^1 \begin{bmatrix} M_{1,1}(1-\mu) & M_{1,2}(1-\mu) & M_{1,3}(1-\mu) \end{bmatrix} (\cdot) d\mu}{M_{1,1}(\zeta = 1) + M_{1,2}(\zeta = 1)} \\ &- \int_0^1 M(\zeta - \mu) V^{-1}(\cdot) d\mu \end{aligned} \tag{5.26}$$

where $M(\zeta)$ is the exponential matrix defined in the same way as in Eq. (5.16) ($M(\zeta) = \mathrm{e}^{V^{-1}(s-\bar{A})\zeta}$), which is a 3×3 matrix and $M_{i,j}(\zeta)$ are each of its elements. If $s \to \lambda_i$, where λ_i is the solution of the eigenvalue problem defined in Eq. 5.14, the denominator of the first term on the right side of Eq. (5.26) goes to zero ($M_{1,1}(\zeta = 1) + M_{1,2}(\zeta = 1) \to 0$) and the resolvent of A^* becomes undefined ($R(s, A^*)(\cdot) \to \infty$), as expected from the resolvent of an operator.

With the resolvent properly determined, it is possible to obtain the discrete time system representation for the Cayley-Tustin time discretization defined in Eqs. (5.24) and (5.23). With the discrete time representation the Model Predicitve Control strategy can be applied to the system, as explained in the following section.

5.7 Model Predictive Controller Design

The MPC design developed in [116] for the finite dimensional linear time invariant systems is extended to the setting of infinite dimensional discrete

setting by considering the following formulation:

$$\begin{aligned} &\min_u \sum_{j=0}^{\infty} \left\langle y\left(\zeta, k+j|\, k\right), Qy\left(\zeta, k+j|\, k\right)\right\rangle \\ &+\left\langle u\left(k+j+1|\, k\right), Ru\left(k+j+1|\, k\right)\right\rangle \end{aligned} \tag{5.27}$$

subject to

$$\begin{aligned} x\left(\zeta, k+j|\, k\right) &= A_d x\left(\zeta, k+j-1|\, k\right) + B_d u\left(k+j|\, k\right) \\ y\left(\zeta, k+j|\, k\right) &= C_d x\left(\zeta, k+j-1|\, k\right) + D_d u\left(k+j|\, k\right) \\ u^{min} &\leq u\left(k+j|\, k\right) \leq u^{max} \\ y^{min} &\leq y\left(\zeta, k+j|\, k\right) \leq y^{max} \end{aligned} \tag{5.28}$$

where inner product $\langle x, y\rangle$ accounts for the spatial integration. The above infinite horizon quadratic optimization problem is reformulated to the finite dimensional (N-horizon length) one as follows:

$$\begin{aligned} &\min_{u^N} \sum_{j=0}^{N} \left\langle y\left(\zeta, k+j|\, k\right), Qy\left(\zeta, k+j|\, k\right)\right\rangle \\ &+\left\langle u\left(k+j+1|\, k\right), Ru\left(k+j+1|\, k\right)\right\rangle + \\ &\left\langle y\left(\zeta, k+N|\, k\right), \bar{Q}y\left(\zeta, k+N|\, k\right)\right\rangle \end{aligned} \tag{5.29}$$

where the $\bar{Q}$ is terminal cost and the stability is enforced by applying the terminal state constraints which are realized as terminal constraints condition associated with the finite number of unstable modes. [34] The $\bar{Q}$ operator is given by:

$$\bar{Q}(\cdot) = \sum_{n=0}^{\infty}\sum_{m=0}^{\infty} -\frac{\langle C\phi_n, QC\phi_m\rangle}{\lambda_n + \bar{\lambda}_m}\langle \cdot, \bar{\psi}_m\rangle\bar{\psi}_n \tag{5.30}$$

And the following constraints condition is imposed in the optimization problem to enforce stability:

$$\left\langle x\left(\zeta, N\right), \psi_U\left(\zeta\right)\right\rangle = 0 \tag{5.31}$$

Therefore, if there is a feasible input given by the optimization problem, the stabilization is achieved by MPC controller through the asymptotic stabilization of the unstable modes with realization of requirement that the unstable modes are placed at zero by at the end of the horizon. Since, the optimisation given by constrained quadratic program is feasible in the zero disturbance case, the feasibility implies stability and optimal stabilizability, in other words this results extends the well know results from the area of finite dimensional MPC theory [115], [116].

5.8 Results

This section shows the results regarding the implementation of the Model Predictive Control. It is divided in two subsections: one considers that the discrete linearized model is also used as the plant model; the other considers the non-linear model presented in Equation (5.1) as the plant model. These scenarios are shown in Figure 5.11.

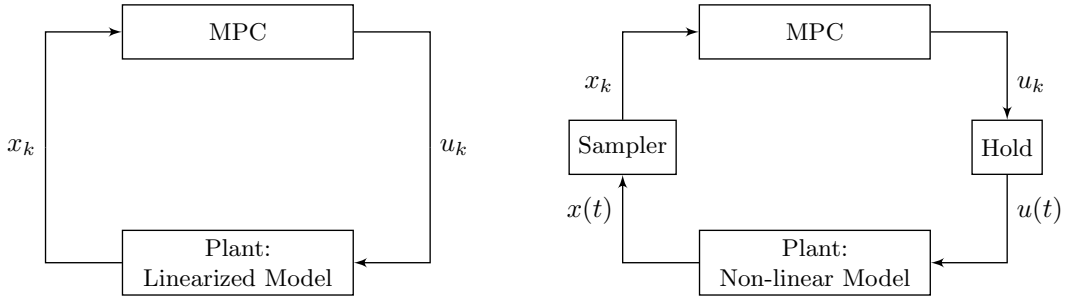

Figure 5.11: Implementation of the MPC: (Left) The MPC model and the plant model are the discrete linear model; (Right) MPC uses the discrete linear model, the plant model is the original non-linear model

5.8.1 Plant: Linear Model

In this section three different scenarios were considered for both stable and unstable steady-states: the open-loop response, the MPC response without any constraints and the MPC response with constrained input. An initial condition different from the steady-states was used in the system. The output considered in the MPC design was the reactor bed temperature. The MPC input $u(t)$ evolution is shown in the simulations studies. As the deviation variable are being used, all variables converge to zero, implying that the system is converging to the considered steady-state of interest. It is expected that the MPC achieves a faster response when the optimal constrained stabilization of already stable steady-state is considered, and it is also expected that MPC is able to stabilize the system when the unstable steady-state is considered.

For the results shown below, one of the stable steady-states shown in Fig. 5.3 was used ($T_f = 550$ K). In this case, the stable steady-state with high

conversion is considered. The choice of steady-state impacts the coefficients presented in the the operator $\mathfrak{A}$ shown in Equation (5.11) (consequently the operator A^* and β of Equation (5.21) also take appropriate values associated with selected steady state). Figure 5.12 shows the response for the three different cases considered. As expected, the open-loop response goes back to the steady-state without any control action (the open-loop response of the output is represented by the dotted solid blue line).

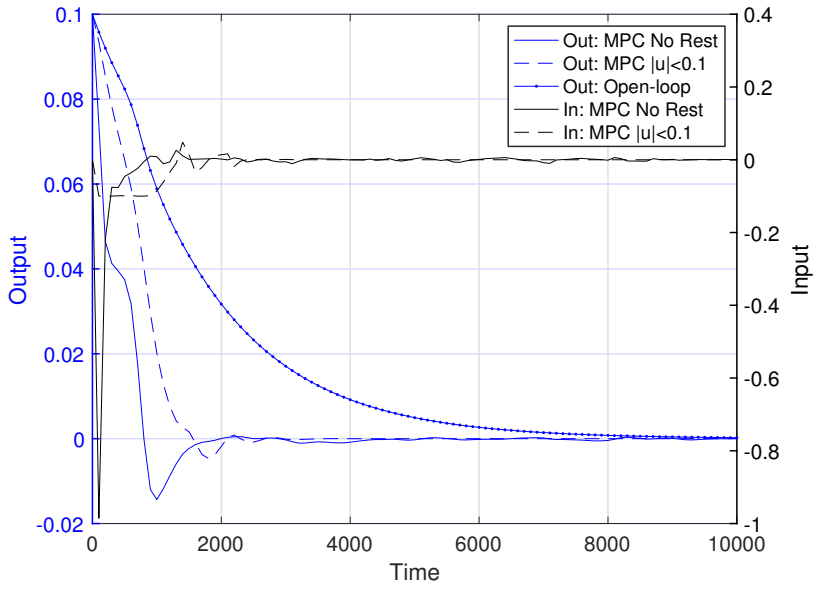

Figure 5.12: Results obtained for one of the stable steady-states.

The output for the MPC without constraints is represented by the solid blue line and the input for this scenario is represented with the solid black line. Notice the magnitude of the input used in this case. The control action at the beginning almost reaches -550 K, which would mean that the feed temperature required would reach 0 K. For this reason, a case with constrained input was considered, which is represented by the blue dashed line (output) and black dashed line (input). The constraint considered for the input in this case was a maximum variation of 10 % in relation to the feed temperature (a variation of ± 55 K). Its is possible to see that, in the beginning, the input required is at the lower limit of the constraint and it stays there for some time until it finally increases and goes back to zero.

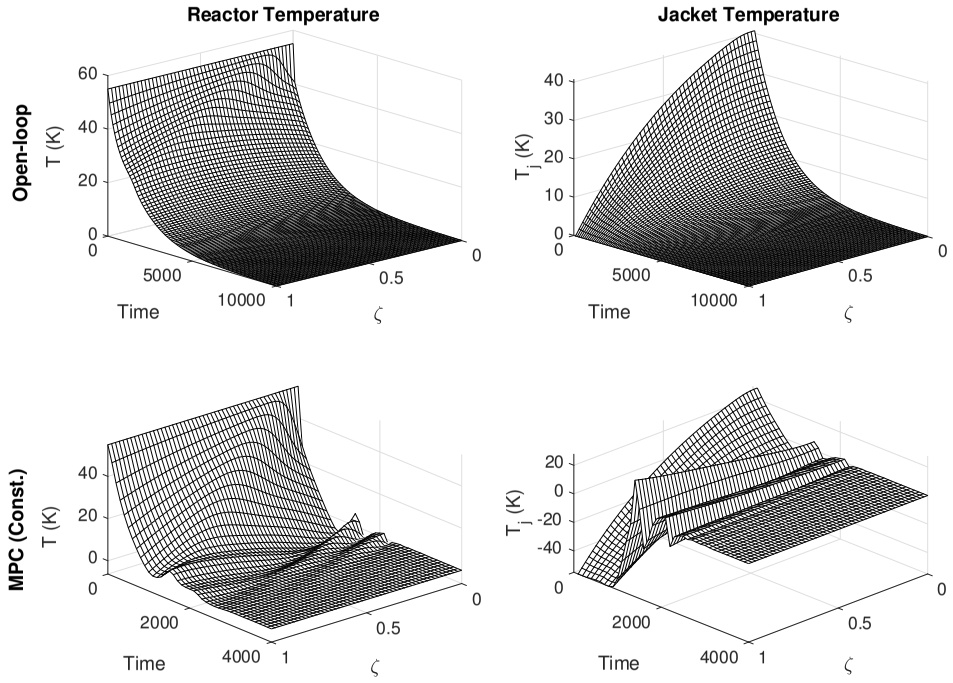

Figure 5.13: Spatial profiles of the jacket temperature obtained for the stable steady-state. (Top row) Open-Loop: (Left) Bed Reactor Temperature; (Right) Jacket Temperature; (Bottom row) Constrained MPC $|\bar{T}_f| \leq 55$ K:(Left) Bed Reactor Temperature; (Right) Jacket Temperature.

For the cases that the MPC was considered, the steady-state was reached in almost one fourth of the time required in the open-loop simulation study, as expected if a controller is used. The spatial profiles of the jacket and reactor temperatures for the open-loop and constrained MPC response are shown in Fig. 5.13. It is possible to see that both the jacket and reactor temperature settle to the steady-state in at most one fourth of the time required to the open-loop response.

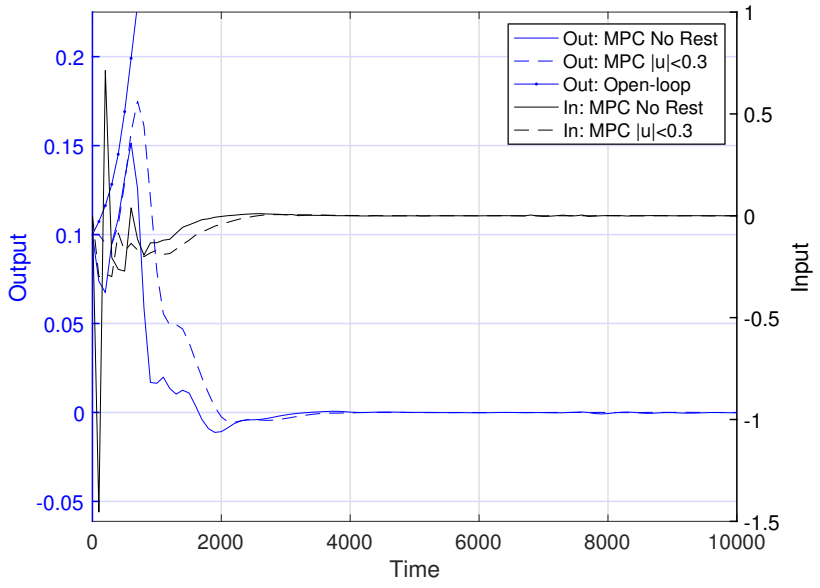

Figure 5.14: Results obtained for the unstable steady-state.

For the next results shown, the unstable steady-state for $T_f = 550$ K, shown in Fig. 5.3, was used. The results for the three different cases considered (Open-loop, unconstrained MPC and constrained MPC) are presented in Fig. 5.14. As expected for an unstable operating condition, the open-loop response grows without bound as no control action is taken (the dotted solid blue line represents this output response). The solid blue line shows output response for the MPC without constraints and the solid black line represents the input for this scenario. Once again, the input magnitude required in this case is not physically feasible. The initial control actions almost reach -800 K, meaning the feed temperature required is around -250 K, not a feasible condition.

Thus, an input constraint was considered again. For the unstable system,

a constraint in the input was a maximum variation of 30 % in relation to the feed temperature, representing a ±165 K variation. The output for this case is represented by the blue dashed line and the input is the black dashed line. As in the case of the stable system, for the first moments, the input required is in the lower limit of the constraint and it stays there for some time until it finally increases and goes back to zero.

The spatial profiles of the jacket and reactor temperatures for the open-loop and constrained MPC response are shown in Fig. 5.15. As expected, in the open-loop response the entire system grows unbounded. As for the closed-loop response, stabilization is achieved and the whole system reaches the steady-state.

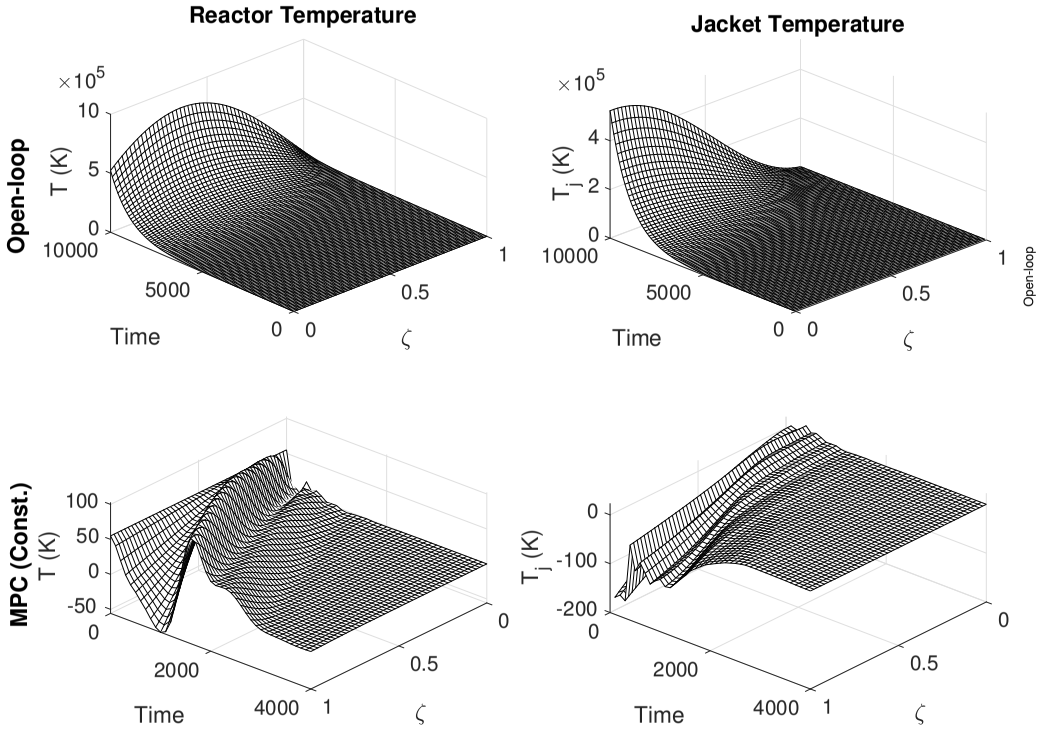

Figure 5.15: Spatial profiles of the jacket temperature obtained for the unstable steady-state:(Top row) Open-Loop: (Left) Bed Reactor Temperature; (Right) Jacket Temperature; (Bottom row) Constrained MPC $|\bar{T}_f| \leq 165$ K:(Left) Bed Reactor Temperature; (Right) Jacket Temperature.

5.8.2 Plant: Non-linear Model

In this section the non-linear model was used as the plant model that apply the actions predicted from the MPC. Two different scenarios were considered: one using the unstable steady-state for a $T_f = 550$ K and the high conversion stable steady-state for the same feed temperature. These results are shown in Figure 5.16. In both cases, the spatial profile obtained at the end of the simulation is the steady-states profiles shown in Fig. 5.3. The MPC using the unstable steady-state takes longer to get to the desired profile than the one with the stable steady-state. In both scenarios, the controller has some trouble in the beginning, as the initial conditions are different from the desired steady-state. As the system gets closer to the linear model steady-state, it is possible to see that the control actions become more reliable and the system converges faster.

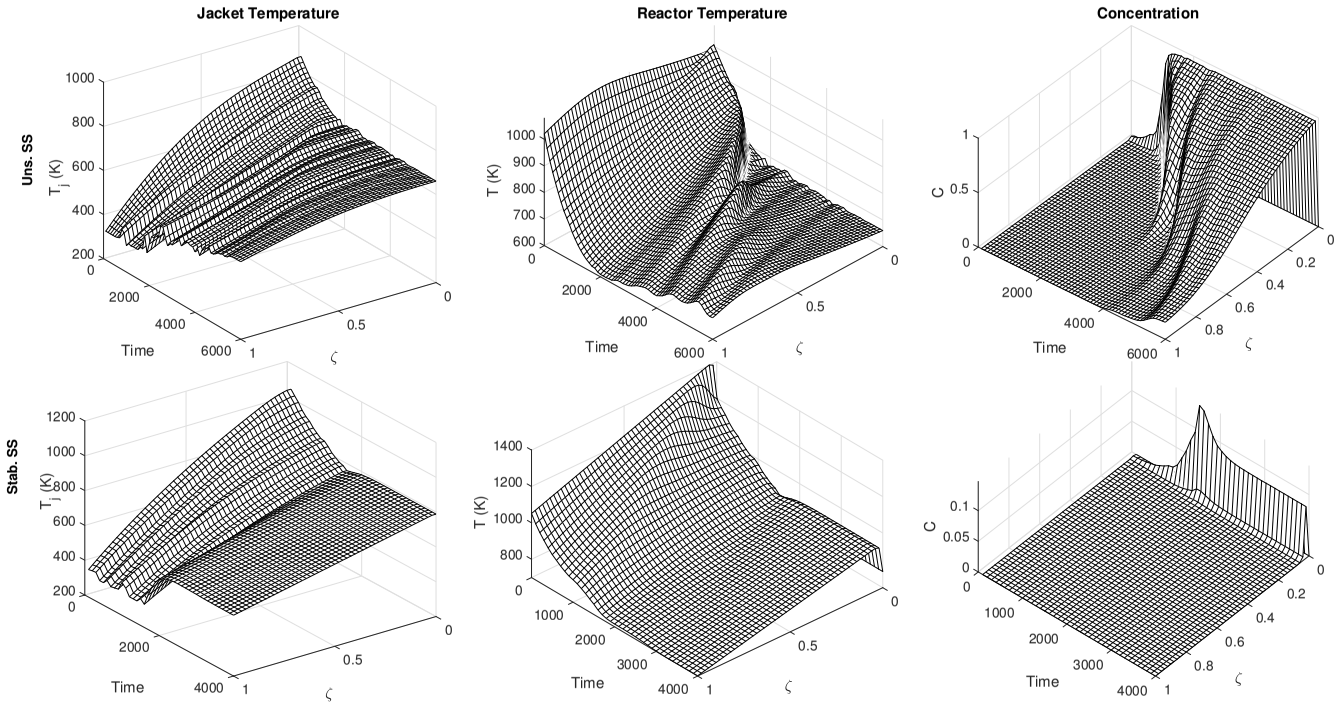

Figure 5.16: Results obtained for the when the non-linear model is used as the plant model, showing, from Left to Right, the jacket temperature, the reactor temperature and the concentration profiles, respectively. (Top Row) MPC model $|\bar{T}_f| \leq 220$ K: Unstable Steady-State; (Bottom Row) MPC model $|\bar{T}_f| \leq 220$ K: Stable Steady-State

5.9 Conclusions

The application of an MPC design to auto-thermal reactor was explored. A boundary control problem realization was considered and a boundary transformation was used to represent the boundary input as an in-domain input. The linearized model around a steady-state was used to achieve a linear representation of the system and the discrete model of the system was obtained by applying a Cayley-Tustin time discretization transformation which preserves the systems characteristics and which does not imply model reduction or approximation.

The model predictive control strategy was applied for the system considering stable and unstable steady-states. As expected, the MPC achieves a faster convergence to the steady-state than the open-loop response if a stable steady-state is considered. For the unstable steady-state, the controller can achieve the system stability. The same results were also achieved when constraints were considered in the system input. When the non-linear model is used as the plant model and the MPC uses the linearized model, it is still possible to make the system converges to the desired steady-state profile.

Acknowledgements

The support for this work is provided by CAPES - 88881.128514/2016-01 (Brazil) and support for Guilherme Ozorio Cassol is gratefully acknowledged.

Chapter 6

Model Predictive Control of a Second-order Hyperbolic transport-reaction process

6.1 Introduction

The transport of a material and/or thermodynamics property at the macroscopic scale is generally described by a parabolic partial differential equation (PDE) obtained by defining the flux across the control volume boundary, for example: by the Fourier's law, for heat transfer; Fick's law, for mass transfer; or Newton's viscosity law, for momentum transfer. In these laws, the gradient in the medium causes an immediate flux. Thus, any localized initial disturbance in the material body is propagated instantly [38]. Experimentally, this assumption does not hold. For instance: materials with non-homogeneous structure [39], or extremely fast thermal disturbances induced by a laser [40] or a flash lamp [41] present thermal waves that travel with finite speeds of propagation. Hence, motivated by the discrepancy between the experimental finite speed of phenomena propagation and the mathematical model - which yields a parabolic partial differential equation -, Cattaneo modified the heat flux to take into account the delay due to the transport, resulting in a hyperbolic PDE for the heat equation, with a finite speed of phenomena propagation [42], [43]. The hyperbolic model of the transport phenomena has been analyzed in different prior contributions. For example: in Surov's work [48], the modified equilibrium model of a heat-conducting, heterogeneous mixture was proposed using

the modified flux, and a set of hyperbolic equations was derived. The study by Nosko [39] proposed different non-Fourier models to simulate temperatures in materials subjected to extremely fast thermal disturbances, specifically for the microscopic sliding contact. Finally, in the work of Abbasi and Malek [49], the optimal control in a biological tissue modeled by a thermal wave equation (a hyperbolic heat equation) was proposed to address the transport phenomena properly. Along these lines of work, specifically for the chemical engineering process, the assumption of a delayed flux can be interesting, as parabolic equations are generally used to represent the reaction-diffusion systems [50], [51]. The controller design for models given by PDEs has been the objective of many studies over the years. One approach for the control of PDEs involves using spatial discretization techniques, converting the PDEs to sets of ODEs, and applying controller design techniques as one would with finite-dimensional systems. The problem with this approach is the resulting large dimension of the controller [107], [123]. When it comes to stabilization of distributed systems, the complexity associated with the design has been addressed with the application of different methodologies [67], [95], [108], [124]–[126], but these contributions only consider the models in the continuous-time setting and do not take into account an optimal constrained control. Additionally, in the design of model-based controllers, a difference between the actual physical plant and the model used in the controller design is challenging, as the deviation in the system dynamics might affect the closed-loop stability and performance characteristics [127], [128]. One of the well-known and fairly utilized control design methodologies in chemical process control that accounts for stabilization and constraints satisfaction is the model predictive control (MPC) [30]. There are a few contributions aimed at the design of MPC for PDEs using different methods, such as spatial discretization, controller design for a class of the Riesz spectral systems with a separable spectrum and piece-wise predictive feedback control [36], [129], [130]. Contrary to the above contributions, in this work, a discrete-time representation of the hyperbolic PDE is used to design the MPC. In particular, a type of Cranck-Nicolson integrator, also known as the Cayley-Tustin time discretization, is considered, which has been shown to

preserve the intrinsic energy and dynamical characteristics of the linear distributed parameter system with finite input and output spaces [29].

Motivated by the above considerations and extending previous results of Xu et al. [34], the second-order hyperbolic PDE obtained for a tubular reactor with a delayed flux is considered, which satisfies the conservation laws and its behavior is observed in experimental results. The controller acts at the boundary of the system and must guarantee closed-loop stabilization, and output/input constraints satisfaction. Furthermore, only the information given by a measured output (output feedback) is given to the controller. Thus, an observer is designed to reconstruct the system states in the discrete-time setting.

To analyze the difference that the modeling assumptions can have on the controller performance on the tubular reactor, this chapter considers both second-order hyperbolic and parabolic equations as representations of the transport-reaction system, emphasizing the former type, which is not commonly used. In the first section, the derivation of the hyperbolic equation for the mass transfer inside the tubular reactor is shown, considering closed boundary conditions. Then, the system properties are derived. In the succeeding sections, controller design is shown, which takes into account an output feedback, differently from the previous contributions. Thus, the observer design in the discrete-time setting is derived by solving the Ricatti operator equation, such that the states can be reconstructed only with the output information. Finally, the numerical simulations show the controller's performance for both types of PDEs and it is possible to see that the different models lead to different responses, specially when an output feedback is used.

6.2 The tubular reactor

Consider a fluid with constant density and diffusivity (D), moving inside a tube with the constant cross-sectional area and velocity (v), as shown in Figure 6.1. A first-order reaction happens inside reactor's tube, and the radial and angular diffusion effects are neglected. The mass balance for the system leads to the following balance equation:

$$\frac{\partial C}{\partial t} = -\frac{\partial F}{\partial \zeta} + r = -\frac{\partial F}{\partial \zeta} + kC \tag{6.1}$$

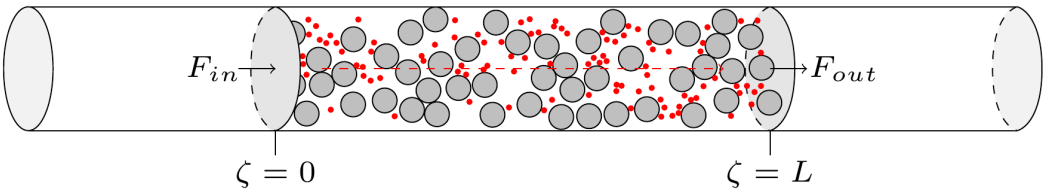

Figure 6.1: Tubular reactor representation.

where F is the mass flux, and r is the reaction term with a constant specific reaction rate (k). For simplification in the notation, throughout the rest of this manuscript, $\partial_t(\cdot)$ will be used to represent $\frac{\partial(\cdot)}{\partial t}$, $\partial_\zeta(\cdot)$, $\partial_{\zeta\zeta}(\cdot)$ and $\partial_{tt}(\cdot)$ for the first partial derivative on space and second derivatives on space and time, respectively. If the mass flux is given by Fick's law and the advective contribution, considering only the axial effects, the following parabolic PDE is obtained:

$$\partial_t C = D\partial_{\zeta\zeta} C - v\partial_\zeta C + kC \tag{6.2}$$

However, Fick's law does not consider any inertial effects. Thus, it could be possible to assume that there is a delay in the mass flux across the boundary, in both diffusive and advective terms, leading to the following flux definition:

$$F = (1 - \tau\partial_t)(-D\partial_\zeta C + vC) \tag{6.3}$$

The mass balance becomes:

$$\partial_t C = (1 - \tau\partial_t)\left[D\partial_{\zeta\zeta} C - v\partial_\zeta C\right] + kC \tag{6.4}$$

If $\tau \to 0$, then $(1 - \tau\partial_t)^{-1} \approx (1 + \tau\partial_t)$, which gives the following second order hyperbolic PDE:

$$\tau\partial_{tt} C + (1 - k\tau)\partial_t C = D\partial_{\zeta\zeta} C - v\partial_\zeta C + kC \tag{6.5}$$

Therefore, this second-order hyperbolic PDE takes into account different physical assumptions. It considers that there is a time lag that happens until the

fluid element particles start moving as a result of the established flux, as proposed by Cattaneo [42] for the heat equation. This time-lag is represented by the parameters τ, if $\tau \to 0$, the propagation phenomena is instantaneous and the parabolic PDE is obtained. Eq. 6.5 also assumes this time-lag affects the advective transport as well.

6.2.1 Boundary Conditions

For the boundary conditions, only closed vessels are considered [51], [60]. Thus, for this type of vessel, there is no dispersion either upstream (right before the inlet of the reactor, at $\zeta = 0^-$) or downstream (right after the outlet, at $\zeta = L^+$). In an open-open vessel, the dispersion occurs both upstream and downstream. The closed-closed boundary conditions can be represented as:

$$vC(0^-) = vC(0^+) - D\partial_\zeta C(0^+) \text{ and } \partial_\zeta C(L^-) = 0 \tag{6.6}$$

which are known as the Danckwerts' Boundary Conditions. In this contribution, we consider that the input is applied at the boundary, specifically, $vC(0^-) = u(t)$.

6.2.2 Control Problem

For the hyperbolic PDE with delay in the total flux, the operator A can be defined as:

$$\partial_t \begin{bmatrix} C(\zeta,t) \\ \partial_t C(\zeta,t) \end{bmatrix} = A \begin{bmatrix} C(\zeta,t) \\ \partial_t C(\zeta,t) \end{bmatrix} = \begin{bmatrix} 0 & 1 \\ \frac{D\partial_{\zeta\zeta}(\cdot) - v\partial_\zeta(\cdot) + k}{\tau} & k - \frac{1}{\tau} \end{bmatrix} \begin{bmatrix} C(\zeta,t) \\ \partial_t C(\zeta,t) \end{bmatrix} \tag{6.7}$$

which is equivalent to writing the PDE shown in Eq. 6.5, with boundary conditions presented in the previous section.

For simplicity, it is considered that $L = 1$ and the measurement of C at the end of the reactor is available (i.e., $y_m(t) = C(\zeta = \zeta_m = 1, t)$). The concentration in the middle of the reactor ($y(t) = C(\zeta = \zeta_y = 0.5, t)$) needs to satisfy a required constraint. This system can also be represented as an

abstract state-space representation $[A, B, C_m, D]$ [16]:

$$\begin{cases} \dot{x}(t) = Ax(t) + Bu(t) \\ y(t) = C_y x(t) \\ y_m(t) = C_m x(t) \end{cases} \tag{6.8}$$

with $x(t) = [C(\zeta, t), \partial_t C(\zeta, t)]^C$, u is the input to the system ($\mathcal{U} \in \Re$, a finite real space), y_m is the measured output ($\mathcal{Y}_m \in \Re$), and y is the constrained output ($\mathcal{Y} \in \Re$), such that:

$$B = \begin{bmatrix} 0 \\ \frac{-1}{\tau} \end{bmatrix} \delta(\zeta - 0); \quad C_y(\cdot) = \int_0^1 \delta(\zeta - \zeta_y)(\cdot)d\zeta; \quad C_m(\cdot) = \int_0^1 \delta(\zeta - \zeta_m)(\cdot)d\zeta \tag{6.9}$$

where $\delta(\zeta)$ is the Dirac delta. The space $\mathcal{X} := C^1(0, 1; \Re^2)$ is equipped with the inner product $\langle x_1, x_2 \rangle_{\mathcal{X}}$:

$$\begin{gathered} \langle x_1, x_2 \rangle_{\mathcal{X}} = \left\langle \begin{bmatrix} C_1 \\ \partial_t C_1 \end{bmatrix}, \begin{bmatrix} C_2 \\ \partial_t C_2 \end{bmatrix} \right\rangle_{\mathcal{X}} = \\ \int_0^1 C_1(\bar{C}_2)d\zeta + \int_0^1 \partial_t C_1(\partial_t \bar{C}_2)d\zeta \end{gathered} \tag{6.10}$$

where, $x_1, x_2 \in \mathcal{X}$, $\bar{C}_2$ and $\partial_t \bar{C}_2$ are the complex conjugates of C_2 and $\partial_t C_2$, respectively. Therefore, A is a linear operator $A : D(A) \subset \mathcal{X} \to \mathcal{X}$, such that one can define the extension A_{-1} of A to $\mathcal{X}_{-1} : \overline{(\mathcal{X}, ||(s_0 - A)^{-1} \cdot ||)}$, where s_0 belongs to the resolvent of A. Finally, one can define B as a linear operator $B \in \mathcal{L}(U, \mathcal{X}_{-1})$ [131].

For the system given by Eqs. 1 and 9, we want to develop a controller that guarantees stabilization and constraints satisfaction while using only the information provided by the (finite) output signal. In this contribution, the second-order hyperbolic PDE and commonly used parabolic PDE are assumed as models in order to compare the controller performance considering the two different model settings.

6.3 System Properties

In this section, the specific properties of the state-space representation given by Eq. 6.8 are defined. These properties are used in the following sections for the observer and controller design.

6.3.1 Eigenvalue Problem

The eigenvalue problem for the hyperbolic PDE is solved in Appendix 6.A, with the boundary conditions defined in the previous section. The resulting characteristic equation for the second-order hyperbolic is given by:

$$\tanh\left(\frac{1}{D}\sqrt{\frac{v^2}{4}+D(\lambda-k)(1+\lambda\tau)}\right)=\frac{-v\sqrt{\frac{v^2}{4}+D(\lambda-k)(1+\lambda\tau)}}{\frac{v^2}{2}+D(\lambda-k)(1+\lambda\tau)} \quad (6.11)$$

which is a non-linear algebraic equation and it is solved numerically. The numerical solution to the above Eq.6.11 yields the value of λ_i, and the corresponding eigenfunctions are defined as (see Appendix 6.A for details):

$$\phi_i=\left[f_{11}(\zeta,\lambda_i)+\frac{v}{D}f_{12}(\zeta,\lambda_i)\right]\begin{bmatrix}1\\ \lambda_i\end{bmatrix}\phi_{1,i}(0) \quad (6.12)$$

6.3.2 Resolvent Operator and Transfer function

The resolvent operator and the systems transfer functions are necessary for the Cayley-Tustin time discretization applied in the ensuing sections. They can be found by applying the *Laplace transformation* to the system of equations shown in Eq. 6.7, which leads to:

$$s\begin{bmatrix}X_1\\ X_2\end{bmatrix}-\begin{bmatrix}x_1(0)\\ x_2(0)\end{bmatrix}=\begin{bmatrix}0 & 1\\ \frac{Dd_{\zeta\zeta}(\cdot)-vd_\zeta(\cdot)+k}{\tau} & k-\frac{1}{\tau}\end{bmatrix}\begin{bmatrix}X_1\\ X_2\end{bmatrix} \quad (6.13)$$

where $X_1=\mathcal{L}\{T(t)\}$, $X_2=\mathcal{L}\{\partial_t T(t)\}$, $x_1(0)=T(0)$ and $x_2(0)=\partial_t T(0)$. Thus, the following system of equations can be written:

$$\begin{cases}X_2=sX_1-x_1(0)\\ \frac{D}{\tau}d_{\zeta\zeta}X_1-\frac{v}{\tau}d_\zeta X_1+\frac{k}{\tau}X_1-\frac{1}{\tau}X_2+kX_2=sX_2-x_2(0)\end{cases} \quad (6.14)$$

by substituting the first equation into the second, the ODE obtained is:

$$\begin{gathered}\tau s^2X_1+\begin{bmatrix}k\tau-s\tau-1 & -\tau\end{bmatrix}\begin{bmatrix}x_1(0)\\ x_2(0)\end{bmatrix}=\\ Dd_{\zeta\zeta}X_1-vd_\zeta X_1+kX_1-sX_1+k\tau sX_1\end{gathered} \quad (6.15)$$

Setting $W_1=X_1$ and $W_2=\partial_\zeta X_1$ leads to the following system of first-order ODEs:

$$d_\zeta\begin{bmatrix}W_1\\ W_2\end{bmatrix}=\begin{bmatrix}0 & 1\\ \frac{(s-k)(\tau s+1)}{D} & \frac{v}{D}\end{bmatrix}\begin{bmatrix}W_1\\ W_2\end{bmatrix}+\begin{bmatrix}0 & 0\\ \frac{k\tau-s\tau-1}{D} & -\frac{\tau}{D}\end{bmatrix}\begin{bmatrix}x_1(0)\\ x_2(0)\end{bmatrix} \quad (6.16)$$

which has the following solution:

$$\begin{aligned}\begin{bmatrix} W_1 \\ W_2 \end{bmatrix} &= \begin{bmatrix} f_{11}(\zeta,s) & f_{12}(\zeta,s) \\ f_{21}(\zeta,s) & f_{22}(\zeta,s) \end{bmatrix} \begin{bmatrix} W_1(0) \\ W_2(0) \end{bmatrix} \\ + \int_0^\zeta \begin{bmatrix} f_{11}(\zeta-\eta,s) & f_{12}(\zeta-\eta,s) \\ f_{21}(\zeta-\eta,s) & f_{22}(\zeta-\eta,s) \end{bmatrix} &\begin{bmatrix} 0 & 0 \\ \frac{k\tau-s\tau-1}{D} & -\frac{\tau}{D} \end{bmatrix} \begin{bmatrix} x_1(0) \\ x_2(0) \end{bmatrix}\end{aligned} \tag{6.17}$$

where $f_{ij}(\zeta,s)$ is defined as in Eq. 6.50 with $\lambda = s$. Considering $u(t) = 0$, the boundary conditions are given by:

$$DW_2(0) - vW_1(0) = 0 \text{ and } W_2(1) = 0 \tag{6.18}$$

resulting in:

$$\begin{aligned} W_1(0) = -\frac{\int_0^1 f_{22}(1-\eta,s) \left[\frac{k\tau-s\tau-1}{D} x_1(0) - \frac{\tau}{D} x_2(0) \right]}{f_{21}(1,s) + \frac{v}{D} f_{22}(1,s)} \implies \\ W_1 = X_1 = \begin{bmatrix} \Gamma_1(\cdot) & \Gamma_2(\cdot) \end{bmatrix} \begin{bmatrix} x_1(0) \\ x_2(0) \end{bmatrix} = \\ \begin{bmatrix} f_{11}(\zeta,s) & f_{12}(\zeta,s) \end{bmatrix} \begin{bmatrix} 1 \\ \frac{v}{D} \end{bmatrix} W_1(0) \\ + \int_0^\zeta f_{12}(\zeta-\eta,s) \begin{bmatrix} \frac{k\tau-s\tau-1}{D} & -\frac{\tau}{D} \end{bmatrix} \begin{bmatrix} x_1(0) \\ x_2(0) \end{bmatrix} \end{aligned} \tag{6.19}$$

with:

$$\begin{aligned} \Gamma_1(\cdot) = -\frac{f_{11}(\zeta,s) + \frac{v}{D} f_{12}(\zeta,s)}{f_{21}(1,s) + \frac{v}{D} f_{22}(1,s)} \int_0^1 f_{22}(1-\eta,s) \frac{k\tau-s\tau-1}{D}(\cdot) d\eta \\ + \int_0^\zeta f_{12}(\zeta-\eta,s) \frac{k\tau-s\tau-1}{D}(\cdot) d\eta \\ \Gamma_2(\cdot) = -\frac{f_{11}(\zeta,s) + \frac{v}{D} f_{12}(\zeta,s)}{f_{21}(1,s) + \frac{v}{D} f_{22}(1,s)} \int_0^1 f_{22}(1-\eta,s) \frac{-\tau}{D}(\cdot) d\eta \\ + \int_0^\zeta f_{12}(\zeta-\eta,s) \frac{-\tau}{D}(\cdot) d\eta \end{aligned} \tag{6.20}$$

Finally, the resolvent operator is defined as:

$$(sI - A)^{-1}\mathbf{x_0} = \begin{bmatrix} X_1 \\ X_2 \end{bmatrix} = \begin{bmatrix} \Gamma_1(\cdot) & \Gamma_2(\cdot) \\ s\Gamma_1(\cdot) - I(\cdot) & s\Gamma_2(\cdot) \end{bmatrix} \begin{bmatrix} x_1(0) \\ x_2(0) \end{bmatrix} \tag{6.21}$$

where $I(\cdot)$ is the identity operator. The same approach is taken to find the transfer function and $(sI-A)^{-1}B$, by considering $\mathbf{x_0} = \mathbf{0}$ and $U(s) \neq 0$. Thus, the solution of the system of ODEs defined in Eq. 6.16 is given by:

$$\begin{bmatrix} W_1 \\ W_2 \end{bmatrix} = \begin{bmatrix} f_{11}(\zeta,s) & f_{12}(\zeta,s) \\ f_{21}(\zeta,s) & f_{22}(\zeta,s) \end{bmatrix} \begin{bmatrix} W_1(0) \\ W_2(0) \end{bmatrix} \tag{6.22}$$

and the boundary conditions:

$$DW_2(0) - vW_1(0) = U(s) \text{ and } W_2(1) = 0 \tag{6.23}$$

leading to:

$$\begin{gathered} W_1(0) = -\frac{\frac{1}{D}f_{22}(1,s)U(s)}{f_{21}(1,s) + \frac{v}{D}f_{22}(1,s)} = aU(s) \implies \\ W_1 = X_1 = \left[af_{11}(\zeta,s) + a\frac{v}{D}f_{12}(\zeta,s)\right]U(s) + \frac{1}{D}f_{12}(\zeta,s)U(s) = \\ \left[af_{11}(\zeta,s) + \left(\frac{av+1}{D}\right)f_{12}(\zeta,s)\right]U(s) = \beta(\zeta)U(s) \end{gathered} \tag{6.24}$$

thus:

$$(sI - A)^{-1}BU(s) = \begin{bmatrix} X_1 \\ X_2 \end{bmatrix} = \begin{bmatrix} \beta(\zeta) \\ s\beta(\zeta) \end{bmatrix} U(s) \tag{6.25}$$

Finally, the transfer functions are:

$$\begin{gathered} G(s) = C_y(sI - A)^{-1}B = X_1(0.5) = \beta(0.5) \\ G_m(s) = C_m(sI - A)^{-1}B = X_1(1) = \beta(1) \end{gathered} \tag{6.26}$$

Remark: For the general state-space representation shown in Eq. 6.8, after finding $(sI - A)^{-1}(\cdot)$ in Eq. 6.21 and $(sI - A)^{-1}B$ in Eq. 6.25, it is possible to define the state-space operators as:

$$B = \begin{bmatrix} 0 \\ \frac{-1}{\tau} \end{bmatrix} \delta(\zeta - 0); \quad C_y(\cdot) = \int_0^1 \delta(\zeta - \zeta_y)(\cdot)d\zeta; \quad C_m(\cdot) = \int_0^1 \delta(\zeta - \zeta_m)(\cdot)d\zeta \tag{6.27}$$

where B was obtained by using $(sI - A)^{-1}(\cdot)$ defined in Eq. 6.21 such that the result is the same as $(sI - A)^{-1}B$ in Eq. 6.25. $\delta(\zeta)$ is the Dirac delta distribution function and $\int_0^1 \delta(\zeta - a)x(\zeta)d\zeta = x(a)$, for $0 \leq a \leq 1$.

6.3.3 Adjoint operator and the bi-orthogonal basis

In the MPC scheme, a stability constraint and the terminal cost are used to guarantee closed-loop stabilization and calculate the cost function after stabilization. These properties can be derived using a bi-orthogonal basis, which is derived in this section. To define this basis, first, the adjoint operator must be obtained, which can be constructed by using the definition of the inner-product shown in Eq. 6.10:

$$\langle Ax, y\rangle = \langle x, A^*y\rangle \tag{6.28}$$

where $x \in \mathcal{X}$, $y \in \mathcal{X}^*$, A is the operator defined in Eq. 6.7 and A^* is the adjoint operator. Using the definition of inner product and expression of operator A one obtains, as shown in Appendix 6.B:

$$\left\langle \begin{bmatrix} x_1 \\ x_2 \end{bmatrix}, \begin{bmatrix} \frac{D\partial_{\zeta\zeta} y_2 + v\partial_\zeta y_2 + k y_2}{\tau} \\ y_1 - \left(-\bar{k} + \frac{1}{\tau}\right) y_2 \end{bmatrix} \right\rangle = \langle x, A^* y \rangle \implies A^* = \begin{bmatrix} 0 & \frac{D\partial_{\zeta\zeta} + v\partial_\zeta + k}{\tau} \\ 1 & k - \frac{1}{\tau} \end{bmatrix} \tag{6.29}$$

with boundary conditions given as:

$$v y_2|_1 + D\partial_\zeta y_2|_1 = 0 \text{ and } \partial_\zeta y_2|_1 = 0 \tag{6.30}$$

By solving the eigenvalue problem for the adjoint operator, the following functions are obtained:

$$\psi_i = \left[g_{11}(\zeta, \lambda_i) + \frac{v}{D} g_{12}(\zeta, \lambda_i) \right] \begin{bmatrix} \lambda_i + \frac{1}{\tau} - k \\ 1 \end{bmatrix} \psi_{2,i}(0) \tag{6.31}$$

with $g_{i,j}$ given by the expressions shown in Eq. 6.50, with $a = \frac{(\lambda - k)(1 + \lambda\tau)}{D}$, $b = -\frac{v}{D}$ and $\zeta_0 = 0$. The derivation of the adjoint operator and its eigenfunctions is shown in Appendix 6.B.

Taking into account the definition of inner product shown in Eq. 6.10

$$\begin{gathered} \langle A\phi_i, \psi_j \rangle = \langle \lambda_i \phi_i, \psi_j \rangle = \lambda_i \langle \phi_i, \psi_j \rangle = \\ \langle A\phi_i, \psi_j \rangle = \langle \phi_i, A^* \psi_j \rangle = \langle \phi_i, \lambda_j \psi_j \rangle = \bar{\lambda}_j \langle \phi_i, \psi_j \rangle \\ \text{or} \\ \langle A\phi_i, \bar{\psi}_j \rangle = \langle \lambda_i \phi_i, \bar{\psi}_j \rangle = \lambda_i \langle \phi_i, \bar{\psi}_j \rangle = \\ \langle A\phi_i, \bar{\psi}_j \rangle = \langle \phi_i, A^* \bar{\psi}_j \rangle = \langle \phi_i, \bar{\lambda}_j \bar{\psi}_j \rangle = \lambda_j \langle \phi_i, \bar{\psi}_j \rangle \end{gathered} \tag{6.32}$$

In the first case, for the equality to hold, $\langle \phi_i, \psi_j \rangle = 0$ if $\lambda_i \neq \bar{\lambda}_j$. Thus, the eigenfunctions are orthogonal to each other, except to the eigenfunction related to their conjugated eigenvalue. In the second case, $\langle \phi_i, \bar{\psi}_j \rangle = 0$ if $\lambda_i \neq \lambda_j$ and the eigenfunctions are orthogonal to each other, except to the eigenfunction related to the same eigenvalue. One can choose $\phi_{1,i}(0)$ in Eq. 6.12 and $\psi_{2,i}(0)$ in Eq. 6.31, such that $\langle \phi_i, \bar{\psi}_j \rangle = 1$.

6.4 Controller Design

The closed-system considered in this contribution is shown in Figure 6.2. In the closed-loop operation, the controller uses an initial estimate of the plant states

to calculate an appropriate input that guarantees the stability and constraints satisfaction up until the end of the control horizon. The input is applied to the plant and the measured output is obtained. With the new information, the observer states are updated and used by the MPC to determine the new input, setting the closed-loop cycle. In the next sections, first, the discrete-time representation of the system, which is also used in the controller design, is shown, followed by the system observer design in the discrete-time setting. Finally, the model predictive control design is presented, using the observer states to calculate the appropriate input that guarantees the system stability and constraints satisfaction.

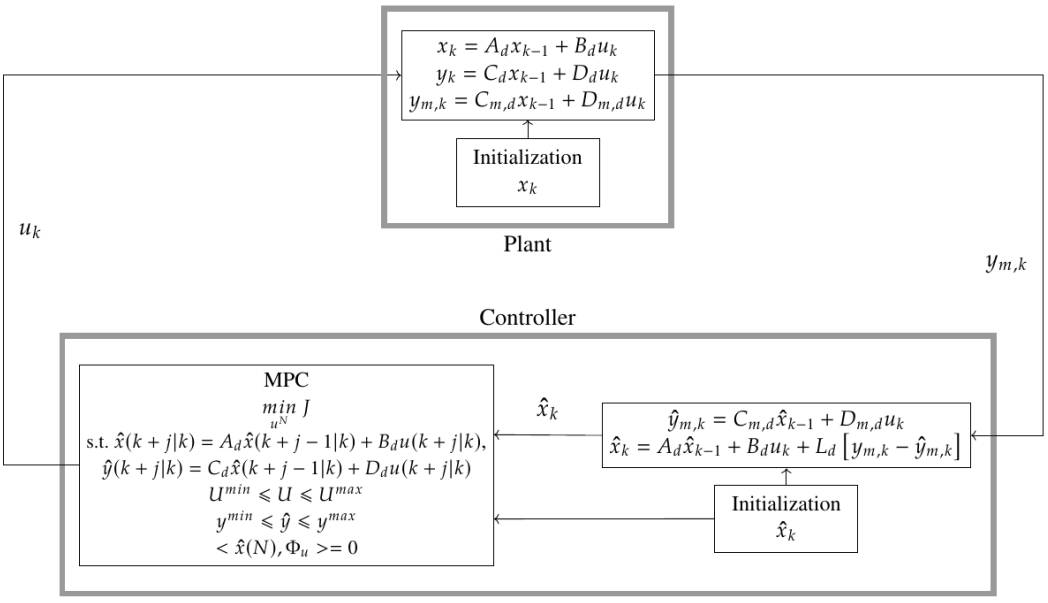

Figure 6.2: Discrete-time closed-loop representation.

6.5 Discrete-time representation

In this section, the discrete representation is obtained for the system. The Cayley-Tustin discrete-time representation is used, which preserves the intrinsic energy, and dynamical characteristics of the system [29].

6.5.1 System representation

Given the system defined in Eq. 6.8, one can apply a structure-preserving time discretization of the dynamical system. The so-called Cayley-Tustin time discretization is derived by applying the Crank-Nicolson midpoint integration rule and assuming piecewise-constant input within the sampled intervals. The discrete system is obtained as:

$$\begin{aligned} x_k &= A_d x_{k-1} + B_d u_k \\ y_k &= C_d x_{k-1} + D_d u_k \\ y_{m,k} &= C_{m,d} x_{k-1} + D_{m,d} u_k \end{aligned} \tag{6.33}$$

where $\delta = 2/\Delta t$, A_d, B_d, C_d, D_d, $C_{m,d}$ and $D_{m,d}$ are the discrete time system operators and are given by:

$$\begin{bmatrix} A_d(\cdot) & B_d \\ C_d(\cdot) & D_d \\ C_{m,d}(\cdot) & D_{m,d} \end{bmatrix} = \begin{bmatrix} -I + 2\delta\left(\delta I - A\right)^{-1}(\cdot) & \sqrt{2\delta}\left(\delta I - A\right)^{-1} B \\ \sqrt{2\delta} C_y \left(\delta I - A\right)^{-1}(\cdot) & G(\delta) \\ \sqrt{2\delta} C_m \left(\delta I - A\right)^{-1}(\cdot) & G_m(\delta) \end{bmatrix} \tag{6.34}$$

$\left(\delta I - A\right)^{-1} = R(\delta, A)$ is defined as the resolvent operator of the operator A, found in Eq. 6.21. $\left(\delta I - A\right)^{-1} B$, $G(\delta) = C_y \left(\delta I - A\right)^{-1} B$ and $G_m(\delta) = C_m \left(\delta I - A\right)^{-1} B$ were defined in Eq. 6.25 and Eq. 6.26 for the system considered, with $s = \delta$. Notice that, although the system in the continuous-time setting does not have a feedthrough operator ($D = D_m = 0$), the discrete-time representation contains feedthrough operators ($D_d = G(\delta) \neq 0$ and $D_{m,d} = G_m(\delta) \neq 0$).

The operators given by Eq. 6.34 are all compact and well-defined, and the issue of boundary (point) actuation or/and observation does not induce mathematical difficulties associated with the continuous counterparts, usually leading to unboundedness.

Assumption 6.1 *A small enough value of Δt is used such that the discrete-time representation of the system shown in Eq. 6.33 is a good approximation of the open-loop system internal dynamics and the finite set of input/output relations.*

Assumption 6.1 presumes there is a large enough δ (small enough Δt) such that the discretization can be applied to unstable systems [34] and is necessary for the development of the controller in the following sessions. For an unstable open-loop system, the following lemma gives an interval for which the discrete representation might be a good approximation of the system:

Lemma 6.1 *For an unstable system, the discrete system* (A_d, B_d, C_d, D_d) *needs to satisfy* $\Delta t < \frac{2}{s(A)}$*, where* $s(A) = \sup\{Re\, z : z \in \sigma(A)\}$*, in order to properly represent the* (A, B, C_y, D) *system dynamics.*

The proof of Lemma 6.1 was shown in previous contributions [132].

6.5.2 System observer

Consider the following Luenberger observer in the discrete-time setting for the system:

$$\begin{aligned} \hat{y}_{m,k} &= C_{m,d}\hat{x}_{k-1} + D_{m,d}u_k \\ \hat{x}_k &= A_d\hat{x}_{k-1} + B_d u_k + L_{o,d}\left[y_{m,k} - \hat{y}_{m,k}\right] \end{aligned} \tag{6.35}$$

where $A_d, B_d, C_{m,d}, D_d$ have been defined previously and $L_{o,d}$ is the observer gain in the discrete-time setting. The observer takes the current values of $y_{m,k}$ and u_k as input and gives the current state estimation $\hat{x}_k$, which the MPC uses to calculate the next input applied to the system. Thus, the proper observer gain ($L_{o,d}$) needs to be found, such that the observer error dynamics, defined as $\hat{e}_k = x_k - \hat{x}_k$, is stable and $\hat{x}_k \to x_k$ as $k \to \infty$. As shown in Appendix 6.D, the following discrete Ricatti equation can be solved to find the appropriate observer gain:

$$\begin{gathered} \langle \bar{Q}_O A_d^* x, A_d^* x\rangle - \langle \bar{Q}_O x, x\rangle \\ -\langle (R_O + C_{m,d}\bar{Q}_O C_{m,d}^*)^{-1} C_{m,d}\bar{Q}_O A_d^* x, C_{m,d}\bar{Q}_O A_d^* x\rangle = \\ -\langle Q_O C_{m,d} x, C_{m,d} x\rangle \end{gathered} \tag{6.36}$$

where the observer gain will then be given as $L_{o,d} = A_d^*\bar{Q}_O C_{m,d}^*(R_O + C_{m,d}\bar{Q}_O C_{m,d}^*)^{-1}$. Solving this equation is the same as solving the equation below:

$$\begin{gathered} A_d\bar{Q}_O A_d^* - \bar{Q}_O - A_d\bar{Q}_O C_{m,d}^*(R_O + C_{m,d}\bar{Q}_O C_{m,d}^*)^{-1} C_{m,d}\bar{Q}_O A_d^* = \\ -C_{m,d}^* Q_O C_{m,d} \end{gathered} \tag{6.37}$$

which is the discrete Ricatti equation generally used for finite (lumped) systems. Solving any of these Ricatti equations is analog to solve the following

discrete Lyapunov equation:

$$\begin{array}{c}\langle \bar{Q}_O(A_d - L_{o,d}C_{m,d})^* x, (A_d - L_{o,d}C_{m,d})^* x\rangle - \langle \bar{Q}_O x, x\rangle = \\ -\langle x, (C_{m,d}^* Q_O C_{m,d} + L_{o,d} R_O L_{o,d}^*)x\rangle\end{array} \tag{6.38}$$

If $\bar{Q}_O$ and Q_O are positive definite operators, the observer error dynamics $A_d - L_{o,d}C_{m,d}$ is stable and the observer states converge to the system states. By using the bi-orthogonal basis of A, the Ricatti equation can be written as:

$$\begin{array}{c}\lambda_M^D \lambda_N^D q_{N,M}^o - q_{N,M}^o \\ -(\lambda_N^D \sum_i c_i q_{N,i}^o)^T (R_O + \sum_i \sum_j c_i^* q_{i,j}^o c_j)^{-1} \overline{(\lambda_M^D \sum_i c_i q_{M,i}^o)} = \\ -(C_{m,d}\psi_N)^T Q_O \overline{(C_{m,d}\psi_M)}\end{array} \tag{6.39}$$

where $c_i = C_{m,d}\phi_i$, ϕ_i are the system eigenfunctions and λ_i^D are the eigenvalues in the discrete-time setting.

Thus, this system of non-linear equations can be solved to find $q_{N,M}^o$ and, consequently, $\bar{Q}_O(\cdot)$ and the observer gain $L_{o,d} = A_d \bar{Q}_O C_{m,d}^*$:

$$\begin{array}{c}\bar{Q}_O(\cdot) = \sum_i^{N_\lambda} \sum_j^{N_\lambda} q_{i,j}^o \langle \phi_i, (\cdot)\rangle \phi_j; \\ L_{o,d}(\zeta) = A_d \bar{Q}_O C_{m,d}^* (R_O + C_{m,d}\bar{Q}_O C_{m,d}^*)^{-1} = \\ \sum_i^{N_\lambda} \sum_j^{N_\lambda} (I + \sum_i \sum_j c_i^* q_{i,j}^o c_j)^{-1} q_{i,j}^o \lambda_j^D \phi_j(\zeta) \langle C_{m,d}\phi_i, 1\rangle\end{array} \tag{6.40}$$

It is important to notice that, for an infinite-dimensional system $N_\lambda \to \infty$, as this type of system has an infinite number of eigenvalues. Thus, we consider an observer gain approximation by using a finite number of eigenvalues. As the system is linear, a direct relationship between the discrete and continuous eigenvalues can be obtained. For the Cayley-Tustin time discretization, this is given by $\lambda_i^D = -1 + \frac{2\delta}{\delta - \lambda_i}$, where λ_i^D and λ_i are the eigenvalues in the discrete and continuous-time setting, respectively. Furthermore, as one expects from a linear system, the eigenfunctions associated with the spatial characteristics are invariant (the same as in the continuous-time setting).

6.6 Model Predictive Control

The MPC design developed in Muske et al. [30] for a finite-dimensional system is a discrete controller design methodology and can be extended to the infinite-dimensional setting [34]. Regarding the regulator design, the following

objective function is considered as the basis of the controller design, which needs to be minimized at each sampling time (k) on an infinite horizon:

$$\begin{aligned}
&\min_{u} \sum_{j=0}^{\infty} \langle \hat{x}(k+j|k), Q\hat{x}(k+j|k)\rangle + \langle u(k+l+1|k), Ru(k+l+1|k)\rangle \\
&\text{s.t.:} \quad \begin{array}{l} \hat{x}(k+j|k) = A_d\hat{x}(k+j-1|k) + B_d u(k+j|k), \\ \hat{y}(k+j|k) = C_d\hat{x}(k+j-1|k) + D_d u(k+j|k), \\ u^{\min} \leqslant u(k+j|k) \leqslant u^{\max}, \\ y^{\min} \leqslant \hat{y}(k+j|k) \leqslant y^{\max} \end{array}
\end{aligned} \tag{6.41}$$

In this equation, $\hat{x}$ and $\hat{y}$ are the system observer states and estimated output, respectively. R is a positive definite matrix (in this case, a scalar, as $u(t) \in \Re^1$) that defines the input cost, Q is positive semidefinite operator associated with the states cost, $k+j|k$ is the future step calculated from the current time k, $u^{\min}$, $u^{\max}$, $y^{\min}$ and $y^{\max}$ are the minimum and maximum input and output constraints. The system is assumed to be stabilized by the end of the control horizon, and the input is zero for $j > N$ (N is the control horizon). This is achieved by adding a stability constraint to the controller design. With these considerations, the infinite horizon objective function given by Eq. 6.41 can be rewritten in a finite horizon:

$$\begin{aligned}
&\min_{u^N} J = \sum_{j=0}^{N-1} \{\langle \hat{x}(k+j|k), Q\hat{x}(k+j|k)\rangle \\
&\qquad +\langle u(k+j+1|k), R_c u(k+j+1|k)\rangle\Big\} \\
&\qquad\quad +\langle \hat{x}(k+N|k), \bar{Q}\hat{x}(k+N|k)\rangle \\
&\text{s.t.:} \quad \begin{array}{l} \hat{x}(k+j|k) = A_d\hat{x}(k+j-1|k) + B_d u(k+j|k), \\ \hat{y}(k+j|k) = C_d\hat{x}(k+j-1|k) + D_d u(k+j|k), \\ u^{\min} \leqslant u(k+j|k) \leqslant u^{\max}, \\ y^{\min} \leqslant \hat{y}(k+j|k) \leqslant y^{\max} \\ \langle \hat{x}(\zeta, k+N), \Psi_U\rangle = 0 \end{array}
\end{aligned} \tag{6.42}$$

where $\bar{Q}$ is the terminal cost and is necessarily a positive definite operator if all the unstable eigenmodes are canceled by the end of the horizon. The bi-orthogonal basis shown in the previous sections can be used to calculate the terminal cost operator ($\bar{Q}$), as shown in Appendix 6.C:

$$\bar{Q}x = -\sum_{i}^{\infty}\sum_{j}^{\infty} \frac{\langle \phi_i, Q\phi_j\rangle}{\lambda_i + \bar{\lambda}_j} \langle x, \bar{\psi}_i\rangle \bar{\psi}_j \tag{6.43}$$

This stability condition is derived from the assumption that, given the biorthonormal basis, for any $x \in \mathcal{X}$, the following holds:

$$\begin{array}{l} x(t,\zeta) = \sum_i^\infty \langle x(t,\zeta), \bar{\psi}_i(\zeta)\rangle \phi_i(\zeta) = \sum_i^\infty a_i(t)\phi_i(\zeta) \implies \\ \dot{x} = \sum_i^\infty \dot{a}_i(t)\phi_i(\zeta) = \sum_i^\infty \langle Ax(t,\zeta), \bar{\psi}_i(\zeta)\rangle \phi_i(\zeta) + Bu(t) \\ = \sum_i^\infty \lambda_i a_i(t)\phi_i(\zeta) + Bu(t) \implies \dot{a}_i(t) = \lambda_i a_i(t) + b_i u(t) \end{array} \tag{6.44}$$

In the last step, the inner product with $\bar{\psi}_j(\zeta)$ was taken and $b_i =< B, \bar{\psi}_i(\zeta) >$. If $< x, \Psi_U >= 0$ (where Ψ_U is the set of unstable eigenfunctions), then $a_U(t) = 0$ and $x(t)$ is exponentially stable ($\dot{a}_i(t) < 0$, as $\Re(\lambda_i) < 0$ for all $\lambda_i \notin \{\lambda_U\}$ - the set of unstable eigenvalues). As the eigenfunctions are the same as in the continuous-time setting, the stability condition remains the same. With the discrete system dynamics, the stability constraint can be further expanded as:

$$\begin{array}{c} \langle x(\zeta, k+N), \Psi_U \rangle = \\ U^T \begin{bmatrix} [(A_d)^{N-1}B_d, \Psi_U] & \dots & [B_d, \Psi_U] \end{bmatrix} + \langle (A_d)^N x(\zeta, k|k), \Psi_U \rangle = 0 \implies \\ \begin{bmatrix} [\Psi_U, (A_d)^{N-1}B_d] & \dots & [\Psi_U, B_d] \end{bmatrix} U + \langle (A_d)^N x(\zeta, k|k), \Psi_U \rangle = 0 \end{array} \tag{6.45}$$

where the transpose was taken and $U = [u^T(k), u^T(k+1), \dots, u^T(k+N)]^T$ is the vector with the inputs up to the control horizon. Finally, Eq. 6.42 can be further simplified by using the system dynamics:

$$\begin{array}{ll} & \min\limits_U \; J = 2U^T G[\hat{x}(\zeta, k|k)] \\ & + U^T H U + \langle \hat{x}(k|k), \bar{Q}\hat{x}(k|k) \rangle \\ \text{s.t.:} & U^{\min} \leqslant U \leqslant U^{\max} \\ & Y^{\min} \leqslant SU + T[\hat{x}(\zeta, k|k)] \leqslant Y^{\max} \\ & \hat{x}_{do}(k+j|k) = A_{do,d}\hat{x}_{do}(k+j-1|k), \\ & S_{IP}U + T_{IP}[\hat{x}(\zeta, k|k)] = 0 \end{array} \tag{6.46}$$

where H is a matrix with elements $h_{i,j}$, for $i = 1, ..., N$ and $j = 1, ..., N$, defined below. $Y^{\min}$ and $Y^{\max}$ are vectors containing the output constraints. It is considered that the constraints are constant, i.e., $y^{\min}(k+j) = y^{\min}$ for $0 \leq j < N$. The elements of the matrices and operators defined on Eq. 6.46 are given by:

$$h_{i,j} = \begin{cases} \left[B_d, \bar{Q}B_d\right] + R, \text{ if } i = j \\ \left[B_d, \bar{Q}(A_d)^{(i-j)}B_d\right], \text{ if } i > j \\ \left[(A_d)^{(j-i)}B_d, \bar{Q}B_d\right], \text{ if } i < j \end{cases}$$

$$G[\cdot] = \begin{bmatrix} [B_d, \bar{Q}A_d(\cdot)] \\ [B_d, \bar{Q}(A_d)^2(\cdot)] \\ \vdots \\ [B_d, \bar{Q}(A_d)^N(\cdot)] \end{bmatrix}, \; T[\cdot] = \begin{bmatrix} C_d(\cdot) \\ C_d(A_d)(\cdot) \\ \vdots \\ C_d(A_d)^{N-1}(\cdot) \end{bmatrix}$$

$$S = \begin{bmatrix} D_d & 0 & \dots & 0 \\ C_dB_d & D_d & \dots & 0 \\ \vdots & \vdots & \ddots & \vdots \\ C_d(A_d)^{N-2}B_d & C_d(A_d)^{N-3}B_d & \dots & D_d \end{bmatrix}$$

$$\begin{aligned} S_{IP} &= \begin{bmatrix} [\Phi_u, (A_d)^{N-1}B_d] & \dots & [\Phi_u, B_d] \end{bmatrix} \\ T_{IP}[\cdot] &= \langle (A_d)^N(\cdot), \hat{\Phi}_u \rangle \\ U &= \begin{bmatrix} u(k+1|k)^T & u(k+2|k)^T & \dots & u(k+N|k)^T \end{bmatrix}^T \end{aligned} \tag{6.47}$$

Thus, considering that this optimization problem is feasible for every k, it is possible to find U for each step, and the values of $u(k)$ are obtained.

6.7 Results

In this section, the simulation results are presented, and the value of the parameters shown in Table 6.1 were considered. For these values, the open-loop system presents an unstable behavior for both the second-order hyperbolic and parabolic PDEs, as shown in the eigenvalue distribution presented in Figure 6.3. For the parabolic PDE, the unstable eigenvalue is located at $\lambda_U \approx 0.15$, whilst for the hyperbolic equation it is at $\lambda_U \approx 0.17$. The difference between the eigenvalues distribution is also noticeable: the parabolic equation has all its eigenvalues located in the real axis, and their values tend to $-\infty$; the hyperbolic PDE, on the other hand, has a finite number of real eigenvalues and its distribution increases in the imaginary axis. The unstable eigenfunctions are presented in Figure 6.3, such that the stability condition given by Eq. 6.45 can be set. For the results shown below, the initial condition for $\partial_t C(t)$, necessary in the hyperbolic PDE, was considered 0 and $C(t = 0, \zeta) = -0.43\zeta^2 + 0.86\zeta + 0.43$ for both PDEs. If only the output feedback is used, the observer initial condition was considered to be zero for all the states. The states cost Q for the parabolic PDE were considered to be

$Q_P x = qx$, where q is a constant. While for the hyperbolic PDE, it was considered $Q_H = \begin{bmatrix} Q_P & 0 \\ 0 & 0 \end{bmatrix}$, such that, only $x(t) = C(t)$ will have a direct weight in the cost function, allowing for the comparison between the two types of models. The integral terms on the discrete operators were approximated by be trapezoidal rule, using $N = 200$ discretization points.

Table 6.1: Parameters used in the simulation.

D	v	k	τ	Δt	R	q	R_O	N	N_λ
0.5	1	1.5	0.1	0.25	40	1	1	200	70

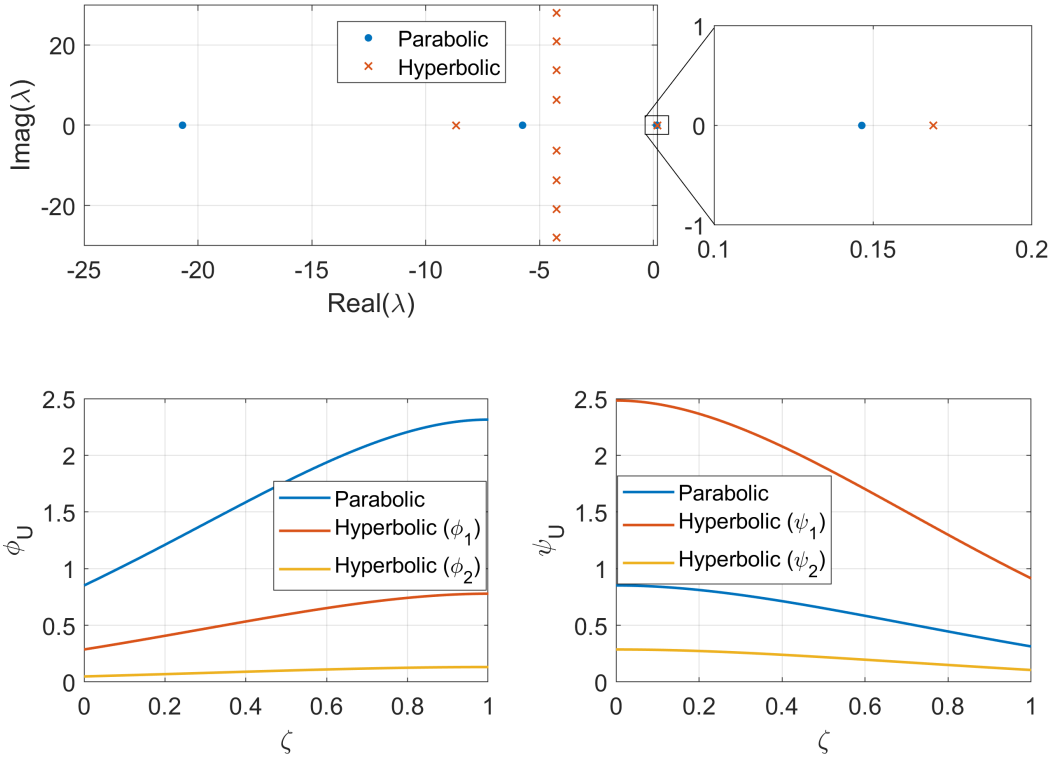

Figure 6.3: (Top): Eigenvalue distribution (left), with a enlarged segment (right), showing the unstable eigenvalues for the conditions shown in Table 6.1; (Bottom): Eigenfunctions - ϕ (Left) - and eigenfunctions of the adjoint operators - ψ (Right) - associated to the unstable eigenvalue;

The results shown in Figure 6.4 consider full-state feedback without constraints on the input or output. For a fair comparison between the parabolic and hyperbolic PDEs, the $||x(k)||$ only takes into account $C(k)$. The input sequence starts differently for the PDEs, with a higher input being applied

to the parabolic model. This is probably due to the speed of propagation; as in the hyperbolic model, the state has a zero initial velocity. Thus, the flux has an initial delay, and the $x(k, \zeta)$ does not increase at the same rate as the parabolic case. However, this also means that, for the hyperbolic case, the input, which is applied at the boundary, will not act in the system as fast as in the parabolic PDE. This is shown in the $||x(k)||$ evolution, where the hyperbolic PDE state remains higher for the initial steps. Finally, due to the higher inputs, the cost function of the parabolic PDE is greater than the hyperbolic case.

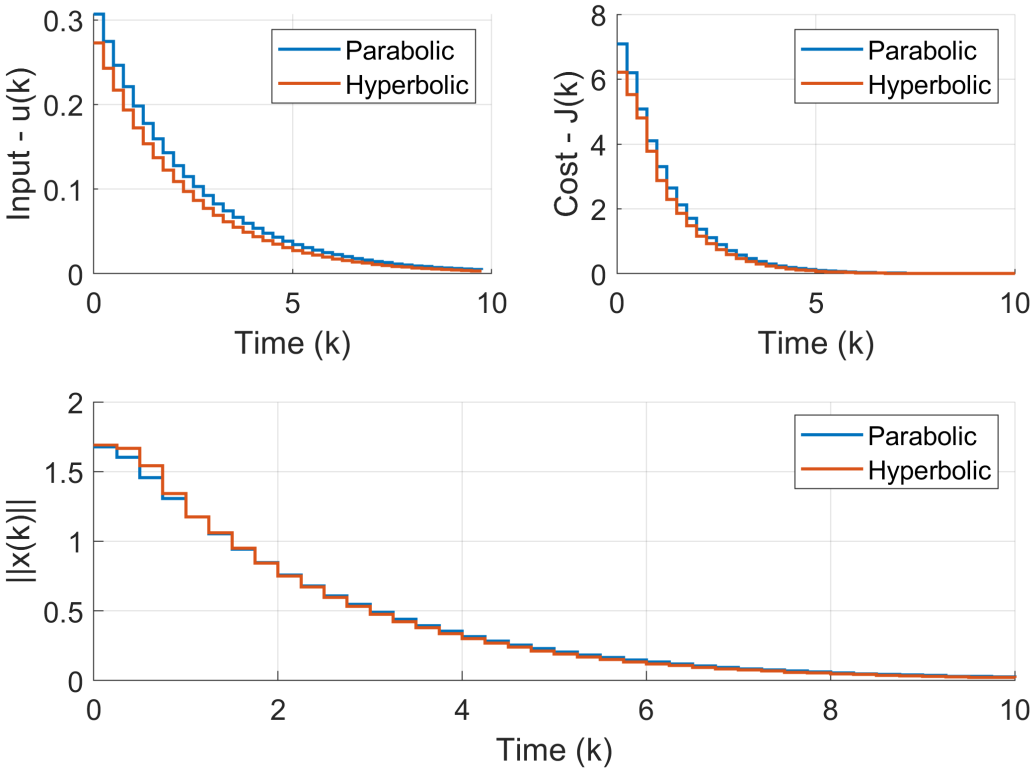

Figure 6.4: Simulations results for the non-constrained MPC with fullstate feedback: (Top-left) Input sequence; (Top-right) MPC Cost Function; (Bottom) State (C) norm;

In the second case, the full-state feedback is considered with an output constraint of $y_{max} = 0.75$. Due to the initial condition, where $y(0) \approx 0.75$, the controller has to make a significant input action to satisfy the constraint in the next time step, as shown in Figure 6.5. Due to the different propagation

speeds between the parabolic and hyperbolic models, the input taken by the hyperbolic case is higher than the parabolic one. This makes the remaining input sequence completely different for the two models, with the controller taking negative inputs for the hyperbolic model and positive for the parabolic equation. As expected, as the input has a direct effect on the cost function, due to the greater action taken in the beginning, the cost of the hyperbolic case is initially higher. Nonetheless, the PDEs are properly stabilized in both cases. The output profile is shown in the bottom-left of Figure 6.6, and it is possible to see that the output constraint is satisfied for the full-state feedback for both hyperbolic and parabolic cases.

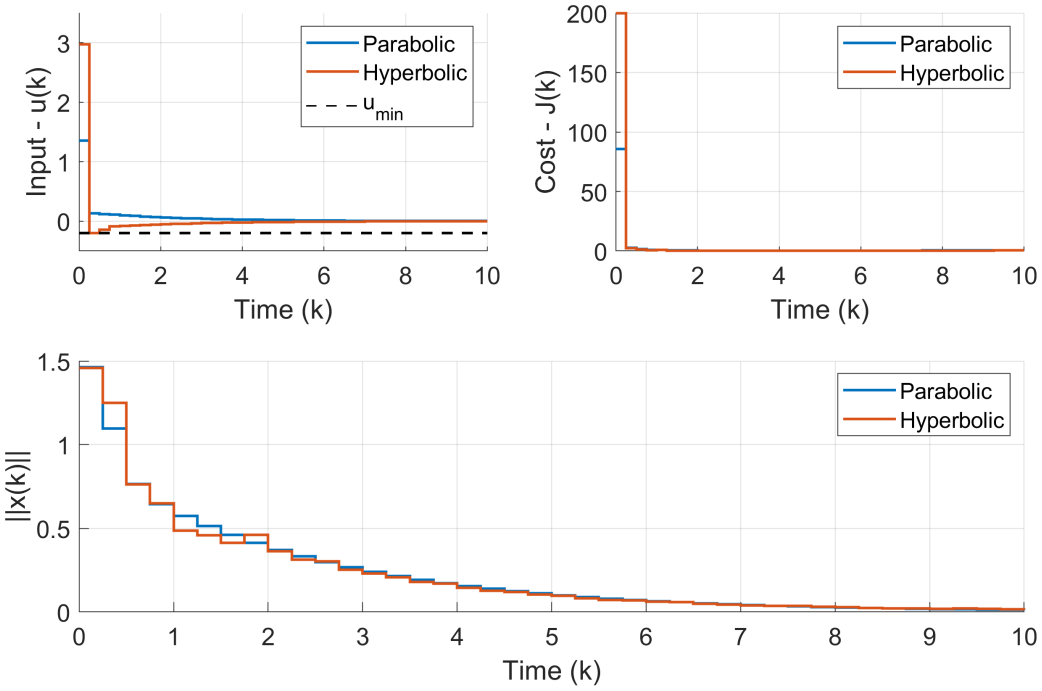

Figure 6.5: Simulations results for the constrained MPC with fullstate feedback: (Top-left) Input sequence; (Top-right) MPC Cost Function; (Bottom) State (C) norm;

The next cases consider that only the output feedback is available to the controller. Thus, the observer designed in the previous section is employed to reconstruct the system states used in the optimization. The observer convergence, represented by the observer error norm, is shown at the top of Figure

6.6. Once again, just the norm of the error between C and $\hat{C}$ is considered. The observer error dynamic is independent of the system stability. Thus, the input sequence does not have any influence on the observer convergence as long as a proper observer gain has been chosen.

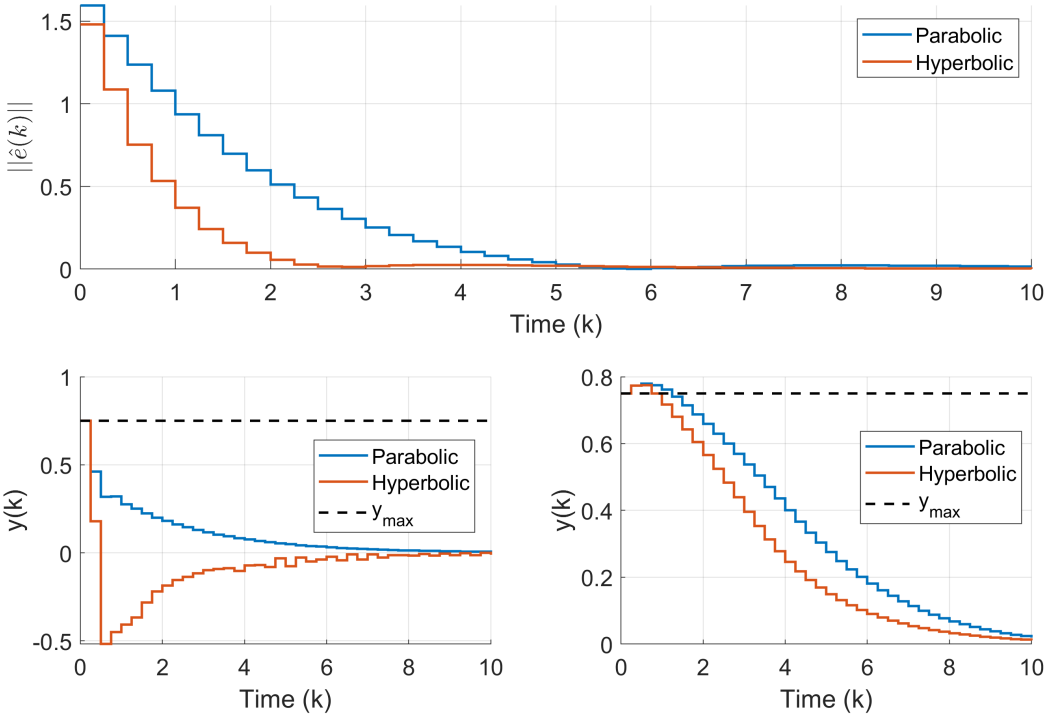

Figure 6.6: Norm of the observer error for $x(k) = C(k)$ for the output feedback controller (Top) and the system output: (Bottom-Left) Fullstate feedback; (Bottom-Right) Output feedback.

For both constrained and unconstrained cases, as the initial observer states are zero, the first input determined by the controller is zero. As the observer states start to change due to the difference between the measured output (y_m) and the predicted measured output ($\hat{y}_m$), the input starts to increase. As the observer converges faster for the hyperbolic case, the input for this PDE increases quicker, leading to a decrease in the state norm ($||x(k)||$), as shown in Figure 6.7.

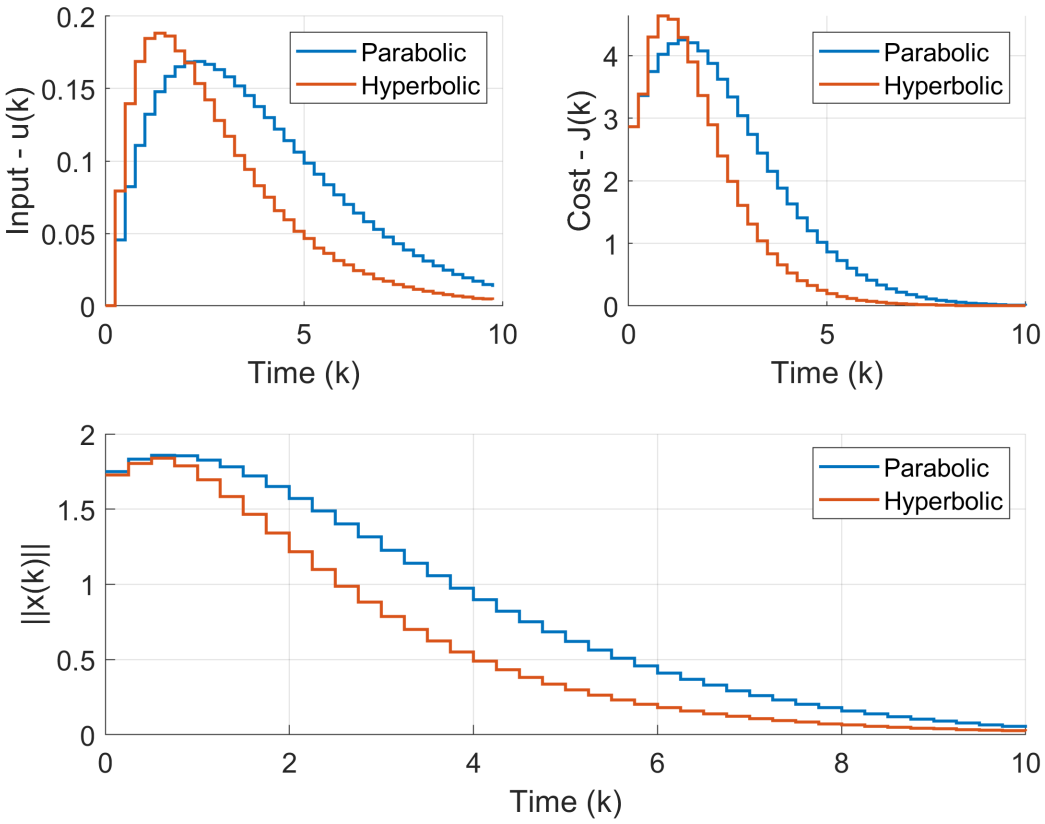

Figure 6.7: Simulations results for the non-constrained MPC with measured output feedback (observer based): (Top-left) Input sequence; (Top-right) MPC Cost Function; (Bottom) State (C) norm;

In the constrained case with output feedback, $u_{max} = 0.15$ and $y_{max} = 0.75$ were considered. In Figure 6.8 and in the bottom-right of Figure 6.6, it is possible to see that, as the observer states are used in the optimization problem, and the measured and constrained outputs are located in different points of the process (at $\zeta = 1$ and $\zeta = 0.5$, respectively), the output constraint is not satisfied until the observer states converge to the system states. However, even with the input constraints, it is possible to stabilize the system, and, after the observer convergence is achieved, the output constraint is satisfied.

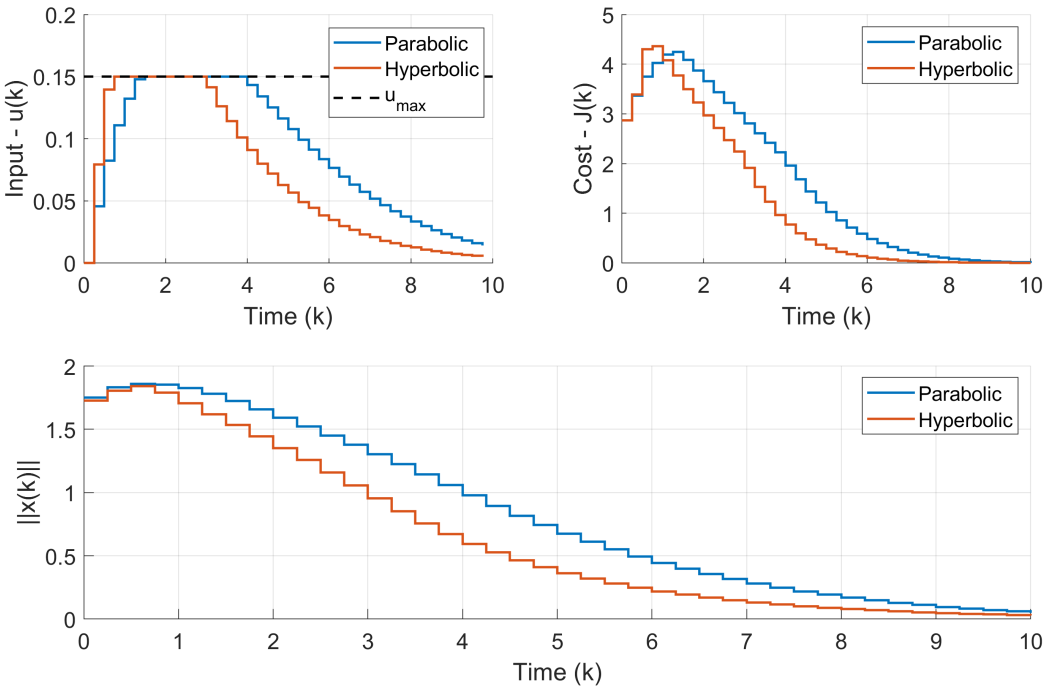

Figure 6.8: Simulations results for the constrained MPC with measured output feedback (observer based): (Top-left) Input sequence; (Top-right) MPC Cost Function; (Bottom) State (C) norm;

Finally, to compare the different results, the total cost ($\sum J(k)$) of each simulation result is shown in Table 6.2. The unconstrained full-state feedback has the lowest value, and the constrained full-state has the highest due to the significant actions taken in the initial steps to satisfy the output constraint. Overall, the cost of the output feedback is higher, even if the input sequences have the lower values, which is due to the increase in the states evolution without the proper control action (i.e., $||x(k)||$ initially increases and only starts decreasing as the observer states converge to the system states). For the constrained case with output feedback, even if the controller takes smaller actions than the unconstrained cases, the input remains at its limit for longer period, hence increasing the total cost.

Table 6.2: Total cost of the optimization problem for the different cases considered: unconstrained fullstate feedback; constrained fullstate feedback; unconstrained output feedback; and, constrained output feedback.

PDE Type	Unconst. Full.	Const. Full.	Uncons. Out.	Const. Out.
Parabolic	39.27	95.08	63.81	65.64
Hyperbolic	34.52	240.63	46.41	49.04

6.8 Conclusion

In this contribution, the difference in the dynamics of a tubular reactor modeled by a parabolic and a second-order hyperbolic PDEs was considered in the model predictive controller design. The discrete representation of the system was obtained by the Cayley-Tustin transformation, used in the controller and observer design.

In the simulation results, a system with one unstable mode was analyzed, such that a stability constraint was used to guarantee the system stability at the end of the control horizon. As an important scenario for practical control application, the output feedback was considered, and an observer was used to provide the controller with the state estimates necessary for the optimization problem. Input and output constraints were considered in the problem, with the measured output located at a different point from the constrained output.

The control actions obtained for both models - the parabolic and the second-order hyperbolic equations - were compared. It is observed that there is a slight difference between the control actions taken by the controller for the case of the full-state feedback without constraints. However, if constraints are present in the system, the controller yields distinct actions for the two different types of PDEs, even with the full-state feedback. The difference becomes larger if only a measured output is available and the observer states have to be used as an estimation for the system states. This is expected, as the different dynamics between the models would lead to different estimations. Finally, as the measured output feedback is generally more physically viable than the full-state feedback, at least for PDE systems, the type of model considered is essential for the proper closed-loop dynamics and performance satisfaction

when it comes to operating such a fundamental system as tubular chemical reactor.

6.A System's eigenvalues and eigenfunctions

In this section, the derivation for the system's characteristic equation and its eigenfunction is shown by defining the eigenvalue problem for the hyperbolic PDE. The following system is obtained from the eigenvalue problem, $A\phi = \lambda\phi$, where A is the operator, ϕ is the eigenfunction, and λ is the eigenvalue. For the operator defined in Eq. 6.7, the following system of ODEs is obtained:

$$\begin{cases} \phi_2 = \lambda\phi_1 \\ \frac{D}{\tau}\partial_{\zeta\zeta}\phi_1 - \frac{v}{\tau}\partial_\zeta\phi_1 + \frac{k}{\tau}\phi_1 - \frac{1}{\tau}\phi_2 + k\phi_2 = \lambda\phi_2 \end{cases} \tag{6.48}$$

resulting in:

$$\begin{gathered} d_\zeta \begin{bmatrix} \phi_1 \\ d_\zeta\phi_1 \end{bmatrix} = \begin{bmatrix} 0 & 1 \\ \frac{(-k+\lambda)(1+\lambda\tau)}{D} & \frac{v}{D} \end{bmatrix} \begin{bmatrix} \phi_1 \\ d_\zeta\phi_1 \end{bmatrix} \implies \\ \begin{bmatrix} \phi_1 \\ d_\zeta\phi_1 \end{bmatrix} = \begin{bmatrix} f_{11}(\zeta,\lambda) & f_{12}(\zeta,\lambda) \\ f_{21}(\zeta,\lambda) & f_{22}(\zeta,\lambda) \end{bmatrix} \begin{bmatrix} \phi_1(\zeta_0) \\ d_\zeta\phi_1(\zeta_0) \end{bmatrix} \end{gathered} \tag{6.49}$$

where the $f_{i,j}$ are given by:

$$\begin{aligned} f_{11}(\zeta,\lambda) &= \mathrm{e}^{\frac{b}{2}(\zeta-\zeta_0)}\left[\cosh\left((\zeta-\zeta_0)\sqrt{\tfrac{b^2}{4}+a}\right) - \tfrac{b}{2}\frac{\sinh\left((\zeta-\zeta_0)\sqrt{\frac{b^2}{4}+a}\right)}{\sqrt{\frac{b^2}{4}+a}}\right] \\ f_{12}(\zeta,\lambda) &= \frac{\mathrm{e}^{\frac{b}{2}(\zeta-\zeta_0)}\sinh\left((\zeta-\zeta_0)\sqrt{\frac{b^2}{4}+a}\right)}{\sqrt{\frac{b^2}{4}+a}} \\ f_{21}(\zeta,\lambda) &= a\frac{\mathrm{e}^{\frac{b}{2}(\zeta-\zeta_0)}\sinh\left((\zeta-\zeta_0)\sqrt{\frac{b^2}{4}+a}\right)}{\sqrt{\frac{b^2}{4}+a}} \\ f_{22}(\zeta,\lambda) &= \mathrm{e}^{\frac{b}{2}(\zeta-\zeta_0)}\left[\cosh\left((\zeta-\zeta_0)\sqrt{\tfrac{b^2}{4}+a}\right) + \tfrac{b}{2}\frac{\sinh\left((\zeta-\zeta_0)\sqrt{\frac{b^2}{4}+a}\right)}{\sqrt{\frac{b^2}{4}+a}}\right] \end{aligned} \tag{6.50}$$

with $a = \frac{(\lambda-k)(1+\lambda\tau)}{D}$, $b = \frac{v}{D}$ and $\zeta_0 = 0$. Applying the boundary conditions results in the condition below:

$$\begin{gathered} \begin{cases} d_\zeta\phi_1(0) = \frac{v}{D}\phi_1(0) \\ f_{21}(1,\lambda)\phi_1(0) + f_{22}(1,\lambda)d_\zeta\phi_1(0) = 0 \end{cases} \implies \\ \phi_1(0)\left[f_{21}(1,\lambda) + \tfrac{v}{D}f_{22}(1,\lambda)\right] = 0 \end{gathered} \tag{6.51}$$

Setting aside the trivial solution, the characteristic equation for this operator is given by $f_{21}(1,\lambda) + \frac{v}{D} f_{22}(1,\lambda) = 0$, which leads to:

$$\tanh\left(\frac{1}{D}\sqrt{\frac{v^2}{4} + D(\lambda - k)(1+\lambda\tau)}\right) = \frac{-v\sqrt{\frac{v^2}{4} + D(\lambda-k)(1+\lambda\tau)}}{\frac{v^2}{2} + D(\lambda-k)(1+\lambda\tau)} \tag{6.52}$$

And the eigenfunctions will be given by:

$$\phi_i = \left[f_{11}(\zeta,\lambda_i) + \frac{v}{D} f_{12}(\zeta,\lambda_i)\right] \begin{bmatrix} 1 \\ \lambda_i \end{bmatrix} \phi_{1,i}(0) \tag{6.53}$$

6.B Adjoint operator and its eigenfunctions

Using the definition of A and the inner product shown in Eq. 6.10:

$$\begin{gathered}
\langle Ax, y\rangle = \left\langle \begin{bmatrix} x_2 \\ \frac{D\partial_{\zeta\zeta}x_1 - v\partial_\zeta x_1 + kx_1}{\tau} - \left(-k + \frac{1}{\tau}\right) x_2 \end{bmatrix}, \begin{bmatrix} y_1 \\ y_2 \end{bmatrix} \right\rangle = \\
\int_0^1 x_2(\bar{y}_1)d\zeta + \int_0^1 \left[\frac{D\partial_{\zeta\zeta}x_1 - v\partial_\zeta x_1 + kx_1}{\tau} - \left(-k + \frac{1}{\tau}\right) x_2\right](y_2)d\zeta = \\
\int_0^1 x_2(\bar{y}_1)d\zeta + \int_0^1 x_2\left[-\left(-k + \frac{1}{\tau}\right)\bar{y}_2\right]d\zeta + \\
\int_0^1 \left[\frac{D\partial_{\zeta\zeta}x_1 - v\partial_\zeta x_1 + kx_1}{\tau}\right](\bar{y}_2)d\zeta
\end{gathered} \tag{6.54}$$

and the last term of this expression is further expanded by applying integration by parts:

$$\begin{gathered}
\int_0^1 \left(\frac{D\partial_{\zeta\zeta}x_1}{\tau}\right)(\bar{y}_2)d\zeta = \left[\frac{D\partial_\zeta x_1}{\tau}\bar{y}_2\right]\Big|_0^1 - \int_0^1 \left(\frac{D\partial_\zeta x_1}{\tau}\right)(\partial_\zeta \bar{y}_2)d\zeta = \\
\left[\tfrac{D\partial_\zeta x_1}{\tau}\bar{y}_2\right]\Big|_0^1 - \left[\tfrac{Dx_1}{\tau}\partial_\zeta\bar{y}_2\right]\Big|_0^1 + \int_0^1 x_1\left(\frac{D\partial_{\zeta\zeta}\bar{y}_2}{\tau}\right)d\zeta \\
\int_0^1 \left(\frac{-v\partial_\zeta x_1}{\tau}\right)(\bar{y}_2)d\zeta = \left[\frac{-vx_1}{\tau}\bar{y}_2\right]\Big|_0^1 + \int_0^1 x_1\left(\frac{v\partial_\zeta\bar{y}_2}{\tau}\right)d\zeta
\end{gathered} \tag{6.55}$$

where $D, k, v, \tau \in \Re$ is considered. Applying the boundary conditions defined in Eq. 6.6 for $u(t) = 0$:

$$\begin{gathered}
\left[\tfrac{D\partial_\zeta x_1}{\tau}\bar{y}_2\right]\Big|_0^1 - \left[\tfrac{Dx_1}{\tau}\partial_\zeta\bar{y}_2\right]\Big|_0^1 + \left[\tfrac{-vx_1}{\tau}\bar{y}_2\right]\Big|_0^1 = \\
\tfrac{1}{\tau}\Big[-\underbrace{(D\partial_\zeta x_1|_0 - vx_1|_0)}_{=0}\bar{y}_2|_0 + D\underbrace{\partial_\zeta x_1|_1}_{=0}\bar{y}_2|_1 \\
-Dx_1|_0\partial_\zeta\bar{y}_2|_0 + x_1|_1(-D\partial_\zeta\bar{y}_2|_1 - v\bar{y}_2|_1)\Big]
\end{gathered} \tag{6.56}$$

giving the following boundary conditions of the adjoint operator:

$$v y_2|_1 + D\partial_\zeta y_2|_1 = 0 \text{ and } \partial_\zeta y_2|_1 = 0 \tag{6.57}$$

And the inner product can be written as:

$$\left\langle \begin{bmatrix} x_1 \\ x_2 \end{bmatrix}, \begin{bmatrix} \frac{D\partial_{\zeta\zeta} y_2 + v\partial_\zeta y_2 + k y_2}{\tau} \\ y_1 - \left(-k + \frac{1}{\tau}\right) y_2 \end{bmatrix} \right\rangle = \langle x, A^* y \rangle \implies A^* = \begin{bmatrix} 0 & \frac{D\partial_{\zeta\zeta} + v\partial_\zeta + k}{\tau} \\ 1 & k - \frac{1}{\tau} \end{bmatrix} \tag{6.58}$$

With the definition of the adjoint operator given in Eq. 6.29 and its boundary conditions given in Eq. 6.30, the eigenvalue problem is solved once more to define the bi-orthogonal basis of the operator. With $A^*\psi = \lambda\psi$, the following system is obtained:

$$\begin{cases} \frac{D}{\tau}\partial_{\zeta\zeta}\psi_2 + \frac{v}{\tau}\partial_\zeta\psi_2 + \frac{k}{\tau}\psi_2 = \lambda\psi_1 \\ \psi_1 - \frac{1}{\tau}\psi_2 + k\psi_2 = \lambda\psi_2 \end{cases} \tag{6.59}$$

resulting in:

$$\psi_1 = \left(\lambda + \frac{1}{\tau} - k\right)\psi_2 \tag{6.60}$$

and

$$\begin{gathered} \frac{d}{d\zeta}\begin{bmatrix} \psi_2 \\ d_\zeta\psi_2 \end{bmatrix} = \begin{bmatrix} 0 & 1 \\ \frac{(\lambda-k)(1+\lambda\tau)}{D} & \frac{-v}{D} \end{bmatrix}\begin{bmatrix} \psi_2 \\ d_\zeta\psi_2 \end{bmatrix} \implies \\ \begin{bmatrix} \psi_2 \\ d_\zeta\psi_2 \end{bmatrix} = \begin{bmatrix} g_{11}(\zeta,\lambda) & g_{12}(\zeta,\lambda) \\ g_{21}(\zeta,\lambda) & g_{22}(\zeta,\lambda) \end{bmatrix}\begin{bmatrix} \psi_2(\zeta_0) \\ d_\zeta\psi_2(\zeta_0) \end{bmatrix} \end{gathered} \tag{6.61}$$

where $g_{i,j}$ is given by the same expression as in Eq. 6.50, with $a = \frac{(\lambda-k)(1+\lambda\tau)}{D}$, $b = -\frac{v}{D}$ and $\zeta_0 = 0$. Applying the boundary conditions of the adjoint operator results in the following:

$$\begin{cases} d_\zeta\psi_2(1) = -\frac{v}{D}\psi_2(1) \\ d_\zeta\psi_2(0) = 0 \end{cases} \implies \psi_2(0)\left[g_{21}(1,\lambda) + \frac{v}{D}g_{11}(1,\lambda)\right] = 0 \tag{6.62}$$

Setting aside the trivial solution, the characteristic equation for this operator is given by $g_{21}(L,\lambda) + \frac{v}{D}g_{11}(L,\lambda) = 0$, which leads to the same expression shown in Eq. 6.11, as expected. The adjoint operator eigenfunctions will be given by:

$$\psi_i = \left[g_{11}(\zeta,\lambda_i) + \frac{v}{D}g_{12}(\zeta,\lambda_i)\right]\begin{bmatrix} \lambda_i + \frac{1}{\tau} - k \\ 1 \end{bmatrix}\psi_{2,i}(0) \tag{6.63}$$

6.C Solution of the Lyapunov Equation and the terminal cost operator

If a system is stable, the cost associated with the system starting at an initial condition x_0, until it reaches the origin at $t \to \infty$ is given by $\langle x_0, \bar{Q}x_0 \rangle$, where $\bar{Q}$ is the solution of the following Lyapunov Equation [16]:

$$\langle Ax_1, \bar{Q}x_2 \rangle + \langle \bar{Q}x_1, Ax_2 \rangle = -\langle x_1, Qx_2 \rangle \tag{6.64}$$

Assuming that $\bar{Q}$ is defined as $\bar{Q} = \sum_i \sum_j q_{i,j} \langle x, \bar{\psi}_i \rangle \bar{\psi}_j$, the elements $q_{i,j}$ of the operator can be found by setting $x_1 = \phi_N$ and $x_2 = \phi_M$, which leads to:

$$\begin{gathered} \langle A\phi_N, \bar{Q}\phi_M \rangle + \langle \bar{Q}\phi_N, A\phi_M \rangle = -\langle \phi_N, Q\phi_M \rangle \\ \implies \langle \lambda_N \phi_N, \textstyle\sum_j q_{M,j} \bar{\psi}_j \rangle + \langle \sum_j q_{N,j} \bar{\psi}_j, \lambda_M \phi_M \rangle \\ = -\langle \phi_N, Q\phi_M \rangle \\ \implies \lambda_N \bar{q}_{M,N} + \bar{\lambda}_M q_{N,M} = -\langle \phi_N, Q\phi_M \rangle \\ \implies q_{N,M} = -\frac{\langle \phi_N, Q\phi_M \rangle}{\lambda_N + \bar{\lambda}_M} \end{gathered} \tag{6.65}$$

where the properties of the inner product and the fact that $\bar{q}_{M,N} = q_{N,M}$ were used. Substituting this in the definition of $\bar{Q}$ leads to Eq. 6.43. As it was shown in Xu et al. [34], the solution of the continuous Lyapunov equation, given by Eq. 6.65 is directly related to the solution of the Lyapunov equation in the discrete-time setting for the Cayley-Tustin discretization.

6.D Solution of the Ricatti Equation for the Observer Design

Considering the Luenberger observer shown in Eq. 6.35, and by defining the observer discrete error as $\hat{e}_k = x_k - \hat{x}_k$ and the observer measurement error as $\hat{e}_{m,k} = y_{m,k} - \hat{y}_{m,k} = C_{m,d}(x_k - \hat{x}_k) = C_{m,d}\hat{e}_k$, the observer error dynamics will be given by:

$$\begin{gathered} \hat{e}_{k+1} = x_{k+1} - \hat{x}_{k+1} = A_d x_k + B_d u_{k+1} - A_d \hat{x}_k - B_d u_{k+1} - L_{o,d}\hat{e}_{m,k} = \\ A_d \hat{e}_k - L_{o,d} C_{m,d} \hat{e}_k = (A_d - L_{o,d} C_{m,d}) \hat{e}_k \end{gathered} \tag{6.66}$$

Thus, a discrete observer gain $L_{o,d}$ needs to be found such that $(A_d - L_{o,d}C_{m,d})$ generates a stable semigroup. By using the duality between observability and controllability, and as similarly shown in Curtain [16], the discrete

Ricatti equation shown in Eq. 6.36 can be solved to find an observer gain that guarantees that $(A_d - L_{o,d}C_{m,d})^*$ is stable, which also implies the stability of $(A_d - L_{o,d}C_{m,d})$. From the duality, the solution of the discrete Ricatti equation minimizes the following quadratic cost:

$$J = \sum_0^\infty \langle C_{m,d}e_k^*, Q_O C_{m,d}e_k^* \rangle + \langle L_{o,d}^* e_k^*, R_O L_{o,d} e_k^* \rangle \tag{6.67}$$

where is the dynamics of the observer error in the dual space (i.e., $e_{k+1}^* = (A_d - L_{o,d}C_{m,d})^* e_k^*$). From the Lyapunov equation shown in Eq. 6.38, the minimum of the cost function will be given as $J_{min} = \langle e_0^*, \bar{Q}_O e_0^* \rangle$, where $\bar{Q}$ is the solution of the discrete Ricatti equation. Eq. 6.36 can also be written as:

$$\begin{gathered} \langle \bar{Q}_O A_d^* x_1, A_d^* x_2 \rangle - \langle \bar{Q}_O x_1, x_2 \rangle \\ -\langle (R_O + C_{m,d}\bar{Q}_O C_{m,d}^*)^{-1} C_{m,d}\bar{Q}_O A_d^* x_1, C_{m,d}\bar{Q}_O A_d^* x_2 \rangle = \\ -\langle Q_O C_{m,d} x_1, C_{m,d} x_2 \rangle \end{gathered} \tag{6.68}$$

for $x_1, x_2 \in \mathcal{X}^*$. By defining the operator in the bi-orthogonal basis of A_d (which has the same eigenfunctions of A), $\bar{Q}_O(\cdot) = \sum_i \sum_j q_{i,j}^o \langle \phi_i, (\cdot) \rangle \phi_j$ and taking $x_1 = \bar{\psi}_N$ and $x_2 = \bar{\psi}_M$, leads to:

$$\begin{gathered} A_d^* x_1 = A_d^* \bar{\psi}_N = \bar{\lambda}_N^D \bar{\psi}_N \\ A_d^* x_2 = A_d^* \bar{\psi}_M = \bar{\lambda}_M^D \bar{\psi}_M \\ \bar{Q}_O x_1 = \bar{Q}_O \bar{\psi}_N = \sum_j q_{N,j}^o \phi_j \\ \bar{Q}_O x_2 = \bar{Q}_O \bar{\psi}_M = \sum_j q_{M,j}^o \phi_j \\ A_d \bar{Q}_O x_1 = A_d \bar{Q}_O \bar{\psi}_N = \sum_j q_{N,j}^o \lambda_j^D \phi_j \\ A_d \bar{Q}_O x_2 = A_d \bar{Q}_O \bar{\psi}_M = \sum_j q_{M,j}^o \lambda_j^D \phi_j \\ C_m \bar{Q}_O A_d^* x_1 = C_m \bar{Q}_O \bar{\lambda}_N^D \bar{\psi}_N = \sum_j q_{N,j}^o \lambda_N^D C_m \phi_j \\ C_m \bar{Q}_O A_d^* x_2 = C_m \bar{Q}_O \bar{\lambda}_M^D \bar{\psi}_M = \sum_j q_{M,j}^o \lambda_M^D C_m \phi_j \\ C_{m,d}\bar{Q}_O C_{m,d}^* = \sum_i \sum_j q_{i,j}^o \langle \phi_i, C_{m,d}^* \rangle C_{m,d}\phi_j = \\ \sum_i \sum_j q_{i,j}^o \langle C_{m,d}\phi_i, 1 \rangle C_{m,d}\phi_j \end{gathered} \tag{6.69}$$

where the properties of the inner product and the bi-orthogonal shown in the previous sections were used. Thus, Eq. 6.66 becomes:

$$\begin{gathered} \langle \sum_j q_{N,j}^o \lambda_j^D \phi_j, \bar{\lambda}_M^D \bar{\psi}_M \rangle - \langle \sum_j q_{N,j}^o \phi_j, \psi_M \rangle - \\ \langle (R_O + \sum_i \sum_j q_{i,j}^o \langle C_{m,d}\phi_i, 1 \rangle C_{m,d}\phi_j)^{-1} \sum_j q_{N,j}^o \lambda_N^D C_m, \sum_j q_{M,j}^o \lambda_M^D C_m \rangle \\ = -\langle Q_O C_{m,d}\bar{\psi}_N, C_{m,d}\bar{\psi}_M \rangle \implies \\ \lambda_M^D \lambda_N^D q_{N,M}^o - q_{N,M}^o \\ -(\lambda_N^D \sum_i c_i q_{N,i}^o)^T (R_O + \sum_i \sum_j c_i^* q_{i,j}^o c_j)^{-1} \overline{(\lambda_M^D \sum_i c_i q_{M,i}^o)} = \\ -(C_{m,d}\psi_N)^T Q_O \overline{(C_{m,d}\psi_M)} \end{gathered} \tag{6.70}$$

6.E Parabolic PDE properties

For the parabolic PDE, the operator A is defined as $AC = D\partial_{\zeta\zeta}C - v\partial_{\zeta}C + kC$ and the boundary conditions are the same as given in Eq. 6.6. If the same boundary input ($C(0^-) = u(t)$), measure output and desired output as the second-order hyperbolic PDE are used, the parabolic properties are defined as:

$$\begin{gathered}(sI-A)^{-1}x_0 = \tfrac{[f_{11}(\zeta,s)+\frac{v}{D}f_{12}(\zeta,s)]}{[f_{21}(1,s)+\frac{v}{D}f_{22}(1,s)]}\int_0^1 f_{22}(1-\eta)\frac{x_0(\eta)}{D} - \int_0^{\zeta} f_{12}(\zeta-\eta)\frac{x_0(\eta)}{D} \\ (sI-A)^{-1}B = [f_{11}(\zeta,s)a + f_{12}(\zeta,s)\tfrac{av+1}{D}];\ a = -\frac{\frac{1}{D}f_{22}(1,s)U(s)}{f_{21}(1,s)+\frac{v}{D}f_{22}(1,s)} \\ C_m(sI-A)^{-1}B = [f_{11}(1,s)a + f_{12}(1,s)\tfrac{av+1}{D}]; \\ C(sI-A)^{-1}B = [f_{11}(0.5,s)a + f_{12}(0.5,s)\tfrac{av+1}{D}];\end{gathered} \tag{6.71}$$

The eigenvalue problem gives the following characteristic equation and eigenfunctions:

$$\begin{gathered}f_{11}(1,\lambda) + \tfrac{v}{D}f_{11}(1,\lambda) = 0 \\ \phi(\zeta,\lambda) = [f_{11}(\zeta,\lambda) + \tfrac{v}{D}f_{12}(\zeta,\lambda)]\phi(0) \\ A^*y = D\partial_{\zeta\zeta}y + v\partial_{\zeta}y + ky,\ D\partial_{\zeta}y(1) + vy(1) = 0\,\&\,\partial_{\zeta}y(0) = 0 \\ \psi(\zeta,\lambda) = g_{11}(\zeta,\lambda)\psi(0)\end{gathered} \tag{6.72}$$

where $f_{i,j}$ is defined in Eq. 6.50 with $a = \frac{\lambda-k}{D}$, $b = \frac{v}{D}$ and $\zeta_0 = 0$, and $g_{i,j}$ with $a = \frac{\lambda-k}{D}$, $b = \frac{-v}{D}$ and $\zeta_0 = 0$. $\phi(0)$ and $\psi(0)$ can be chosen such that $\langle\phi_i, \bar{\psi}_j\rangle = 1$ for $i = j$ and $\langle\phi_i, \bar{\psi}_j\rangle = 0$ for $i \neq j$.

Chapter 7

Conclusions and Future Work

7.1 Conclusions

Throughout this thesis, the modeling and control of systems modelled by hyperbolic PDEs were analyzed from the continuous to the discrete-time settings. Chemical transport-reaction processes and a water canal were the systems considered for the analysis and/or control.

Chapter 2 analyzed the difference in the dynamics between the parabolic and second-order hyperbolic PDEs, as the latter is generally used as a standard model for diffusive processes. The second-order hyperbolic PDE considers a delay in the transport due to the initial inertia, which gives it a finite speed of propagation seen in experimental results. In the non-delayed diffusion, any initial disturbance in the material body is propagated instantly with maximum rate, a characteristic of the parabolic equation. To analyze the differences between the hyperbolic and parabolic PDEs, a one-dimensional heat diffusion problem, an axial tubular reactor, and a phase change system were considered as processes of interest.

For the heat equation and the tubular reactor, the difference in the dynamic of the two equations was investigated by performing the eigenvalues analysis and presenting the results of the numerical simulations. Overall, the properties' rate of change showed a noticeable distinction from the hyperbolic and parabolic equations. For the system with a phase transition (modeled as a Stefan problem), the type of flux influences the interface's dynamics.

The difference in the dynamics can be crucial for some applications. If

a model-based controller is considered, even though it is possible to guarantee some degree of robustness in the closed-loop, the controller's performance would be affected.

In Chapter 3, the controller design in the continuous-time setting was developed assuming two different layouts of a heat exchanger system. Delayed boundary feedback and a boundary input were considered for both configurations, requiring a system transformation to deal with these conditions. The transformed system had a corresponding in-domain input instead of the boundary input, and the transport delay was turned into an equivalent transport equation.

For unstable operation conditions, it was shown that output feedback is not sufficient to stabilize the system. Thus, a full-state feedback control law was used. Unfortunately, as the information for all states of a DPS is hardly available, an observer was designed to reconstruct the system states. The computer simulations demonstrated the controller's capability to stabilize the system, achieve output tracking of the desired signal, and reject the disturbances.

The transition from the continuous-time setting to the discrete-time was made in Chapter 4. The regulator for the Saint-Venant-Exner model was developed to achieve proper closed-loop stability and output tracking. The backstepping methodology was used in the continuous-time setting to map the closed-loop system and the observer error dynamics to stable target systems, guaranteeing the system stability and observer convergence. A reference signal generated by an exosystem was considered for the output tracking problem. With the stabilization and tracking achieved in the continuous-time setting, the discrete regulator was explored by developing a direct relation to the control law and observer gain in the continuous-time setting. The simulations results showed the regulator performance.

Finally, Chapters 5 and 6 considered the optimal constrained control problem. Chapter 5 analyzed an autothermal reactor with boundary actuation. The linearized model around a steady-state was used to achieve a linear representation of the system, followed by a boundary transformation to represent

the boundary input as an in-domain input. The model predictive controller was designed based on the transformed system, and the discrete model was obtained by applying a Cayley-Tustin time discretization transformation. The control strategy was applied considering stable and unstable steady-states, where the optimal system response and constraints satisfaction were possible using the designed controller. When the system's non-linear model is assumed as the plant model, and the MPC uses the linearized model, it is still possible to make the system converge to the desired steady-state profile.

Chapter 6 assessed the effect of the different dynamics of the second-order hyperbolic and the parabolic PDEs showed in Chapter 2 on the controller closed-loop performance. The output feedback was considered, and an observer was used to provide the state estimates. Input and output constraints were assumed in the control problem. The difference in the control actions taken by the controller was small if full-state feedback was available and no constraints were imposed. If constraints were present in the system, the controller yielded distinct actions for the two different types of PDEs. The difference is notable if only the measured output is available. Thus, as expected, the model considered is essential for the proper closed-loop dynamics and performance satisfaction.

7.2 Future Work

This thesis considered the modeling and control of DPS, specifically those modelled by hyperbolic equations, without using early lumping in both the continuous and discrete-time settings. There remain many open questions regarding this subject, and a number of them are briefly mentioned here, considering the work in production and future possibilities.

The difference in the dynamics analyzed in Chapter 2 is also being considered for materials under phase-change for problems in two and three dimensional cases. This will be done using the enthalpy technique presented in [133] and [134]. Furthermore, the hyperbolic models used in Chapters 2 and 6 can be extended to other applications such as: cardiac alternans [135], [136], cryosurgery [137], and phase change with convection [138].

The regulator design considered in Chapter 3 guarantees the system stability, proper tracking, and disturbance rejection. Yet, it does not account for any optimal conditions when it comes to performance, which is a possible extension to be considered. This could also be coupled to an advanced control strategy as the MPC design showed in Chapter 5, such that the constrained optimal stabilization and tracking problem could be considered.

The operators considered were all differential operators. The controller design taking into account partial integral-differential equations - that arise from populational balances - is being studied.

The models studied here were all representations of transport-reaction processes in one-dimensional spaces. A packed bed reactor - a system that can be represented by a two-dimensional model - and the controller design for the system are under study.

References

[1] R. Aris and A. Varma, "Stirred pots and empty tubes," in *Chemical reactor theory: a review*, Englewood Cliffs, N.J.: Prentice-Hall, 1977, pp. 79–155.

[2] B. A. Francis and W. M. Wonham, "The Internal Model Principle of Linear Control Theory," *Automatica*, vol. 12, no. 1, pp. 457–465, 1976.

[3] R. Aris, *Introduction to the Analysis of Chemical Reactors*. 1965, pp. 7–14.

[4] P. Christofides, *Nonlinear and Robust Control of PDE Systems: Methods and Applications to Transport-Reaction Processes*. 2001.

[5] P. Danckwerts, "Continuous flow systems. distribution of residence times," *Chemical Engineering Science*, vol. 2, no. 1, pp. 1–13, 1953.

[6] X. Xu and S. Dubljevic, "The state feedback servo-regulator for countercurrent heat-exchanger system modelled by system of hyperbolic PDEs," *European Journal of Control*, vol. 29, pp. 51–61, 2016.

[7] R. Curtain, M. Demetriou, and K. Ito, "Adaptive compensators for perturbed positive real infinite dimensional systems," *International Journal of Applied Mathematics and Computer Science*, vol. 13, no. 4, pp. 441–452, 2003.

[8] A. Smyshlyaev and M. Krstic, "Backstepping observers for a class of parabolic PDEs," *Systems and Control Letters*, vol. 54, no. 7, pp. 613–625, 2005.

[9] E. J. Davison, "The Robust Control of a Servomechanism Problem for Linear Time-Invariant Multivariable Systems," *IEEE Transactions on Automatic Control*, vol. 21, no. 1, pp. 25–34, 1976.

[10] B. A. Francis, "The Linear Multivariable Regulator Problem," *Siam J. Control and Optimization*, vol. 15, no. 3, pp. 3–8, 1977.

[11] A. Alizadeh Moghadam, I. Aksikas, S. Dubljevic, and J. F. Forbes, "Boundary optimal (LQ) control of coupled hyperbolic PDEs and ODEs," *Automatica*, vol. 49, no. 2, pp. 526–533, 2013.

[12] T. Kobayashi, "Regulator problem for infinite-dimensional systems," *Systems and Control Letters*, vol. 3, no. 1, pp. 31–39, 1983.

[13] C. I. Byrnes, I. G. Lauko, D. S. Gilliam, and V. I. Shubov, "Output regulation for linear distributed parameter systems," *IEEE Trans. Autom. Contr.*, vol. 2, pp. 170–194, 2000.

[14] X. Xu and S. Dubljevic, "Finite-dimensional output feedback regulator for a mono-tubular heat exchanger process," *IFAC-PapersOnLine*, vol. 49, no. 8, pp. 54–59, 2016.

[15] X. Xu, S. Pohjolainen, and S. Dubljevic, "Finite-dimensional regulators for a class of regular hyperbolic PDE systems," *International Journal of Control*, vol. 7179, pp. 1–18, 2017.

[16] R. F. Curtain and H. Zwart, *An introduction to Infinite-Dimensional Linear Systems Theory*. New York: Springer-Verlag, 1995.

[17] A. Bensoussan, G. Prato, M. Delfour, and S. Mitter, *Representation and Control of Infinite Dimensional Systems*. Birkhauser, Boston, 2007.

[18] D. Dochain, "State observers for tubular reactors with unknown kinetics," *Journal of Process Control*, vol. 10, no. 2, pp. 259–268, 2000.

[19] A. Vande Wouver and M. Zeitz, "State estimation in distributed parameter systems," *Control Systems, Robotics, and Automation*, vol. 14, no. 92, 2009.

[20] O. Boubaker, J. Babary, and M. Ksouri, "Variable structure estimation and control of nonlinear distributed parameter bioreactors," vol. 4, 1998, pp. 3770–3774.

[21] P. Ligarius and J.-F. Couchouron, "Asymptotic observers for a class of evolution equations. a nonlinear approach [observateurs asymptotiques pour une classe d'équations d'évolution. une approche non linéaire]," *Comptes Rendus de l'Academie des Sciences - Series I: Mathematics*, vol. 324, no. 3, pp. 355–360, 1997.

[22] D. Dochain, "State observation and adaptive linearizing control for distributed parameter (bio)chemical reactors," *International Journal of Adaptive Control and Signal Processing*, vol. 15, no. 6, pp. 633–653, 2001.

[23] A. Schaum, J. Moreno, and J. Alvarez, "Dissipativity-based globally convergent observer design for a class of tubular reactors," vol. 17, 2008.

[24] A. Schaum, J. Moreno, E. Fridman, and J. Alvarez, "Observer design for a class of transport-reaction systems: A direct Lyapunov approach," vol. 6, 2009, pp. 284–289.

[25] X. Xu, B. Huang, and S. Dubljevic, "Optimal continuous-time state estimation for linear finite and infinite-dimensional chemical process systems with state constraints," *Journal of Process Control*, vol. 35, pp. 127–142, 2015.

[26] N. Kazantzis and C. Kravaris, "Time-discretization of nonlinear control systems via Taylor methods," *Computers and Chemical Engineering*, vol. 23, no. 6, pp. 763–784, 1999.

[27] K. J. Astrom and B. Wittenmark, *Computer-controlled Systems: Theory and Design (2nd Ed.)* Upper Saddle River, NJ, USA: Prentice-Hall, Inc., 1990, ISBN: 0-13-168600-3.

[28] L. C. Hairer E. and G. Wanner, *Geometric Numerical Integration: Structure-Preserving Algorithms for Ordinary Differential Equations* (Springer Series in Computational Mathematics). Berlin: Springer, 2002, vol. 31.

[29] V. Havu and J. Malinen, "The Cayley transform as a time discretization scheme," *Numerical Functional Analysis and Optimization*, vol. 28, no. 7-8, pp. 825–851, 2007.

[30] K. R. Muske and J. B. Rawlings, "Model predictive control with linear models," *AIChE Journal*, vol. 39, no. 2, pp. 262–287, 1993.

[31] S. Dubljevic, P. Mhaskar, N. H. El-Farra, and P. D. Christofides, "Predictive control of transport-reaction processes," *Computers & Chemical Engineering*, vol. 29, no. 11, pp. 2335–2345, 2005.

[32] A. Alessio and A. Bemporad, "A survey on explicit model predictive control," in *Nonlinear Model Predictive Control: Towards New Challenging Applications*, L. Magni, D. M. Raimondo, and F. Allgower, Eds. Berlin, Heidelberg: Springer Berlin Heidelberg, 2009, pp. 345–369.

[33] E. Pahija, F. Manenti, I. M. Mujtaba, and F. Rossi, "Assessment of control techniques for the dynamic optimization of (semi-)batch reactors," *Computers & Chemical Engineering*, vol. 66, pp. 269–275, 2014.

[34] Q. Xu, "Model Predictive and Nonlinear Control of Transport-Reaction Process Systems," Ph.D. dissertation, University of Alberta, 2017, p. 197.

[35] S. Dubljevic, N. H. El-Farra, P. Mhaskar, and P. D. Christofides, "Predictive control of parabolic PDEs with state and control constraints," in *Proceedings of the 2004 American Control Conference*, vol. 1, Jun. 2004, 254–260 vol.1.

[36] S. Dubljevic and P. D. Christofides, "Predictive control of parabolic PDEs with boundary control actuation," *Chemical Engineering Science*, vol. 61, no. 18, pp. 6239–6248, 2006.

[37] S. Dubljevic and P. D. Christofides, "Predictive output feedback control of parabolic partial differential equations (PDEs)," *Industrial & Engineering Chemistry Research*, vol. 45, no. 25, pp. 8421–8429, 2006.

[38] C. I. Christov and P. M. Jordan, "Heat conduction paradox involving second-sound propagation in moving media.," *Physical review letters*, vol. 94 15, pp. 154–301, 2005.

[39] O. Nosko, "Hyperbolic heat conduction at a microscopic sliding contact with account of adhesion-deformational heat generation and wear," *International Journal of Thermal Sciences*, vol. 137, pp. 101–109, 2019.

[40] J. Li, Y. Gu, and Z. Guo, "Analysis of the phenomena of non-Fourier heat conduction in switch-q laser processing for reducing the core loss of grain-oriented silicon steel," *Journal of Materials Processing Technology*, vol. 74, no. 1, pp. 292–297, 1998.

[41] A. Banerjee, A. A. Ogale, C. Das, K. Mitra, and C. Subramanian, "Temperature distribution in different materials due to short pulse laser irradiation," *Heat Transfer Engineering*, vol. 26, no. 8, pp. 41–49, 2005.

[42] C. Cattaneo, "On a form of heat equation which eliminates the paradox of instantaneous propagation," *C. R. Acad. Sci. Paris*, pp. 431–433, 1958.

[43] P. Vernotte, "Les paradoxes de la theorie continue de l'equation de la chaleur," *C. R. Acad. Sci. Paris*, vol. 246, pp. 3154–3155, 1958.

[44] A. E. Fischer and J. E. Marsden, "The Einstein evolution equations as a first-order quasi-linear symmetric hyperbolic system, i," *Communications in Mathematical Physics*, vol. 28, no. 1, pp. 1–38, Oct. 1972.

[45] A. C. King, D. J. Needham, and N. H. Scott, "The effects of weak hyperbolicity on the diffusion of heat," *Proceedings: Mathematical, Physical and Engineering Sciences*, vol. 454, no. 1974, pp. 1659–1679, 1998.

[46] I. Novikov, "Solution of the linear one-dimensional inverse heat-conduction problem on the basis of a hyperbolic equation," *Journal of Engineering Physics*, vol. 40, pp. 668–672, 1981.

[47] K. Mitra, S. Kumar, A. Vedevarz, and M. K. Moallemi, "Experimental evidence of hyperbolic heat conduction in processed meat," *Journal of Heat Transfer*, vol. 117, no. 3, pp. 568–573, Aug. 1995.

[48] V. Surov, "Hyperbolic model of a single-speed, heat-conductive mixture with interfractional heat transfer," *High Temp*, vol. 56, pp. 890–899, 2018.

[49] G. Abbasi and A. Malek, "Pointwise optimal control for cancer treatment by hyperthermia with thermal wave bioheat transfer," *Automatica*, vol. 111, p. 108 579, 2020.

[50] D. Dochain, "Analysis of the multiplicity of equilibrium profiles in tubular reactor models," *IFAC-PapersOnLine*, vol. 49, no. 18, pp. 903–908, 2016.

[51] H. S. Fogler, *Elements of chemical reaction engineering*, 5 edition. Prentice Hall, 2016, p. 992, ISBN: 0133887510.

[52] H. Gomez, I. Colominas, F. Navarrina, J. París, and M. Casteleiro, "A hyperbolic theory for advection-diffusion problems: Mathematical foundations and numerical modeling," *Archives of Computational Methods in Engineering*, vol. 17, pp. 191–211, Jun. 2010.

[53] A. Compte and R. Metzler, "The generalized Cattaneo equation for the description of anomalous transport processes," *Journal of Physics A: Mathematical and General*, vol. 30, no. 21, pp. 7277–7289, Nov. 1997.

[54] R. Klages, G. Radons, and I. Sokolov, *Anomalous Transport: Foundations and Applications*. Wiley, 2008.

[55] T. F. Nonnenmacher, "Derivation of exact non-linear constitutive equations: A simple model for a non-linear diffusion theory," vol. 9, no. 3, pp. 171–176, 1984.

[56] S. Godoy and L. S. Garcia-Colin, "From the quantum random walk to classical mesoscopic diffusion in crystalline solids," *Phys. Rev. E*, vol. 53, pp. 5779–5785, 6 Jun. 1996.

[57] P. D. Christofides and P. Daoutidis, "Nonlinear feedback control of parabolic PDE systems," in *Nonlinear Model Based Process Control*, R. Berber and C. Kravaris, Eds. Dordrecht: Springer Netherlands, 1998, pp. 371–399.

[58] L. Rubenstein, *The Stefan problem, by L.I. Rubenstein* (Translations of mathematical monographs). American Mathematical Society, 1971.

[59] O. Cassol and S. Dubljevic, "Hyperbolicity of the heat equation," 2019 IFAC Workshop on Thermodynamic Foundations of Mathematical Systems Theory, 2019.

[60] S. J. Parulekar and D. Ramkrishna, "Tubular reactor stability revisited without the Danckwerts boundary conditions," *Chemical Engineering Science*, vol. 39, no. 3, pp. 455–469, 1984.

[61] S. Gupta, *The Classical Stefan Problem. Basic Concepts, Modelling and Analysis*. North-Holland: Applied mathematics and Mechanics, 2003.

[62] J. Gunnarsson, I. Sinclair, and F. Alanis, "Compact Heat Exchangers: Improving Heat Recovery," *Chemical engineering*, vol. 116, no. 2, pp. 44–47, 2009.

[63] N. Kunimatsu, "Stability analysis of heat-exchanger equations with boundary feedbacks," *Journal of Mathematical Control & Information*, vol. 15, pp. 317–330, 1998.

[64] J. A. Villegas, H. Zwart, Y. Le Gorrec, and B. Maschke, "Exponential stability of a class of boundary control systems," *IEEE Transactions on Automatic Control*, vol. 54, no. 1, pp. 142–147, 2009.

[65] H. Sano, "Exponential Stability of Heat Exchangers with Delayed Boundary Feedback.," *IFAC-PapersOnLine*, vol. 49, no. 8, pp. 43–47, 2016.

[66] C. Prieur, J. Winkin, and G. Bastin, "Robust boundary control of systems of conservation laws," *Mathematics of Control, Signals, and Systems*, vol. 20, no. 2, pp. 173–197, Jun. 2008.

[67] M. Krstic and A. Smyshlyaev, *Boundary control of PDEs: A course on backstepping designs*. Philadelphia: SIAM, 2008.

[68] G. Bastin and J. Coron, *Stability and Boundary Stabilization of 1-D Hyperbolic Systems* (Progress in Nonlinear Differential Equations and Their Applications). Springer International Publishing, 2016.

[69] M. Krstic and A. Smyshlyaev, "Backstepping boundary control for first-order hyperbolic PDEs and application to systems with actuator and sensor delays," *Systems & Control Letters*, vol. 57, no. 9, pp. 750–758, 2008.

[70] F. Di Meglio, R. Vazquez, and M. Krstic, "Stabilization of a system of coupled first-order hyperbolic linear PDEs with a single boundary input," *IEEE Transactions on Automatic Control*, vol. 58, no. 12, pp. 3097–3111, 2013.

[71] J. Deutscher, "A backstepping approach to the output regulation of boundary controlled parabolic PDEs," *Automatica*, vol. 57, pp. 56–64, 2015, ISSN: 0005-1098.

[72] J. Deutscher and S. Kerschbaum, "Output regulation for coupled linear parabolic PIDEs," *Automatica*, vol. 100, pp. 360–370, 2019.

[73] X. Xu and S. Dubljevic, "Output regulation boundary control of first-order coupled linear mimo hyperbolic PIDE systems," *International Journal of Control*, vol. 93, no. 3, pp. 410–423, 2018.

[74] T. Khambanonda, A. Palazoglu, and J. Romagnoli, "A transformation approach to nonlinear process control," *AIChE Journal*, vol. 37, no. 7, 1991.

[75] Y. S. Malleswararao and M. Chidambaram, "Non-linear controllers for a heat exchanger," *Journal of Process Control*, vol. 2, no. 1, pp. 17–21, 1992.

[76] A. Maidi, M. Diaf, and J. P. Corriou, "Boundary geometric control of a counter-current heat exchanger," *Journal of Process Control*, vol. 19, no. 2, pp. 297–313, 2009.

[77] A. Maidi, M. Diaf, and J. P. Corriou, "Boundary control of a parallel-flow heat exchanger by input-output linearization," *Journal of Process Control*, vol. 20, no. 10, pp. 1161–1174, 2010.

[78] J. D. Álvarez, L. J. Yebra, and M. Berenguel, "Repetitive control of tubular heat exchangers," *Journal of Process Control*, vol. 17, no. 9, pp. 689–701, 2007.

[79] A. Michel and A. Kugi, "Model based control of compact heat exchangers independent of the heat transfer behavior," *Journal of Process Control*, vol. 24, no. 4, pp. 286–298, 2014.

[80] V. Natarajan, D. S. Gilliam, and G. Weiss, "The State Feedback Regulator Problem for Regular Linear Systems," *IEEE Transactions on Automatic Control*, vol. 59, no. 10, pp. 2708–2723, 2014.

[81] D. Bonvin, R. G. Rinker, and D. A. Mellichamp, "Dynamic Analysis and Control of a Tubular Autothermal Reactor at an Unstable State," *Chemical Engineering Science*, vol. 35, pp. 603–612, 1980.

[82] D. Bonvin, R. Rinker, and D. Mellichamp, "On Controlling an Autothermal Fixed-bed Reactor at an Unstable State-II:Discrimination among rival models to achieve suitable internal structure," *Chemical Engineering Science*, vol. 38, no. 2, pp. 245–255, 1983.

[83] D. Bonvin, R. Rinker, and D. Mellichamp, "On controlling an autothermal fixed-bed reactor at an unstable state-i: Steady-state and dynamic modeling," *Chemical Engineering Science*, vol. 38, no. 2, pp. 233–244, 1983.

[84] T. Hämäläinen and S. Pohjolainen, "Robust Regulation of Distributed Parameter Systems with Infinite-Dimensional Exosystems," *SIAM Journal on Control and Optimization*, vol. 48, no. 8, pp. 4846–4873, Jan. 2010.

[85] L. Paunonen and S. Pohjolainen, "Internal Model Theory for Distributed Parameter Systems," *SIAM Journal on Control and Optimization*, vol. 48, no. 7, pp. 4753–4775, Jan. 2010.

[86] L. Paunonen and S. Pohjolainen, "Robust controller design for infinite-dimensional exosystems," *International Journal of Robust and Nonlinear Control*, vol. 24, no. 5, pp. 825–858, Mar. 2014.

[87] C.-Z. Xu and G. Sallet, "Proportional and integral regulation of irrigation canal systems governed by the st venant equation," *IFAC Proceedings Volumes*, vol. 32, no. 2, pp. 2274–2279, 1999, 14th IFAC World Congress 1999, Beijing, Chia, 5-9 July.

[88] X. Litrico and V. Fromion, "H_∞ control of an irrigation canal pool with a mixed control politics," *IEEE Transactions on Control Systems Technology*, vol. 14, no. 1, pp. 99–111, 2006.

[89] C. Prieur and J. de Halleux, "Stabilization of a 1-d tank containing a fluid modeled by the shallow water equations," *Systems & Control Letters*, vol. 52, no. 3, pp. 167–178, 2004.

[90] A. Diagne, M. Diagne, S. Tang, and M. Krstic, "Backstepping stabilization of the linearized Saint-Venant–Exner model," *Automatica*, vol. 76, pp. 345–354, 2017.

[91] O. Aamo, "Disturbance Rejection in 2x2 Linear Hyperbolic Systems," *IEEE Transactions on Automatic Control*, vol. 58, no. 5, pp. 1095–1106, 2013.

[92] J. Deutscher, "Output regulation for linear distributed-parameter systems using finite-dimensional dual observers," *Automatica*, vol. 47, no. 11, pp. 2468–2473, 2011.

[93] R. Mlayeh, S. Toumi, and L. Beji, "Backstepping boundary observer based-control for hyperbolic PDE in rotary drilling system," *Applied Mathematics and Computation*, vol. 322, pp. 66–78, 2018.

[94] A. Deutschmann, L. Jadachowski, and A. Kugi, "Backstepping-based boundary observer for a class of time-varying linear hyperbolic PIDEs," *Automatica*, vol. 68, pp. 369–377, 2016.

[95] J. Deutscher, N. Gehring, and R. Kern, "Output feedback control of general linear heterodirectional hyperbolic ODE–PDE–ODE systems," *Automatica*, vol. 95, pp. 472–480, 2018.

[96] I. Karafyllis and M. Krstic, "Sampled-data boundary feedback control of 1-d linear transport PDEs with non-local terms," *Systems & Control Letters*, vol. 107, pp. 68–75, 2017.

[97] I. Karafyllis and M. Krstic, "Sampled-data boundary feedback control of 1-d parabolic PDEs," *Automatica*, vol. 87, pp. 226–237, 2018.

[98] R. Engel and G. Kreisselmeier, "A continuous-time observer which converges in finite time," *IEEE Transactions on Automatic Control*, vol. 47, no. 7, pp. 1202–1204, Jul. 2002.

[99] J. Deutscher, "Finite-time output regulation for linear 2×2 hyperbolic systems using backstepping," *Automatica*, vol. 75, pp. 54–62, 2017.

[100] S. Dubljevic and J.-P. Humaloja, "Model predictive control for regular linear systems," `arXiv:0706.1234 [math.FA]`, 2018.

[101] N. Besseling, "Stability analysis in continuous and discrete time," Undefined, Ph.D. dissertation, University of Twente, Jan. 2012.

[102] M. Izadi, J. Abdollahi, and S. S. Dubljevic, "PDE backstepping control of one-dimensional heat equation with time-varying domain," *Automatica*, vol. 54, pp. 41–48, 2015.

[103] M. Izadi and S. Dubljevic, "Backstepping output-feedback control of moving boundary parabolic PDEs," *European Journal of Control*, vol. 21, pp. 27–35, 2015.

[104] H. Kanoh, "Control of Heat Exchangers by Placement of Closed-Loop Poles," *IFAC Proceedings Volumes*, vol. 24, no. 8, pp. 409–414, 1991.

[105] H. Sano, "Exponential stability of a mono-tubular heat exchanger equation with output feedback," *Systems and Control Letters*, vol. 50, no. 5, pp. 363–369, 2003.

[106] B. Z. Guo and X. Y. Liang, "Differentiability of the C0-semigroup and failure of Riesz basis for a mono-tubular heat exchanger equation with output feedback: A case study," *Semigroup Forum*, vol. 69, no. 3, pp. 462–471, 2004.

[107] W. H. Ray, *Advanced Process Control*. New York, New York: McGraw-Hill, 1981.

[108] I. Aksikas, J. J. Winkin, and D. Dochain, "Optimal LQ-feedback regulation of a nonisothermal plug flow reactor model by spectral factorization," *IEEE Transactions on Automatic Control*, vol. 52, no. 7, pp. 1179–1193, 2007.

[109] I. Aksikas, A. Fuxman, J. F. Forbes, and J. J. Winkin, "LQ control design of a class of hyperbolic PDE systems: Application to fixed-bed reactor," *Automatica*, vol. 45, no. 6, pp. 1542–1548, 2009.

[110] Shang H., J. F. Frobes, and M. Guay, "Model Predictive Control for Quasilinear Hyperbolic Distributed Parameter Systems," *Ind. & Eng. Chem. Res.*, vol. 43, pp. 2140–2149, 2004.

[111] Y. Yang and S. Dubljevic, "Boundary model predictive control of thin film thickness modelled by the kuramoto-sivashinsky equation with input and state constraints," *Journal of Process Control*, vol. 23, no. 9, pp. 1362–1379, 2013.

[112] L. Liu, B. Huang, and S. Dubljevic, "Model predictive control of axial dispersion chemical reactor," *Journal of Process Control*, vol. 24, no. 11, pp. 1671–1690, 2014.

[113] I. Bonis, W. Xie, and C. Theodoropoulos, "A linear model predictive control algorithm for nonlinear large-scale distributed parameter systems," *AIChE Journal*, vol. 58, no. 3, pp. 801–811, 2012.

[114] L. Ai and Y. San, "Model predictive control for nonlinear distributed parameter systems based on ls-svm," *Asian Journal of Control*, vol. 15, no. 5, pp. 1407–1416, 2013.

[115] D. Q. Mayne, "Model Predictive Control," *Automatica*, vol. 50, no. 12, pp. 2967–2986, Dec. 2014.

[116] J. B. Rawlings and D. Q. Mayne, *Model predictive control: Theory and design*. Nob Hill Pub., 2009.

[117] P. O. Scokaert, D. Q. Mayne, and J. B. Rawlings, "Suboptimal model predictive control (feasibility implies stability)," *IEEE Trans. Auto. Cont.*, vol. 44, pp. 648–654, 1999.

[118] D. Bonvin, R. Rinker, and D. Mellichamp, "On Controlling an Autothermal Fixed-bed Reactor at an Unstable State-III: Model reduction and control strategies which avoid state estimation," *Chemical Engineering Science*, vol. 38, no. 4, pp. 607–618, 1983.

[119] C. Wong, D. Bonvin, D. Mellichamp, and R. Rinker, "On controlling an autothermal fixed-bed reactor at an unstable state-iv: Model fitting and control of the laboratory reactor," *Chemical Engineering Science*, vol. 38, no. 4, pp. 619–633, 1983.

[120] P. H. Gusciora and A. S. Foss, "Detecting and avoiding unstable operation of autothermal reactors," *AIChE Journal*, vol. 35, no. 6, pp. 881–890, 1989.

[121] S. G. Metchis and A. S. Foss, "Averting extinction in autothermal catalytic reactor operations," *AIChE Journal*, vol. 33, no. 8, pp. 1288–1299, 1987.

[122] H. B. Keller, "Lectures on numerical methods in bifurcation problems," *Applied Mathematics*, vol. 217, p. 50, 1987.

[123] M. J. Balas, "Feedback control of linear diffusion processes," *International Journal of Control*, vol. 29, no. 3, pp. 523–534, 1979.

[124] P. Christofides and P. Daoutidis, "Finite-dimensional control of parabolic pde systems using approximate inertial manifolds," *Journal of Mathematical Analysis and Applications*, vol. 216, no. 2, pp. 398–420, 1997.

[125] P. D. Christofides, *Nonlinear and Robust Control of PDE Systems: Methods and Applications to transport reaction processes*. Birkhauser, 2000.

[126] I. Aksikas, A. A. Moghadam, and J. F. Forbes, "Optimal linear–quadratic control of coupled parabolic–hyperbolic PDEs," *International Journal of Control*, vol. 90, no. 10, pp. 2152–2164, 2017.

[127] L. O. Santos and L. T. Biegler, "A tool to analyze robust stability for model predictive controllers," *Journal of Process Control*, vol. 9, no. 3, pp. 233–246, 1999.

[128] A. Nafsun and N. Yusoff, "Effect of model-plant mismatch on mpc controller performance," English, *Journal of Applied Sciences*, vol. 11, no. 21, pp. 3579–3585, 2011.

[129] P. Dufour, Y. Touré, D. Blanc, and P. Laurent, "On nonlinear distributed parameter model predictive control strategy: On-line calculation time reduction and application to an experimental drying process," *Computers & Chemical Engineering*, vol. 27, no. 11, pp. 1533–1542, 2003.

[130] A. Armaou and A. Ataei, "Piece-wise constant predictive feedback control of nonlinear systems," *Journal of Process Control*, vol. 24, no. 4, pp. 326–335, 2014.

[131] T. Marius and G. Weiss, *Observation and Control for Operator Semigroups*. Jan. 2009, vol. 11.

[132] G. O. Cassol and S. Dubljevic, "Discrete output regulator design for the linearized Saint–Venant–Exner model," *Processes*, vol. 8, no. 8, 2020.

[133] Y. Belhamadia, A. Fortin, and É. Chamberland, "Anisotropic mesh adaptation for the solution of the stefan problem," *Journal of Computational Physics*, vol. 194, no. 1, pp. 233–255, 2004.

[134] Y. Belhamadia, A. Fortin, and É. Chamberland, "Three-dimensional anisotropic mesh adaptation for phase change problems," *Journal of Computational Physics*, vol. 201, no. 2, pp. 753–770, 2004.

[135] A. Hazim, Y. Belhamadia, and S. Dubljevic, "Mechanical perturbation control of cardiac alternans," *Physical Review E*, vol. 97, p. 052 407, 5 2018. DOI: 10.1103/PhysRevE.97.052407.

[136] A. Hazim, Y. Belhamadia, and S. Dubljevic, "Effects of mechano-electrical feedback on the onset of alternans: A computational study," *Chaos: An Interdisciplinary Journal of Nonlinear Science*, vol. 29, no. 6, p. 063 126, 2019. DOI: 10.1063/1.5095778.

[137] A. Fortin and Y. Belhamadia, "Numerical prediction of freezing fronts in cryosurgery: Comparison with experimental results," *Computer methods in biomechanics and biomedical engineering*, vol. 8, no. 4, pp. 241–249, 2005.

[138] Y. Belhamadia, A. Fortin, and T. Briffard, "A two-dimensional adaptive remeshing method for solving melting and solidification problems with convection," *Numerical Heat Transfer, Part A: Applications*, vol. 76, no. 4, pp. 179–197, 2019.